Electronic Thesis and Dissertation Repository

3-31-2021 2:00 PM

Experimental, theoretical, and translational studies of RBC distribution in capillary networks

Asher Mendelson, *The University of Western Ontario*

Supervisor: Ellis, Christopher G, *The University of Western Ontario*
: Goldman, Daniel, *The University of Western Ontario*
A thesis submitted in partial fulfillment of the requirements for the Doctor of Philosophy degree in Medical Biophysics
© Asher Mendelson 2021

Abstract

The purpose of this thesis was to evaluate the physiology of red blood cell (RBC) distribution in skeletal muscle capillary networks. Because this is the terminal site of oxygen exchange in the microcirculation, characterization of this fundamental process informs an understanding of how microvascular blood flow regulation matches oxygen supply with local tissue demand. Prior studies in this field have focused on small groups of capillaries, and have not linked capillary network structure with functional measurements, nor evaluated the temporal complexity of RBC distribution over physiologically-relevant scales. It is also unclear how the functional units called capillary modules – comprised of parallel capillaries from arteriole to venule – relate together within large capillary networks. In this thesis, we employed multiple methodologies to achieve this goal with preclinical animal models, theoretical simulations, and translational studies in human patients. First, we used intravital videomicroscopy of resting extensor digitorum longus muscle in rats and discovered that skeletal muscle capillary networks are organized into columns of interconnected capillary modules spanning thousands of microns – a structure we called the Capillary Fascicle. We showed that capillary-RBC hemodynamics are heterogeneous within a module and between modules. Next, we evaluated capillary module hemodynamics and demonstrated that RBC flow is independent of module resistance, providing evidence for regulation of driving pressure at the level of the capillary module, that requires pre- and post-capillary mechanisms of control. Using a dual-phase mathematical model of blood flow within artificial capillary module geometries, we showed that RBC flow heterogeneity is an intrinsic property of capillary module structure,

and that variations to inflow hematocrit and pressure impact RBC distribution as a consequence of the rheological properties of microvascular blood flow. Finally, we used high-resolution near-infrared spectroscopy to monitor the temporal variability of hemoglobin content in skeletal muscle of patients in the intensive care unit (ICU). We showed that RBC perfusion characteristics are not consistent between patients, and that ICU interventions directly impact microvascular RBC distribution. Together, these studies support a theory of capillary networks as active participants in microvascular blood flow regulation, with structural features of capillary networks contributing to functional characteristics of RBC distribution.

Keywords: Microcirculation, capillary, capillary networks, red blood cell, physiology, skeletal muscle, blood flow, blood flow regulation, intravital microscopy, mathematical model, rheology, biophysics, intensive care, critical care, near-infrared spectroscopy, hemoglobin, hemodynamic monitoring

Summary for Lay Audience

Capillaries are the smallest blood vessels in the microcirculation, and red blood cells (RBCs) contain hemoglobin that carries oxygen throughout the body. Oxygen is fundamentally exchanged at the level of the capillary network, making the study of RBC distribution in capillary networks very important for understanding how the microcirculation regulates oxygen delivery. Prior studies of capillary biology has focused on small groups of capillaries (called capillary modules) and have not linked capillary network structure with function, nor described how capillary modules relate within large capillary networks. The purpose of this thesis was to evaluate the physiology of RBC distribution in skeletal muscle capillary networks. We employed a variety of techniques ranging from animal models, to theoretical simulations, and clinical studies with human patients. First, we used microscopy in living rodents to examine RBC flow in resting skeletal muscle. We discovered that capillary networks are organized into columns of interconnected capillary modules– a structure we called the Capillary Fascicle. We also showed that blood flow control is actively adjusted in capillary modules through changes to perfusion pressure. We used mathematical simulations to understand how the structure of the capillary modules and the properties of blood flow in the microcirculation affect RBC distribution. Finally, we used near-infrared spectroscopy (a non-invasive monitoring technology that uses light) to investigate the physiology of RBC distribution in patients in the intensive care unit (ICU). We showed that the patterns of RBC flow in the microcirculation are not consistent between patients, and are impacted by ICU interventions including medications and the ventilator. Together, these results provide a

novel and comprehensive description of RBC distribution in skeletal muscle capillary networks, and suggest that capillary networks participate in blood flow regulation and oxygen delivery.

Co-Authorship Statement

This thesis contains the following manuscripts that have been accepted, submitted, or are in preparation for submission:

Chapter 1: This chapter was written by Asher Mendelson. Section 1.8 was adapted from a review article entitled "*Advances in Translational Imaging of the Microcirculation*" published in *Microcirculation*. Co-authors are Marie Guerraty, Akanksha Bhargava, Janaka Senarathna, Asher Mendelson, and Arvind Pathak. Asher Mendelson was the primary author for the near-infrared spectroscopy section of the review article, used in this thesis. Portions of the review article contributed by the other authors were not used.

Chapter 2: This chapter represents work based on a manuscript entitled "*The Capillary Fascicle in skeletal muscle: structural and functional physiology of RBC distribution in capillary networks*," published in *The Journal of Physiology*. Asher Mendelson is first author for this work; co-authors are Stephanie Milkovich, Timothy Hunter, Raashi Vijay, Yun-Hee Choi, Shaun Milkovich, Edward Ho, Daniel Goldman, and Christopher Ellis. Asher Mendelson was responsible for study concept and experimental design, the completion of all experiments, data analysis, statistical analysis, data interpretation, preparing the figures, and drafting the manuscript. Stephanie Milkovich assisted with experiments. Timothy Hunter, Raashi Vijay, and Shaun Milkovich assisted with data analysis, under the direction of Asher Mendelson. Yun-Hee Choi provided guidance on statistical analysis. Edward Ho (as part of his undergraduate thesis) designed the software that generated the synthetic module geometries, under the supervision of Asher Mendelson,

and using the dual-phase blood flow model created by Daniel Goldman. Daniel Goldman and Christopher Ellis, as co-supervisors for Asher Mendelson, contributed to study concept, experimental design, and data interpretation. All authors reviewed a draft of the manuscript prior to submission for publication.

Chapter 3: This manuscript is in preparation and has not been submitted. Asher Mendelson is first author for this work; co-authors are Edward Ho, Shayla Scott, Raashi Vijay, Timothy Hunter, Christopher Ellis, and Daniel Goldman. Asher Mendelson was responsible for study concept and experimental design, the completion of all experiments, data analysis, statistical analysis, data interpretation, preparing the figures, and drafting the chapter. Edward Ho (as part of his undergraduate thesis) designed the software that generated the synthetic module geometries, under the supervision of Asher Mendelson, and using the dual-phase blood flow model created by Daniel Goldman. Shayla Scott (as part of her undergraduate thesis) completed the plasma flow analysis from the experimental data, under the supervision of Asher Mendelson and Daniel Goldman. Raashi Vijay and Timothy Hunter assisted with data analysis, under the direction of Asher Mendelson. Daniel Goldman and Christopher Ellis, as co-supervisors for Asher Mendelson, contributed to study concept, experimental design and data interpretation.

Chapter 4: This chapter represents work based on a manuscript entitled "*Dynamic tracking of microvascular hemoglobin content for continuous perfusion monitoring in the intensive care unit: pilot feasibility study,*" that was published in *Journal of Clinical Monitoring and Computing* in October 2020. Asher Mendelson is the first author for this work; co-authors are Ajay Rajaram, Daniel Bainbridge, Keith St. Lawrence, Tracey

Bentall, Michael Sharpe, Mamadou Diop, and Christopher Ellis. Asher Mendelson was responsible for study design, data collection in the ICU, data analysis, statistical analysis, data interpretation, preparation of the figures, and drafting the manuscript. Ajay Rajaram, under the supervision of Mamadou Diop and Keith St. Lawrence, designed and built the NIRS system used in the study, with assistance from Asher Mendelson. Tracey Bentall assisted with patient recruitment in the ICU. Daniel Bainbridge and Michael Sharpe provided clinical direction for experimental design and data interpretation. Mamadou Diop and Keith St. Lawrence provided guidance with data interpretation. Christopher Ellis conceptualized the study, secured funding, designed the wavelet software used for analysis, and provided guidance with data interpretation. All authors reviewed the manuscript prior to submission.

Chapter 5: This chapter was written by Asher Mendelson.

Acknowledgment

Deciding to embark on a doctoral degree following a decade of clinical medical training was not a decision I took lightly, but one that has proven to be the most rewarding of my academic career. I entered this degree with many unknowns, and have emerged with the tools and roadmap necessary to embark on a successful career of lifelong investigation and discovery.

To my supervisors, Chris Ellis and Daniel Goldman, it is hard to express the gratitude I have for sharing your knowledge with me. Each of you have patiently nurtured my curiosity, while providing a positive space for me to grow as a scientist and human being. Your passion for teaching, and for the microcirculation, is inspiring. Throughout the inevitable challenges encountered during this degree, you gave me motivation, support, and the magic words every student needs to hear: "you can do it, I know you can."

I would also like to acknowledge my collaborators on all the research projects: Mamadou, Keith, and Ajay at Lawson Optics; Dan, Mike, and Tracey at LHSC; Yun-Hee in Biostatistics. All of you have given me insight and new perspective, reminding me that science is a team sport where everybody brings skills to the table, and the final product is more than the sum of its parts.

To Steph, my trusted companion in the lab, you have been one of the best teachers I could hope for as I learned many challenging experimental techniques and life lessons; thank you for always laughing at my jokes and keeping me focused on the bright side. I would also like to acknowledge the other members of the lab for their helpful discussion

and support over the years. Moreover, I am grateful for all the undergraduate students that have come through the lab, who contributed to the work in this thesis and showed me the value of teaching and mentoring research trainees.

I would like to thank the patients and families in the ICU who consented to the clinical study in this thesis, and acknowledge the sacrifice of the many lab animals that were used to generate the preclinical data. In all cases, the contributions have been immeasurable and will continue to bear fruit with the knowledge gained from this work.

To my family, thank you for listening to all my heartache, self-doubt, frustration. It is hard to imagine completing this thesis without your love and support. I promise this is that last degree that I get.

And to Rachel, the love of my life that I met during the early years of this degree. Your gentle kindness and soft heart bring me joy every day. You have been by my side for every step of this journey, picked me up when I was down, and kept me looking forward when all I wanted to do is turn back. Marrying you was the single greatest accomplishment of this time in my life. Above all else, you have taught me that what matters the most cannot be found in a textbook or a science experiment. You are my best friend and the next chapter of our life, and every chapter thereafter, is dedicated to you.

Table of Contents

List of Tables

List of Figures

List of Abbreviations

1A: Feeding arteriole

2A: Arcade arteriole

3A: Transverse arteriole

4A: Terminal arteriole

CF: Capillary Fascicle

CM: Capillary module

CVP: Central venous pressure

D: Diameter

DAMP: Damage-associated molecular patterns

EC: Endothelial cells

EDF: Extended depth of focus

EDL: Extensor digitorum longus

FOV: Field of view

[Hb]: Concentration of hemoglobin

Hb: Deoxy-hemoglobin

Hb-O2: Oxy-hemoglobin

HbT: Total hemoglobin

Hct: Hematocrit

H_D: Discharge hematocrit

H_T: Tube hematocrit

HVM: Handheld vital microscopy

ICU: Intensive care unit

iNOS: Inducible nitric oxide synthase

l: Length

LD: Lineal density

LPS: Lipopolysaccharide, endotoxin

MAP: Mean arterial pressure

MFI: Microvascular flow index

MHC: Microvascular hemoglobin content

mmHg: Millimeters of mercury

NET: Neutrophil extracellular traps

NIRS: Near-infrared spectroscopy

N_{par}: Number of parallel capillaries

O_2: Oxygen

PAMP: Pathogen-associated molecular patterns

PCV: Post-capillary venule

pO2: Partial pressure of oxygen

pCO2: Partial pressure of carbon dioxide

PPV: Proportion of perfused vessels

Q: Blood flow

QO_2: Oxygen delivery

r: radius

RBC: Red blood cell

SR_{rbc}: RBC supply rate

SR_{module}: Capillary module RBC supply rate

SpO_2: Arterial oxygen saturation

StO_2: Tissue oxygen saturation

TLR: Toll-like receptor

V_b: Blood velocity

V_c: Cell velocity

VO_2: Oxygen consumption

VOT: Vascular occlusion test

V_{rbc}: RBC velocity

μm: micrometer

ΔP: Driving pressure, pressure gradient

ΔOD: Change in optical density

η: Apparent viscosity, viscosity

CHAPTER 1: INTRODUCTION

1.1 Purpose and Hypotheses

The microcirculation defines the portion of the cardiovascular system comprising the smallest blood vessels throughout the body. Because of the direct interface with all organs, the microcirculation is tasked with the fundamental homeostatic roles of the cardiovascular system including oxygen and nutrient delivery, waste removal, fluid exchange, coagulation, and immune signaling. Microvascular dysfunction has been implicated in the pathophysiology of numerous diseases, both acute and chronic, in every organ system, and can result from both depressed and exaggerated physiological responses.

We can surmise that chief among these functions is the delivery of oxygen to all cells throughout the body, which is essential to ensure adequate cellular respiration and thus to sustain life. This is achieved by convective transport (i.e. blood flow) within the circulatory system over large distances, and diffusive transport from the microcirculation into surrounding tissue. All vertebrates (except the Antarctic icefish [251]) utilize specialized cells called erythrocytes (red blood cells, RBCs), that contain millions of hemoglobin proteins that reversibly bind oxygen for transport and delivery. Thus, a detailed understanding of microvascular oxygen exchange cannot be complete without a simultaneous description of the RBC distribution therein. Far from being passive, the interaction between the microcirculation and RBCs is a dynamic relationship that matches tissue demand with oxygen supply in real-time. To accomplish this task, the

microcirculation has structural features that are conducive to RBC delivery and oxygen exchange within an organ, and functional mechanisms that distribute RBCs with exquisite spatial and temporal accuracy in response to feedback signals within the system [67, 220, 247].

Capillary networks represent the primary exchange vessels of the microcirculation and are therefore a critical step in the oxygen pathway. Network topology and capillary hematocrit determine the functional surface area available for diffusion, whereas capillary-RBC hemodynamics define the convective transport of oxygen through the network (i.e. capillary perfusion). Often, studies have provided topological details of capillary networks with no functional data, or conversely capillary-RBC hemodynamics are recorded with no spatial localization. When these components have been reported together, it has been with the limited scale of only a small number of capillaries in a small volume of tissue, thereby restricting the scope of interpretation. Moreover, it has long been recognized that heterogeneity is a hallmark of the microcirculation [58, 220], and that physiological parameters in capillary networks exhibit dramatic variability even under normal conditions. This reinforces that accurate characterization and understanding of capillary physiology requires comprehensive experimental sampling over a larger volume of tissue and linkages between structure and function.

One organ of specific interest to oxygen transport is skeletal muscle, given its remarkable ability to increase oxygen metabolism and blood flow from rest to peak exercise. Skeletal muscle fibres (myocytes) can often have lengths exceeding many thousands of microns in small animals and even centimeters in humans, far longer than any

individual capillary. Previous work has identified the capillary module as the basic functional unit of complex capillary networks – comprising a group of parallel-flowing capillaries originating from a single terminal arteriole and draining into a post-capillary venule. Despite the longstanding recognition that capillary modules in skeletal muscle are indeed linked to form larger capillary networks [49, 254], most researchers still think about the microcirculation as a 'linear' system whereby all modules behave independently from each other, with segregated inflow and outflow vessels controlling one module at a time. This linear model becomes increasingly deficient when the heterogeneity of module topology is considered, and it also fails to address how blood flow can be coordinated over large scales to meet the energy requirements of contracting muscle. At present, we can conclude that a functionally-relevant and anatomically-informed framework for RBC distribution in skeletal muscle capillary networks is still needed in order to faithfully investigate how RBC supply is regulated.

Also contributing to the physiology of RBC distribution in skeletal muscle capillary networks is the structure of the capillary module, and the unique biophysical properties of blood flow in the microcirculation. Unlike traditional branching networks of the arteriolar tree, capillary modules are organized with a relatively large number of capillaries arising from a single terminal arteriole over a very short distance and within each module there are multiple capillary segments arising from diverging and converging bifurcations. Moreover, blood flow in the microcirculation does not exist as a homogenous medium, but rather as particulate RBCs suspended in plasma; in capillaries with very narrow internal diameter, RBCs have important interactions with the vessel wall that may affect their hemodynamics. Computational models of microvascular blood flow have been used to better understand

these properties within arteriolar systems, or within groups of capillaries unconnected to the surrounding microvasculature, but have rarely been systematically applied to a completed capillary module that includes both inflow and outflow vessels. These boundary conditions are important for understanding how RBC distribution is manifested in capillary modules, and how these modules can link together to form large capillary networks that span the length of a muscle. Moreover, by applying biophysical calculations to in vivo experimental data and computational models, we gain insights into the physiological mechanisms of flow regulation.

The clinical applications for physiological studies of RBC distribution are numerous, but have particular relevance in the field of critical care medicine, where patients suffer life-threatening organ dysfunction due to diseases like sepsis, cardiac arrest, and trauma. Inadequate oxygen delivery is an essential criteria for diagnosing circulatory shock, that presents with both cardiovascular collapse and profound microvascular dysfunction. Importantly, the presence of normal systemic hemodynamics does not preclude the existence of microvascular dysfunction, and microvascular parameters actually correlate better with adverse outcomes. Early recognition of perfusion abnormalities can alert clinicians and prompt reversal of the condition with targeted interventions. In recent years, non-invasive techniques have been developed to interrogate the microcirculation at the bedside, including sublingual videomicroscopy and near-infrared spectroscopy. While each of these modalities have technical advantages and limitations, they have rarely demonstrated the ability to affect outcomes when incorporated into treatment protocols. This may be explained, in part, by their inability to accurately represent the physiological complexity of RBC distribution within the underlying

microcirculation during the onset of microvascular dysfunction. There is an urgent need for a new approach to noninvasively monitor the microvasculature that captures this complexity.

In order to advance the understanding of RBC distribution in the microcirculation, three studies have been conceived that span the breadth of scientific investigation: preclinical experimentation to establish a new framework for interpreting microvascular flow regulation, theoretical modeling to uncover novel relationships in the experimental data complemented by computation simulations to further test these findings, and translational applications based on the insights gained from experimental data to address unmet challenges in the clinical setting:

Chapter 2: The Capillary Fascicle in skeletal muscle: structural and functional physiology of RBC distribution in capillary networks.

> *Purpose:* Using intravital videomicroscopy, we characterize RBC distribution in rodent skeletal muscle and link network topology with functional capillary-RBC hemodynamics in large capillary networks. The Capillary Fascicle is introduced as a series of interconnected capillary modules that link together in large columns spanning many thousands of microns in parallel with muscle fibres.

Hypothesis: Capillary networks demonstrate spatial and temporal heterogeneity at the level of individual capillaries, within capillary modules and between modules. Structure-function analysis of the Capillary Fascicle will demonstrate the presence of microvascular flow regulation at the level of the capillary module.

Chapter 3: Biophysical properties of RBC and plasma flow distribution in capillary modules

Purpose: Building on these findings, we apply biophysical equations of microvascular blood flow to the in vivo experimental data. This analysis delineates the differential behaviors of RBC and plasma flow distribution, and the interactions between flow, resistance and pressure at the level of interconnected capillary modules. Using a dual-phase computational model of blood flow within capillary module geometries, we analyze the effect of pressure and hematocrit boundary conditions on flow distribution within individual capillary modules, and between connected modules.

Hypothesis: Capillary module blood flow is largely independent of module hemodynamic resistance, signifying that the regulation of driving pressure across the module is an important mechanism of microvascular flow regulation. The interconnected structure of capillary modules suggests the need for pre- and post-capillary loci of blood flow control. RBC and plasma distributions within capillary modules are affected by the particulate nature of blood flow and viscosity-dependent changes to capillary resistance, implying the need for multiple coordinated and time-dependent mechanisms of flow regulation.

Chapter 4: Dynamic tracking of microvascular hemoglobin content for continuous perfusion monitoring in the intensive care unit: pilot feasibility study.

Purpose: To develop an optical system using high-resolution near-infrared spectroscopy to monitor RBC distribution in the peripheral microcirculation in humans, and to test the feasibility of this monitoring system in the intensive care unit (ICU).

Hypothesis: The time-dependent variability in microvascular hemoglobin content reflects the complex physiology of RBC distribution within the underlying microcirculation. Time series analysis using wavelet transform can reveal heterogeneous perfusion characteristics between patients and interactions between the microcirculation and systemic ICU interventions including vasoactive medications and mechanical ventilation.

In the ensuing sections of the introduction, we provide an overview of the current state of knowledge regarding structure and function of capillary networks and their potential contribution to microvascular flow regulation (Chapter 2). Next, we discuss the unique biophysical properties of blood flow in the microcirculation and their implications on network-level RBC flow distribution (Chapter 3). Finally, we outline the physiology of microvascular dysfunction and circulatory shock in the ICU, as well as past and current efforts to monitor global oxygen delivery, microvascular function, and peripheral perfusion in critical care (Chapter 4).

1.2 Capillary networks in skeletal muscle – organization, physiology, and flow regulation

Capillary networks are the fundamental site of oxygen exchange between the microcirculation and surrounding tissue. Because of this essential role in the oxygen exchange pathway, alterations to capillary network structure and function can have profound implications for the ability of organs to maintain homeostasis and respond to increased energy demands under stress conditions or in disease states [204, 205]. Skeletal muscle is the largest organ by mass in the body [45, 134], accounting for approximately 40% of total body weight. Due to its specialized function in locomotion, skeletal muscle also has the widest range of metabolic requirements, whereby oxygen consumption can increase 100-fold from rest to peak exercise; this change in oxygen consumption and muscle work is accompanied by a linear increase in blood flow [187, 203], indicating exquisite mechanisms for matching oxygen demand with supply. Thus, capillary networks in skeletal muscle are an ideal system to study the physiology of oxygen exchange and blood flow regulation.

In the early 20th century, August Krogh was the first scientist to recognize the role of capillaries in oxygen exchange [141, 142], and proposed simple diffusion as the primary biophysical method by which this was achieved. For his description of the *Krogh cylinder* – the volume of tissue surrounding a perfused capillary – and the regulation of oxygen delivery from capillaries into muscle tissue, he was awarded the Nobel Prize in 1920. This work also highlighted the importance of capillary architecture in oxygen exchange by

proposing a maximal radius of tissue (and therefore inter-capillary distance) that supports oxygen diffusion from a single capillary. To accommodate changes in oxygen consumption with locomotion, Krogh hypothesized that non-flowing capillaries are recruited to facilitate oxygen exchange by shortening the diffusion distance between capillaries into the surrounding muscle tissue (see counterpoint to the capillary recruitment hypothesis below).

Over time, these theories have evolved with more sophisticated experimental and computational studies. In the 1960s and 1970s, work in this field was largely restricted to ex-vivo geometric analysis. Plyley and Groom [201] utilized microfil silicon elastomere perfusion of the frog sartorius muscle to elucidate the geometry of a single "capillary unit" - the group of parallel flowing capillaries originating from a terminal arteriole (TA) and draining to a post-capillary venule (PCV). They identified the internal branching structure inside this unit, consisting of converging and diverging bifurcations (Figure 1.1), and described capillary segments as the unbranched vessels that together form the total path length for the network; notably, they showed that path lengths are Gaussian, and the occurrence of branch points along the capillary path length follows a Poisson distribution, suggesting a degree of stochasticity in generating this architecture.

Further capillary geometry analysis was undertaken by Skalak and Schmid-Schönbein using carbon ink [254], to quantify the number of parallel capillaries, nodal branch points, and arteriolar/venular connections (Figure 1.1). Ratios between these values yielded metrics that were used to compare capillary architecture between control and spontaneously hypertensive rats, showing differences between both groups. Skalak also identified the alternating pattern of TA and PCV that insert into these capillary networks

forming a columnar structure parallel with muscle fibres, which he called a "capillary bundle."
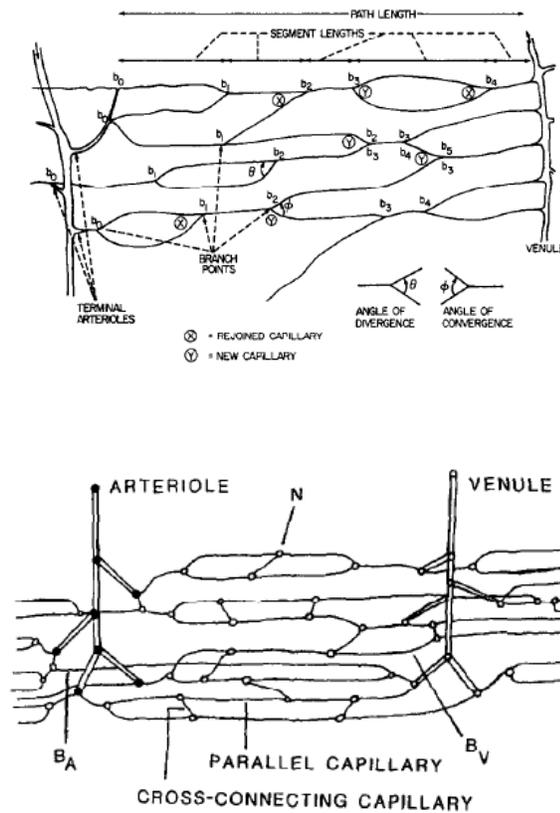
Figure 1.1: Structure of the capillary module
Top: described by Plyley and Groom [201] consisting of capillary segments with converging and diverging bifurcations.
Bottom: described by Skalak and Schmid-Schönbein [254] consisting of parallel capillaries with cross-connections. Reproduced with permission.

Geometric analysis was further enhanced with in vivo measurements of capillary perfusion. Honig [115], combined geometric data with velocities from Burton [28] to demonstrate that RBC transit time through a capillary network was highly variable. Tyml [271] used video-microscopy of the frog sartorius to show that capillaries exhibit both temporal and spatial heterogeneity with regards to RBC velocity and transit time, and also mapped these functional parameters back onto an beautiful network figure. Sarelius

pioneered the use of fluorescently-labelled erythrocytes in the hamster cremaster and cheek pouch to directly measure RBC transit time and hematocrit [239]. With this technique, she demonstrated heterogeneity in RBC velocity, transit time and RBC flux, as well as a dissociation between anatomical path length (i.e. distance between TA and PCV) and functional path length (i.e. the length traversed by an RBC through the network) [238]; interestingly, Sarelius found that hyperemia did not significantly alter the proportion of RBCs that travel through shorter or longer paths, which may suggest that module topology is an important determinant of RBC distribution.

To understand the origins of the observed heterogeneity in capillary physiology, the interaction of arterioles with skeletal muscle capillary networks has also been a subject of investigation. Organization of the arteriolar system in skeletal muscle comprises large feeding arterioles (1A) into the muscle, which then branch into arcade arterioles (2A) forming interconnected loops [72, 243]; these arcade arterioles branch further (often at 90 degrees from the arcade arteriole) into transverse arterioles (3A) that run linearly across a muscle region [282]; finally, transverse arterioles give rise to terminal arterioles (4A) that flow directly into capillary networks. Zweifach established that the pressures and flows throughout the arteriolar system in skeletal muscle are highly variable [282], up to and including the 4A terminal arterioles. Lund and colleagues [164] described the grouping of capillaries into "modules" (units) supplied by a single terminal arteriole. Delashaw and Duling [49] examined the hamster tibialis anterior muscle, and identified "unit pairs" which comprised two capillary modules supplied by a common terminal arteriole and draining into two separate post-capillary venules in opposite directions. Using various stimuli, including hyperoxia, muscle contraction, and phenylephrine, they showed that the flow

response for unit pairs was almost always synchronous between modules, and increased or decreased in unison for both modules. Segal expanded this observation to note that although unit pairs are undoubtedly linked by a common terminal arteriole, adjacent unit pairs are only partially aligned across the muscle length and sometimes arise from different sections of the arteriolar tree [71]. Sweeney and Sarelius [263] observed similar findings regarding the grouped nature of capillary flow, and found that control of blood flow to capillary modules occurred upstream from the 4A arterioles, likely at the 3A position; further investigation revealed that distribution of RBCs between capillary modules could be spatially organized, and the branch position of the 4A arteriole along the length of the 3A vessel was an important determinant of its dilatory response [80, 240]. Yet, Ellis and colleagues [63] showed substantial RBC flow heterogeneity even in a capillary module supplied by a single 4A arteriole, which is inversely related to RBC supply rate from the terminal arteriole (i.e. increased supply rate will decrease RBC heterogeneity); this suggested that although heterogeneity in flow and pressure distribution between proximal arterioles can account from some of the observed heterogeneity in capillary networks, the geometry of capillary networks themselves and the rheology of RBCs through these networks provides an intrinsic source of heterogeneity observed in experimental studies. For the purposes of consistency, the term capillary module will be used for the remainder of this thesis to denote the group of parallel capillaries between TA and PCV.

Despite these insights regarding the physiology of RBC distribution between arterioles and capillary networks, questions still remained regarding how capillaries might participate in microvascular flow regulation and coordinate a hyperemic response in skeletal muscle. Arterioles have classically been viewed as the primary regulators of

microvascular blood flow [247], and intrinsic arteriolar properties to maintain flow homeostasis and accommodate functional hyperemia have been well-described. Myogenic tone provides a feedback loop, such that increases to intraluminal pressure will lead to vasoconstriction of the arteriolar smooth muscle [47]; shear-dependent vasodilation, mediated by nitric oxide, provides an opposing mechanism that prevents biophysical stress from damaging resistance vessels due to increased blood flow during hyperemia [97]. These signals, as well as sympathetic innervation of vascular smooth muscle, are integrated along the arteriolar tree [267], and conducted vasodilation of depolarizing signals that travel via the vascular endothelium to call for increased flow from proximal arterioles [11]. Undoubtedly, these complex mechanisms support the theory that blood flow control occurs in arterioles, through alterations to vascular resistance. However, this fails to address whether a hyperemic flow response requires contribution from capillaries themselves: this physiology could be explained by the "metabolic hypothesis" that vasodilatory substances produced from contracting skeletal muscle diffuse directly from active muscle into adjacent arterioles.

Anatomically, a "capillary-centric" hypothesis for flow regulation is attractive because capillaries are ideally located between muscle fibres to sense local changes in skeletal muscle metabolism and oxygen consumption. Moreover, given the size of capillary modules, the distance to the closest 4A and 3A arterioles is too far and the hyperemic response is too quick (less than a second) for vasoactive metabolites to diffuse to arterioles within a reasonable timeframe [186]. Because capillaries contain no contractile smooth muscle, the capillary-centric hypothesis may appear dubious. However, experimental evidence does indeed exist that capillaries can communicate directly with arterioles to elicit

a hyperemic response. Dietrich demonstrated that locally-applied norepinephrine on capillaries produced a negative flow response on those capillaries despite no change in their diameter [52], presumably via arteriolar vasoconstriction. This was further explored by Dietrich and Tyml, revealing that this response was not attributed to diffusion of the metabolic stimulus to the arteriole, sympathetic nerve activity, or communication from vein to arteriole [53]. Upstream vasodilation responses by arterioles to capillary stimulation has also been noted with other vasoactive metabolites including acetylcholine, and adenosine or pinacidil which open ATP-sensitive potassium channels [38, 39, 256, 270]. The above studies by Cohen also showed that electrical stimulation of muscle contraction over a region of capillaries could yield a similar vasodilatory response in upstream arterioles, and inhibition of gap-junction communication with halothane or hyperosmotic glucose reduces this effect [38]. Berg and colleagues [22] illustrated the exquisite spatial localization of this phenomenon: even though capillary module stimulation generated an upstream response by 2A, 3A, and 4A arterioles, there was no spillover of this arteriolar hyperemia into unstimulated capillary modules that were supplied by the above arterioles. Other mechanisms for microvascular signaling include oxygen-dependent ATP release from RBCs, triggering a depolarization event on the capillary endothelium [65, 69]. Taken together, this data conclusively supports the theory that capillaries can serve as effective sensors of metabolic demand and communicators with the arteriolar system.

Regarding capillary recruitment, although this had originally been proposed by Krogh to explain how capillary networks accommodate increased oxygen delivery to myocytes to meet increased metabolic demand, subsequent empirical evidence and re-interpretation of Krogh's work refutes this claim [203, 204]. The overwhelming majority

(>80%) of capillaries are perfused at rest [16, 41, 66, 136, 195], and the non-perfused capillaries observed by Krogh were likely a fixation artifact that misrepresented low-flow (but not zero flow) capillaries. Importantly, not all perfused capillaries contribute equally to oxygen exchange at rest, but rather that heterogenous resting capillary hemodynamics will all approach maximal thresholds during reactive hyperemia; capillary hematocrits all trend towards systemic levels and capillary velocities increase many-fold above resting values. This change from baseline is most significant for low flow capillaries, but does not imply they were recruited de novo [205].

In concert with these experimental studies, computational modeling has shown the importance of considering capillary network physiology when evaluating the ability of the microcirculation to deliver oxygen. Federspiel and Popel [74] demonstrated that the particulate nature of blood is essential for calculating the diffusive characteristics of oxygen from capillaries into muscle tissue. Specifically, the number of RBCs in a capillary and their spacing between plasma gaps are the main determinants of resistance to oxygen diffusion, and that discrete models differed significantly when compared to blood as a homogenous medium. This insight underscores why capillaries with low RBC flow participate very little in oxygen transport at baseline, but can increase their contribution with functional hyperemia. Popel was one of the first to identify that capillary flow heterogeneity may have implications for oxygen transport [206]. This was complemented by work from Pittman and Ellsworth that suggested that oxygen is exchanged through diffusion and convection between all microvessels (arterioles, capillaries, and venules), which underscores the importance of network architecture in characterizing oxygen transport [70, 199, 200]. Lo and colleagues [161] illustrated how control of oxygen delivery

through sensing at the level of the capillaries – as opposed to the arterioles – resulted in more uniform and resilient oxygen delivery over a range of metabolic consumption rates. Goldman quantified the process of diffusional exchange in capillary networks, showing definitively that low-flow capillaries can receive oxygen from adjacent capillaries and participate in oxygen exchange [90]; More recently, Liu and colleagues showed how variations in fibre size and metabolic activity between fibre types contributes to oxygen heterogeneity in muscle tissue [159]. Fraser developed an oxygen exchange model using realistic 3D mapping of capillary networks [81], and further confirmed that diffusional exchange between capillaries can serve as a buffer to prevent tissue dysoxia under normal conditions. Lücker and colleagues illustrated that changes to capillary hematocrit have a greater impact on oxygen exchange than changes to RBC velocity [163], and how diffusive exchange between capillaries reduces tissue dysoxia in reconstructed cerebral capillary networks [162]. Together, this body of literature indicates that capillary networks plays an essential role in the physiology of microvascular oxygen delivery.

1.3 Biophysical properties of blood flow in the microcirculation

Although there is no exact size cutoff, it is generally accepted that the microcirculation denotes vessels with internal diameter less than 100-150 microns [151, 207], with upper estimates of 300 microns [214]. These vessels have the largest cross-sectional surface area of the cardiovascular system and are the greatest contributor to overall vascular resistance. The physiological functions of the microcirculation are made possible by the unique biophysical properties of blood flow within small microvessels [219, 220]. In the large arteries and veins of the systemic circulation, blood is considered a homogenous fluid whose flow mechanics are determined mostly by inertial forces [246]. By contrast, blood flow within the microcirculation is dominated by viscous forces that are determined by an exceedingly low Reynolds number (Re << 1), thereby implying that inertial forces can be neglected [246]. The explanation for this shift in mechanical properties is explained in part by the cross-sectional area that greatly reduces the flow velocities in microvessels. Rather than a homogenous fluid, blood flow in the microcirculation should be viewed as the sum of its discrete components: red blood cells (RBCs) suspended in aqueous plasma. Plasma is mostly water with some macromolecular proteins, and overall flow remains Newtonian (viscosity independent of shear rate); RBCs exist as deformable bi-concave structures that interact with each other and the vessel wall [158]. For the purposes of these theories, the volume of blood occupied by platelets and white blood cells is negligible.

How do these two blood components behave in microvessels, and what effects does this have on the nature of blood flow? RBCs will migrate away from the vessel wall due to the radial velocity profile resulting in higher hematocrits towards the center of a vessel [220, 246]. Moreover, the endothelial surface layer (ESL) contains numerous glycoproteins

that exclude RBCs causing a cell-free layer that also retards plasma flow. These differences in flow speed between plasma and RBC components lead to differences in transit time within a microvessel, such that the RBC volume fraction (tube hematocrit, H_T) is always lower than the RBC flow fraction (discharge hematocrit, H_D). These relationships have been defined by Albrecht (1979):

$$\frac{H_T}{H_D} = \frac{v_b}{v_c}$$

Where v_b and v_c are the flow velocities of blood (rbc + plasma) and cells (rbc), respectively. This reduction in tube hematocrit in the microcirculation relative to discharge hematocrit is known as the *Fahraeus effect*, and becomes more pronounced as blood flows through progressively smaller microvessels, with the strongest effect in the diameter range 7-30μm [93]. Using empirical data from the mesenteric microcirculation, Pries and colleagues [217] derived a parametric equation that defines the alterations to this ratio as a function of vessel diameter (D):

$$\frac{H_T}{H_D} = H_D + (1 - H_D) * (1 + 1.7e^{-0.415D} - 0.6e^{-0.011D})$$

This reduction in tube hematocrit also partially contributes to another observed phenomenon of microvascular blood flow – the reduction in apparent viscosity (η) in microvessels relative to the viscosity of blood in the systemic circulation. The *Fahraeus-Lindqvist effect* defines these diameter- and hematocrit-dependent viscosity observations, and has been described for *in vitro* experiments with glass tubes [211]; Pries [218] also

derived another set of parametric equations through *in vivo* observations of microvascular networks:

$$\eta_{vivo} = \left[1 + \left(\eta^*_{0.45} - 1\right) * \frac{(1-H_D)^C - 1}{(1-0.45)^C - 1} * \left(\frac{D}{D-1.1}\right)^2\right] * \left(\frac{D}{D-1.1}\right)^2$$

Where $\eta^*_{0.45} = 6 * e^{-0.085D} + 3.2 - 2.44e^{-0.06D^{0.645}}$

and $C = (0.8 + e^{-0.075D}) * \left(-1 + \frac{1}{1+10^{-11}*D^{12}}\right) + \left(-1 + \frac{1}{1+10^{-11}*D^{12}}\right)$

Notably, as vessel diameter approaches a critical lower limit (below 5µm), the single-file nature of RBC flow, and interactions between RBCs and the vessel wall cause dramatic increases in viscosity – the *reverse Fahraeus-Lindqvist effect*. It has been suggested that the discrepancies between the nadir of the Fahraeus and Fahraeus-Lindqvist curves can be explained by cell-cell interactions in flowing blood [246].

Taken together, these equations allow application of Poiseuille's law to the microcirculation, such that the flow of blood (Q) through a cylindrical tube is determined by the pressure gradient across the tube (ΔP), as well as length (l), diameter (D), and viscosity (η):

$$Q = \left(\frac{\pi}{128} * \frac{D^4}{l} * \frac{1}{\eta}\right) * \Delta P$$

The assumptions that microvessels are perfect cylinders is an over-simplification, but can nevertheless be viewed as a reasonable approximation for the purposes of flow modeling.

One of the important consequences of Poiseuille's law is that small variations in vessel diameter have dramatic effects on resistance and blood flow.

The consequences of dual-phase blood flow also have implications to the partition of blood at microvascular bifurcations. Because RBC flow migrates towards the center of the blood vessel, the edges of a vessel become relatively RBC-deplete (cell-free layer). Consequently, at bifurcations, when the fraction of blood flow into a daughter vessel is low, this blood is mainly drawn from this outer layer of the vessel; the resultant "plasma skimming" or "phase separation" at bifurcations will cause an even lower proportion of RBC flow in the daughter vessel than would be expected from the proportion of blood flow. In fact, a lower limit of blood flow into a daughter vessel is identified under which no RBC flow will occur, and it will be only plasma flow [217]. Conversely, it can be stated that daughter vessels with higher proportion of blood flow will receive an exaggerated proportion of RBC flow.

These observations were made mathematically by Levin [150], and empirically by Klitzman [137] and Schmid-Schönbein [242], with parametric formulae for a sigmoidal relationship established by Pries [215]. Important determinants of this relationship are the discharge hematocrit of the parent vessel, as well as the diameters of the parent and both daughter vessels. Fraser and colleagues [82] showed that this relationship holds true even in capillaries where RBCs travel in single-file, and therefore have a binary choice for direction to each daughter vessel. Representation of this phenomenon is shown in Figure 1.2:
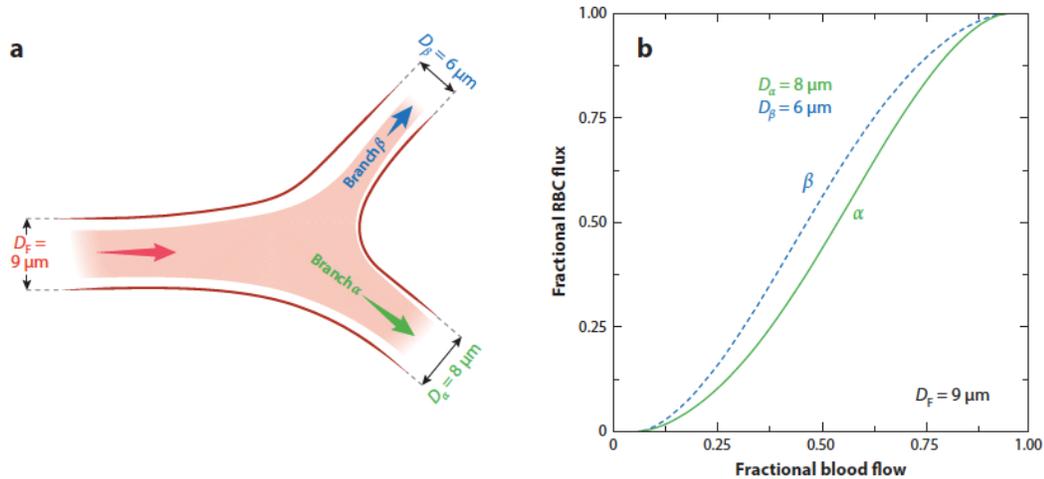
Figure 1.2: Effect of phase-separation at microvascular bifurcations. Daughter vessels with low blood flow will receive a disproportionately lower amount of RBC flow, also known as "plasma skimming." This is shown schematically (a) as well as mathematically (b). Note the lower limit of blood flow (x-intercept) under which no RBC flow occurs. Reproduced from Secomb [246]

These biophysical principles for individual microvessels have important implications for the distribution of RBC and blood flow throughout large composite microvascular networks. Consider firstly that network topology is markedly heterogeneous, with variations in vessel lengths and diameters throughout the vascular tree, even for vessels of the same order [212]; consequently, vessel segment resistance and hemodynamics will have a corresponding degree of heterogeneity [213]. With progressive bifurcations down the arteriolar network and successive increase in cross-sectional area, this asymmetric distribution of blood flow at bifurcations will synergized with the vessel Fahraeus effect to cause marked reductions in overall hematocrit – denoted as the *network Fahraeus effect* [216]. This phenomenon is most pronounced in capillaries, where mean hematocrit is lowest compared to the systemic circulation, and hematocrit values

demonstrate the widest heterogeneity between capillary segments [117]. Dilation of daughter arterioles reduces the plasma-skimming at bifurcations, and draws more RBC flow from the centre flow path of the parent vessel; invariably these centre RBCs have higher RBC oxygenation than those at the vessel wall. This results in decreased hematocrit heterogeneity and increased RBC oxygen saturation within the downstream network [68]. Whole-brain simulations of capillary blood flow suggest that the pathway effect caused by shorter distances for superficial capillary networks produces a depth-dependent hematocrit gradient within the brain [102], which also results in more uniform oxygen delivery in deeper layers of cortex [152]. Additionally, RBC dynamics have been proposed by Schmid and colleagues [244] as a mechanism that smooths outflow velocities from brain capillary networks, which itself has advantages for maintaining stable perfusion and oxygen delivery.

Time-dependent computational models and experiments have contributed further to our understanding of how RBC rheology interacts with network topology to affect RBC distribution. Fung predicted that the phase separation at microvascular bifurcations was self-regulating, insofar as the preferential distribution of RBCs to one daughter branch would eventually be counteracted by the hematocrit-dependent increase in vessel resistance [83]. Recently, Baloch and Bagchi demonstrated with discrete cell simulations of RBC flow in reconstructed microvascular networks that temporal heterogeneity in RBC distribution is even more pronounced than spatial heterogeneity [13]. Furthermore, the biophysics of RBC rheology within simulated microvascular networks can generate spontaneous oscillations and non-linear temporal patterns leading to unsteady-state blood flow characteristics [46, 79, 87].

Finally, it should be noted that most computational modeling has been designed using either simple diverging branches of the arteriolar tree, or repeating geometries of capillary networks (e.g. honeycomb). Rarely, if ever, has the interaction between these two systems been systematically investigated together; given the implications for microvascular control and communication between capillaries and arterioles, these relationships require further evaluation and analysis.

Taken together it becomes clear that (i) microvascular blood flow is not governed by the same principles as blood flow within large vessels, (ii) the biophysical properties of blood flow within individual microvessels contribute to functional heterogeneity on the network level, and (iii) network structure supports the functional requirements of microvascular networks for maintaining adequate oxygen delivery.

1.4 Pathogenesis of microvascular dysfunction in sepsis and critical illness

The microcirculation is increasingly recognized as a central factor in the pathogenesis of critical illness [9, 10, 182, 194]. This has been described most extensively in the context of sepsis, but also for other common ICU diseases including trauma, cardiac arrest, and following major surgery. Because of the diffuse systemic inflammatory response that characterizes the early host response of sepsis, microvascular dysfunction is ubiquitous, and is considered a cardinal feature of the disease [67, 119].

Sepsis is defined as the dysregulated host response to infection that causes life-threatening organ dysfunction [252]. Sepsis is responsible every year for a staggering 20% (one fifth !!) of all worldwide deaths [233], disproportionately affecting low- and middle-income countries in Africa and Asia. Although survivorship has been steadily improving over the past 30 years, sepsis is still a deadly disease, with mortality estimates of approximately 30%-35% [44, 146, 174, 236]. Sepsis accounts for over half of all hospital-related deaths [160] and is the most common cause of admission to the intensive care unit. When presenting with hypotension and organ failure, sepsis is defined as 'septic shock,' and confers additional mortality risk [165, 277]. In the United States, sepsis is the most costly in-hospital disease [268], with annual health care expenditures estimated upwards of $20B [112, 196]. Patients that survive sepsis suffer from long-term sequelae including weakness, cognitive dysfunction, increased cardiovascular risk, reduced quality of life, reduced productivity, and increased utilization of health care resources [209, 210]. Recognizing this global health priority, the World Health Organization adopted a

resolution in 2017 to improve the prevention, diagnosis, and clinical management of sepsis [224].

Microvascular dysfunction in sepsis begins with activation of the endothelium, and change to a pro-inflammatory phenotype for endothelial cells (ECs) [122, 126]. Pathogens, bacterial toxins, and bacterial degradation products directly activate endothelial cell-surface receptors that recognize pathogen-associated molecular patterns (PAMPs), as well as circulating damage-associated molecular patterns (DAMPs) released from injured human cells [202, 223]. The classic example of this would be activation of endothelial cells via the toll-like receptor 4 (TLR4) with lipopolysaccharide (LPS, endotoxin), a component of the cell surface of gram-negative bacteria. This EC pro-inflammatory phenotype results in shedding of the endothelial glycocalyx [272], disrupted endothelial barrier function and increased vascular permeability [116, 192]. Activated ECs also have pro-coagulopathic and anti-fibrinolytic phenotype, causing adhesion of fibrin, complement factors, and platelets together, eventually leading to widespread microthrombosis and disseminated intravascular coagulation [23, 36, 249, 259, 260]. Because the microcirculation interacts with every organ in the body, these effects will compound with impaired cellular function [29], and contribute to multi-system organ failure.

Leukocyte response to pathogen invasion will synergize with direct endothelial activation to potentiate the vicious cycle of inflammation and microvascular dysfunction in sepsis. Macrophages and neutrophils will secrete inflammatory cytokines in response to infection – e.g. tumor necrosis factor alpha (TNF-α) interleukin 6 (IL-6) – that act on ECs in a similar manner to EC-pathogen interaction [280]. These cytokines promote upregulation of cell-surface adhesion molecules and cause rolling, adhesion, and activation

of circulating neutrophils [154]. Activated neutrophils produce free-radicals to kill bacteria, but also cause off-target damage to surrounding tissue [33]. Simultaneously, they secrete neutrophil extra-cellular traps (NETs) which consist of cell-free DNA and anti-microbial enzymes to combat pathogens; these NETs are easily incorporated into fibrin microthrombi and exacerbate the microvascular coagulopathy of sepsis [51]. Finally, as activated neutrophils transmigrate across the vascular endothelium, they secrete proteases that further disrupt cell junctions, EC barrier function, and cause further tissue damage [192].

From a hemodynamic perspective, endothelial activation causes vasodilation through upregulation by ECs of inducible nitric oxide synthase (iNOS) acting on arteriolar smooth muscle and contributes to the observed hypotension in sepsis [18]. This increase in nitric oxide production occurs heterogeneously throughout the microcirculation contributing to inappropriate shunting of blood flow through microvascular networks [178]. Moreover, arterioles demonstrate decreased adrenergic sensitivity and hypo-responsiveness to catecholamines that exacerbates sepsis-induced hypotension [27, 135]. Sepsis-associated cardiomyopathy is a well-recognized feature of hemodynamic impairment in septic shock, and is mediated through TLR4-induced cardiomyocyte dysfunction, mitochondrial dysfunction, and alterations to the coronary microcirculation [78, 98, 258]

At the level of the capillary network, sepsis causes microvascular alterations that impair oxygen transport. Reduced RBC velocity, RBC supply rate, and RBC oxygen saturation are routinely observed [16, 66], signifying impaired convective transport of oxygen. Stopped-flow capillaries are considered a hallmark feature of sepsis, first

described by Lam and colleagues [143] and corroborated in subsequent experimental studies [16, 66, 198]; consequently, diffusion capacity of capillary networks is reduced. Breakdown of inter-cellular gap junctions impairs conducted signalling from capillaries to upstream arterioles [153], which limits communication and blood flow regulation throughout the microvascular network. Furthermore, sepsis reduces the ability for RBCs to release ATP and to signal appropriately in the setting of RBC hypoxia [17], and decreases RBC deformability which contributes to RBC maldistribution in capillary networks [19]. Using computational modeling, Goldman demonstrated how flow heterogeneity in sepsis (particularly increased stopped-flow capillaries) accounts for much of the pathological supply dependency that is encountered with this disease [91, 92]. Finally, increased cellular metabolic rate and impaired mitochondrial oxygen utilization provide additional stresses to the system [29], such that energy requirements are many times above resting levels, and cells are unable to utilize oxygen efficiently even if oxygen demand was met by increased supply. Overall, microvascular and cellular factors synergize together to produce multiple defects in the oxygen pathway that contribute to organ failure and death.

Despite the recognition that microvascular dysfunction plays a pivotal role in the pathogenesis of sepsis specifically, and critical illness in general, evaluation of circulatory shock (as the cardiovascular manifestation of critical illness) rarely incorporates microvascular assessment outside of experimental studies. In the following section, we discuss various techniques that have been utilized to monitor circulatory shock, and the ongoing knowledge gaps that can be addressed with future research.

1.5 Circulatory shock - overview

Patients suffering from diseases in the ICU frequently require support for organ failure, including mechanical ventilation (lungs) or hemodialysis (kidneys). Circulatory shock represents failure of the cardiovascular system (heart and blood vessels), and has been reported with an overall prevalence of 33% in the ICU setting [237]. Inadequate end-organ perfusion is an essential condition for the diagnosis of shock [32, 275], and is related to insufficient oxygen delivery and distribution by the circulation, as well as dysfunctional oxygen extraction and metabolism at the cellular level. Arterial hypotension – systolic blood pressure less than 90 mmHg or mean arterial pressure less than 70 mmHg – is commonly present, but not always required for shock to occur; hypotension can be masked by sympathetic activation in young patients and by pre-existing hypertension in older adults [32, 275].

Shock can be classified into four main categories based on the pathophysiology of circulatory failure [278]: (1) hypovolemic (hemorrhage, fluid loss), (2) cardiogenic (myocardial infarction, aortic insufficiency) (3) obstructive (pulmonary embolism, cardiac tamponade), and (4) distributive (sepsis, anaphylaxis). The first three mechanisms represent decreased cardiac output and inadequate oxygen delivery (i.e. 'low-flow states'), whereas distributive shock is associated with low systemic vascular resistance, and normal or supranormal cardiac output. In a large trial of more than 1600 ICU patients with undifferentiated shock [5], sepsis was by far the most common etiology (62%) followed next by cardiac (16%) and hypovolemia (16%), and rarely obstructive shock (2%). These categories are not considered mutually exclusive, and one disease often causes shock

through multiple mechanisms (e.g. vasoplegia and cardiac dysfunction with sepsis, low flow and reperfusion injury after cardiac arrest).

Treatment of shock in the ICU is aimed at reversing the underlying cause of the condition and providing hemodynamic support for the failing circulatory system [275]. Broadly, hemodynamic support consists of three classes of medications: (1) intravenous fluids - comprising either crystalloid (normal saline, ringer's lactate) or colloids (albumin, blood products) - to restore effective circulating volume, preload, and cardiac output (2) vasopressors (or 'pressors') to increase blood pressure via vasoconstriction, augmenting systemic vascular resistance and perfusion pressure to vital organs, and venoconstriction to augment venous return, and (3) inotropes that increase cardiac contractility and heart rate, with the overall goal to increase cardiac output, blood flow, and oxygen delivery. The rapid diagnosis of shock is essential in order to initiate resuscitation, restore circulatory function, and prevent the sequelae from organ failure. As this diagnosis of shock is being made, clinicians must decide from a variety of potential treatments and interventions, and monitor for signs of response to therapy. These goals require the continuous synthesis of clinical, biochemical, and hemodynamic information at the bedside.

1.6 Systemic hemodynamic monitors

Hemodynamic monitoring for circulatory shock in the ICU has traditionally focused on macrovascular measurements, most notably continuous heart rate and arterial blood pressure monitoring that comprise the basic standard of care for most ICUs worldwide. Non-invasive measures of cardiac output can be derived from arterial pressure waveform analysis [191, 265], but have not been shown to directly improve outcomes when

used in clinical settings [264]. Measurements of cardiac preload such as central venous pressure (CVP) have ultimately been shown as poor markers of fluid responsiveness [170, 181]. Most recently, bedside echocardiography has emerged as a versatile non-invasive tool that is easily available to clinicians for monitoring the cardiac function in the ICU [274]. It should be noted, however, that echocardiography has not yet been shown to improve outcomes for patients with shock when incorporated into a resuscitation protocol [253].

One of the main limitations of conventional hemodynamic monitors is the assumption that systemic hemodynamics are an appropriate surrogate for end-organ perfusion. In a landmark trial of resuscitation for sepsis, Rivers and colleagues [228] established early goal-directed therapy (EGDT) within 6 hours in the emergency department using a treatment protocol incorporating MAP, CVP, and central venous oxygen saturation (ScvO2). In this randomized controlled trial (263 patients, one hospital, one country), EGDT demonstrated significant survival benefit for patients with septic shock over usual care, and became ubiquitously adopted throughout the world [50]. Remarkably, three large randomized controlled trials later retested this same EGDT protocol (3723 patients, 138 hospitals, seven countries), and showed no benefit for survival compared with standard therapy [232]. These results can be explained in part as an evolution of standards of care for sepsis resuscitation over the ensuing decades, that build on many of the philosophies that were pioneered by Rivers; the other explanation is that macrovascular targets are insufficient to guide resuscitation. Currently, only MAP remains as a macrovascular target within the Surviving Sepsis Guidelines [226], and proposals for

personalized MAP targets have been further suggested based on age or pre-existing hypertension [131, 148].

Invasive measurements of cardiac output derived from the pulmonary-artery catheter were used routinely in the 1990s, but have largely been abandoned after failing to demonstrate benefit in randomized trials [103, 227], and potentially even harm for some ICU patients [37]. These catheters were used not only used for measuring cardiac output, but also for calculating total body oxygen consumption using the Fick equation:

$$\dot{V}O_2 = \dot{Q} * (C_aO_2 - C_vO_2)$$

Whereby $\dot{V}O_2$ is the total body oxygen consumption, $\dot{Q}$ is the cardiac output, and C_aO_2 and C_vO_2 are the oxygen content in arterial and venous blood, respectively. The oxygen content of blood is determined by hemoglobin content, hemoglobin saturation, and partial pressure of oxygen. Global oxygen delivery was previously considered a therapeutic target for resuscitation in circulatory shock, but this approach has not been supported with empirical evidence. Ronco and colleagues did not find a change to oxygen consumption, despite augmenting global oxygen delivery with transfusion or inotropes [230, 231], and found that patients with critical illness do not experience global oxygen supply dependency [229]. Moreover, randomized controlled trials targeting supranormal oxygen delivery did not show any benefit [86, 105]. Thus, we conclude that while defects in the oxygen pathway are clearly identified in critical illness, they cannot be corrected with manipulation of systemic oxygen delivery parameters.

Because of these deficiencies with systemic hemodynamic monitoring and systemic oxygen delivery and consumption, new tools have been developed to evaluate oxygen delivery within the microcirculation at the bedside. The two modalities that have been most commonly applied in clinical resuscitation research are handheld vital microscopy of the sublingual microcirculation, and near-infrared spectroscopy (NIRS) of skeletal muscle. The main take-home points from this body of literature indicate that (i) microvascular parameters are strong predictors of adverse ICU outcomes, (ii) microvascular dysfunction can persist despite normalization of systemic hemodynamics, and (iii) microvascular response to conventional therapy is highly heterogeneous.

1.7 Microvascular monitors – Sublingual handheld vital microscopy

Handheld vital microscopy (HVM) is an optical technology that utilizes side-stream dark field illumination with LED lights in a ring surrounding the sublingual tissue [89]; more recently, incident dark field illumination is an updated version of the technology [4]. Both systems allow for direct visualization of the microcirculation, predominantly focused on microvessels with sizes up to 20μm. HVM detects RBC flow, and provides quantitative and semi-quantitative analysis of convective and diffusive indices of oxygen transport [121], including the proportion of perfused vessels (PPV), perfused capillary density, and microvascular flow index (MFI); MFI is a quadrant-based score that identifies stopped, intermitted, sluggish, and fully-perfused vessels. Heterogeneity index is a functional marker of RBC distribution within the microcirculation that reflects maldistribution from both stopped flow and over-perfusion from microvascular shunting [257]. Recently, HVM

has been able to measure RBC velocity using space-time images [54], similar to the intravital microscopy techniques developed by Ellis for preclinical models [64]. Hilty and Ince have also attempted to quantify the volume flow fraction of RBCs within an HVM field of view, which they denote as tissue RBC perfusion [113]. Image analysis has often been a time-consuming task that prevented application of HVM in real-time, however automated video analysis has recently been developed to streamline this process [30, 114]. Technical limitations of HVM should be acknowledged. Recorded videos are only captured for short periods, typically ranging from 5-30 seconds, and are sensitive to artifacts from saliva, uneven illumination, and from over-pressure or under-pressure of the vascular bed with the probe. See technical review by Massey and Shapiro for comprehensive details [171].

Nevertheless, within the scope of these technical limitations, HVM analysis has revealed substantial insight into the impact of microvascular dysfunction in critical illness. De Backer and colleagues were among the first to identify loss of microvascular perfusion in septic patients using sublingual HVM [7], and further showed that PPV, but not cardiac output or MAP, was an independent predictor of ICU mortality using multivariate analysis [8]. HVM-derived indices of perfusion were also noted by Hernandez to correlate with mortality, organ failure, lactate, and vasopressor requirements but not systemic hemodynamics [107]. Sakr demonstrated that PPV was lower in non-survivors vs survivors of sepsis, and that these alterations persisted for the duration of ICU stay despite resolution of circulatory shock [235]; similar persistence of microvascular dysfunction was noted by Trzeciak during resustiation of non-survivors even though blood pressure and central venous oxygenation were normalized [269]. Edul and colleagues showed that RBC

velocity was reduced in patients with sepsis, and similar flow reductions were observed regardless of normal or depressed cardiac output [130].

Sublingual HVM has been directly compared with intestinal microvascular flow, which was only possible in selected studies of surgical patients with colostomy or ileostomy access. Boerma and colleagues found that these two vascular beds did not correlate in terms of MFI on the first day of admission to ICU with abdominal sepsis, but that most of them all normalized to the same values by the third day [24]. Edul et. al. compared sublingual and intestinal microvascular perfused vessel density at baseline and after administration of a fluid bolus, and found no correlation either before or with the change in both vascular territories [62]; in this series changes in sublingual, but not intestinal microcirculation, tracked with changes in systemic hemodynamics. This would suggest that while sublingual HVM is clearly correlated with ICU outcomes, it may not serve as a surrogate for mesenteric perfusion throughout the alimentary tract. Another unanswered question is whether the sublingual microcirculation, dominated by connective tissue and venous plexus, and subjected to a wide variety of environmental temperatures and oxygen contents, is an appropriate vascular bed with similar capacity for dynamic flow regulation compared with the brain or skeletal muscle.

Ince describes the concept of 'hemodynamic coherence' to denote the appropriate response between macrovascular therapy and the microcirculation under normal conditions, and the breakdown of these relationships in critical illness [120]. The loss of hemodynamic coherence may partly explain why macrovascular resuscitation targets have proved deficient, as described above. De Backer found that administration of the inotrope

dobutamine was successful in augmenting PPV, but these changes were independent from changes in MAP or cardiac output [6]. Pranskunas and colleagues showed that patients with low baseline MFI responded better following fluid administration with improvements to organ failure, whereas patients with normal MFI at baseline did not derive significant benefit from fluid bolus, despite both groups having a similar change in systemic hemodynamics [208]. Dubin and colleagues showed that low baseline capillary density was predictive of a positive microvascular response to augmented blood pressure with norepinephrine, whereas patients with normal capillary density at baseline saw a reduction in microvascular perfusion with the same intervention [57]. Similarly, low baseline microvascular metrics appear to be a potential tool for selecting patients with favorable response to RBC transfusion regardless of systemic hemoglobin levels [234, 241]. These studies illustrate some of the deficiencies with relying exclusively on systemic hemodynamics, and demonstrate the added value of microvascular monitoring in the management of patients with circulatory failure.

1.8 Microvascular monitors – Near-infrared spectroscopy

First described by Jöbsis in 1977 [125], near-infrared spectroscopy (NIRS) is a common modality that has been used to evaluate the human microcirculation. This technique leverages the optical properties of biological tissue, including good penetration of near-infrared light (650-900nm) through skin, subcutaneous tissue, muscle and skull [12, 75]. NIRS has the advantage of being continuous and non-invasive, and is considered an indirect modality for microvascular monitoring, insofar as images of the tissue are not acquired for visualization. Rather, light is trans-illuminated through the tissue, the intensity

is recovered by one or multiple fibre optic receivers, and photons are counted on a spectrophotometer with a high temporal resolution (>10Hz). By applying the physical principles of biomedical optics, information can be derived from the underlying microcirculation and the micro-environment [245]. The main organs that are interrogated with NIRS are brain and skeletal muscle [15, 77, 144], although NIRS has also been used with internal organs such as adult bladder [261], and pediatric kidneys [21, 34], abdominal/mesentery [34, 132, 197], and liver [279].

Chromophores are substances that absorb light, and their absorption properties will vary between chromophores and as a function of wavelength in the NIRS spectrum [12]. Oxyhemoglobin (Hb-O2), deoxyhemoglobin (Hb) and water are the dominant chromophores in human tissue that display biological variability, i.e. dynamically change over time; importantly, Hb-O2 and Hb have different optical absorption in the NIRS spectrum, which allows them to be discriminated using at least two wavelengths. Given that hemoglobin is contained exclusively within red blood cells (RBC), NIRS can primarily be viewed as a physiological evaluation of RBC distribution and oxygen transport in microvascular networks [73]. Although, the separation of two distinct hemoglobin chromophores is optically and computationally valid, this does not relate physiologically to how oxygen is transported in the microcirculation. Hemoglobin will never exist in exclusively oxy- or deoxy- states, and RBC oxygen saturation is the aggregate of millions of hemoglobin proteins (each with four O_2 binding sites); in this regard, we can better characterize hemoglobin as having O_2 saturation-dependent optical absorption properties that exist on a continuum between 0% and 100% [124]. Furthermore, chromophores such as melanin, bilirubin, lipids, and water contribute to overall tissue absorbance, but do not

change during the NIRS recording. NIRS interrogation of skeletal muscle has the important addition of myoglobin (Mb) - an intracellular iron-containing protein that binds oxygen in myocytes - that contributes significantly (60-90%) to overall NIRS signal [15, 48, 168]. Hemoglobin and myoglobin have almost identical absorption spectra, and separating them with NIRS is difficult. While the content of myoglobin does not change over time, the oxygenation status of the myoglobin chromophore will change based on skeletal muscle oxygen metabolism (e.g. during exercise) [48]. Hemoglobin, by contrast, will vary in both oxygen status and content and reflects microvascular transport of oxygen and utilization in surrounding tissue.

Continuous-wave NIRS simply measures the intensity of light that interacts with biological medium and is received by a light detector [245]; this modality is simple, inexpensive, and can be recorded at a high sampling rate, but cannot differentiate between light that is absorbed or scattered. Because scattering is unknown, quantification of absolute chromophore concentration with NIRS cannot be calculated, representing one of the classic limitations of traditional continuous-wave NIRS [173]. However, if we assume that scattering does not change significantly over the duration of measurement (i.e. that changes in scattering are minimal compared to changes in absorption), continuous-wave NIRS can measure the change from baseline in chromophore concentration, measured in arbitrary units [245].

The NIRS signal is derived from blood contained in arterioles, capillaries, and venules of less than 1mm diameter [15, 128, 185]. The most common metrics reported with NIRS are total hemoglobin (HbT) denoted as the sum of both hemoglobin chromophores

(Hb-O2 + Hb), and tissue oxygen saturation (StO2) defined as the ratio (Hb-O2/HbT). Changes in HbT reflect dynamic changes in blood volume, microvascular hematocrit, and blood flow velocity [15, 73]. StO2 is considered a measure of regional venous oxygen saturation because the majority of blood in the microcirculation resides in the venular system [77]. The isosbestic wavelength of hemoglobin defines the wavelength where the extinction coefficients for HbO2 and Hb chromophores are equal; in the near-infrared spectrum, this occurs approximately at 798nm. Changes in absorption at the isosbestic wavelength are sensitive to changes to HbT concentration, independent of oxygen saturation [12].

Although outside the scope of this thesis, the application of NIRS for monitoring the cerebral microcirculation is extensive, particularly for neonates [85], cardiac surgery patients [35], cardiac arrest [248], and for assessing cerebral autoregulation in critical care [147, 283]. Skeletal muscle/somatic tissue has the advantage of being easily accessible for physiological interrogation, and has therefore been another focus for NIRS researchers studying microvascular oxygen delivery and metabolism [15]. The typical source detector distance of 3-4cm for somatic NIRS will give a depth of tissue penetration of approximately 1.5cm [76]. The most common muscle groups that are measured are the quadriceps (vastus lateralis, rectus femoris), forearm (flexor digitorum profundus), and thenar eminence (abductor policis brevis), but other superficial muscle groups such as gastrocnemius, deltoid, and intercostals have also been evaluated [76]. Adipose and soft tissue thickness will impact NIRS measurements from skeletal muscle – particularly quantification of StO2 and absolute chromophore concentration - and should be considered when undertaking an experimental protocol [43].

The primary metric evaluated with somatic NIRS is StO2, representing a regional assessment of the balance between oxygen supply (blood flow and oxygen content) and tissue oxidative metabolism (uptake and consumption). Notably, StO2 values are spatially heterogeneous, even within the same muscle [138, 179, 281]. Somatic/peripheral NIRS also allows for dynamic vascular occlusion tests (VOT) to derive additional information about regional blood flow and oxygen kinetics [15, 95, 128]. The VOT can be performed with occlusion of the limb using a blood pressure cuff, and by measuring NIRS signal on the distal section of the upper or lower extremity. Venous occlusion occurs when the cuff is inflated above diastolic blood pressure but below systolic blood pressure (~60-80 mmHg), and blood can enter the limb but outflow is severely restricted; changes to blood volume then result from a new flow equilibrium and/or accommodation by the capacitance venous system. The rate of HbT and Hb increase during the initial linear phase of the occlusion is a measurement of local microvascular blood flow and oxygen consumption, respectively [31, 166]. During arterial occlusion, the cuff is inflated above systolic blood pressure (~130-150 mmHg) creating a closed system where there is no blood flow and constant blood volume. Under these conditions, the rate of decrease in Hb-O2 and/or StO2 is used to quantify local muscle oxygen consumption. When the cuff is released, the reperfusion slope can also be quantified, including the post-occlusive reactive hyperemia (PORH) where an overshoot for StO2 occurs above baseline; these metrics are proposed as a measure of microvascular reactivity.

Evaluation of skeletal muscle oxygenation with somatic NIRS has been applied in many clinical conditions. Exercise physiology is an obvious field that benefits from regional assessment of oxygen metabolism, and many protocols for continuous,

intermittent, isometric, concentric, maximal, and sub-maximal exercise have been proposed [95]. Oxygen extraction fraction and oxygen consumption can be determined with StO2 and Hb measurements during the onset of exercise, and the rate of reoxygenation in the immediate post-recovery phase is used as a surrogate for determining muscle oxidative capacity [95, 140]. Koga and colleagues utilized time-resolved spectroscopy to differentiate superficial from deep muscle layers in the lower extremity, and showed that muscle oxygenation kinetics were markedly different between muscle layers at the onset and termination of exercise, likely reflecting differences in fibre type and muscle recruitment profiles [139]. All these parameters are intimately related to microvascular blood flow and diffusion capacity of capillary networks, and are affected by endurance training [25, 96, 184] and medical conditions such as congestive heart failure [100, 133, 190], diabetes [20], and peripheral arterial disease [167, 273].

In the ICU, somatic NIRS has been investigated for providing quantitative and reproducible measurements of the peripheral microcirculation, including skin, soft tissue, and underlying skeletal muscle [175, 183]. For patients with sepsis, numerous studies have demonstrated that persistently low StO2 and/or blunted response during VOT are prognostic markers for poor ICU outcomes [189, 255]. Leone and colleagues, as well as Lima and colleagues both found that low StO2 was a poor prognostic marker in sepsis despite all patients achieving adequate systemic resuscitation targets with EGDT [149, 156]. Interestingly, incorporation of StO2-guided therapy into a treatment protocol did not show benefit over routine care [188]; this may signify an important distinction for the application of this technology (prognostic vs therapeutic monitoring) or the limitations of StO2 as a metric of microvascular perfusion. In addition to sepsis, the correlation of NIRS

metrics with ICU outcomes has also been evaluated in the general ICU population [56], trauma patients [40, 55, 61, 225], and patients with cardiogenic shock [193].

Overall, NIRS provides an evaluation of microvascular oxygen delivery, and local oxygen metabolism that can be applied to human skeletal muscle in numerous clinical settings. While there have been many advances in the field, lack of consistency in experimental protocols and terminology between research groups has made comparing results between studies challenging. In addition to serving as a reliable prognostic and diagnostic marker of disease, future research should determine how to incorporate NIRS into the management of ICU patients to guide therapy and interventions.

1.9 Biochemical and perfusion monitoring in critical care

Elevated serum lactate is a biochemical marker that is associated with increasing severity of shock and poor outcomes [180], and reflects a shift in cellular energy production and utilization towards glycolysis and away from oxidative phosphorylation [14]; this shift is mediated in part through cellular beta-adrenergic signalling and through intracellular inflammation pathways. Lactate can be directed as an alternative fuel source from the cytosol into mitochondria, and used as a high-energy metabolite that is shuttled from skeletal muscle to supply vital organs (e.g. heart, brain) in a biochemical pathway known as the Cori cycle [84]. In sepsis, elevated serum lactate has been shown as an independent predictor of mortality [177, 266], and a prognosticator for clinical deterioration in the emergency department [222, 250]. The inability to clear lactate over the first 24 hours of ICU admission is also a strong predictor of death [172], and lactate appears to be a stronger predictor of poor outcomes for ICU patients with sepsis than arterial hypotension [94]. This

is also supported by the concept of "cryptic shock" in which hyperlactemia in the presence of normal arterial pressure has a very high mortality [118, 221].

Lactate-based protocols are another framework for guiding resuscitation in patients with sepsis. First introduced by Jones and colleagues [127], 10% reduction in serum lactate levels in the first 6 hrs was shown as equivalent to conventional EGDT therapy. Jansen and colleagues [123] showed that an even more aggressive lactate-guided protocol of 20% reduction every 2 hours may improve outcomes for ICU patients in the initial phase of resuscitation; interestingly, the survival benefit observed by Jansen occurred despite no differences in serum lactate kinetics between the groups, which may suggest that the treatment was effective irrespective of the changes in lactate concentration. Frequent measurements of serum lactate have subsequently been incorporated into international guidelines for the management of septic shock [226]. Although lactate production has traditionally been attributed as a surrogate for anaerobic glycolysis and cellular oxygen deficit (and thus poor perfusion that is amenable to resuscitation), there is evidence to suggest that cells will produce lactate as a stress response through aerobic glycolysis even in the presence of adequate oxygen delivery [84, 262]. This may suggest that although lactate is a strong prognosticator for poor outcomes, it cannot be considered an appropriate therapeutic target [106, 169].

Clinical signs of hypoperfusion are evident through physiological 'windows' that provide direct insight into organ function [276] – altered mental status (brain), decreased urine output (kidney), and mottled periphery (skin). The skin is most accessible organ in the body, and palpation of the peripheral extremities is an essential component of the

physical exam for patients in the ICU [176]. However, in order to be considered an appropriate monitor for circulatory shock, it is necessary to quantify the degree of hypo-perfusion with objective metrics. Many different standardized assessments have been proposed, including a mottling score of the lower extremity, capillary refill time (CRT), central-to-toe and toe-to-room temperature gradients [88, 101, 104, 155]. Although these measurements may appear crude, bedside markers of peripheral perfusion correlate strongly with ICU outcomes [1, 2, 59, 129, 145] and highlight the value of this clinical assessment.

Ironically, the simplest forms of clinical perfusion monitoring have only recently been considered as true resuscitation markers for critical illness that may enhance, or even replace, systemic hemodynamics [60, 99]. Ait-Oufella and colleagues [1, 2] examined patients with sepsis at 6 hours after initial resuscitation, and found that abnormal CRT or mottling score was predictive of ICU mortality whereas cardiac index and MAP were not; there was also no correlation between CRT and cardiac index. Similarly, Lima and colleagues [157] evaluated CRT at 24 hours after ICU admission, and found no differences in systemic hemodynamics between patients with normal or abnormal perfusion status. Coudroy et. al [42] showed that the value of skin mottling for predicting mortality in a large ICU cohort (791 patients) regardless of other organ failure, and Dumas [59] showed the prognostic value of mottling scores was independent of systemic hemodynamics and dose of vasopressors. CRT has also shown to relate to indices of visceral organ perfusion measured by doppler ultrasonography [26]. Moreover, the kinetics of peripheral perfusion are favorable for real-time hemodynamic monitoring. Lara and colleagues [145] found that normalization of CRT after fluid administration in the emergency department substantially

reduced mortality risk compared to patients with persistently abnormal CRT. These changes in CRT can precede lactate clearance within the first 6 hours of resuscitation [108, 110], and are much faster than resolution of either sublingual or NIRS-derived metrics [111].

Moving beyond the EGDT pioneered by Rivers, these physiological concepts have culminated in a recent randomized controlled trial (424 patients, 28 hospitals, 5 countries) comparing perfusion-guided resuscitation with lactate-guided resuscitation strategies [109]. In this study, patients received fluids and vasoactive medications in a step-wise adaptive protocol with triggers for escalating care based on perfusion status or persistently elevated serum lactate. The patients randomized to perfusion status demonstrated a trend to reduced 28-day mortality (p=0.06), and significantly reduced secondary outcomes of organ failure at 72 hrs (p=0.045). These findings highlight the practical application and value of clinical perfusion monitoring to not only predict poor outcomes, but to prospectively guide therapy.

In summary, circulatory shock continues to pose significant mortality risk to ICU patients and reflects disruption of the complex relationship between macrovascular and microvascular oxygen delivery. Monitoring of systemic hemodynamics provides an incomplete assessment of the cardiovascular derangements that contribute to adverse outcomes. Although many studies have conclusively demonstrated the prognostic value of microvascular monitoring, this body of literature is mainly comprised of single-centre studies, and heterogeneity in terminology and protocols have often limited the ability of researchers to synthesize this data for meaningful interpretation and comparison.

Moreover, it is worth mentioning that any monitor itself will never improve outcomes unless it is tied to a specific and appropriate intervention that follows from the monitoring information. This continues to be the Achilles heel for these modalities, that have often failed to provide direction for clinicians on actionable items and next steps in resuscitation. Part of these setbacks are attributed to the technical challenges surrounding these monitoring modalities, and their dissociation from the physiological phenomenon that they seek to understand. For example, short video sequences of sublingual HVM for less than a minute would rarely capture the extent of perfusion heterogeneity that accompanies microvascular dysfunction; StO2 measurements with NIRS mostly reflect venous oxygen saturation that changes over hours; lactate is routinely generated in ICU patients despite adequate oxygen delivery. In this regard, perfusion monitoring appears to be more amenable to incorporation into clinical practice given its accessibility at the bedside, the temporal association with real-time changes to circulatory physiology, and the common-sense fidelity with established clinical management strategies.

1.10 General Summary

Investigating RBC distribution in capillary networks requires a multi-scale and multi-modal approach, using methods derived from experimental, theoretical, and translational science. Current understanding of the structure and functional heterogeneity of skeletal muscle capillary networks (section 1.2) is limited to isolated capillaries and capillary modules, which does not adequately consider how these capillary networks are organized over larger scales or participate in flow regulation with the broader microcirculation. The biophysical properties of blood flow in the microcirculation (section

1.3) likely have important and unique implications for RBC flow distribution in capillary networks and capillary modules that may point to mechanisms regarding how this flow regulation in capillary networks is achieved. And while dysfunctional microvascular oxygen delivery is a significant contributor to the pathogenesis of circulatory shock in the ICU (sections 1.4, 1.5), our ability to monitor this phenomenon at the bedside (sections 1.6, 1.7, 1.8) is limited by technologies that are not grounded in physiological principles of RBC distribution.

The goal of this thesis is to provide a physiologically-informed and quantifiable framework for characterizing RBC distribution in capillary networks and to strengthen linkages between preclinical and clinical evaluation of microvascular oxygen delivery.

1.11 References

1. **Ait-Oufella H, Bige N, Boelle PY, et al** (2014) Capillary refill time exploration during septic shock. *Intensive Care Med* 40:958–964.

2. **Ait-Oufella H, Lemoinne S, Boelle PY, et al** (2011) Mottling score predicts survival in septic shock. *Intensive Care Med* 37:801–807.

3. **Albrecht KH, Gaehtgens P, Pries A, Heuser M** (1979) The Fahraeus effect in narrow capillaries (i.d. 3.3 to 11.0 μm). *Microvasc Res* 18:33–47.

4. **Aykut G, Veenstra G, Scorcella C, et al** (2015) Cytocam-IDF (incident dark field illumination) imaging for bedside monitoring of the microcirculation. *Intensive Care Med Exp* 3:4.

5. **De Backer D, Biston P, Devriendt J, et al** (2010) Comparison of dopamine and norepinephrine in the treatment of shock. *N Engl J Med* 362:779–89.

6. **De Backer D, Creteur J, Dubois M-JJ, et al** (2006) The effects of dobutamine on microcirculatory alterations in patients with septic shock are independent of its systemic effects*. *Crit Care Med* 34:403–408.

7. **De Backer D, Creteur J, Preiser JC, et al** (2002) Microvascular blood flow is altered in patients with sepsis. *Am J Respir Crit Care Med* 166:98–104.

8. **De Backer D, Donadello K, Sakr Y, et al** (2013) Microcirculatory alterations in patients with severe sepsis: Impact of time of assessment and relationship with outcome. *Crit Care Med* 41:791–799.

9. **De Backer D, Donadello K, Taccone F, et al** (2011) Microcirculatory alterations: potential mechanisms and implications for therapy. *Ann Intensive Care* 1:27.

10. **De Backer D, Orbegozo Cortes D, Donadello K, Vincent J-L** (2014) Pathophysiology of microcirculatory dysfunction and the pathogenesis of septic shock. *Virulence* 5:73–9.

11. **Bagher P, Segal SS** (2011) Regulation of blood flow in the microcirculation: role of conducted vasodilation. *Acta Physiol* 202:271–284.

12. **Bakker A, Smith B, Ainslie P, Smith K** (2012) Near-Infrared Spectroscopy. In: Applied Aspects of Ultrasonography in Humans. InTech, pp 65–88

13. **Balogh P, Bagchi P** (2017) Direct Numerical Simulation of Cellular-Scale Blood Flow in 3D Microvascular Networks. *Biophys J* 113:2815–2826.

14. **Bar-Or D, Carrick M, Tanner A, et al** (2018) Overcoming the Warburg Effect: Is it the key to survival in sepsis? *J Crit Care* 43:197–201.

15. **Barstow TJ** (2019) Understanding near infrared spectroscopy and its application to skeletal muscle research. *J Appl Physiol* 126:1360–1376.

16. **Bateman RM, Sharpe MD, Goldman D, et al** (2008) Inhibiting nitric oxide overproduction during hypotensive sepsis increases local oxygen consumption in rat skeletal muscle. *Crit Care Med* 36:225–231.

17. **Bateman RM, Sharpe MD, Jagger JE, Ellis CG** (2015) Sepsis impairs microvascular autoregulation and delays capillary response within hypoxic capillaries. *Crit Care* 19:1–14.

18. **Bateman RM, Sharpe MD, Ellis CG** (2003) Bench-to-bedside review: microvascular dysfunction in sepsis--hemodynamics, oxygen transport, and nitric oxide. *Crit Care* 7:359–73.

19. **Bateman R, Sharpe M, Singer M, Ellis C** (2017) The Effect of Sepsis on the Erythrocyte. *Int J Mol Sci* 18:1932.

20. **Bauer TA, Reusch JEB, Levi M, Regensteiner JG** (2007) Skeletal Muscle Deoxygenation After the Onset of Moderate Exercise Suggests Slowed Microvascular Blood Flow Kinetics in Type 2 Diabetes. *Diabetes Care* 30:2880–2885.

21. **Beck J, Loron G, Masson C, et al** (2017) Monitoring Cerebral and Renal Oxygenation Status during Neonatal Digestive Surgeries Using Near Infrared Spectroscopy. *Front Pediatr* 5:.

22. **Berg BR, Cohen KD, Sarelius IH** (1997) Direct coupling between blood flow and metabolism at the capillary level in striated muscle. *Am J Physiol Circ Physiol* 272:H2693–H2700.

23. **Bermejo-Martin J, Martín-Fernandez M, López-Mestanza C, et al** (2018) Shared Features of Endothelial Dysfunction between Sepsis and Its Preceding Risk Factors (Aging and Chronic Disease). *J Clin Med* 7:400.

24. **Boerma EC, van der Voort PHJ, Spronk PE, Ince C** (2007) Relationship between sublingual and intestinal microcirculatory perfusion in patients with abdominal sepsis*. *Crit Care Med* 35:1055–1060.

25. **Brizendine JT, Ryan TE, Larson RD, McCully KK** (2013) Skeletal muscle metabolism in endurance athletes with near-infrared spectroscopy. *Med Sci Sports Exerc* 45:869–75.

26. **Brunauer A, Koköfer A, Bataar O, et al** (2016) Changes in peripheral perfusion relate to visceral organ perfusion in early septic shock: A pilot study. *J Crit Care* 35:105–109.

27. **Burgdorff A-M, Bucher M, Schumann J** (2018) Vasoplegia in patients with sepsis and septic shock: pathways and mechanisms. *J Int Med Res* 46:1303–1310.

28. **Burton K, Johnson P** (1972) Reactive hyperemia in individual capillaries of skeletal muscle. *Am J Physiol Content* 223:517–524.

29. **Carré JE, Singer M** (2008) Cellular energetic metabolism in sepsis: The need for a systems approach. *Biochim Biophys Acta - Bioenerg* 1777:763–771.

30. **Carsetti A, Aya HD, Pierantozzi S, et al** (2017) Ability and efficiency of an automatic analysis software to measure microvascular parameters. *J Clin Monit Comput* 31:669–676.

31. **Casavola C, Paunescu LA, Fantini S, Gratton E** (2000) Blood flow and oxygen consumption with near-infrared spectroscopy and venous occlusion: spatial maps and the effect of time and pressure of inflation. *J Biomed Opt* 5:269.

32. **Cecconi M, De Backer D, Antonelli M, et al** (2014) Consensus on circulatory shock and hemodynamic monitoring. Task force of the European Society of Intensive Care Medicine. *Intensive Care Med* 40:1795–1815.

33. **Cepinskas G, Wilson JX** (2008) Inflammatory Response in Microvascular Endothelium in Sepsis: Role of Oxidants. *J Clin Biochem Nutr* 42:175–184.

34. **Chakravarti SB, Mittnacht AJC, Katz JC, et al** (2009) Multisite Near-Infrared Spectroscopy Predicts Elevated Blood Lactate Level in Children After Cardiac Surgery. *J Cardiothorac Vasc Anesth* 23:663–667.

35. **Chan MJ, Chung T, Glassford NJ, Bellomo R** (2017) Near-Infrared Spectroscopy in Adult Cardiac Surgery Patients: A Systematic Review and Meta-Analysis. *J Cardiothorac Vasc Anesth* 31:1155–1165.

36. **Chang JC** (2019) Sepsis and septic shock: endothelial molecular pathogenesis associated with vascular microthrombotic disease. *Thromb J* 17:10.

37. **Chittock DR, Dhingra VK, Ronco JJ, et al** (2004) Severity of illness and risk of death associated with pulmonary artery catheter use. *Crit Care Med* 32:911–5.

38. **Cohen KD, Berg BR, Sarelius IH** (2000) Remote arteriolar dilations in response to muscle contraction under capillaries. *Am J Physiol Circ Physiol* 278:H1916–H1923.

39. **Cohen KD, Sarelius IH** (2002) Muscle contraction under capillaries in hamster muscle induces arteriolar dilatation via K ATP channels and nitric oxide. *J Physiol* 539:547–555.

40. **Cohn SM, Nathens AB, Moore FA, et al** (2007) Tissue oxygen saturation predicts the development of organ dysfunction during traumatic shock resuscitation. *J Trauma - Inj Infect Crit Care* 62:44–54.

41. **Copp SW, Ferreira LF, Herspring KF, et al** (2009) The effects of aging on capillary hemodynamics in contracting rat spinotrapezius muscle. *Microvasc Res* 77:113–9.

42. **Coudroy R, Jamet A, Frat J-P, et al** (2015) Incidence and impact of skin mottling over the knee and its duration on outcome in critically ill patients. *Intensive Care Med* 41:452–9.

43. **Craig JC, Broxterman RM, Wilcox SL, et al** (2017) Effect of adipose tissue thickness, muscle site, and sex on near-infrared spectroscopy derived total-[hemoglobin + myoglobin]. *J Appl Physiol* 123:1571–1578.

44. **Daviaud F, Grimaldi D, Dechartres A, et al** (2015) Timing and causes of death in septic shock. *Ann Intensive Care* 5:16.

45. **Davidson LE, Kelley DE, Heshka S, et al** (2014) Skeletal muscle and organ masses differ in overweight adults with type 2 diabetes. *J Appl Physiol* 117:377–382.

46. **Davis JM, Pozrikidis C** (2014) Self-sustained Oscillations in Blood Flow Through a Honeycomb Capillary Network. *Bull Math Biol* 76:2217–2237.

47. **Davis MJ** (2012) Perspective: physiological role(s) of the vascular myogenic response. *Microcirculation* 19:99–114.

48. **Davis ML, Barstow TJ** (2013) Estimated contribution of hemoglobin and myoglobin to near infrared spectroscopy. *Respir Physiol Neurobiol* 186:180–187.

49. **Delashaw JB, Duling BR** (1988) A study of the functional elements regulating capillary perfusion in striated muscle. *Microvasc Res* 36:162–171.

50. **Dellinger RP, Levy MM, Rhodes A, et al** (2013) Surviving sepsis campaign: international guidelines for management of severe sepsis and septic shock: 2012. *Crit Care Med* 41:580–637.

51. **Denning N-L, Aziz M, Gurien SD, Wang P** (2019) DAMPs and NETs in Sepsis. *Front Immunol* 10:2536.

52. **Dietrich HH** (1989) Effect of locally applied epinephrine and norepinephrine on blood flow and diameter in capillaries of rat mesentery. *Microvasc Res* 38:125–135.

53. **Dietrich HH, Tyml K** (1992) Capillary as a communicating medium in the microvasculature. *Microvasc Res* 43:87–99.

54. **Dobbe JGG, Streekstra GJ, Atasever B, et al** (2008) Measurement of functional microcirculatory geometry and velocity distributions using automated image analysis. *Med Biol Eng Comput* 46:659–670.

55. **Domizi R, Damiani E, Scorcella C, et al** (2019) Association between sublingual microcirculation, tissue perfusion and organ failure in major trauma: A subgroup analysis of a prospective observational study. *PLoS One* 14:e0213085.

56. **Donati A, Damiani E, Domizi R, et al** (2016) Near-infrared spectroscopy for assessing tissue oxygenation and microvascular reactivity in critically ill patients: A prospective observational study. *Crit Care* 20:1–10.

57. **Dubin A, Pozo MO, Casabella CA, et al** (2009) Increasing arterial blood pressure with norepinephrine does not improve microcirculatory blood flow: A prospective study. *Crit Care* 13:1–8.

58. **Duling BR, Damon DH** (1987) An examination of the measurement of flow heterogeneity in striated muscle. *Circ Res* 60:1–13.

59. **Dumas G, Lavillegrand JR, Joffre J, et al** (2019) Mottling score is a strong predictor of 14-day mortality in septic patients whatever vasopressor doses and other tissue perfusion parameters. *Crit Care* 23:1–9.

60. **Dünser MW, Takala J, Brunauer A, Bakker J** (2013) Re-thinking resuscitation: leaving blood pressure cosmetics behind and moving forward to permissive hypotension and a tissue perfusion-based approach. *Crit Care* 17:326.

61. **Duret J, Pottecher J, Bouzat P, et al** (2015) Skeletal muscle oxygenation in severe trauma patients during haemorrhagic shock resuscitation. *Crit Care* 19:1–7.

62. **Edul VSK, Ince C, Navarro N, et al** (2014) Dissociation between sublingual and gut microcirculation in the response to a fluid challenge in postoperative patients with abdominal sepsis. *Ann Intensive Care* 4:1–9.

63. **Ellis CG, Wrigley SM, Groom AC** (1994) Heterogeneity of red blood cell perfusion in capillary networks supplied by a single arteriole in resting skeletal muscle. *Circ Res* 75:357–368.

64. **Ellis CG, Ellsworth ML, Pittman RN, Burgess WL** (1992) Application of image analysis for evaluation of red blood cell dynamics in capillaries. *Microvasc Res* 44:214–25.

65. **Ellis CG, Milkovich S, Goldman D** (2012) What is the efficiency of ATP signaling from erythrocytes to regulate distribution of O(2) supply within the microvasculature? *Microcirculation* 19:440–50.

66. **Ellis CG, Bateman RM, Sharpe MD, et al** (2002) Effect of a maldistribution of microvascular blood flow on capillary O(2) extraction in sepsis. *Am J Physiol Heart Circ Physiol* 282:H156-64.

67. **Ellis CG, Jagger J, Sharpe M** (2005) The microcirculation as a functional system. *Crit Care* 9 Suppl 4:S3-8.

68. **Ellsworth ML, Ellis CG, Goldman D, et al** (2009) Erythrocytes: Oxygen Sensors and Modulators of Vascular Tone. *Physiology* 24:107–116.

69. **Ellsworth ML, Ellis CG, Sprague RS** (2016) Role of erythrocyte-released ATP in the regulation of microvascular oxygen supply in skeletal muscle. *Acta Physiol (Oxf)* 216:265–76.

70. **Ellsworth M, Ellis C, Popel A, Pittman R** (1994) Role of Microvessels in Oxygen Supply to Tissue. *Physiology* 9:119–123.

71. **Emerson GG, Segal SS** (1997) Alignment of microvascular units along skeletal muscle fibers of hamster retractor. *J Appl Physiol* 82:42–48.

72. **Engelson ET, Skalak TC, Schmid-Schönbein GW** (1985) The microvasculature in skeletal muscle. I. Arteriolar network in rat spinotrapezius muscle. *Microvasc Res* 30:29–44.

73. **Fantini S** (2014) Dynamic model for the tissue concentration and oxygen saturation of hemoglobin in relation to blood volume, flow velocity, and oxygen consumption: Implications for functional neuroimaging and coherent hemodynamics spectroscopy (CHS). *Neuroimage* 85:202–221.

74. **Federspiel WJ, Popel AS** (1986) A theoretical analysis of the effect of the particulate nature of blood on oxygen release in capillaries. *Microvasc Res* 32:164–89.

75. **Ferrari M, Mottola L, Quaresima V** (2004) Principles, Techniques, and Limitations of Near Infrared Spectroscopy. *Can J Appl Physiol* 29:463–487.

76. **Ferrari M, Muthalib M, Quaresima V** (2011) The use of near-infrared spectroscopy in understanding skeletal muscle physiology: recent developments. *Philos Trans R Soc A Math Phys Eng Sci* 369:4577–4590.

77. **Ferrari M, Quaresima V** (2012) Near Infrared Brain and Muscle Oximetry: From the Discovery to Current Applications. *J Near Infrared Spectrosc* 20:1–14.

78. **Flynn A, Chokkalingam Mani B, Mather PJ** (2010) Sepsis-induced cardiomyopathy: a review of pathophysiologic mechanisms. *Heart Fail Rev* 15:605–611.

79. **Forouzan O, Yang X, Sosa JM, et al** (2012) Spontaneous oscillations of capillary blood flow in artificial microvascular networks. *Microvasc Res* 84:123–132.

80. **Frame MD, Sarelius IH** (1993) Regulation of capillary perfusion by small arterioles is spatially organized. *Circ Res* 73:155–63.

81. **Fraser GM, Goldman D, Ellis CG** (2012) Microvascular Flow Modeling using In Vivo Hemodynamic Measurements in Reconstructed 3D Capillary Networks. *Microcirculation* 19:510–520.

82. **Fraser GM, Milkovich S, Goldman D, Ellis CG** (2012) Mapping 3-D functional capillary geometry in rat skeletal muscle in vivo. *Am J Physiol Circ Physiol* 302:H654–H664.

83. **Fung Y-C** (1973) Stochastic flow in capillary blood vessels. *Microvasc Res* 5:34–48.

84. **Garcia-Alvarez M, Marik P, Bellomo R** (2014) Sepsis-associated hyperlactatemia. *Crit Care* 18:503.

85. **Garvey AA, Dempsey EM** (2018) Applications of near infrared spectroscopy in the neonate. *Curr Opin Pediatr* 30:209–215.

86. **Gattinoni L, Brazzi L, Pelosi P, et al** (1995) A trial of goal-oriented hemodynamic therapy in critically ill patients. SvO2 Collaborative Group. *N Engl J Med* 333:1025–32.

87. **Geddes JB, Carr RT, Wu F, et al** (2010) Blood flow in microvascular networks: a study in nonlinear biology. *Chaos* 20:045123.

88. **van Genderen ME, van Bommel J, Lima A** (2012) Monitoring peripheral perfusion in critically ill patients at the bedside. *Curr Opin Crit Care* 18:273–9.

89. **Goedhart PT, Khalilzada M, Bezemer R, et al** (2007) Sidestream Dark Field (SDF) imaging: a novel stroboscopic LED ring-based imaging modality for clinical assessment of the microcirculation. *Opt Express* 15:15101.

90. **Goldman D, Popel AS** (2000) A computational study of the effect of capillary network anastomoses and tortuosity on oxygen transport. *J Theor Biol* 206:181–94.

91. **Goldman D, Bateman RM, Ellis CG** (2004) Effect of sepsis on skeletal muscle oxygen consumption and tissue oxygenation: interpreting capillary oxygen transport data using a mathematical model. *Am J Physiol Circ Physiol* 287:H2535–H2544.

92. **Goldman D, Bateman RM, Ellis CG** (2006) Effect of decreased O2 supply on skeletal muscle oxygenation and O2 consumption during sepsis: role of heterogeneous capillary spacing and blood flow. *Am J Physiol Heart Circ Physiol* 290:H2277-85.

93. **Goldsmith HL, Cokelet GR, Gaehtgens P** (1989) Robin Fahraeus: evolution of his concepts in cardiovascular physiology. *Am J Physiol Circ Physiol* 257:H1005–H1015.

94. **Gotmaker R, Peake SL, Forbes A, Bellomo R** (2017) Mortality is Greater in Septic Patients With Hyperlactatemia Than With Refractory Hypotension. *SHOCK* 48:294–300.

95. **Grassi B, Quaresima V** (2016) Near-infrared spectroscopy and skeletal muscle oxidative function in vivo in health and disease: a review from an exercise physiology perspective. *J Biomed Opt* 21:091313.

96. **Grey TM, Spencer MD, Belfry GR, et al** (2015) Effects of age and long-term endurance training on VO2 kinetics. *Med Sci Sports Exerc* 47:289–98.

97. **Gutterman DD, Chabowski DS, Kadlec AO, et al** (2016) The Human Microcirculation: Regulation of Flow and beyond. *Circ Res* 118:157–172.

98. **Habimana R, Choi I, Cho HJ, et al** (2020) Sepsis-induced cardiac dysfunction: a review of pathophysiology. *Acute Crit Care* 35:57–66.

99. **Hallisey SD, Greenwood JC** (2019) Beyond Mean Arterial Pressure and Lactate: Perfusion End Points for Managing the Shocked Patient. *Emerg Med Clin North Am* 37:395–408.

100. **Hanada A** (2000) Dissociation between muscle metabolism and oxygen kinetics during recovery from exercise in patients with chronic heart failure. *Heart* 83:161–166.

101. **Hariri G, Joffre J, Leblanc G, et al** (2019) Narrative review: clinical assessment of peripheral tissue perfusion in septic shock. *Ann Intensive Care* 9:1–9.

102. **Hartung G, Vesel C, Morley R, et al** (2018) Simulations of blood as a suspension predicts a depth dependent hematocrit in the circulation throughout the cerebral cortex. *PLOS Comput Biol* 14:e1006549.

103. **Harvey S, Harrison DA, Singer M, et al** (2005) Assessment of the clinical effectiveness of pulmonary artery catheters in management of patients in intensive care (PAC-Man): a randomised controlled trial. *Lancet* 366:472–477.

104. **Hasanin A, Mukhtar A, Nassar H** (2017) Perfusion indices revisited. *J Intensive Care* 5:1–8.

105. **Hayes MA, Timmins AC, Yau EH, et al** (1994) Elevation of systemic oxygen delivery in the treatment of critically ill patients. *N Engl J Med* 330:1717–22.

106. **Hernandez G, Bellomo R, Bakker J** (2019) The ten pitfalls of lactate clearance in sepsis. *Intensive Care Med* 45:82–85.

107. **Hernandez G, Boerma EC, Dubin A, et al** (2013) Severe abnormalities in microvascular perfused vessel density are associated to organ dysfunctions and mortality and can be predicted by hyperlactatemia and norepinephrine requirements in septic shock patients. *J Crit Care* 28:.

108. **Hernandez G, Luengo C, Bruhn A, et al** (2014) When to stop septic shock resuscitation: clues from a dynamic perfusion monitoring. *Apidologie* 4:1–9.

109. **Hernández G, Ospina-Tascón GA, Damiani LP, et al** (2019) Effect of a Resuscitation Strategy Targeting Peripheral Perfusion Status vs Serum Lactate Levels on 28-Day Mortality among Patients with Septic Shock: The ANDROMEDA-SHOCK Randomized Clinical Trial. *JAMA - J Am Med Assoc* 321:654–664.

110. **Hernandez G, Pedreros C, Veas E, et al** (2012) Evolution of peripheral vs metabolic perfusion parameters during septic shock resuscitation. A clinical-physiologic study. *J Crit Care* 27:283–8.

111. **Hernandez G, Regueira T, Bruhn A, et al** (2012) Relationship of systemic, hepatosplanchnic, and microcirculatory perfusion parameters with 6-hour lactate clearance in hyperdynamic septic shock patients: an acute, clinical-physiological, pilot study. *Ann Intensive Care* 2:44.

112. **Higgins AM, Brooker JE, Mackie M, et al** (2020) Health economic evaluations of sepsis interventions in critically ill adult patients: a systematic review. *J Intensive Care* 8:5.

113. **Hilty MP, Ince C** (2020) Automated quantification of tissue red blood cell perfusion as a new resuscitation target. *Curr Opin Crit Care* 26:273–280.

114. **Hilty MP, Guerci P, Ince Y, et al** (2019) MicroTools enables automated quantification of capillary density and red blood cell velocity in handheld vital microscopy. *Commun Biol* 2:217.

115. **Honig CR, Feldstein ML, Frierson JL** (1977) Capillary lengths, anastomoses, and estimated capillary transit times in skeletal muscle. *Am J Physiol Circ Physiol* 233:H122–H129.

116. **Hotchkiss RS, Moldawer LL, Opal SM, et al** (2016) Sepsis and septic shock. *Nat Rev Dis Prim* 2:16045.

117. **House SD, Lipowsky HH** (1987) Microvascular hematocrit and red cell flux in rat cremaster muscle. *Am J Physiol Circ Physiol* 252:H211–H222.

118. **Hwang SY eo., Shin TG u., Jo IJ oo., et al** (2014) Association between hemodynamic presentation and outcome in sepsis patients. *Shock* 42:205–210.

119. **Ince C** (2005) The microcirculation is the motor of sepsis. *Crit Care* 9:13–19.

120. **Ince C** (2015) Hemodynamic coherence and the rationale for monitoring the microcirculation. *Crit Care* 19:S8.

121. **Ince C, Boerma EC, Cecconi M, et al** (2018) Second consensus on the assessment of sublingual microcirculation in critically ill patients: results from a task force of the European Society of Intensive Care Medicine. *Intensive Care Med* 44:281–299.

122. **Ince C, Mayeux PR, Nguyen T, et al** (2016) The endothelium in sepsis. *Shock* 45:259–70.

123. **Jansen TC, van Bommel J, Schoonderbeek FJ, et al** (2010) Early lactate-guided therapy in intensive care unit patients: a multicenter, open-label, randomized controlled trial. *Am J Respir Crit Care Med* 182:752–61.

124. **Japee SA, Pittman RN, Ellis CG** (2005) A new video image analysis system to study red blood cell dynamics and oxygenation in capillary networks. *Microcirculation* 12:489–506.

125. **Jöbsis FF** (1977) Noninvasive, infrared monitoring of cerebral and myocardial oxygen sufficiency and circulatory parameters. *Science* 198:1264–7.

126. **Joffre J, Hellman J, Ince C, Ait-Oufella H** (2020) Endothelial Responses in Sepsis. Am J Respir Crit Care Med. https://doi.org/10.1164/rccm.201910-1911TR

127. **Jones AE** (2010) Lactate Clearance vs Central Venous Oxygen Saturation as Goals of Early Sepsis Therapy<subtitle>A Randomized Clinical Trial</subtitle> *Jama* 303:739.

128. **Jones S, Chiesa ST, Chaturvedi N, Hughes AD** (2016) Recent developments in near-infrared spectroscopy (NIRS) for the assessment of local skeletal muscle microvascular function and capacity to utilise oxygen. *Artery Res* 16:25.

129. **Jouffroy R, Saade A, Tourtier JP, et al** (2019) Skin mottling score and capillary refill time to assess mortality of septic shock since pre-hospital setting. *Am J Emerg Med* 37:664–671.

130. **Kanoore Edul VS, Ince C, Vazquez AR, et al** (2016) Similar microcirculatory alterations in patients with normodynamic and hyperdynamic septic shock. *Ann Am Thorac Soc* 13:240–247.

131. **Kato R, Pinsky MR** (2015) Personalizing blood pressure management in septic shock. *Ann Intensive Care* 5:41.

132. **Kaufman J, Almodovar MC, Zuk J, Friesen RH** (2008) Correlation of abdominal site near-infrared spectroscopy with gastric tonometry in infants following surgery for congenital heart disease*. *Pediatr Crit Care Med* 9:62–68.

133. **Kemps HMC, Prompers JJ, Wessels B, et al** (2010) Skeletal muscle metabolic recovery following submaximal exercise in chronic heart failure is limited more by O2 delivery than O2 utilization. *Clin Sci* 118:203–210.

134. **Kim KM, Jang HC, Lim S** (2016) Differences among skeletal muscle mass indices derived from height-, weight-, and body mass index-adjusted models in assessing sarcopenia. *Korean J Intern Med* 31:643–650.

135. **Kimmoun A, Ducrocq N, Levy B** (2013) Mechanisms of vascular hyporesponsiveness in septic shock. *Curr Vasc Pharmacol* 11:139–49.

136. **Kindig CA, Richardson TE, Poole DC** (2002) Skeletal muscle capillary hemodynamics from rest to contractions: implications for oxygen transfer. *J Appl Physiol* 92:2513–20.

137. **Klitzman B, Johnson PC** (1982) Capillary network geometry and red cell distribution in hamster cremaster muscle. *Am J Physiol* 242:H211-9.

138. **Koga S, Barstow TJ, Okushima D, et al** (2015) Validation of a high-power, time-resolved, near-infrared spectroscopy system for measurement of superficial and deep muscle deoxygenation during exercise. *J Appl Physiol* 118:1435–1442.

139. **Koga S, Okushima D, Barstow TJ, et al** (2017) Near-infrared spectroscopy of superficial and deep rectus femoris reveals markedly different exercise response to superficial vastus lateralis. *Physiol Rep* 5:e13402.

140. **Koga S, Rossiter HB, Heinonen I, et al** (2014) Dynamic heterogeneity of exercising muscle blood flow and O2 utilization. *Med Sci Sports Exerc* 46:860–76.

141. **Krogh A** (1919) The number and distribution of capillaries in muscles with calculations of the oxygen pressure head necessary for supplying the tissue. *J Physiol* 52:409–15.

142. **Krogh A** (1919) The supply of oxygen to the tissues and the regulation of the capillary circulation. *J Physiol* 52:457–74.

143. **Lam C, Tyml K, Martin C, Sibbald W** (1994) Microvascular perfusion is impaired in a rat model of normotensive sepsis. *J Clin Invest* 94:2077–2083.

144. **Lange F, Tachtsidis I** (2019) Clinical Brain Monitoring with Time Domain NIRS: A Review and Future Perspectives. *Appl Sci* 9:1612.

145. **Lara B, Enberg L, Ortega M, et al** (2017) Capillary refill time during fluid resuscitation in patients with sepsis-related hyperlactatemia at the emergency department is related to mortality. *PLoS One* 12:1–9.

146. **Law AC, Stevens JP, Walkey AJ** (2019) National Trends in Timing of Death Among Patients With Septic Shock, 1994–2014. *Crit Care Med* 47:1493–1496.

147. **Lee KF, Wood MD, Maslove DM, et al** (2019) Dysfunctional cerebral autoregulation is associated with delirium in critically ill adults. *J Cereb Blood Flow Metab* 39:2512–2520.

148. **Leone M, Asfar P, Radermacher P, et al** (2015) Optimizing mean arterial pressure in septic shock: A critical reappraisal of the literature. *Crit Care* 19:1–7.

149. **Leone M, Blidi S, Antonini F, et al** (2009) Oxygen tissue saturation is lower in nonsurvivors than in survivors after early resuscitation of septic shock. *Anesthesiology* 111:366–371.

150. **Levin M, Dawant B, Popel AS** (1986) Effect of dispersion of vessel diameters and lengths in stochastic networks. *Microvasc Res* 31:223–234.

151. **Levy BI, Ambrosio G, Pries AR, Struijker-Boudier HAJ** (2001) Microcirculation in Hypertension. *Circulation* 104:735–740.

152. **Li B, Esipova T V, Sencan I, et al** (2019) More homogeneous capillary flow and oxygenation in deeper cortical layers correlate with increased oxygen extraction. *Elife* 8:.

153. **Lidington D, Ouellette Y, Li F, Tyml K** (2003) Conducted vasoconstriction is reduced in a mouse model of sepsis. *J Vasc Res* 40:149–158.

154. **Liew PX, Kubes P** (2019) The Neutrophil's Role During Health and Disease. *Physiol Rev* 99:1223–1248.

155. **Lima A, Bakker J** (2015) Clinical assessment of peripheral circulation. *Curr Opin Crit Care* 21:226–31.

156. **Lima A, van Bommel J, Jansen TC, et al** (2009) Low tissue oxygen saturation at the end of early goal-directed therapy is associated with worse outcome in critically ill patients. *Crit Care* 13:S13.

157. **Lima A, Jansen TC, van Bommel J, et al** (2009) The prognostic value of the subjective assessment of peripheral perfusion in critically ill patients. *Crit Care Med* 37:934–938.

158. **Lipowsky HH** (2005) Microvascular rheology and hemodynamics. *Microcirculation* 12:5–15.

159. **Liu G, Mac Gabhann F, Popel AS** (2012) Effects of Fiber Type and Size on the Heterogeneity of Oxygen Distribution in Exercising Skeletal Muscle. *PLoS One* 7:e44375.

160. **Liu V, Escobar GJ, Greene JD, et al** (2014) Hospital deaths in patients with sepsis from 2 independent cohorts. *JAMA* 312:90–2.

161. **Lo A, Fuglevand AJ, Secomb TW** (2003) Oxygen delivery to skeletal muscle fibers: effects of microvascular unit structure and control mechanisms. *Am J Physiol - Hear Circ Physiol* 285:H955–H963.

162. **Lücker A, Secomb TW, Barrett MJP, et al** (2018) The Relation Between Capillary Transit Times and Hemoglobin Saturation Heterogeneity. Part 2: Capillary Networks. *Front Physiol* 9:.

163. **Lücker A, Secomb TW, Weber B, Jenny P** (2017) The relative influence of hematocrit and red blood cell velocity on oxygen transport from capillaries to tissue. *Microcirculation* 24:e12337.

164. **Lund N, Damon DH, Damon DN, Duling BR** (1987) Capillary grouping in hamster tibials anterior muscles: flow patterns, and physiological significance. *Int J Microcirc Clin Exp* 5:359—372.

165. **Maheshwari K, Nathanson BH, Munson SH, et al** (2018) The relationship between ICU hypotension and in-hospital mortality and morbidity in septic patients. *Intensive Care Med* 44:857–867.

166. **Malagoni AM, Felisatti M, Mandini S, et al** (2010) Resting Muscle Oxygen Consumption by Near-Infrared Spectroscopy in Peripheral Arterial Disease: A Parameter to be Considered in a Clinical Setting? *Angiology* 61:530–536.

167. **Manfredini F, Malagoni AM, Mandini S, et al** (2012) Near-Infrared Spectroscopy Assessment Following Exercise Training in Patients With Intermittent Claudication and in Untrained Healthy Participants. *Vasc Endovascular Surg* 46:315–324.

168. **Marcinek DJ, Amara CE, Matz K, et al** (2007) Wavelength Shift Analysis: A Simple Method to Determine the Contribution of Hemoglobin and Myoglobin to In Vivo Optical Spectra. *Appl Spectrosc* 61:665–669.

169. **Marik PE** (2019) Lactate guided resuscitation—nothing is more dangerous than conscientious foolishness. *J Thorac Dis* 11:S1969–S1972.

170. **Marik PE, Cavallazzi R** (2013) Does the central venous pressure predict fluid responsiveness? An updated meta-analysis and a plea for some common sense. *Crit Care Med* 41:1774–1781.

171. **Massey MJ, Shapiro NI** (2016) A guide to human in vivo microcirculatory flow image analysis. *Crit Care* 20:1–10.

172. **Masyuk M, Wernly B, Lichtenauer M, et al** (2019) Prognostic relevance of serum lactate kinetics in critically ill patients. *Intensive Care Med* 45:55–61.

173. **Matcher SJ, Cooper CE** (1994) Absolute quantification of deoxyhaemoglobin concentration in tissue near infrared spectroscopy. *Phys Med Biol* 39:1295–312.

174. **Mayr FB, Yende S, Angus DC** (2014) Epidemiology of severe sepsis. *Virulence* 5:4–11.

175. **Mesquida J, Gruartmoner G, Espinal C, et al** (2013) Skeletal Muscle Oxygen Saturation (StO2) Measured by Near-Infrared Spectroscopy in the Critically Ill Patients. *Biomed Res Int* 2013:1–8.

176. **Metkus TS, Kim BS** (2015) Bedside Diagnosis in the Intensive Care Unit. Is Looking Overlooked? *Ann Am Thorac Soc* 12:1447–1450.

177. **Mikkelsen ME, Miltiades AN, Gaieski DF, et al** (2009) Serum lactate is associated with mortality in severe sepsis independent of organ failure and shock. *Crit Care Med* 37:1670–7.

178. **Miranda M, Balarini M, Caixeta D, Bouskela E** (2016) Microcirculatory dysfunction in sepsis: pathophysiology, clinical monitoring, and potential therapies. *Am J Physiol - Hear Circ Physiol* 311:H24–H35.

179. **Miura H, McCully K, Hong L, et al** (2001) Regional Difference of Muscle Oxygen Saturation and Blood Volume during Exercise Determined by Near Infrared Imaging Device. *Jpn J Physiol* 51:599–606.

180. **Mizock BA, Falk JL** (1992) Lactic acidosis in critical illness. *Crit Care Med* 20:80–93.

181. **Monnet X, Marik PE, Teboul JL** (2016) Prediction of fluid responsiveness: an update. *Ann Intensive Care* 6:1–11.

182. **Moore JPR, Dyson A, Singer M, Fraser J** (2015) Microcirculatory dysfunction and resuscitation: Why, when, and how. *Br J Anaesth* 115:366–375.

183. **Možina H, Podbregar M** (2015) Near infrared spectroscopy for evaluation of skeletal muscle tissue oxygenation in different types of shock. *Signa Vitae* 10:10–24.

184. **Murias JM, Kowalchuk JM, Paterson DH** (2010) Speeding of Vo2 kinetics with endurance training in old and young men is associated with improved matching of local O2 delivery to muscle O2 utilization. *J Appl Physiol* 108:913–922.

185. **Murkin JM, Arango M** (2009) Near-infrared spectroscopy as an index of brain and tissue oxygenation. *Br J Anaesth* 103:i3–i13.

186. **Murrant CL, Lamb IR, Novielli NM** (2017) Capillary endothelial cells as coordinators of skeletal muscle blood flow during active hyperemia. *Microcirculation* 24:1–10.

187. **Murrant CL, Sarelius IH** (2015) Local control of blood flow during active hyperaemia: what kinds of integration are important? *J Physiol* 593:4699–4711.

188. **Nardi O, Zavala E, Martin C, et al** (2018) Targeting skeletal muscle tissue oxygenation (StO_2) in adults with severe sepsis and septic shock: a randomised controlled trial (OTO-StS Study). *BMJ Open* 8:e017581.

189. **Neto AS, Pereira VGM, Manetta JA, et al** (2014) Association between static and dynamic thenar near-infrared spectroscopy and mortality in patients with sepsis. *J Trauma Acute Care Surg* 76:226–233.

190. **Niemeijer VM, Spee RF, Schoots T, et al** (2016) Limitations of skeletal muscle oxygen delivery and utilization during moderate-intensity exercise in moderately impaired patients with chronic heart failure. *Am J Physiol Circ Physiol* 311:H1530–H1539.

191. **O'Rourke MF** (2009) Time domain analysis of the arterial pulse in clinical medicine. *Med Biol Eng Comput* 47:119–129.

192. **Opal SM, van der Poll T** (2015) Endothelial barrier dysfunction in septic shock. *J Intern Med* 277:277–293.

193. **Ostadal P, Kruger A, Vondrakova D, et al** (2014) Noninvasive assessment of hemodynamic variables using near-infrared spectroscopy in patients experiencing cardiogenic shock and individuals undergoing venoarterial extracorporeal membrane oxygenation. *J Crit Care* 29:690.e11-690.e15.

194. **Østergaard L, Granfeldt A, Secher N, et al** (2015) Microcirculatory dysfunction and tissue oxygenation in critical illness. *Acta Anaesthesiol Scand* 59:1246–1259.

195. **Padilla DJ, McDonough P, Behnke BJ, et al** (2006) Effects of Type II diabetes on capillary hemodynamics in skeletal muscle. *Am J Physiol Heart Circ Physiol* 291:H2439–H2444.

196. **Paoli CJ, Reynolds MA, Sinha M, et al** (2018) Epidemiology and Costs of Sepsis in the United States-An Analysis Based on Timing of Diagnosis and Severity Level. *Crit Care Med* 46:1889–1897.

197. **Patel AK, Lazar DA, Burrin DG, et al** (2014) Abdominal Near-Infrared Spectroscopy Measurements Are Lower in Preterm Infants at Risk for Necrotizing Enterocolitis. *Pediatr Crit Care Med* 15:735–741.

198. **Piper RD, Pitt-Hyde M, Li F, et al** (1996) Microcirculatory changes in rat skeletal muscle in sepsis. *Am J Respir Crit Care Med* 154:931–937.

199. **Pittman RN** (2011) Oxygen gradients in the microcirculation. *Acta Physiol* 202:311–322.

200. **Pittman RN** (1995) Influence of Microvascular Architecture on Oxygen Exchange in Skeletal Muscle. *Microcirculation* 2:1–18.

201. **Plyley MJ, Sutherland GJ, Groom AC** (1976) Geometry of the capillary network in skeletal muscle. *Microvasc Res* 11:161–173.

202. **van der Poll T, Opal SM** (2008) Host-pathogen interactions in sepsis. *Lancet Infect Dis* 8:32–43.

203. **Poole DC, Copp SW, Hirai DM, Musch TI** (2011) Dynamics of muscle microcirculatory and blood-myocyte O(2) flux during contractions. *Acta Physiol (Oxf)* 202:293–310.

204. **Poole DC, Copp SW, Ferguson SK, Musch TI** (2013) Skeletal muscle capillary function: Contemporary observations and novel hypotheses. *Exp Physiol* 98:1645–1658.

205. **Poole DC** (2019) Edward F. Adolph Distinguished Lecture. Contemporary model of muscle microcirculation: gateway to function and dysfunction. *J Appl Physiol* 127:1012–1033.

206. **Popel AS, Charny CK, Dvinsky AS** (1986) Effect of Heterogeneous Oxygen Delivery on the Oxygen Distribution in Skeletal Muscle. *Math Biosci* 81:91–113.

207. **Popel AS, Johnson PC** (2005) Microcirculaton and Hemorheology. *Annu Rev Fluid Mech* 37:43–69.

208. **Pranskunas A, Koopmans M, Koetsier PM, et al** (2013) Microcirculatory blood flow as a tool to select ICU patients eligible for fluid therapy. *Intensive Care Med* 39:612–619.

209. **Prescott HC, Angus DC** (2018) Enhancing Recovery From Sepsis: A Review. *JAMA* 319:62–75.

210. **Prescott HC, Iwashyna TJ, Blackwood B, et al** (2019) Understanding and Enhancing Sepsis Survivorship. Priorities for Research and Practice. *Am J Respir Crit Care Med* 200:972–981.

211. **Pries AR, Neuhaus D, Gaehtgens P** (1992) Blood viscosity in tube flow: dependence on diameter and hematocrit. *Am J Physiol Circ Physiol* 263:H1770–H1778.

212. **Pries AR, Secomb TW, Gaehtgens P** (1995) Structure and hemodynamics of microvascular networks: heterogeneity and correlations. *Am J Physiol Circ Physiol* 269:H1713–H1722.

213. **Pries AR, Secomb TW, Gaehtgens P** (1996) Relationship between structural and hemodynamic heterogeneity in microvascular networks. *Am J Physiol - Hear Circ Physiol* 270:545–553.

214. **Pries AR, Secomb TW, Gaehtgens P** (1996) Biophysical aspects of blood flow in the microvasculature. *Cardiovasc Res* 32:654–667.

215. **Pries AR, Ley K, Claassen M, Gaehtgens P** (1989) Red cell distribution at microvascular bifurcations. *Microvasc Res* 38:81–101.

216. **Pries AR, Ley K, Gaehtgens P** (1986) Generalization of the Fahraeus principle for microvessel networks. *Am J Physiol* 251:H1324-32.

217. **Pries AR, Secomb TW, Gaehtgens P, Gross JF** (1990) Blood flow in microvascular networks. Experiments and simulation. *Circ Res* 67:826–834.

218. **Pries AR, Secomb TW, Gessner T, et al** (1994) Resistance to blood flow in microvessels in vivo. *Circ Res* 75:904–915.

219. **Pries AR** (2019) Microvascular hemodynamics: System properties. *Biorheology* 56:1–13.

220. **Pries AR, Secomb TW** (2008) Blood Flow in Microvascular Networks. In: Microcirculation. Elsevier, pp 3–36

221. **Puskarich MA, Trzeciak S, Shapiro NI, et al** (2011) Outcomes of patients undergoing early sepsis resuscitation for cryptic shock compared with overt shock. *Resuscitation* 82:1289–1293.

222. **Puskarich MA, Illich BM, Jones AE** (2014) Prognosis of emergency department patients with suspected infection and intermediate lactate levels: a systematic review. *J Crit Care* 29:334–9.

223. **Raymond SL, Holden DC, Mira JC, et al** (2017) Microbial recognition and danger signals in sepsis and trauma. *Biochim Biophys Acta - Mol Basis Dis* 1863:2564–2573.

224. **Reinhart K, Daniels R, Kissoon N, et al** (2017) Recognizing Sepsis as a Global Health Priority — A WHO Resolution. *N Engl J Med* 377:414–417.

225. **Reisner AT, Edla S, Liu J, et al** (2016) Muscle Oxygen Saturation Improves Diagnostic Association Between Initial Vital Signs and Major Hemorrhage: A Prospective Observational Study. *Acad Emerg Med* 23:353–357.

226. **Rhodes A, Evans LE, Alhazzani W, et al** (2017) Surviving Sepsis Campaign: International Guidelines for Management of Sepsis and Septic Shock: 2016. *Intensive Care Med* 43:304–377.

227. **Richard C, Warszawski J, Anguel N, et al** (2003) Early use of the pulmonary artery catheter and outcomes in patients with shock and acute respiratory distress syndrome: a randomized controlled trial. *JAMA* 290:2713–20.

228. **Rivers E, Nguyen B, Havstad S, et al** (2001) Early goal-directed therapy in the treatment of severe sepsis and septic shock. *N Engl J Med* 345:1368–77.

229. **Ronco JJ, Fenwick JC, Tweeddale MG, et al** (1993) Identification of the critical oxygen delivery for anaerobic metabolism in critically ill septic and nonseptic humans. *JAMA* 270:1724–30.

230. **Ronco JJ, Fenwick JC, Wiggs BR, et al** (1993) Oxygen consumption is independent of increases in oxygen delivery by dobutamine in septic patients who have normal or increased plasma lactate. *Am Rev Respir Dis* 147:25–31.

231. **Ronco JJ, Phang PT, Walley KR, et al** (1991) Oxygen consumption is independent of changes in oxygen delivery in severe adult respiratory distress syndrome. *Am Rev Respir Dis* 143:1267–73.

232. **Rowan KM, Angus DC, Bailey M, et al** (2017) Early, goal-directed therapy for septic shock - A patient-level meta-analysis. *N Engl J Med* 376:2223–2234.

233. **Rudd KE, Johnson SC, Agesa KM, et al** (2020) Global, regional, and national sepsis incidence and mortality, 1990-2017: analysis for the Global Burden of Disease Study. *Lancet (London, England)* 395:200–211.

234. **Sakr Y, Chierego M, Piagnerelli M, et al** (2007) Microvascular response to red blood cell transfusion in patients with severe sepsis*. *Crit Care Med* 35:1639–1644.

235. **Sakr Y, Dubois M-J, De Backer D, et al** (2004) Persistent microcirculatory alterations are associated with organ failure and death in patients with septic shock*. *Crit Care Med* 32:1825–1831.

236. **Sakr Y, Jaschinski U, Wittebole X, et al** (2018) Sepsis in Intensive Care Unit Patients: Worldwide Data From the Intensive Care over Nations Audit. *Open forum Infect Dis* 5:ofy313.

237. **Sakr Y, Reinhart K, Vincent J-L, et al** (2006) Does dopamine administration in shock influence outcome? Results of the Sepsis Occurrence in Acutely Ill Patients (SOAP) Study. *Crit Care Med* 34:589–97.

238. **Sarelius IH** (1986) Cell flow path influences transit time through striated muscle capillaries. *Am J Physiol Hear Circ Physiol* 250:H899–H907.

239. **Sarelius IH, Duling BR** (1982) Direct measurement of microvessel hematocrit, red cell flux, velocity, and transit time. *Am J Physiol Circ Physiol* 243:H1018–H1026.

240. **Sarelius IH** (1993) Cell and oxygen flow in arterioles controlling capillary perfusion. *Am J Physiol* 265:H1682-7.

241. **Scheuzger J, Zehnder A, Meier V, et al** (2020) Sublingual microcirculation does not reflect red blood cell transfusion thresholds in the intensive care unit-a prospective observational study in the intensive care unit. *Crit Care* 24:18.

242. **Schmid-Schönbein GW, Skalak R, Usami S, Chien S** (1980) Cell distribution in capillary networks. *Microvasc Res* 19:18–44.

243. **Schmid-Schönbein GW, Skalak TC, Firestone G** (1987) The microvasculature in skeletal muscle. V. The microvascular arcades in normotensive and hypertensive rats. *Microvasc Res* 34:385–93.

244. **Schmid F, Barrett MJP, Obrist D, et al** (2019) Red blood cells stabilize flow in brain microvascular networks. *PLOS Comput Biol* 15:e1007231.

245. **Scholkmann F, Kleiser S, Metz AJ, et al** (2014) A review on continuous wave functional near-infrared spectroscopy and imaging instrumentation and methodology. *Neuroimage* 85:6–27.

246. **Secomb TW** (2017) Blood Flow in the Microcirculation. *Annu Rev Fluid Mech* 49:443–461.

247. **Segal SS** (2005) Regulation of blood flow in the microcirculation. *Microcirculation* 12:33–45.

248. **Sekhon MS, Smielewski P, Bhate TD, et al** (2016) Using the relationship between brain tissue regional saturation of oxygen and mean arterial pressure to determine the optimal mean arterial pressure in patients following cardiac arrest: A pilot proof-of-concept study. *Resuscitation* 106:120–125.

249. **Semeraro N, Ammollo CT, Semeraro F, Colucci M** (2015) Coagulopathy of Acute Sepsis. *Semin Thromb Hemost* 41:650–8.

250. **Shapiro NI, Howell MD, Talmor D, et al** (2005) Serum lactate as a predictor of mortality in emergency department patients with infection. *Ann Emerg Med* 45:524–8.

251. **Sidell BD** (2006) When bad things happen to good fish: the loss of hemoglobin and myoglobin expression in Antarctic icefishes. *J Exp Biol* 209:1791–1802.

252. **Singer M, Deutschman CS, Seymour C, et al** (2016) The third international consensus definitions for sepsis and septic shock (sepsis-3). *JAMA - J Am Med Assoc* 315:801–810.

253. **Singh K, Mayo P** (2018) Critical care echocardiography and outcomes in the critically ill. *Curr Opin Crit Care* 24:316–321.

254. **Skalak TC, Schmid-Schönbein GW** (1986) The microvasculature in skeletal muscle. IV. A model of the capillary network. *Microvasc Res* 32:333–347.

255. **Skarda DE, Mulier KE, Myers DE, et al** (2007) Dynamic near-infrared spectroscopy measurements in patients with severe sepsis. *Shock* 27:348–353.

256. **Song H, Tyml K** (1993) Evidence for sensing and integration of biological signals by the capillary network. *Am J Physiol Circ Physiol* 265:H1235–H1242.

257. **Spronk PE, Zandstra DF, Ince C** (2004) Bench-to-bedside review: Sepsis is a disease of the microcirculation. *Crit Care* 8:462.

258. **Stanzani G, Duchen MR, Singer M** (2019) The role of mitochondria in sepsis-induced cardiomyopathy. *Biochim Biophys Acta - Mol Basis Dis* 1865:759–773.

259. **Stearns-Kurosawa DJ, Osuchowski MF, Valentine C, et al** (2011) The pathogenesis of sepsis. *Annu Rev Pathol* 6:19–48.

260. **de Stoppelaar SF, van 't Veer C, van der Poll T** (2014) The role of platelets in sepsis. *Thromb Haemost* 112:666–77.

261. **Stothers L, Shadgan B, Macnab A** (2008) Urological applications of near infrared spectroscopy. *Can J Urol* 15:4399–409.

262. **Suetrong B, Walley KR** (2016) Lactic Acidosis in Sepsis: It's Not All Anaerobic: Implications for Diagnosis and Management. *Chest* 149:252–61.

263. **Sweeney TE, Sarelius IH** (1989) Arteriolar control of capillary cell flow in striated muscle. *Circ Res* 64:112–120.

264. **Takala J, Ruokonen E, Tenhunen JJ, et al** (2011) Early non-invasive cardiac output monitoring in hemodynamically unstable intensive care patients: A multi-center randomized controlled trial. *Crit Care* 15:R148.

265. **Thiele RH, Durieux ME** (2011) Arterial waveform analysis for the anesthesiologist: Past, present, and future concepts. *Anesth Analg* 113:766–776.

266. **Thomas-Rueddel DO, Poidinger B, Weiss M, et al** (2015) Hyperlactatemia is an independent predictor of mortality and denotes distinct subtypes of severe sepsis and septic shock. *J Crit Care* 30:439.e1-439.e6.

267. **Thomas GD, Segal SS** (2004) Neural control of muscle blood flow during exercise. *J Appl Physiol* 97:731–738.

268. **Torio CM, Moore BJ** (2006) National Inpatient Hospital Costs: The Most Expensive Conditions by Payer, 2013: Statistical Brief #204

269. **Trzeciak S, McCoy J V., Phillip Dellinger R, et al** (2008) Early increases in microcirculatory perfusion during protocol-directed resuscitation are associated with reduced multi-organ failure at 24 h in patients with sepsis. *Intensive Care Med* 34:2210–2217.

270. **Twynstra J, Ruiz DA, Murrant CL** (2012) Functional coordination of the spread of vasodilations through skeletal muscle microvasculature: implications for blood flow control. *Acta Physiol* 206:229–241.

271. **Tyml K, Ellis CG, Safranyos RG, et al** (1981) Temporal and spatial distributions of red cell velocity in capillaries of resting skeletal muscle, including estimates of red cell transit times. *Microvasc Res* 22:14–31.

272. **Uchimido R, Schmidt EP, Shapiro NI** (2019) The glycocalyx: a novel diagnostic and therapeutic target in sepsis. *Crit Care* 23:16.

273. **Vardi M, Nini A** (2008) Near-infrared Spectroscopy for Evaluation of Peripheral Vascular Disease. A Systematic Review of Literature. *Eur J Vasc Endovasc Surg* 35:68–74.

274. **Vieillard-Baron A, Millington SJ, Sanfilippo F, et al** (2019) A decade of progress in critical care echocardiography: a narrative review. *Intensive Care Med* 45:770–788.

275. **Vincent J, De Backer D** (2013) Circulatory Shock. *N Engl J Med* 369:1726–1734.

276. **Vincent JL, Ince C, Bakker J** (2012) Clinical review: Circulatory shock - an update: a tribute to Professor Max Harry Weil. *Crit Care* 16:1–5.

277. **Vincent JL, Nielsen ND, Shapiro NI, et al** (2018) Mean arterial pressure and mortality in patients with distributive shock: a retrospective analysis of the MIMIC-III database. *Ann Intensive Care* 8:.

278. **Weil MH, Shubin H** (1971) Proposed reclassification of shock states with special reference to distributive defects. *Adv Exp Med Biol* 23:13–23.

279. **Weiss M, Schulz G, Teller I, et al** (2004) Tissue oxygenation monitoring during major pediatric surgery using transcutaneous liver near infrared spectroscopy. *Paediatr Anaesth* 14:989–95.

280. **Wiersinga WJ, Leopold SJ, Cranendonk DR, van der Poll T** (2014) Host innate immune responses to sepsis. *Virulence* 5:36–44.

281. **Wolf U, Wolf M, Choi JH, et al** (2007) Regional differences of hemodynamics and oxygenation in the human calf muscle detected with near-infrared spectrophotometry. *J Vasc Interv Radiol* 18:1094–101.

282. **Zweifach BW, Kovalcheck S, De Lano F, Chen P** (1981) Micropressure-flow relationships in a skeletal muscle of spontaneously hypertensive rats. *Hypertension* 3:601–614.

283. **Zweifel C, Dias C, Smielewski P, Czosnyka M** (2014) Continuous time-domain monitoring of cerebral autoregulation in neurocritical care. *Med Eng Phys* 36:638–645.

CHAPTER 2: THE CAPILLARY FASCICLE IN SKELETAL MUSCLE: STRUCTURAL AND FUNCTIONAL PHYSIOLOGY OF RBC DISTRIBUTION IN CAPILLARY NETWORKS

2.1 Introduction

Capillary networks are the fundamental site of oxygen (O_2) exchange in the microcirculation. Given their complexity and scale, understanding how capillary networks participate in microvascular oxygen exchange has proven challenging, but not insurmountable [76, 81, 105]. Skeletal muscle comprises the largest organ by mass and largest capillary bed in the body [80], and impaired microvascular oxygen exchange in skeletal muscle contributes to exercise limitation in aging, and for patients with diabetes, congestive heart failure, and COPD [79]. Fundamentally, the structure of capillary networks determines their geometric resistance to blood flow, and the surface area for diffusional O_2 exchange between perfused capillaries and surrounding tissue. Capillary-red blood cell (RBC) hemodynamics determine the convective O_2 delivery of flowing blood [61], that can be denoted as 'capillary perfusion' within microvascular networks.

The capillary module (CM) - also referred to as capillary unit or capillary bundle element - is classically considered the building block of complex capillary networks. Capillaries are oriented longitudinally between muscle fibres, and are grouped into modules of parallel-flowing microvessels arising from a terminal arteriole (TA) and

draining to a post-capillary venule (PCV) [8, 19, 64, 96]. Because they originate from a single TA, blood flow will change together for all capillaries in a module although module structure and RBC rheology suggest these changes may not manifest uniformly for all capillary segments [19, 93, 98]. CMs typically comprise 10-20 vessels, with length of 500-1000μm, width of 200-500μm, and depth of 100-200μm, depending on the species and muscle [69]; capillary segments will form converging and diverging internal bifurcations within the module [77]. However, this singular microvascular unit fails to address how blood flow is regulated along the entire length of the contracting muscle fibres, requiring coordination from numerous CMs [69]. The target volume of tissue supplied by a CM is also unclear since CMs are wider than individual muscle fibres, and are not spatially associated with motor units or muscle recruitment [33, 41]. These discordances may partly be explained by the anatomical observation that TAs in skeletal muscle supply blood for two CMs flowing in opposite directions and PCVs similarly receive blood flow from two CMs [10, 19, 84, 96, 101]. However, detailed description of this structure and implications for microvascular flow regulation are currently not known.

Herein, we will refer to the column of interconnected CMs in skeletal muscle as the Capillary Fascicle (CF). The interconnected architecture of capillary networks has been noted in many organs, with a mesh-like lattice described in the brain [62, 74, 97] or hexagonal lattice in the lung [42] and liver [89]. Skeletal muscle, by contrast, has a columnar architecture with muscle fibres of many millimeters (small animals) or even centimeters (humans) in length, and regional oxygen metabolism can increase up to 100-fold from rest to peak exercise with commensurate 20-fold increase in blood flow [52, 55] - the widest range for any organ in the body; these factors provide anatomical constraints

and functional demands on the organization of capillary networks. Previous studies using intravital videomicroscopy have derived detailed hemodynamic data for capillary segments within one individual CM [27, 38], or from random sampling of capillaries distributed throughout the network [5, 17, 31, 56, 71]. In this regard, capillary hemodynamics have lacked spatial context from the CF, thereby limiting the interpretation of functional data. Quantifying capillary-RBC hemodynamics at the level of multiple CMs is needed to gain insights into the regulation of blood flow within the CF. Furthermore, although heterogeneity is considered a hallmark of microvascular blood flow and is a vital characteristic of healthy microvascular systems [88], very little is known about heterogeneity relative to the anatomical structure of the CF. Even at rest, capillary-RBC hemodynamics in skeletal muscle demonstrate substantial spatial and temporal variation [27, 81, 101], and this is often under-appreciate from capillary-RBC hemodynamic studies comprising modest datasets of capillaries (dozens to hundreds) with experimental data per capillary derived from short periods of measurement (10-60 seconds). Overall, these knowledge gaps suggest the need for a more comprehensive and thorough analysis strategy.

Using a systems physiology approach, we characterize the structure and function of the Capillary Fascicle in resting skeletal muscle using a robust dataset derived from in-vivo capillary perfusion. We evaluate the heterogeneity of RBC distribution and the interaction between capillary-RBC hemodynamics and CM topology using label-free intravital imaging and processing. This study provides an updated model of complex capillary networks in skeletal muscle, and demonstrates how non-homogenous functional units of blood flow participate together in microvascular flow regulation.

2.2 Methods

All experiments were conducted in accordance with local animal ethics committee approval (REB 2019-053), in compliance with ARRIVE guidelines [73], Canadian Council for Animal Care, and ethical policies of the Journal. This was a prospective observational study with no comparison groups (i.e. only control animals). Sample size was determined to sufficiently account for between-subject variability, but no formal sample size calculations were undertaken. There was no inclusion/exclusion criteria or blinding of results.

2.2.1 Experimental Protocol – Rodent Extensor Digitorum Longus Muscle

Juvenile male Sprague-Dawley rats were used for this study (n=9, Charles River Laboratories, purchased at 90g approximately 7-8 weeks), with an experimental protocol described previously by our group [39]. Animals were housed in the animal care facility at the University of Western Ontario for seven days prior to the experiment (2-3 animals per cage), with free access to food and water and 12-hour light-dark cycles. Animals were selected randomly on the day of the experiment. Anesthesia was induced with intraperitoneal injection of sodium pentobarbital (6.5 mg/100g), and animals were maintained at 37°C throughout the duration of the experiment. This cohort was comprised of naïve animals (n=2), and sham animals (n=7) with 5-mm lower-midline abdominal incision and intraperitoneal instillation of 0.6 mL normal saline; incision was subsequently closed with silk suture. Sham procedure conforms with fecal-induced peritonitis model of sepsis developed by our group [51]. Tracheostomy was performed and the animals were

ventilated at a rate of 70-74 breaths per minute with a gas composition of 30% O_2 and 70% nitrogen (Harvard Instruments). The left common carotid artery was cannulated with polyethelene tubing, and connected to a pressure transducer for continuous heart rate and blood pressure monitoring (MicroMed); continuous data were averaged over the duration of the experiment to generate a mean blood pressure for each animal. The right internal jugular vein was cannulated with silastic tubing and infused with normal saline (0.5 mL/hr) for the duration of the experiment.

The extensor digitorum longus (EDL) muscle was externalized with blunt dissection [102] and the distal tendon was released from the hindlimb and secured with a silk ligature [31]. The animal was placed on the microscope stage, and the EDL muscle was positioned on a glass coverslip over the objective at its resting in-situ length and orientation. Warmed Plasma-Lyte 148 solution (Baxter Healthcare) was applied on the muscle, which was then covered with an O_2-impermeable membrane (Saran wrap, Dow Chemical Company) and a coverslip to isolate the muscle from the environment. Arterial blood gas was obtained at baseline to monitor systemic physiological and respiratory parameters (iSTAT, Abbott Point of Care). The EDL muscle was allowed to equilibrate for 30 minutes prior to video capture. Maintenance doses of pentobarbital (2.2mg/100g) were administered intravenously as needed to maintain appropriate analgesia and depth of anesthesia, tested every 60 minutes by blink response and changes to heart rate and blood pressure. This was a terminal experiment with intravenous euthanasia dose of sodium pentobarbital administered at the end of the experiment (12mg/100g).

2.2.2 Dual-wavelength intravital videomicroscopy

In-vivo video sequences were recorded from perfused capillary networks in resting skeletal muscle with intravital videomicroscopy. We used an inverted microscope (Olympus IX81) and a dual-wavelength camera system as described previously [2, 3]. All video recordings were captured with the 10X objective for 2 minutes duration at 20.6 frames per second (2520 frames). The EDL muscle was trans-illuminated with a 75-watt Xenon lightsource, and the transmitted light passed through a DualCam parfocal beam-splitter that allows for simultaneous video capture on two digital video cameras (Rolera-XR, QImaging) using custom capture software (Neovision). Light to each camera was filtered for either the isosbestic wavelength (452/454nm) or oxygen-dependent wavelength (438/440nm) of hemoglobin. These wavelengths were selected for their sensitivity to changes in hemoglobin content and RBC oxygen saturation, and their ability to generate strong contrast between RBCs, plasma, and surrounding muscle tissue. RBC hemodynamics can be measured using either wavelength individually, whereas RBC oxygen saturation would require calculating the ratio of optical density at these wavelengths [53].

2.2.3 Functional Images – Pseudo-optical density and extended depth of focus

2-minute videos recorded with intravital videomicroscopy were converted from the light captured on the camera chip (696 x 520 pixels) using custom software to generate functional images that provide quantitative physiological information. Functional images

yield detailed geometric data on individual capillary segments (diameter, length, volume) and overall topology of the network; they are also used to guide the acquisition of hemodynamic data from individual segments [54]. Intravital videomicroscopy was recorded from overlapping fields of view (FOV) to reconstruct the CL as an interconnected network of capillary modules.

Pseudo-optical density (psOD) images were generated from the maximum and minimum light intensity levels (I_{max}, I_{min}) at every pixel in the FOV over the 2520 frames with the equation $psOD(x, y) = log_{10} \frac{I_{max}(x,y)}{I_{min}(x,y)}$. psOD images yield high contrast images of the capillary lumen as RBCs (hemoglobin with high extinction coefficient) and plasma gaps (light intensity of the background tissue) flow through the vessel. Thus, only pixels comprising moving RBCs will be registered with this method, as opposed to background tissue which does not have varying intensity.

Because capillaries are positioned at different focal depths within the muscle, multiple videos at sequential z-planes were captured for each FOV to increase the number of capillaries in the dataset. For 7/9 networks, an extended depth of focus (EDF) recording at each FOV was also performed, whereby the focal plane of the microscope was manually adjusted down and back up through the muscle during a 2 minute recording to form a continuous z-stack of approximately 100μm. By converting the EDF video into a psOD functional image, this method is able to obtain a label-free 2D projection of perfused capillaries within the z-stack.

2.2.4 Topological classification of capillary modules in the Capillary Fascicle

The structure of the CF is derived from overlapping maps of functional images (n=9 networks). The CF denotes the expansive network of interconnected CMs arranged in columns oriented parallel with skeletal muscle fibres. CMs are defined as the group of parallel-flowing capillary segments originating from a single TA and draining into a single PCV with the associated internal bifurcations [8, 19, 64, 96]. Using 3D reconstruction software [39], a column of capillary modules is shown in Figure 2.1 to illustrate CF structure and the quantification methods for module topology. Two operators (TH, RV) worked together to abstract the data from network maps; analysis strategy was coordinated, direct measurements were performed separately, and final quality review was performed by one operator to ensure consistency (TH). Module length is defined as the average distance between inflowing and outflowing capillary segments, i.e. the distance between TA and PCV. Module width is defined as the total distance across all parallel-flowing capillary segments, and is taken as the mean from three measurements at the arteriolar, middle, and venular locations along the module. When a gap of tissue exists between horizontally-adjacent modules, the distance was split between them. Module volume (mm^3) is defined as ($length * width * depth$), with a standardized 100μm depth used throughout this study.
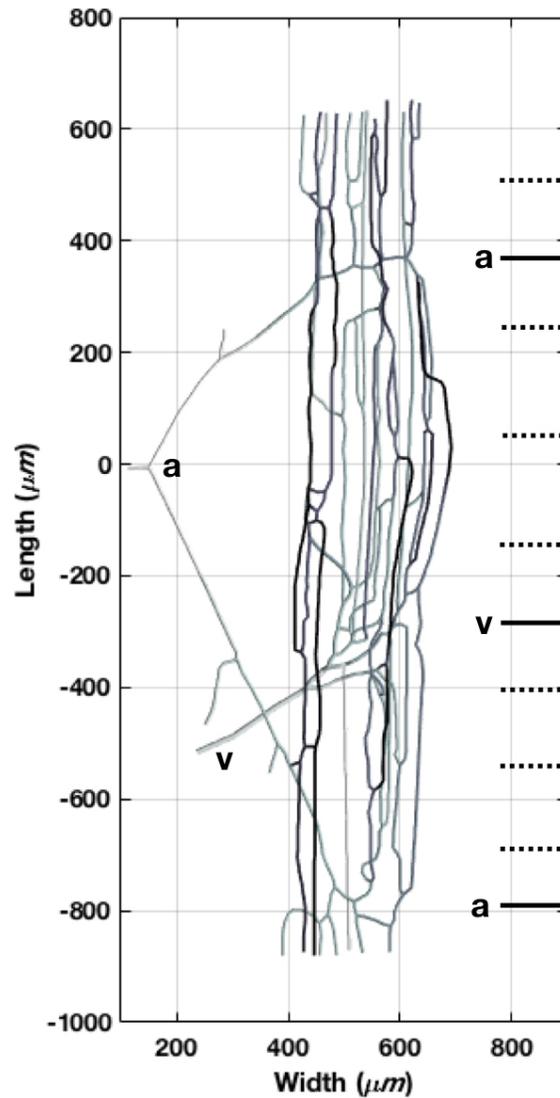
Figure 2.1: Capillary Fascicle (CF) in skeletal muscle.
3D rendering generated from functional images derived from intravital videomicroscopy of the rodent extensor digitorum longus muscle; greyscale is used for depth. The CF comprises interconnected capillary modules (CM), linked together to form continuous columns. Terminal arteriole (a) and post-capillary venule (v) are seen feeding and draining the modules from deeper in the muscle. Note that arterioles feed two CMs flowing in opposite directions, and venules similarly collect blood from two CMs. Module length is defined as the distance between inflowing and outflowing vessels (solid lines). Module width and the number of parallel capillaries (N_{par}) are taken as the mean from three measurements along each module (hashed lines). CMs contain converging and diverging bifurcations, and do not have standardized length, width, or parallel capillaries.

The number of parallel capillaries in a module (N_{par}) was derived from CMs in the 7/9 networks with EDF protocol. N_{par} was taken as the mean from three measurements at the arteriolar, middle, and venular locations along the CM by drawing lines perpendicular to RBC flow and counting the number of capillary segments intersecting each line [31]. Note that N_{par} can be non-integer, such as 8.33 from averaging 8, 9, and 8 parallel capillaries at three locations. Similarly, capillary density (cap/mm^2) was defined as $\frac{N_{par}}{width * depth}$, averaged from the measurements at three module locations. This metric is analogous to the 2D capillary density measurements derived with cross-sectional muscle histology.

2.2.5 Capillary hemodynamic measurements

Capillary segments are defined in this study as unbranched capillary microvessels that result from stochastic diverging and converging bifurcations within a capillary module [77, 101]. Capillary segments are often shorter than the full length between TA and PCV, although some unbranched capillaries traverse the entire length of the module [91].

The intravital videos were post-processed using custom software for quantifying RBC-capillary hemodynamics, with details previously published by our group [2, 39, 49, 53]. Briefly, 2-min intravital videos were reviewed by the operator, and capillary segments were manually selected from a co-registered functional image by placing a window over the desired capillary segment. The software determines the edges of the RBC column defining the lumen of the vessel, from which capillary diameters and volume are determined, and the capillary centerline is positioned along the vessel. Extraction of light

intensity data from the centerline records the position of RBCs in the capillary for each frame over the duration of the video. The resulting space-time image (STI), one for each wavelength, shows the dynamic passage of RBCs through the capillary. As many capillary segments as possible were evaluated from each FOV, with the operator excluding segments in a FOV that are completely out-of-focus or with overlapping capillaries. Segments with exceedingly high hematocrit or RBC velocity were also excluded, as technical considerations preclude accurate measurements of these vessels with our software. These exclusions comprise approximately 10% of capillary segments per FOV. The number of stopped-flow capillaries was also counted in each FOV to evaluate how many of these capillary segments are present in resting skeletal muscle.

The fundamental metrics of capillary-RBC hemodynamics are RBC velocity (V_{rbc}, μm/sec), lineal density (LD, RBC/mm) as a surrogate for hematocrit (Hct, %), and RBC supply rate (SR_{rbc}, RBC/s) where $SR_{rbc} = V_{rbc} * LD * \frac{1mm}{1000\mu m}$; RBC supply rate has also been referred to as RBC flux or erythrocyte flux [9, 27, 80]. SR_{rbc} defines the number of RBCs flowing through an individual capillary per unit time, and plays a critical role in the biophysics of capillary oxygen exchange with surrounding myocytes [36]. STIs are used to calculate frame-by-frame capillary hemodynamics (2520 frames) as originally described by Ellis [28]. Data were generated from STIs for both wavelengths, and were manually inspected (AAM) and compared to the original video for artifacts and accuracy; any concerns with data quality were reviewed with a second operator (SM). The wavelength with superior quality was used to generate summary hemodynamics for each capillary segment as the mean over the 2-min video. RBC O_2 saturation measurements were accurate

only when both intravital wavelengths are in perfect focus and alignment between cameras; these conditions were met for a minority of capillary segments at 10X magnification, whereas the emphasis of this analysis is capillary-RBC hemodynamics.

2.2.6 Calculation of capillary diameter and hematocrit

Capillary hematocrit was calculated from the experimentally-derived LD parameter using the equation: $Hct = \frac{LD * RBC_{vol}}{\pi r^2} * \frac{1mm}{1000\mu m}$, whereby RBC_{vol} is the reported mean volume of a rat erythrocyte (65 μm^3, Canham *et al.*, 1984), and r is the capillary radius (μm). Because vessels will blur and over-estimate capillary radius when they are not crisply in focus, all capillary radii above 3μm were set to 3μm (i.e. capillary diameter 6μm), consistent with values reported in the literature [39, 83, 96]. Hematocrit is calculated for physiological reference only since it is sensitive to this focus artifact. LD is used for quantitative analysis in this study as a more reliable empirical measurement.

2.2.7 *Spatial and temporal classification of capillary modules in the Capillary Fascicle*

As illustrated in Figure 2.2, capillary segments were assigned a nomenclature to group them within a module, and the modules are numbered within the CF for each capillary network. When the same capillary segment is measured in more than one video (e.g. at different z-planes or overlapping FOVs) the summary hemodynamics from each 2-minute video are averaged to create a composite mean for the capillary segment. Temporal heterogeneity between repeated capillary measurements was represented as the

%normalized range of 2-minute summary values compared to the composite mean for the

capillary segment: $\frac{max-min}{mean} * 100$.
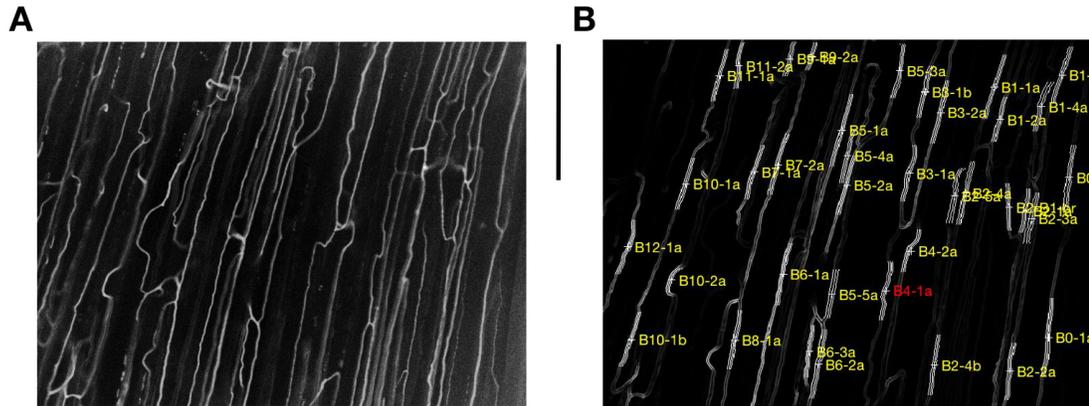
Figure 2.2: Capillary-RBC hemodynamic analysis of the Capillary Fascicle.
Functional images derived from intravital videomicroscopy (A) guide the analysis using custom software. Capillary segments are selected (B) and assigned a nomenclature to record their spatial location inside capillary modules. Frame-by-frame analysis is performed over the 2-minute video recording, generating summary hemodynamics for RBC velocity (µm/s), lineal density (RBC/mm), and RBC supply rate (RBC/s). This particular field of view yielded over 30 capillary segments for analysis. Scale bar = 250 µm.

Spatially-distinct and temporally-resolved capillary segments with corresponding RBC-capillary hemodynamics were sorted into capillary modules for each CF network. Mean module hemodynamics represent the average values for all segments within a CM, as well as a coefficient of variation (%CV) representing the spatial distribution of hemodynamics between capillary segments. RBC transit time for a module (seconds) is estimated as $\frac{Length}{(V_{rbc})_{mean}}$, where $(V_{rbc})_{mean}$ is the mean RBC velocity for capillary segments in the module.

2.2.8 Capillary module RBC supply rate

Capillary module RBC supply rate (SR$_{module}$, RBC/s) represents the total number of RBCs flowing through a CM per second, and is an important metric when considering convective oxygen transport in the CF [38]. Ideally, SR$_{module}$ would be calculated with perfect accuracy by measuring RBC flow for all capillary segments arising from the TA, all capillary segments draining to the PCV, or by resolving the mass balance for converging and diverging bifurcations inside the module. However, this was rarely possible due to technical and time constraints with video acquisition. SR$_{module}$ was therefore approximated from experimental data with the equation: $SR_{module} = (SR_{rbc})_{mean} * N_{par}$, whereby $(SR_{rbc})_{mean}$ is the mean RBC supply rate for capillary segments in the module, and N_{par} is the number of parallel capillaries in the module (see above). Note that due to internal bifurcations, the number of segments in a module is almost always greater than the number of parallel capillaries, and that experimental sampling of capillary segments is incomplete. Both of these circumstances lead to sampling error when calculating SR$_{module}$ from experimental data, with this error being minimized by increasing the number of measured segments.

The amount of error from under-sampling of capillary segments to estimate SR$_{module}$ was quantified with a series of synthetic CMs and a dual-phase mathematical blood flow model developed by Goldman and Popel [47] using established rheological properties [86, 87]. Experimental "coverage" for each module was defined as the ratio of

measured segments to parallel capillaries (N_{par}): for example, 11 capillary segments measured from a module with 8.33 parallel capillaries would have 132% coverage; 8 capillary segments measured from a module of 10 parallel capillaries would have 80% coverage.

Three synthetic CM geometries were generated to approximate the mean dimensions of length, width, and N_{par} from the experimental data (Figure 2.3). The number of internal bifurcations (converging and diverging) for the three CMs was 8, 9, and 10, respectively, and all modules had more capillary segments than parallel capillaries. We sampled all combinations of segments at increasing levels of experimental coverage (10%-150%) to generate a hypothetical dataset from the CMs. The estimated SR_module was calculated with the same equation used for the experimental data: $SR_{module} = (SR_{rbc})_{mean} * N_{par}$. These values were compared with the true SR_module from the model, and establish a degree of sampling error for various levels of coverage. We hypothesize that at least 67% coverage is required to ensure the accuracy of SR_module values included in the final dataset.
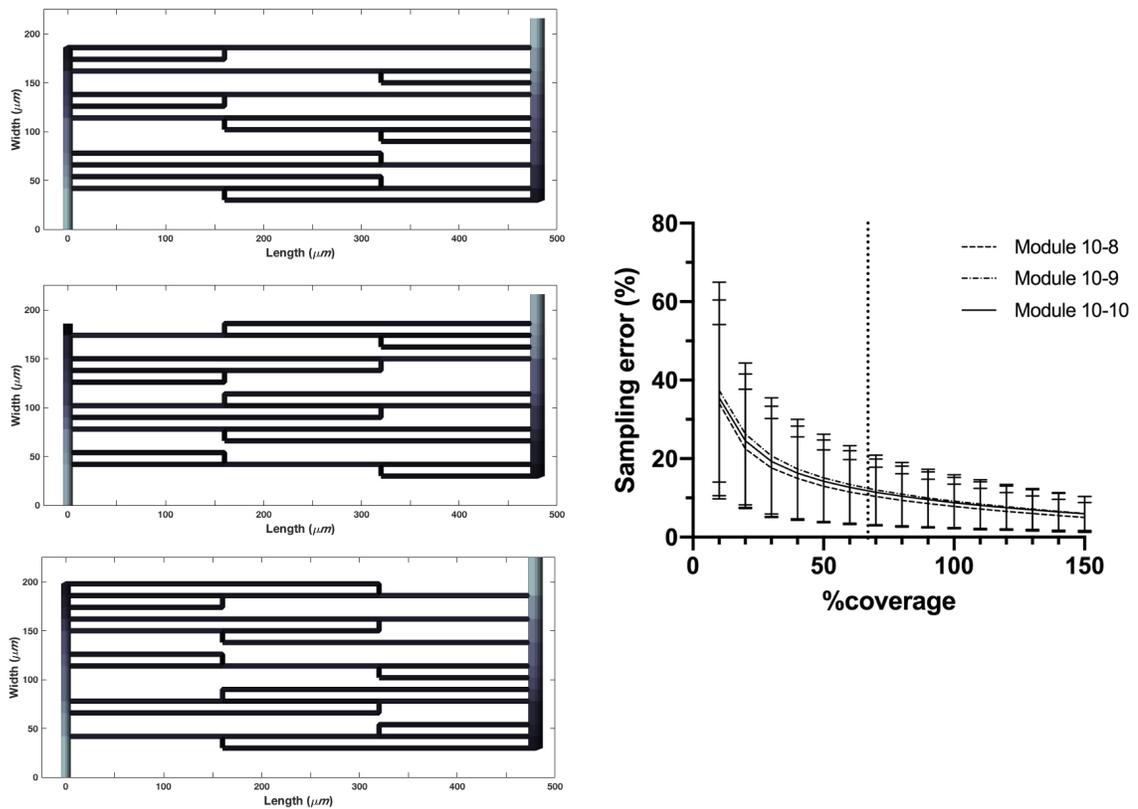
Figure 2.3: Three synthetic capillary modules used to estimate the error from experimental under-sampling

Synthetic modules were generated with the same approximate dimensions (length, width, parallel capillaries) as the average module from the dataset; dual-phase mathematical blood flow model is applied. Blood flow is from terminal arteriole (bottom left), through the capillary module, and to the post-capillary venule (top right). Increasing levels of experimental coverage reduce the sampling error when calculating total capillary module RBC supply rate (SR$_{module}$), with a 67% sampling threshold (hashed line) yielding a mean error of approximately 12%. Data presented as mean +/- SD.

2.2.9 Statistical methods

Datasets were summarized with descriptive statistics (PRISM Graphpad v8), including frequency distribution, mean and standard deviation (SD), median and interquartile range, and coefficient of variation ($\%CV = \frac{SD}{mean} * 100$). Mean capillary

density of the CMs was compared between EDF and non-EDF networks using student's

unpaired t-test. Correlation between systemic parameters (MAP, pO2) and mean SR_{rbc} for

the animals was analyzed with simple linear regression. Correlation was reported as a

slope, [95% confidence interval], and the coefficient of determination (R^2) that defines the

proportion of variance in the dependent variable that can be attributed to the predictor.

Lines of regression are plotted only for figures with significant correlation.

Linear mixed effects regression was used to evaluate the relationships between

hemodynamic variables and topological features in the CF. Simple linear regression from

the pooled dataset would incorrectly assume that all capillaries and CMs are independent

measurements, when in reality they were derived from a small group of animals. To

account for repeated measures from the same animal and biological variability between

animals, a linear mixed effects model was used (SPSS v26). The fixed effect defines the

correlation across all measurements, and the random effect (random slope and random

intercept) allows different lines of regression for each animal. R^2 for linear mixed effects

models has been adapted by Nakagawa and colleagues [70]:

$$R^2 = \frac{\sigma_f{}^2}{\sigma_f{}^2 + \sigma_\alpha{}^2 + \sigma_\epsilon{}^2}$$

Whereby $\sigma_f{}^2$ is the variance of the fixed predicted values, $\sigma_\alpha{}^2$ is the variance of the random

effects, and $\sigma_\epsilon{}^2$ is the variance of the residuals in the model. This R^2 for linear mixed

effects models represents the proportion of variance explained by fixed factors, which

signifies the same concept as with simple linear regression.

2.3 Results

2.3.1 Animal physiology and systemic hemodynamics

Mean data (SD) are presented: Weight (g) 173.33 (10.89), Arterial blood gas analysis: pH 7.46 (0.04); pCO2 (mmHg) 40.90 (5.50); pO2 (mmHg) 89.33 (16.05); bicarbonate (mmol/L) 29.06 (2.74); lactate (mmol/L) 1.06 (0.34). Hemodynamic monitoring: mean arterial pressure (mmHg) 78.29 (9.99), range: 64.32-90.16; systolic blood pressure (mmHg) 93.36 (11.79); diastolic blood pressure (mmHg) 64.76 (10.42); heart rate (beats per minute) 384.01 (38.38). These results demonstrate adequate systemic hemodynamics, oxygenation and ventilation, and serum lactate levels indicate adequate tissue perfusion. All rats had a mean arterial pressure (MAP) greater than 60 mmHg at the time of videomicroscopy. As shown in Figure 2.4, mean capillary RBC supply rate for each animal was not correlated with MAP (linear regression: 0.06289 [-0.1906-0.3164], R^2=0.05; p=0.5759), or pO2 (linear regression: 0.01571 [-0.1453-0.1767], R^2=0.01; p=0.8241), indicating that microvascular hemodynamics are independent from systemic parameters.
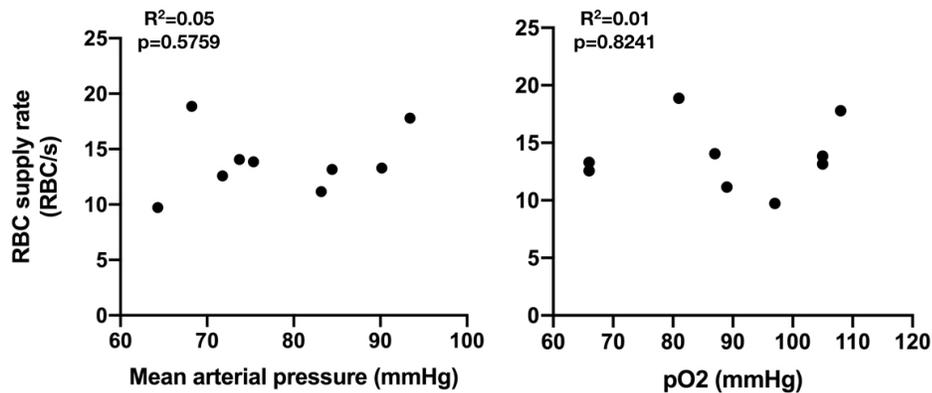
Figure 2.4: Relationship between systemic parameters and capillary-RBC hemodynamics under normal resting conditions.
Mean RBC supply rate per animal is not correlated with mean arterial pressure or arterial partial pressure of oxygen (pO2) (n=9 animals, 1491 capillary segments).

2.3.2 Capillary Fascicle structure and topology

A composite map for one representative CF network with labelled arterioles and venules is shown in Figure 2.5. Capillaries are oriented parallel to muscle fibres in continuous columns spanning thousands of microns, i.e. to the limit of observed muscle. TAs and PCVs are inserted along the columns in an alternating fashion, giving rise to the interconnected CM structure that defines the CF. The width of CF columns can be one or multiple CMs across. The border of each fascicular column is noted with a distinct longitudinal tissue gap and lack of capillary vascularity, whereas CMs within the same CF column are in closer horizontal proximity. The insertions of microvessels into the CF appears coordinated, insofar as TAs and PCVs are partially aligned between adjacent modules and columns. Most capillaries in a module will drain into a PCV, but a small

minority of capillaries bridge vertically between modules and bypass the PCV. The collecting venule system that drains the CF is visible in the background of the EDF image, whereas the arteriolar system that supplies the CF is not evident since it originates deeper in the tissue.
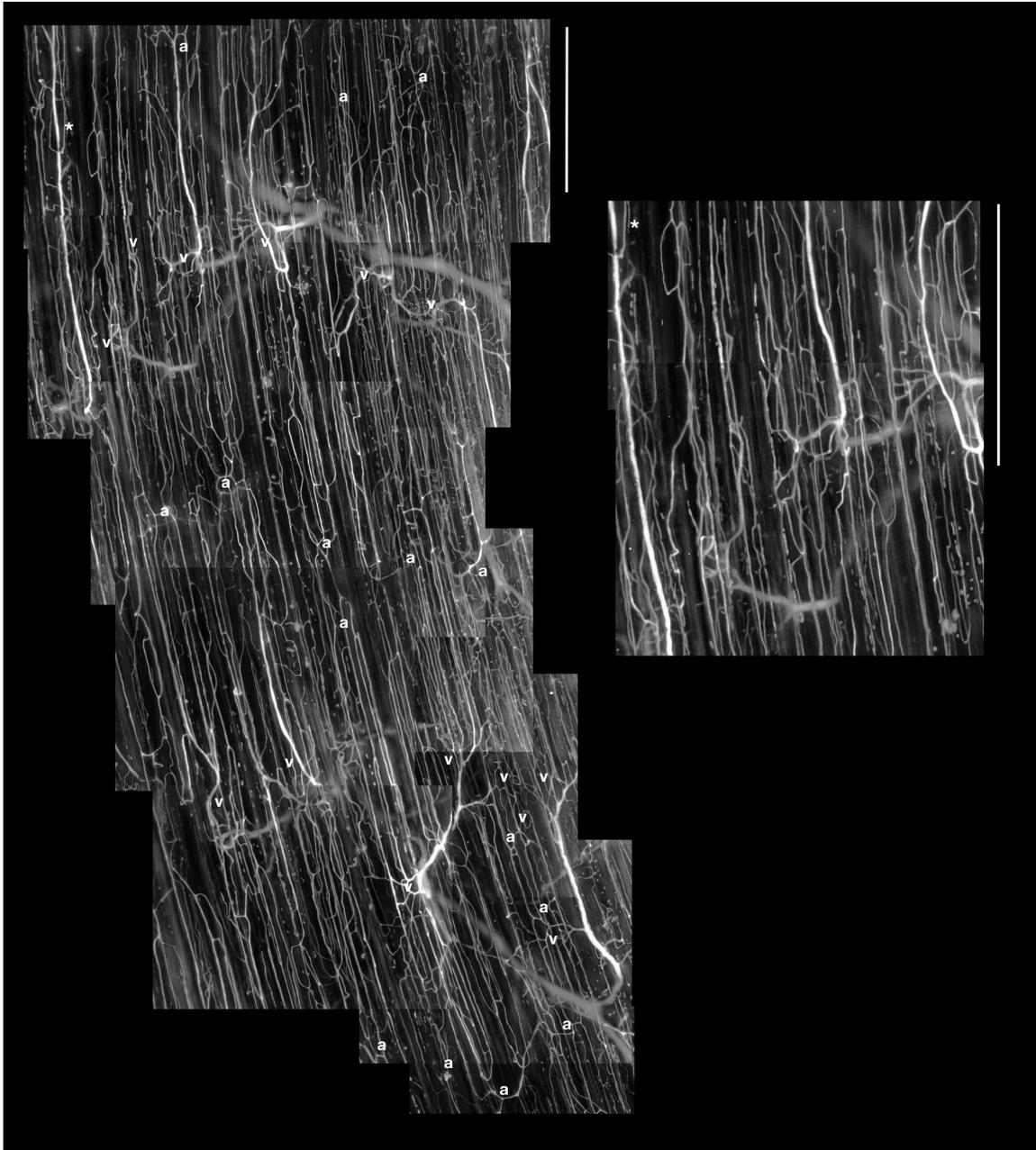
Figure 2.5: Capillary Fascicle (CF) in the rodent extensor digitorum longus muscle. Functional images are derived from 10X intravital videomicroscopy (inverted microscope, Olympus IX81) and stitched together to generate capillary networks. Filter applied to the image to enhance contrast between vessels and background tissue. The CF is a series of interconnected capillary modules forming continuous columns spanning thousands of microns that align naturally with the dimensions of the muscle fascicle. Zoomed section (*) highlights the tissue gaps between CF columns. Arterioles (a) and venules (v) are inserted into the CF in an alternating fashion with partial alignment across the muscle. Collecting venule system is visible in the background of the image. Scale bar = 500μm

Geometric and topological parameters of the capillary modules (n=9 networks, 327 modules) are reported in Table 2.1. The dimensions of the "average module" for the dataset are length 481μm, width 157μm, and 9.51 parallel capillaries. The 90th percentile for module length and width are 716μm, and 240μm, respectively; 90th percentile for N_{par} is 15.03 parallel capillaries. Spatial heterogeneity of module dimensions, as determined by %CV, is lowest for capillary density (23%) and highest for CM volume (56%). On average, there are more capillaries on the venular end of the module than arising from the arteriole, represented by a mean PCV/TA ratio of 1.24, although this ratio was inverted for 17% of the modules.

	No. of measurements	Mean (SD)	%CV
Module Length (μm)	247	481.07 (174.22)	36.22
Module Width (μm)	316	157.00 (53.41)	34.02
Module volume (mm³)	242	0.0078 (0.0044)	55.99
N_{par} (#)	248	9.51 (4.09)	43.01
Capillary v/a ratio	202	1.24 (0.35)	28.61
Capillary density (cap/mm²)	247	579.14 (131.49)	22.70

Table 2.1: Geometric and topological classification of capillary modules in the Capillary Fascicle.
Module dimensions (length, width, volume) are derived from nine networks, and module topology (parallel capillaries, capillary density) is derived from seven networks with extended depth of focus protocol. N_{par} denotes the number of parallel capillaries in a module. Capillary v/a ratio denotes the ratio of capillaries at the venular vs arteriolar end of the module. Capillary density is analogous to 2D capillary density derived from cross-sectional muscle histology.

Because of the orientation of capillaries parallel to muscle fibres, there is a strong correlation between module width and N_{par} (linear mixed effects: 0.0583 [0.0521, 0.0645], R^2=0.70, p<0.0001) indicating that wider modules will have more parallel capillaries; however, there is no correlation between module width and capillary density (linear mixed effects: 0.0252 [-0.2915, 0.3418], R^2=0.01, p=0.8758). There is no correlation between module length and N_{par} (linear mixed effects: 0.0015 [-0.0013, 0.0044], R^2=0.01, p=0.2929) or capillary density (linear mixed effects: 0.0640 [-0.0321, 0.1601], R^2=0.01, p=0.1904).

To evaluate the utility of the EDF protocol for registering more vessels in the functional image, N_{par} and capillary density was compared from modules with EDF protocol (n=7 networks, 248 modules) versus the non-EDF modules (n=2 networks, 69 modules). As shown in Figure 2.6, the EDF protocol substantially increased N_{par} (student's unpaired t-test: 9.51 vs 5.72, mean difference = 3.79 [2.80, 4.79]; p<0.0001) and capillary density (students unpaired t-test: 579.14 vs 428.28, mean difference = 150.87 [117.28, 184.44]; p<0.0001). These data support the use of EDF as an augmented label-free method for measuring Capillary Fascicle topology with intravital videomicroscopy.
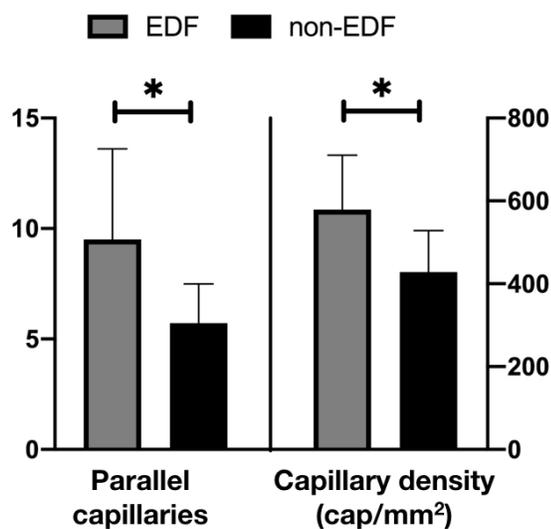
Figure 2.6: Comparison of extended depth of focus (EDF) versus non-EDF functional images.
Capillary modules quantified from EDF images (n=248) had significantly more parallel capillaries and higher capillary density when compared with non-EDF modules (n=69). Data are presented as mean and SD; * p<0.0001.

2.3.3 Capillary-RBC hemodynamics

Capillary-RBC hemodynamics for V_{rbc}, LD, and SR_{rbc} (n=9 networks, 1491 segments) are reported in Table 2.2 with corresponding histograms in Figure 2.7. Mean capillary hematocrit is 13.19% (6.56) for resting capillaries in rodent EDL muscle. There is a bimodal distribution of RBC velocity measurements, with a main peak approximately around 200 μm/s and a second peak around 600 μm/s. Capillary LD follows approximately normal distribution and SR_{rbc} is a right-skewed distribution. In total, there were 130 stopped-flow capillaries, representing an additional 8.72% above the quantified dataset of perfused capillaries.

		No. of measurements	Mean (SD)	%CV
Capillary segments	V_{rbc} (μm/s)	1491	245.40 (147.4)	60.08
	Lineal density (RBC/mm)	1491	55.98 (24.54)	43.83
	Hematocrit (%)	1491	13.19 (6.56)	49.76
	SR_{rbc} (RBC/s)	1491	13.96 (11.63)	83.35
Capillary modules	V_{rbc} (RBC/s)	112	246.49 (91.22)	37.01
	Lineal density (RBC/mm)	112	54.54 (14.36)	26.34
	SR_{rbc} (RBC/s)	112	13.57 (5.72)	42.15
	SR_{module} (RBC/s)	89	131.49 (82.16)	62.50
	Transit time (s)	100	2.43 (1.21)	49.86

Table 2.2: RBC-capillary hemodynamics for the Capillary Fascicle in resting extensor digitorum longus muscle.

RBC velocity (V_{rbc}), lineal density, and RBC supply rate (SR_{rbc}) are recorded for at least 2 minutes from capillary segments using dual-wavelength intravital videomicroscopy (n=9 networks). Capillary segments are grouped into capillary modules, and mean hemodynamics are reported for modules with at least 67% experimental sampling.
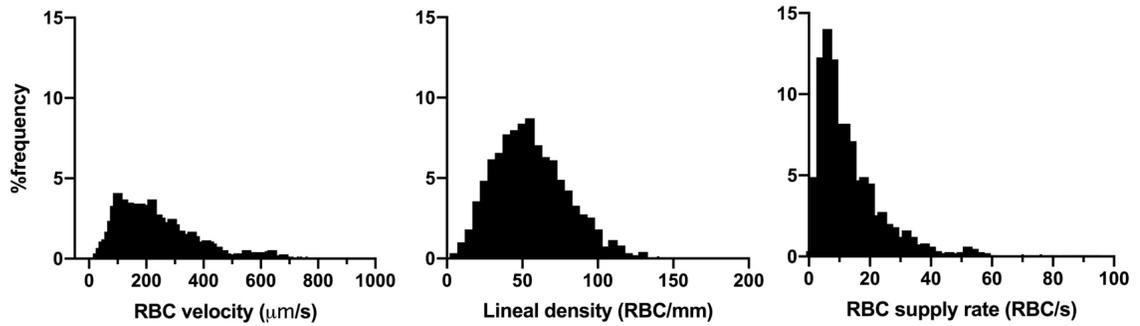
Figure 2.7: Frequency distribution for capillary-RBC hemodynamics in the Capillary Fascicle

Correlation between primary capillary-RBC hemodynamic variables is shown in Figure 2.8. SR_{rbc} is correlated with V_{rbc} (linear mixed effects: 0.0601 [0.0549, 0.0653], R^2=0.61, p<0.0001) and LD (linear mixed effects: 0.2810 [0.2291, 0.3329], R^2=0.36, p<0.0001), which is not surprising given the multiplicative relationship between these three variables (SR_{rbc}=V_{rbc} x LD). Interestingly, there is no correlation between V_{rbc} and LD for the capillary segments (linear mixed effects: 0.0113 [-0.0006, 0.0231], R^2=0.01, p=0.0601), signifying that these hemodynamic variables are independent when evaluated in large capillary datasets; this is demonstrated as a random scatter plot.
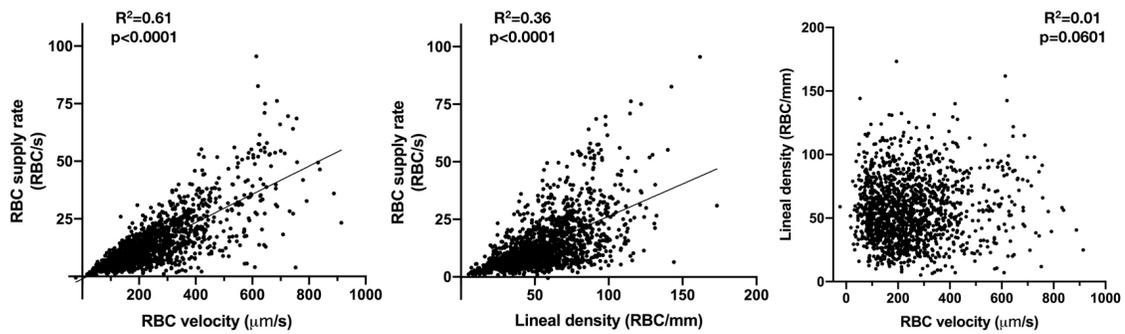
Figure 2.8: Correlation for capillary-RBC hemodynamics in the Capillary Fascicle. There are significant linear correlations between RBC velocity, lineal density, and RBC supply rate. However, RBC velocity and lineal density are not correlated with each other (n=9 networks, 1491 capillary segments).

Temporal variation in capillary-RBC hemodynamics was assessed for 561 capillary segments in the dataset with repeated 2-minute video measurements. As shown in Figure 2.9, there is moderate but persistent temporal variation in the 2-minute mean capillary hemodynamics, as indicated by a median %variability for V_{rbc} 25% (11-44), LD 20% (8-36), and SR_{rbc} 29% (14-52). A subset (15-25%) of capillary segments demonstrated temporal variation greater than 50%, indicating a subpopulation of segments with substantial changes in hemodynamic values between repeated measurements.
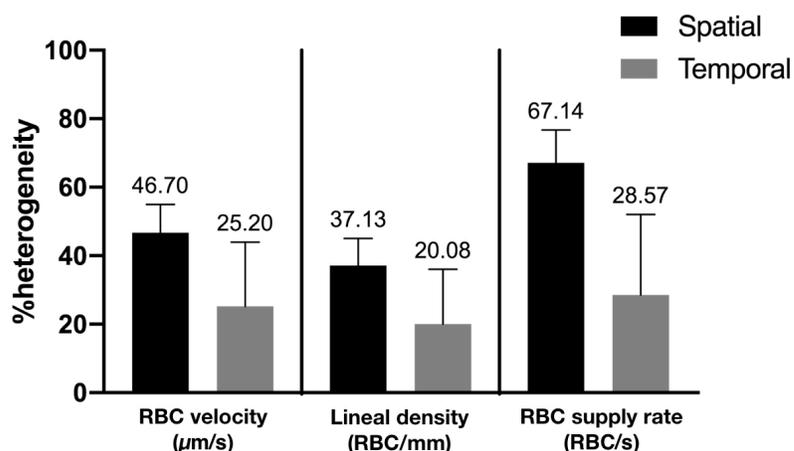
Figure 2.9: Spatial and temporal heterogeneity of capillary segments in the Capillary Fascicle.
Spatial heterogeneity is defined as the %CV of capillary segment hemodynamics within a module (n=9 networks, 112 modules, 967 segments). Temporal heterogeneity is defined as the %normalized range of summary hemodynamics between repeated 2-min measurements of the same capillary segment (n=9 networks, 561 segments). Data presented as median and interquartile range.

2.3.4 Capillary module hemodynamics

Sampling error for SR$_{module}$ with increasing level of coverage was calculated for three synthetic CMs, and reported in Figure 2.3. Mean error for modules greater than 67% coverage was low (12%), supporting the use of this threshold for accurate calculation of module hemodynamics.

Capillary segments were spatially organized to generate mean module hemodynamics (i.e. average hemodynamics for the capillary segments in the module). In this dataset, 112 modules (n=9 networks, 967 segments) had at least 67% coverage, with a median of 7 (5-11) capillary segments measured per module. Mean module hemodynamics were not different to values derived from capillary segments (Table 2). Mean RBC transit

time per module is 2.43 (1.21) seconds (n=9 networks, 100 modules); SR_{module} is 131.49 (82.16) RBC/s, calculated from modules with at least 67% coverage and EDF protocol (n=7 networks, 89 modules, 851 segments).

Spatial heterogeneity for capillary-RBC hemodynamics was calculated as %CV for capillary segments in a module (n=9 networks, 112 modules, 967 segments). As shown in Figure 2.9, CMs demonstrate significant spatial heterogeneity, indicated by median %CV values of V_{rbc} 47% (34-55), LD 37% (28-45), and SR_{rbc} 67% (50-77). As shown in Figure 2.10, %CV was not correlated with the mean module hemodynamics for V_{rbc} (linear mixed effects: 0.0173 [-0.0137, 0.0483], R^2=0.01, p=0.2703) or LD (linear mixed effects: -0.1310 [-0.3086, 0.0466], R^2=0.02, p=0.1466) and weakly correlated with SR_{rbc} (linear mixed effects: 0.9061 [0.0283, 1.7839], R^2=0.06, p=0.0451). This data signifies that capillary modules in resting skeletal muscle have similar degrees of spatial heterogeneity regardless of mean module hemodynamics.
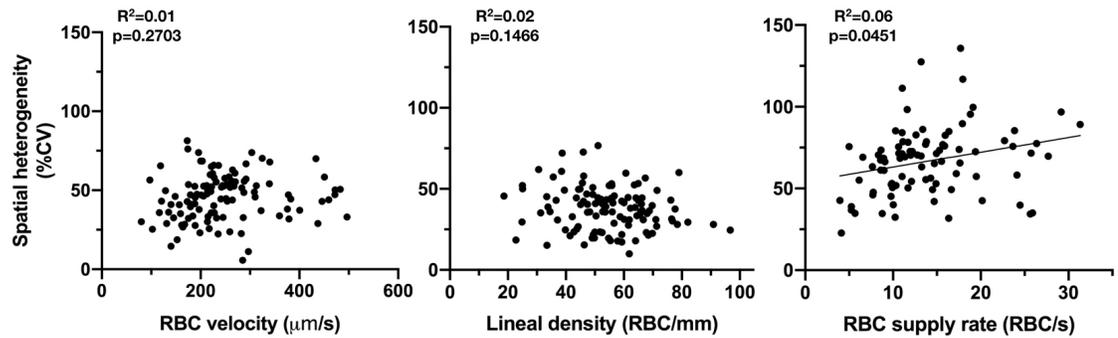
Figure 2.10: Capillary module spatial heterogeneity versus mean module hemodynamics. There is no correlation for RBC velocity and lineal density, and weak positive correlation for RBC supply rate.

2.3.5 Structure-function relationships in the Capillary Fascicle

The correlation between CM topology (width, length, N_{par}) and module hemodynamics (V_{rbc}, LD, SR_{rbc}, and SR_{module}) was examined in the CF. There was no correlation between module width and mean module hemodynamics (linear mixed effect: V_{rbc} 0.0510 [-0.2648, 0.3668], R^2=0.01, p=0.7496; LD 0.0155 [-0.0440, 0.0751], R^2=0.01, p=0.6035; SR_{rbc} 0.0089 [-0.0116, 0.0294], R^2=0.01, p=0.3925).

Module length and N_{par} (i.e. parallel flow paths) are major determinants of hemodynamic resistance for a capillary module. As indicated in Figure 2.11, neither variable was a substantial predictor of mean module hemodynamics. Module length was not correlated with V_{rbc} (linear mixed effects: 0.0671 [-0.0192, 0.1533], R^2=0.02,

p=0.1259) or LD (linear mixed effects: 0.0095 [-0.0058, 0.0248], R^2=0.02, p=0.2010), and weak positive correlation with SR_{rbc} (linear mixed effects: 0.0075 [0.0017, 0.0132], R^2=0.05, p=0.0112). N_{par} was not correlated with mean module hemodynamics (linear mixed effects: V_{rbc} 0.9489 [-3.9070, 5.8048], R^2=0.01, p=0.6986; LD 0.1745 [-0.8272, 1.1762], R^2=0.01, p=0.7219; SR_{rbc} 0.1603 [-0.1905, 0.5112], R^2=0.01, p=0.3446). Together, this data indicates that module RBC hemodynamics in resting skeletal muscle are largely independent from module resistance.

SR_{module} is not correlated with module length (linear mixed effects: 0.0877 [-0.0084, 0.1838], R^2=0.04, p=0.0727). However, SR_{module} is strongly correlated with N_{par} (linear mixed effects: 15.5121 [11.4855, 19.5387], R^2=0.60, p<0.0001) and module width (linear mixed effects: 0.9145 [0.6341, 1.1949], R^2=0.38, p<0.0001). This is to be expected given that module width and N_{par} are topologically related, and N_{par} is used directly to calculate SR_{module}.
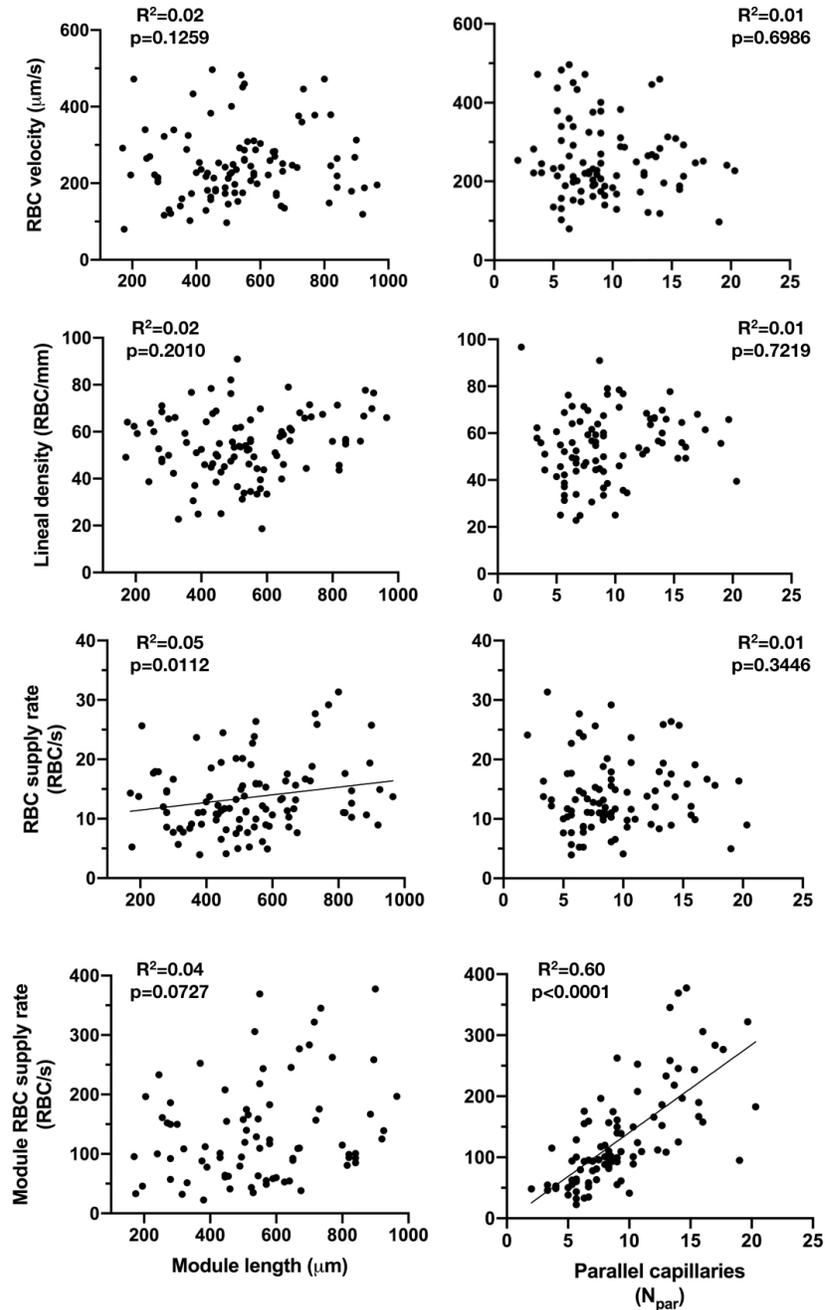
Figure 2.11: Structure-function relationships for capillary modules in the Capillary Fascicle.

There is no correlation between module length, mean RBC velocity, and lineal density. There is weak correlation between module length and mean RBC supply rate, and no correlation with total module RBC supply rate. Similarly, there is no correlation between the number of parallel capillaries in a module (N_{par}) and mean module RBC velocity, lineal density or RBC supply rate. There is a strong correlation between N_{par} and total module RBC supply rate.

2.4 Discussion

This analysis of capillary-RBC hemodynamics is the largest experimentally-derived dataset and largest network imaging to date of *in vivo* RBC perfusion in skeletal muscle. The Capillary Fascicle is introduced as an updated paradigm for describing blood flow in capillary networks. By linking capillary modules together into columns, the CF supports blood flow over thousands of microns, thereby providing a physiologically-grounded framework for oxygen exchange with surrounding muscle tissue. The CF exhibits structural and functional heterogeneity at different levels of scale, and network-level analysis of structure-function relationships provides direct evidence for microvascular flow regulation at the level of the capillary module. The findings of the current study inform a significant shift regarding how capillary-RBC perfusion is characterized in skeletal muscle. Previous *in vivo* and histological analysis has focused on the relationship between individual capillaries and single muscle fibres. Rather, within the CF paradigm, the columns of interconnected CMs interface naturally with the dimensions of the muscle fascicle comprised of numerous muscle fibres, and the muscle fascicle becomes the target volume of tissue for oxygen delivery by the microcirculation.

The columnar ultrastructure of the CF in skeletal muscle, illustrated in Figure 2.1 and Figure 2.5, organizes capillary networks on the intermediate scale (mesoscale), providing a conceptual bridge between individual capillary segments, capillary modules, and whole-organ perfusion [94]. Although this current study does not directly visualize muscle fibres and fascicle boundaries, certain anatomical relationships can be inferred: the CF is supported by the endomysium surrounding individual muscle fibres [10], with similar

vascular columns observed in the endoneurium of peripheral nerves [66]; the perimysium is a clear boundary of the muscle fascicle that necessitates penetrating vessels to connect the CF with higher-order arterioles and venules between fascicles. It has been proposed that 3D characterization of capillary network structure from tissue histology is more accurate than standard 2D cross-section for evaluating capillary-myocyte interactions and oxygen exchange with surrounding muscle tissue [13, 35, 104]. In this regard, the CF will inform future analysis and computational modeling to better understand how the microcirculation delivers oxygen to a muscle fascicle.

The quantitative capillary-RBC hemodynamics for resting skeletal muscle in the current study are within the physiological range expected in rodent models, and are in agreement with previously reported literature [2, 3, 5, 17, 29, 31, 37, 56, 57, 71, 91, 92, 101]. These metrics were independent from systemic blood pressure or oxygenation in the present cohort over a wide range of values (Figure 2.4), signifying the microcirculation as a distinct hemodynamic compartment of the cardiovascular system with capacity for autoregulation. Capillary networks exhibit a significant reduction in microvascular hematocrit compared with systemic values, that can be explained by the "network Fahraeus effect" [85] observed experimentally in this study, and others mentioned above. Topological analysis of the CMs in the rat EDL reveal mean length and width of CMs in our study that are less than those reported previously for hamster tibialis anterior and retractor [33, 64] and other species [10], but correspond with the dimensions reported by our group using the rat EDL [39]. Capillary density measurements are concordant with those reported by some groups [103], while others have reported values lower [68], or higher [20, 21]. These differences can likely be explained by calculations in this study

derived on the basis of individual modules (as opposed to tissue histology of large sections of muscle), the uniform estimation of muscle depth, and the location of our microscopy in the distal and superficial portion of the muscle.

More important, however, than mean values is the marked heterogeneity for capillary-RBC hemodynamics and CM topology that exists within these capillary networks. The wide dispersion implies that summary network values are unlikely to convey the true complexity of the system [88], and might lead to inaccurate assumptions if applied uniformly in analysis or modeling. In this study, a similar degree of spatial heterogeneity in capillary-RBC hemodynamics is evident among capillaries within the dataset, modules within the dataset, and capillaries within a module – as indicated by the %CV values in Table 2.2 and Figure 2.9. The degree of spatial heterogeneity inside a module is also independent of the mean module hemodynamics (Figure 2.10), perhaps determined by module topology such as internal converging and diverging bifurcations. This analysis reinforces that heterogeneity is an intrinsic feature of microvascular physiology, and conveys the properties of scale-invariance and self-similarity in the CF that are often observed in fractal systems such as the microcirculation [45, 46]. This heterogeneity extends not only in space, but also as a function of time (Figure 2.9), even when comparing averages from 2-minute videos for capillary hemodynamics. Taken together, this data underscores the value of spatially-resolved classification and prolonged recording of experimental data, and will inform future experimental approaches and modeling design for evaluating capillary networks.

Understanding the physiological heterogeneity of RBC distribution in capillary networks under normal resting conditions is essential for comparison with exercise and disease states. A muscle fascicle contains dozens to hundreds of myocytes of varying fibre types and sizes, with differing basal levels of oxygen metabolism and supply-demand (i.e. QO_2/VO_2) ratios for matching blood flow in adjacent capillaries [58, 60]. Moreover, motor units comprise muscle fibres that are dispersed throughout the fascicle, resulting in heterogenous patterns of activation during locomotion [11, 34]. The CF is therefore ideally designed in a modular fashion to accommodate this metabolic heterogeneity, comprised of CMs with differing sizes, capillary densities, and rates of blood flow; this allows for spatially-resolved supply-demand matching of oxygen delivery between the CF and surrounding muscle tissue [52]. Given the irregular shapes, sizes, and fibre composition of muscle fascicles, it is unclear how many capillary fascicles are associated with each muscle fascicle. This is particularly relevant when considering the difference in structure between longitudinal muscles such as the extensor digitorum longus used in this study, and more planar muscles such as the spinotrapezius. While the columnar structure of the CF would be maintained in both cases given the association with linear muscle fibres, it is likely that muscle architecture is a major determinant of CF structure; this should be further explored with dedicated *in vivo* labelling for connective tissue and fibre type.

The contiguous CF structure, visualized in this study using advanced label-free videomicroscopy techniques, and the low number of stopped-flow capillaries (8.72%), confirms that the overwhelming majority of capillaries in skeletal muscle support RBC perfusion at rest. However, the lack of correlation between capillary RBC velocity and lineal density over the large dataset (Figure 2.8), and significant heterogeneity of capillary-

RBC hemodynamics within a module (Figure 2.9), implies a degree of stochasticity and the absence of flow regulation on the level of individual capillaries. This is possible because capillary segments within a module support diffusional O_2 exchange between themselves, such that segments with generous RBC supply rate can offload oxygen to surrounding capillaries with low perfusion [47, 48, 75]. Notably, the mitochondrial and myoglobin systems also form reticular lattices within and between myocytes [14, 44], and participate to distribute oxygen exchange and oxidative capacity throughout large volumes of muscle tissue according to locoregional metabolic demands. These factors together, as well as low O_2 extraction fraction and intact O_2 regulation mechanisms [32], make it unlikely that heterogeneity in RBC distribution will cause dysoxia within healthy resting skeletal muscle [40]. Rather, heterogeneous capillary-RBC perfusion in the Capillary Fascicle should be viewed as a normal feature of these complex non-linear systems, and reflects the capacity of the network to adapt to external stressors or changes in energy requirements [95].

By contrast, exercise will increase capillary perfusion to support increased O_2 metabolism and decrease network heterogeneity [27, 100], such that capillaries – even those with negligible perfusion at rest – approach systemic hematocrit levels and maximal RBC supply rate [78]. Experimental data [3, 22, 29, 31, 59, 71, 72] and computational modeling [40, 48, 49, 82] from disease states (e.g. sepsis, ischemia, heart failure, diabetes) has shown that pathological changes in capillary flow heterogeneity can result in substantial changes in tissue oxygenation and O_2 utilization, and this relationship is also affected by total flow and tissue O_2 consumption rate. By contrasting disease models with the dataset provided in this study, future research can delineate what features constitute

pathological heterogeneity, the mechanisms responsible for these observations, and how they might be ameliorated with therapeutic interventions.

The strength of the current study is the linkage of network topology and hemodynamics by grouping capillary segments into modules, the large number of CMs included in the dataset, and the statistical treatment of repeated measures. These factors provide an opportunity to evaluate network-level physiological relationships in the CF. Using this approach, emergent properties of the biological system are identified that would not be evident from microscopic or macroscopic scales or from individual components [1, 6], such as when considering small groups of capillaries [4, 39, 63], or the total of all capillaries within an organ [43, 50]. For example, due to changes in CM hemodynamic resistance, a passive microvascular system without flow regulation would yield an inverse relationship between module hemodynamics and module length, and positive relationship with the number of parallel capillaries (due to increased parallel flow paths). Remarkably, these relationships are absent in our dataset (Figure 2.11), and could never have been predicted when considering modules in isolation. In fact, module length in the dataset exhibits a weak positive correlation with mean SR_{rbc} (i.e. longer modules have slightly higher mean RBC supply rate), which is the opposite of what would be expected from a passive system.

Because these passive relationships are not observed, the findings from this study provide direct evidence for active microvascular flow regulation at the level of the capillary module; importantly, these observations are made in the absence of local pharmacological interventions (e.g. vasoconstrictors, vasodilators, channel inhibitors) or electrical

stimulation that directly influence capillary-RBC hemodynamics in skeletal muscle. When considering Ohm's law, it becomes apparent that this is best achieved through regulation of capillary module perfusion pressure (ΔP) for a wide range of hemodynamic resistances; this strategy adjusts total module RBC supply rate (SR_{module}) to support oxygen exchange with the surrounding muscle fascicle. By linking modules together to form expansive columns, the CF is able to control blood flow within discrete sections of tissue, yet this also explains why capillary networks can be viewed as space-filling above certain cutoff lengths [62]. Although direct manipulation of module resistance (e.g. via pre-capillary sphincters or metarterioles) could theoretically yield similar results, this would require an enormous amount of finite control at the capillary level and the presence of these contractile structures in skeletal muscle is not supported by empirical observations [90]. As noted above, diffusional oxygen exchange between capillary segments also obviates the need for hemodynamic control of individual capillaries. This interpretation of the data is consistent with the theory that capillary perfusion pressure (ΔP) and hydrostatic pressure (P_C) are regulated together [18], and supports the theory of capillary networks as the origin for the stimulus of microvascular flow regulation [30, 69], with the primary goal to ensure adequate oxygen delivery. Evidence in the literature clearly demonstrates the ability of stimulated capillary networks to elicit a flow response from the arteriolar tree [7, 16, 23, 24] and further mechanistic studies suggest this is achieved through conducted signaling via endothelial gap junctions between capillaries and arterioles [15, 25, 99], and O_2-dependent ATP release from RBCs in capillary networks [30, 32].

The Capillary Fascicle is ideally suited for signaling changes in tissue metabolic demand to the arteriolar system given the intimate relationship with the muscle fascicle. However, the CF structure raises important questions regarding how this flow regulation is accomplished. The insertion of terminal arterioles into CF columns will arise from different sections of the arteriolar tree [33], with higher pressure from the proximal arteriolar system potentially creating a gradient along the length of the column. It has been proposed that interconnected CMs are conducive to smoothing pressure variability arising from TAs and PCVs inserted into the CF, particularly if these vessels become suddenly occluded [96]. Furthermore, TAs simultaneously feed multiple CMs with different resistances, implying that a TA hyperemic response would preferentially "steal" towards the module with lower resistance, while depriving the other module of adequate blood flow. These factors together would suggest the need for both pre-capillary and post-capillary mechanisms of flow regulation to ensure ΔP is maintained across the CM within a physiological range; post-capillary regulation would ensure blood flow is distributed correctly between two modules with shared TA by independently regulating ΔP for each module. There is already evidence for active dilation of venules following stimulated contraction in rodent skeletal muscle [65], and for myogenic responses from isolated venules that are modulated by norepinephrine and removal of the endothelium [26]; these observations have not been resolved at the level of CMs or the CF. Venules possess all of the necessary components required to participate in microvascular flow regulation, including sympathetic innervation, vascular smooth muscle, endothelial gap junctions, nitric oxide, and ion channels [67]. Currently, this hypothesis is not well-established, and requires exploration and validation with more empirical evidence.

Experimental limitations of this study should be noted. Anesthesia has an effect on systemic hemodynamics and will modulate, but not obliterate, local mechanisms of flow regulation (particularly sympathetic tone). In this regard, we can expect that mean values and degree of heterogeneity may differ between anesthetized and awake animals; nevertheless, the main findings regarding CF structure, intrinsic heterogeneity, length-independence of capillary-RBC module hemodynamics, and the implications for capillary flow regulation should be maintained. The absence of correlation over a wide range of systemic hemodynamics (MAP, pO2) in this cohort supports pooling of data and the generalization of our findings, especially given the statistical treatment of between-subject variability; however, direct evaluation of how these systemic variables may affect capillary-RBC hemodynamics is better tested using controlled interventions (e.g. hypovolemia, adjustment of ventilation) and repeated measurements in the same animal. Capillary hemodynamics were not collected from segments with excessive hematocrit or RBC velocity, causing a selection bias that under-represents these capillaries within the dataset. To minimize the error associated with incomplete capillary sampling, calculations of module hemodynamics were restricted to modules with at least 67% coverage. The decision to capture video sequences at 10X magnification to acquire capillary hemodynamics data from as many segments as possible meant we were unable to consistently measure RBC O_2 saturation. Although video sequences were captured at both wavelengths for O_2 saturation analysis, the spatial resolution of the cameras at 10X magnification was not sufficient to make accurate measurements on more than a small subset of capillary segments. Lastly, the higher order arteriolar and venular trees are deeper in the muscle than can be resolved with our microscope, and connections into the CF are

not well delineated. It can be expected that advances in intravital videomicroscopy and other imaging modalities (e.g. laser scanning confocal microscopy, multiphoton microscopy) will overcome many of these challenges and permit future investigation of these knowledge gaps.

In conclusion, the Capillary Fascicle is an updated physiological framework for describing RBC distribution in skeletal muscle capillary networks. Fascicular columns of interconnected CMs interface naturally with muscle fascicles, strongly suggesting that the muscle fascicle is the target volume of tissue for matching O_2 supply to O_2 demand, rather than individual capillaries and muscle fibres. Network-level analysis illustrates the intrinsic heterogeneity of microvascular physiology, and provides a robust dataset in healthy resting muscle that can be compared with diseases states. Evidence of microvascular flow regulation at the level of the CM suggests that capillary networks are the primary origin for the signal that regulates flow distribution to capillary modules.

2.5 References

1.   **Aderem A** (2005) Systems Biology: Its Practice and Challenges. *Cell* 121:511–513.

2.   **Akerstrom T, Goldman D, Nilsson F, et al** (2020) Hyperinsulinemia does not cause de novo capillary recruitment in rat skeletal muscle. *Microcirculation* 27:.

3.   **Arpino J-M, Nong Z, Li F, et al** (2017) Four-Dimensional Microvascular Analysis Reveals That Regenerative Angiogenesis in Ischemic Muscle Produces a Flawed Microcirculation. *Circ Res* 120:1453–1465.

4.   **Balogh P, Bagchi P** (2017) Direct Numerical Simulation of Cellular-Scale Blood Flow in 3D Microvascular Networks. *Biophys J* 113:2815–2826.

5.   **Bateman RM, Sharpe MD, Goldman D, et al** (2008) Inhibiting nitric oxide overproduction during hypotensive sepsis increases local oxygen consumption in rat skeletal muscle. *Crit Care Med* 36:225–231.

6.   **Batterman RW, Green S** (2020) Steel and bone: mesoscale modeling and middle-out strategies in physics and biology. Synthese. https://doi.org/10.1007/s11229-020-02769-y

7.   **Berg BR, Cohen KD, Sarelius IH** (1997) Direct coupling between blood flow and metabolism at the capillary level in striated muscle. *Am J Physiol Circ Physiol* 272:H2693–H2700.

8.   **Berg BR, Sarelius IH** (1995) Functional capillary organization in striated muscle. *Am J Physiol* 268:H1215-22.

9.   **Berg BR, Sarelius IH** (1996) Erythrocyte flux in capillary networks during maturation: implications for oxygen delivery. *Am J Physiol* 271:H2263-73.

10. **Bloch EH, Iberall AS** (1982) Toward a concept of the functional unit of mammalian skeletal muscle. *Am J Physiol Integr Comp Physiol* 242:R411–R420.

11. **Bodine-Fowler S, Garfinkel A, Roy RR, Edgerton VR** (1990) Spatial distribution of muscle fibers within the territory of a motor unit. *Muscle Nerve* 13:1133–1145.

12. **Canham PB, Potter RF, Woo D** (1984) Geometric accommodation between the dimensions of erythrocytes and the calibre of heart and muscle capillaries in the rat. *J Physiol* 347:697–712.

13. **Čebašek V, Eržen I, Vyhnal A, et al** (2010) The estimation error of skeletal muscle capillary supply is significantly reduced by 3D method. *Microvasc Res* 79:40–46.

14. **Clanton TL** (2019) Managing the power grid: how myoglobin can regulate PO 2 and energy distribution in skeletal muscle. *J Appl Physiol* 126:787–790.

15. **Cohen KD, Berg BR, Sarelius IH** (2000) Remote arteriolar dilations in response to muscle contraction under capillaries. *Am J Physiol Circ Physiol* 278:H1916–H1923.

16. **Cohen KD, Sarelius IH** (2002) Muscle contraction under capillaries in hamster muscle induces arteriolar dilatation via K ATP channels and nitric oxide. *J Physiol* 539:547–555.

17. **Copp SW, Ferreira LF, Herspring KF, et al** (2009) The effects of aging on capillary hemodynamics in contracting rat spinotrapezius muscle. *Microvasc Res* 77:113–9.

18. **Davis MJ, Hill MA, Kuo L** (2011) Local Regulation of Microvascular Perfusion. In: Comprehensive Physiology. John Wiley & Sons, Inc., Hoboken, NJ, USA

19. **Delashaw JB, Duling BR** (1988) A study of the functional elements regulating capillary perfusion in striated muscle. *Microvasc Res* 36:162–171.

20. **Deveci D, Marshall JM, Egginton S** (2002) Chronic Hypoxia Induces Prolonged Angiogenesis in Skeletal Muscles of Rat. *Exp Physiol* 87:287–291.

21. **Deveci D, Marshall JM, Egginton S** (2001) Relationship between capillary angiogenesis, fiber type, and fiber size in chronic systemic hypoxia. *Am J Physiol Heart Circ Physiol* 281:H241-52.

22. **Diederich E, Behnke BJ, McDonough P, et al** (2002) Dynamics of microvascular oxygen partial pressure in contracting skeletal muscle of rats with chronic heart failure. *Cardiovasc Res* 56:479–486.

23. **Dietrich HH** (1989) Effect of locally applied epinephrine and norepinephrine on blood flow and diameter in capillaries of rat mesentery. *Microvasc Res* 38:125–135.

24. **Dietrich HH, Tyml K** (1992) Microvascular flow response to localized application of norepinephrine on capillaries in rat and frog skeletal muscle. *Microvasc Res* 43:73–86.

25. **Dietrich HH, Tyml K** (1992) Capillary as a communicating medium in the microvasculature. *Microvasc Res* 43:87–99.

26. **Dornyei G, Monos E, Kaley G, Koller A** (1996) Myogenic responses of isolated rat skeletal muscle venules: modulation by norepinephrine and endothelium. *Am J Physiol Circ Physiol* 271:H267–H272.

27. **Ellis CG, Wrigley SM, Groom AC** (1994) Heterogeneity of red blood cell perfusion in capillary networks supplied by a single arteriole in resting skeletal muscle. *Circ Res* 75:357–368.

28. **Ellis CG, Ellsworth ML, Pittman RN, Burgess WL** (1992) Application of image analysis for evaluation of red blood cell dynamics in capillaries. *Microvasc Res* 44:214–25.

29. **Ellis CG, Goldman D, Hanson M, et al** (2010) Defects in oxygen supply to skeletal muscle of prediabetic ZDF rats. *Am J Physiol Circ Physiol* 298:H1661–H1670.

30. **Ellis CG, Milkovich S, Goldman D** (2012) What is the efficiency of ATP signaling from erythrocytes to regulate distribution of O(2) supply within the microvasculature? *Microcirculation* 19:440–50.

31. **Ellis CG, Bateman RM, Sharpe MD, et al** (2002) Effect of a maldistribution of microvascular blood flow on capillary O(2) extraction in sepsis. *Am J Physiol Heart Circ Physiol* 282:H156-64.

32. **Ellsworth ML, Ellis CG, Sprague RS** (2016) Role of erythrocyte-released ATP in the regulation of microvascular oxygen supply in skeletal muscle. *Acta Physiol (Oxf)* 216:265–76.

33. **Emerson GG, Segal SS** (1997) Alignment of microvascular units along skeletal muscle fibers of hamster retractor. *J Appl Physiol* 82:42–48.

34. **Enoka RM** (1995) Morphological Features and Activation Patterns of Motor Units. *J Clin Neurophysiol* 12:538–559.

35. **Eržen I, Janáček J, Kubínová L** (2011) Characterization of the capillary network in skeletal muscles from 3D data. *Physiol Res* 60:1–13.

36. **Federspiel WJ, Popel AS** (1986) A theoretical analysis of the effect of the particulate nature of blood on oxygen release in capillaries. *Microvasc Res* 32:164–89.

37. **Ferreira LF, Padilla DJ, Musch TI, Poole DC** (2006) Temporal profile of rat skeletal muscle capillary haemodynamics during recovery from contractions. *J Physiol* 573:787–97.

38. **Fraser GM, Goldman D, Ellis CG** (2012) Microvascular Flow Modeling using In Vivo Hemodynamic Measurements in Reconstructed 3D Capillary Networks. *Microcirculation* 19:510–520.

39. **Fraser GM, Milkovich S, Goldman D, Ellis CG** (2012) Mapping 3-D functional capillary geometry in rat skeletal muscle in vivo. *Am J Physiol Circ Physiol* 302:H654–H664.

40. **Fraser GM, Sharpe MD, Goldman D, Ellis CG** (2015) Impact of Incremental Perfusion Loss on Oxygen Transport in a Capillary Network Mathematical Model. *Microcirculation* 22:348–359.

41. **Fuglevand AJ, Segal SS** (1997) Simulation of motor unit recruitment and microvascular unit perfusion: spatial considerations. *J Appl Physiol* 83:1223–1234.

42. **Gil J** (2011) Microcirculation of the Lung: Functional and Anatomic Aspects. In: Textbook of Pulmonary Vascular Disease. Springer US, Boston, MA, pp 13–24

43. **Di Giovanna AP, Tibo A, Silvestri L, et al** (2018) Whole-Brain Vasculature Reconstruction at the Single Capillary Level. *Sci Rep* 8:12573.

44. **Glancy B, Hartnell LM, Malide D, et al** (2015) Mitochondrial reticulum for cellular energy distribution in muscle. *Nature* 523:617–620.

45. **Glenny RW, Robertson HT, Yamashiro S, Bassingthwaighte JB** (1991) Applications of fractal analysis to physiology. *J Appl Physiol* 70:2351–2367.

46. **Goldberger AL, Amaral LAN, Hausdorff JM, et al** (2002) Fractal dynamics in physiology: Alterations with disease and aging. *Proc Natl Acad Sci* 99:2466–2472.

47. **Goldman D, Popel AS** (2000) A computational study of the effect of capillary network anastomoses and tortuosity on oxygen transport. *J Theor Biol* 206:181–94.

48. **Goldman D, Bateman RM, Ellis CG** (2004) Effect of sepsis on skeletal muscle oxygen consumption and tissue oxygenation: interpreting capillary oxygen transport data using a mathematical model. *Am J Physiol Circ Physiol* 287:H2535–H2544.

49. **Goldman D, Bateman RM, Ellis CG** (2006) Effect of decreased O2 supply on skeletal muscle oxygenation and O2 consumption during sepsis: role of heterogeneous capillary spacing and blood flow. *Am J Physiol Heart Circ Physiol* 290:H2277-85.

50. **Hartung G, Vesel C, Morley R, et al** (2018) Simulations of blood as a suspension predicts a depth dependent hematocrit in the circulation throughout the cerebral cortex. *PLOS Comput Biol* 14:e1006549.

51. **Hayward NE** (2013) Development of a translational animal model of sepsis. Western University

52. **Heinonen I, Koga S, Kalliokoski KK, et al** (2015) Heterogeneity of Muscle Blood Flow and Metabolism. *Exerc Sport Sci Rev* 43:117–124.

53. **Japee SA, Pittman RN, Ellis CG** (2005) A new video image analysis system to study red blood cell dynamics and oxygenation in capillary networks. *Microcirculation* 12:489–506.

54. **Japee SA, Ellis CG, Pittman RN** (2004) Flow visualization tools for image analysis of capillary networks. *Microcirculation* 11:39–54.

55. **Joyner MJ, Casey DP** (2015) Regulation of increased blood flow (hyperemia) to muscles during exercise: a hierarchy of competing physiological needs. *Physiol Rev* 95:549–601.

56. **Kindig CA, Richardson TE, Poole DC** (2002) Skeletal muscle capillary hemodynamics from rest to contractions: implications for oxygen transfer. *J Appl Physiol* 92:2513–20.

57. **Klitzman B, Duling BR** (1979) Microvascular hematocrit and red cell flow in resting and contracting striated muscle. *Am J Physiol Circ Physiol* 237:H481–H490.

58. **Koga S, Rossiter HB, Heinonen I, et al** (2014) Dynamic heterogeneity of exercising muscle blood flow and O2 utilization. *Med Sci Sports Exerc* 46:860–76.

59. **Lam C, Tyml K, Martin C, Sibbald W** (1994) Microvascular perfusion is impaired in a rat model of normotensive sepsis. *J Clin Invest* 94:2077–2083.

60. **Liu G, Mac Gabhann F, Popel AS** (2012) Effects of Fiber Type and Size on the Heterogeneity of Oxygen Distribution in Exercising Skeletal Muscle. *PLoS One* 7:e44375.

61. **Lo A, Fuglevand AJ, Secomb TW** (2003) Oxygen delivery to skeletal muscle fibers: effects of microvascular unit structure and control mechanisms. *Am J Physiol - Hear Circ Physiol* 285:H955–H963.

62. **Lorthois S, Cassot F** (2010) Fractal analysis of vascular networks: Insights from morphogenesis. *J Theor Biol* 262:614–633.

63. **Lücker A, Secomb TW, Barrett MJP, et al** (2018) The Relation Between Capillary Transit Times and Hemoglobin Saturation Heterogeneity. Part 2: Capillary Networks. *Front Physiol* 9:.

64. **Lund N, Damon DH, Damon DN, Duling BR** (1987) Capillary grouping in hamster tibials anterior muscles: flow patterns, and physiological significance. *Int J Microcirc Clin Exp* 5:359—372.

65. **Marshall JM, Tandon HC** (1984) Direct observations of muscle arterioles and venules following contraction of skeletal muscle fibres in the rat. *J Physiol* 350:447–459.

66. **Mizisin AP, Weerasuriya A** (2011) Homeostatic regulation of the endoneurial microenvironment during development, aging and in response to trauma, disease and toxic insult. *Acta Neuropathol* 121:291–312.

67. **Monos E, Bérczi V, Nádasy G, et al** (1995) Local control of veins: biomechanical, metabolic, and humoral aspects. *Physiol Rev* 75:611–666.

68. **Murakami S, Fujinoc H, Takeda I, et al** (2010) Comparison of capillary architecture between slow and fast muscles in rats using a confocal laser scanning microscope. *Acta Med Okayama* 64:11–8.

69. **Murrant CL, Lamb IR, Novielli NM** (2017) Capillary endothelial cells as coordinators of skeletal muscle blood flow during active hyperemia. *Microcirculation* 24:1–10.

70. **Nakagawa S, Schielzeth H** (2013) A general and simple method for obtaining R^2 from generalized linear mixed-effects models. *Methods Ecol Evol* 4:133–142.

71. **Padilla DJ, McDonough P, Behnke BJ, et al** (2006) Effects of Type II diabetes on capillary hemodynamics in skeletal muscle. *Am J Physiol Heart Circ Physiol* 291:H2439–H2444.

72. **Padilla DJ, McDonough P, Behnke BJ, et al** (2007) Effects of Type II diabetes on muscle microvascular oxygen pressures. *Respir Physiol Neurobiol* 156:187–195.

73. **Percie du Sert N, Hurst V, Ahluwalia A, et al** (2020) The ARRIVE guidelines 2.0: Updated guidelines for reporting animal research. *PLoS Biol* 18:e3000410.

74. **Peyrounette M, Davit Y, Quintard M, Lorthois S** (2018) Multiscale modelling of blood flow in cerebral microcirculation: Details at capillary scale control accuracy at the level of the cortex. *PLoS One* 13:e0189474.

75. **Pittman RN** (2011) Oxygen gradients in the microcirculation. *Acta Physiol* 202:311–322.

76. **Pittman RN** (2013) Oxygen Transport in the Microcirculation and Its Regulation. *Microcirculation* 20:117–37.

77. **Plyley MJ, Sutherland GJ, Groom AC** (1976) Geometry of the capillary network in skeletal muscle. *Microvasc Res* 11:161–173.

78. **Poole DC, Copp SW, Hirai DM, Musch TI** (2011) Dynamics of muscle microcirculatory and blood-myocyte O(2) flux during contractions. *Acta Physiol (Oxf)* 202:293–310.

79. **Poole DC, Behnke BJ, Musch TI** (2020) The role of vascular function on exercise capacity in health and disease. *J Physiol* JP278931.

80. **Poole DC, Copp SW, Ferguson SK, Musch TI** (2013) Skeletal muscle capillary function: Contemporary observations and novel hypotheses. *Exp Physiol* 98:1645–1658.

81. **Poole DC** (2019) Edward F. Adolph Distinguished Lecture. Contemporary model of muscle microcirculation: gateway to function and dysfunction. *J Appl Physiol* 127:1012–1033.

82. **Popel AS, Charny CK, Dvinsky AS** (1986) Effect of Heterogeneous Oxygen Delivery on the Oxygen Distribution in Skeletal Muscle. *Math Biosci* 81:91–113.

83. **Potter RF, Groom AC** (1983) Capillary diameter and geometry in cardiac and skeletal muscle studied by means of corrosion casts. *Microvasc Res* 25:68–84.

84. **Price R, Owens G, Skalak T** (1994) Immunohistochemical identification of arteriolar development using markers of smooth muscle differentiation. *Circ Res* 75:520–527.

85. **Pries AR, Ley K, Gaehtgens P** (1986) Generalization of the Fahraeus principle for microvessel networks. *Am J Physiol* 251:H1324-32.

86. **Pries AR, Secomb TW, Gaehtgens P, Gross JF** (1990) Blood flow in microvascular networks. Experiments and simulation. *Circ Res* 67:826–834.

87. **Pries AR, Secomb TW, Gessner T, et al** (1994) Resistance to blood flow in microvessels in vivo. *Circ Res* 75:904–15.

88. **Pries AR, Secomb TW** (2008) Blood Flow in Microvascular Networks. In: Microcirculation. Elsevier, pp 3–36

89. **Rezania V, Marsh R, Coombe D, Tuszynski J** (2013) A physiologically-based flow network model for hepatic drug elimination I: regular lattice lobule model. *Theor Biol Med Model* 10:52.

90. **Sakai T, Hosoyamada Y** (2013) Are the precapillary sphincters and metarterioles universal components of the microcirculation? An historical review. *J Physiol Sci* 63:319–331.

91. **Sarelius IH** (1986) Cell flow path influences transit time through striated muscle capillaries. *Am J Physiol Hear Circ Physiol* 250:H899–H907.

92. **Sarelius IH, Duling BR** (1982) Direct measurement of microvessel hematocrit, red cell flux, velocity, and transit time. *Am J Physiol Circ Physiol* 243:H1018–H1026.

93. **Sarelius IH** (1993) Cell and oxygen flow in arterioles controlling capillary perfusion. *Am J Physiol* 265:H1682-7.

94. **Secomb TW, Pries AR** (2011) The microcirculation: physiology at the mesoscale. *J Physiol* 589:1047–52.

95. **Seely AJE, Macklem P** (2012) Fractal variability: an emergent property of complex dissipative systems. *Chaos* 22:013108.

96. **Skalak TC, Schmid-Schönbein GW** (1986) The microvasculature in skeletal muscle. IV. A model of the capillary network. *Microvasc Res* 32:333–347.

97. **Smith AF, Doyeux V, Berg M, et al** (2019) Brain Capillary Networks Across Species: A few Simple Organizational Requirements Are Sufficient to Reproduce Both Structure and Function. *Front Physiol* 10:.

98. **Sweeney TE, Sarelius IH** (1989) Arteriolar control of capillary cell flow in striated muscle. *Circ Res* 64:112–120.

99. **Twynstra J, Ruiz DA, Murrant CL** (2012) Functional coordination of the spread of vasodilations through skeletal muscle microvasculature: implications for blood flow control. *Acta Physiol* 206:229–241.

100. **Tyml K, Cheng L** (1995) Heterogeneity of red blood cell velocity in skeletal muscle decreases with increased flow. *Microcirculation* 2:181–93.

101. **Tyml K, Ellis CG, Safranyos RG, et al** (1981) Temporal and spatial distributions of red cell velocity in capillaries of resting skeletal muscle, including estimates of red cell transit times. *Microvasc Res* 22:14–31.

102. **Tyml K, Mathieu-Costello O, Budreau CH** (1992) Distribution of red blood cell velocity in capillary network, and endothelial ultrastructure, in aged rat skeletal muscle. *Microvasc Res* 44:1–13.

103. **Tyml K, Mathieu-Costello O, Cheng L, Noble EG** (1999) Differential microvascular response to disuse in rat hindlimb skeletal muscles. *J Appl Physiol* 87:1496–1505.

104. **Zeller-Plumhoff B, Daly KR, Clough GF, et al** (2017) Investigation of microvascular morphological measures for skeletal muscle tissue oxygenation by image-based modelling in three dimensions. *J R Soc Interface* 14:20170635.

105. **Zeller-Plumhoff B, Roose T, Clough GF, Schneider P** (2017) Image-based modelling of skeletal muscle oxygenation. *J R Soc Interface* 14:20160992.

CHAPTER 3: BIOPHYSICAL PROPERTIES OF RBC AND PLASMA FLOW DISTRUBTION IN CAPILLARY MODULES

3.1 Introduction

Blood flow in the microcirculation is governed by unique biophysical properties that are of important consequence when considering the regulation and distribution of oxygen in microvascular networks. Unlike the systemic circulation, where blood is considered a homogenous medium, blood flow within microvessels less than 300μm in diameter is characterized as a dual-phase non-Newtonian fluid consisting of red blood cells (RBCs) suspended in aqueous plasma [49, 56]. Because of the tendency of RBCs to migrate away from the vessel wall, and the ability of the endothelial surface layer (ESL) to retard plasma flow, these two blood components have different flow rates and radial velocity profiles. These critical phenomena cause a reduction in both the volume fraction (i.e. tube hematocrit) of RBCs in microvessels (Fahraeus effect) and a reduction in apparent viscosity of blood flow compared to larger vessels (Fahraeus-Lindqvist effect) – both have been described in seminal works by Pries [47, 48] using empirical data from mesenteric microvascular networks. Moreover, the relative cell-free layer at the edge of the vessel wall results in uneven distribution of RBC flow at bifurcations, such that the daughter vessel with low flow receives even less RBC flow (plasma skimming), and the daughter vessel

with high flow receives even more RBC flow than would be predicted by the proportion of total blood flow [45, 52].

Together, these three cardinal biophysical laws of microvascular blood flow (Fahraeus effect, Fahraeus-Lindqvist effect, bifurcation law) have important consequences when applied over large microvascular networks. For example, the Fahraeus effect within individual microvessels will cause, on average, a reduction in hematocrit compared to the systemic circulation as vessels decrease in diameter down the arteriolar network [46]. The Fahraeus-Lindqvist effect offsets an untenable increase to resistance that would otherwise be associated with vessel diameters in microcirculation. The bifurcation law, when considered through successive branches of the arteriolar system, is one of the main causes for functional heterogeneity in RBC flow and hematocrit distribution [50], and one of the mechanisms by which vasodilation in upstream arterioles can homogenize hematocrit and oxygen delivery in downstream capillary networks. Pries has also shown that variations to network topology and geometry both contribute functional heterogeneity [43, 44], thereby highlighting how the structure of microvascular networks participates with the above-mentioned biophysical properties to generate the observed physiology of blood flow in the microcirculation. However, network structure and biophysics are not sufficient in and of themselves to achieve the homeostatic roles of the microcirculation. Working in concert with these components, active mechanisms of flow regulation are employed to ensure that microvascular oxygen supply is matched with tissue metabolic demand [9, 10, 27, 57]; mechanisms of flow regulation also ensure that biophysical parameters such as shear, flow, pressure, and resistance are maintained within a physiological range to prevent mechanical damage to microvessels.

Capillary networks have a fundamental role in the microcirculation, as the terminal site of oxygen and substrate exchange with surrounding tissue. This is of significance in all organs, but will be specifically explored here for skeletal muscle, given the remarkable range of oxygen consumption and blood flows that can be achieved from rest to peak exercise. Although capillaries are governed by the same biophysical properties as resistance arterioles and venules, important structural differences exist that require special attention. Unlike the traditional branching systems of arterioles and venules, capillary networks are comprised of interconnected capillary modules (CMs), consisting of a group of parallel-flowing capillaries originating from a terminal arteriole (TA) and draining into a post-capillary venule (PCV) [38, 39, 60]; it has also been recognized that TAs will supply multiple CMs flowing in opposite directions, and PCVs will receive blood from multiple CMs [11, 60, 62]. Unlike the arteriolar and venular trees where bifurcations invariably result in two daughters from a parent vessel, terminal arterioles and post-capillary venules will interact with many capillaries in very close succession. Within a capillary module, internal bifurcations can be either converging or diverging [39], and the diameter of these vessels does not adhere to the reductions in vessel diameter that are dictated by Murray's law [59]. These features may have important considerations that affect the distribution of RBCs and plasma within a capillary module. As has been shown previously using computational modeling, heterogeneity of RBC distribution can have important consequences for oxygen delivery and exchange [15, 21, 25, 31].

Furthermore, while we can acknowledge that the locus of flow regulation in the microcirculation resides upstream in resistance arterioles [2], this theory does not consider how capillary networks might participate in this process, or how the interconnected

structure of CMs impacts the ability of arterioles to exclusively determine flow through capillary networks. Because of their anatomic arrangement and association with a single terminal arteriole, RBC flow will change together for all capillaries in a module [11, 51, 61], however this does not describe how specific hemodynamic mechanisms of flow regulation (e.g. vasodilation, pressure changes, hematocrit changes) interact with the structure of a capillary module to affect the magnitude and distribution of blood flow within capillary segments.

These considerations have further implications when viewed through the new paradigm of the Capillary Fascicle, described in Chapter 2. Although capillary modules have been mostly treated in isolation, they exist within columns spanning thousands of microns. This perspective shifts from small volumes of tissue, and focuses on blood flow regulation within the entire muscle fascicle. In order to understand how this process is achieved during coordinated activities (i.e. contraction) over many modules, we need to better describe the mechanisms of microvascular control for each functional unit, and their immediate neighbors.

In this study, we use experimentally-derived data from resting skeletal muscle capillary networks to understand the relationship between hemodynamic variables at the level of the capillary module. By applying the biophysical principles of blood flow in the microcirculation, we illustrate how flow regulation might be achieved within complex capillary networks. Using computational modeling in simulated capillary modules, we describe the impact of variations to boundary conditions on RBC and plasma flow distribution. Together, these experiments provide evidence that the dual-phase nature of

blood and the structure of capillary modules have important consequences for flow regulation in the microcirculation.

3.2 Methods

3.2.1 Capillary segment hemodynamics derived from experimental dataset

A rodent model of intravital videomicroscopy of resting extensor digitorum longus (EDL) muscle was used, as described previously by our group [20], and in section 2.2.1 of this thesis. Briefly, juvenile male Sprague-Dawley rats (n=9) were anesthetized with intravenous pentobarbital, and the EDL muscle was dissected, exteriorized, and placed on the objective of an inverted microscope (Olympus IX81) and dual-wavelength camera system (Rolera-XR, QImaging). The wavelengths are selected to provide maximum contrast between flowing RBCs and surrounding muscle tissue, in order to obtain accurate measurements of RBC hemodynamics. 2-minute video recordings were made from overlapping fields of view to generate hemodynamic data from large capillary networks, thereby providing a robust dataset for computational analysis.

The intravital videos were post-processed using custom software for quantifying RBC-capillary hemodynamics, with details previously published by our group [1, 20, 25, 30]. An operator selects the capillary segment for analysis, and the software generates a frame-by-frame space time image (STI) that determines the flow of RBCs down the centerline of the vessel. STIs are used to calculate frame-by-frame capillary hemodynamics (2520 frames) as originally described by Ellis [13]. The fundamental metrics of capillary-

RBC hemodynamics are RBC velocity (V_{rbc}, μm/sec), lineal density (LD, RBC/mm) as a surrogate for hematocrit (Hct, %), and RBC supply rate (SR_{rbc}, RBC/s) where $SR_{rbc} = V_{rbc} * LD * \frac{1mm}{1000\mu m}$; SRrbc defines the number of RBCs flowing through an individual capillary per unit time.

Capillary segments are grouped into capillary modules (CM), which are considered the building block of complex capillary networks. CMs are defined as parallel-flowing capillaries originating from a single terminal arteriole and draining into a single post-capillary venule [38, 39, 60]. This analysis provides spatial localization of capillary hemodynamics for functional interpretation of blood flow at the level of the CM.

3.2.2 RBC and plasma distribution within capillary modules derived from experimental dataset

In the microcirculation blood exists in a dual phase, with distinct RBC and plasma components; this is particularly notable in capillary networks with single-file RBC flow and distinct plasma gaps between RBCs. Using this experimentally-derived dataset and rheological properties of the microcirculation, the distribution of RBC and plasma flow within CMs was calculated. RBC supply rate of capillary segments was measured directly from experimental datasets, as described above. This variable has units of RBC/s, and can also be reported as a volume (nL/s) of RBC flow:

$$Q_{rbc} = SR_{rbc} * RBC_{vol} * \frac{1\ nL}{10^6\ \mu m^3}$$

where RBC_{vol} is the reported mean volume of a rat erythrocyte (65 μm³, Canham *et al.*, 1984).

Capillary tube hematocrit (H_T) was calculated from the experimentally-derived LD parameter using the equation:

$$H_T = \frac{LD \ * \ RBC_{vol}}{\pi r^2} * \frac{1mm}{1000 \mu m}$$

where r is the capillary radius in microns. A measurement error for capillary radius was systematically encountered for out-of-focus vessels, that will blur the edges and over-estimate capillary diameter. This was adjusted by setting an upper limit of capillary diameter to 6μm (radius 3μm), consistent with values reported in the literature [20, 41, 60].

Plasma flow for capillary segments is not measured directly, but is derived from experimental measurements of Q_{rbc} and H_T using rheological equations. The first step is the conversion of capillary tube hematocrit (H_T) to capillary discharge hematocrit (H_D); H_T is an RBC volume fraction, and H_D is an RBC flow fraction. The reduction of H_T relative to H_D as a function of microvessel diameter (D, μm) - known as the Fahraeus effect - is due to the cell-free layer of blood at the wall of the microvessel that causes differential speed of RBC and plasma flow. This relationship is defined by the empirical formula from Pries (1990):

$$\frac{H_T}{H_D} = H_D + (1 - H_D) * (1 + 1.7e^{-0.415D} - 0.6e^{-0.011D})$$

With this dataset, H_D and Q_{rbc} are used to solve for capillary blood flow (Q_{blood}) given that $H_D = \frac{Q_{rbc}}{Q_{blood}}$; capillary plasma flow (Q_{plasma}) is then solved with the equation:

$$Q_{blood} = Q_{rbc} + Q_{plasma}$$

This analysis, derived fundamentally by the application of the Fahraeus effect to capillary-RBC hemodynamics, allows for simultaneous quantification of RBC and plasma flow in skeletal muscle capillary networks. Mean values for RBC and plasma flow are used to estimate module blood flow (see below). The coefficient of variation ($\%CV = \frac{SD}{mean} *$ 100) of Q_{rbc} and Q_{plasma} represents the spatial distribution of RBC and plasma flow, respectively, for capillary segments in a module. To minimize sampling error, only CMs with hemodynamic measurements of at least 67% experimental coverage (defined as the ratio of measured capillary segments to parallel capillaries) were included in analysis, defined as the ratio of measured capillary segments to parallel capillaries; this yielded a low rate of sampling error (~12%) as described in section 2.2.8 of this thesis.

3.2.3 Estimation of capillary module resistance and module driving pressure derived from experimental dataset

Poiseuille's law for blood flow within a cylindrical tube can be extended to approximate the pressure-flow relationship in a capillary module comprised of several parallel microvessels:

$$(Q_{blood})_{module} = \frac{\Delta P}{\left(\frac{128\,\eta\,l}{\pi D^4} * \frac{1}{N_{par}}\right)}$$

Where D is the mean diameter of capillary segments (5.94 μm in this experimental dataset), N_{par} is the number of parallel capillaries in the module, l is module length, η is module viscosity, and ΔP is the driving pressure across the capillary module. The bracketed term is equal to the module resistance (R_{module}), whereby viscosity is the functional component of resistance and $\frac{l}{N_{par}}$ is considered the geometric resistance of a capillary module; because capillary diameter is fixed in these calculations, it does not contribute to the analysis. CM topology was quantified for module length and N_{par} using extended depth of focus (EDF) functional images derived from intravital videomicroscopy, as described in section 2.2.4 of this thesis. Lengths and flows are calculated in cm and cm³/s; viscosity units were converted from pascal seconds (Pa*s) into millimeters of mercury seconds (mmHg*s).

CM viscosity was calculated using the mean of H_D values from capillary segments, and applying the empirical equations for η_{vivo} [48], that define the hematocrit- and diameter-dependent alterations in blood viscosity for the microcirculation – also known as the Fahraeus-Lindqvist effect. $(Q_{blood})_{module}$ is estimated from mean RBC and plasma flow values multiplied by the number of parallel capillaries:

$$(Q_{blood})_{module} = (Q_{rbc})_{module} + (Q_{plasma})_{module}$$

$$= (Q_{rbc})_{mean} * N_{par} + (Q_{plasma})_{mean} * N_{par}$$

Finally, coming back to Poiseuille's law, ΔP can now be solved to calculate the driving pressure (mmHg) across a capillary module for a given blood flow and resistance.

$$\Delta P_{module} = (Q_{blood})_{module} * R_{module}$$

3.2.3 Hemodynamic relationships for capillary modules and module pairs

In a passive microvascular system, blood flow would be strongly determined by network resistance; at the level of the CM, the following inverse relationship would be expected:

$$Q_{module} \propto \frac{1}{R_{module}}$$

This correlation is tested for total blood flow, as well as RBC and plasma flow for each CM in the dataset.

Moreover, it has been well-recognized that terminal arterioles (TA) supply blood to two CMs flowing in opposite directions, and similarly post-capillary venules (PCV) will receive blood from two CMs [11, 60, 62]. This anatomical relationship provides an opportunity to compare blood flow in capillary module pairs with a shared boundary condition – either a common TA or PCV.

Consider two capillary modules, CM_1 and CM_2, supplied by a common TA; because of their anatomical connection, variations in blood flow will change together for both modules and have a shared inflow pressure and blood supply. In a passive

microvascular system, the distribution of blood flow between modules would be determined exclusively by module resistance. More specifically, the ratio of resistances between modules would determine the ratio of blood flow - the module with higher resistance would have proportionally less perfusion. As given by Ohm's law, the ratio of resistances R_1 and R_2, and blood flows, Q_1 and Q_2 would be inversely correlated:

$$\frac{R_1}{R_2} \propto \frac{Q_2}{Q_1}$$

For example, a module with double the resistance should receive half the blood flow compared to the pair module – provided that driving pressure between modules is equal ($\Delta P_1 = \Delta P_2$). Deviations from this relationship would be explained by differences in ΔP between modules, stochastic variability, or experimental errors for calculating module flow and resistance. Two capillary modules that share a common PCV do not have similar constraint on shared blood supply and inflow pressure, but do have a common outflow pressure. Nevertheless, the same relationships between resistance and blood flow would still be expected if driving pressures were equal and blood flow was determined by module resistance. In all pairs, R_1 was arbitrarily defined as the module with higher resistance, such that the ratio of resistance was always greater than 1.

By contrast to example described above, the microcirculation is viewed as a physiological system with active flow regulation [2, 14]. For capillary networks, we hypothesize that this is achieved through independent control of ΔP across each capillary module. Under conditions of active flow regulation, disparities in module resistance

between pairs would need to be compensated with a similar pressure differential between modules:

$$\frac{R_1}{R_2} \propto \frac{\Delta P_1}{\Delta P_2}$$

The module with higher resistance would receive proportionally higher driving pressure, otherwise it would be vulnerable to under-perfusion. The greater the asymmetry of module resistances, the more pressure differential would be required to overcome this imbalance.

Pressure differential between module pairs was assessed, and was defined as the difference in driving pressures ($\Delta P_1 - \Delta P_2$), whereby ΔP_1 is the driving pressure across the module with higher resistance (R_1) and ΔP_2 is the driving pressure across the second module with lower resistance (R_2). Note that this pressure differential can be positive or negative, depending on which module has a higher driving pressure.

3.2.4 *Computational modeling of capillary module boundary conditions*

A summary of all computational experiments is outlined in Table 3.1, and all module geometries are shown in Figures 3.1 and 3.2. In order to determine the impact of variations in capillary module boundary conditions on the distribution of RBC and plasma flow, synthetic CMs were constructed with the approximate dimensions of the average CM from the experimental dataset outlined in chapter 2 (see Table 2.1): length 480μm, width 150-170μm, and 9.5-10.5 parallel capillaries. Before proceeding with interconnected modules, as observed in realistic capillary networks, we evaluated a single CM with a short

inlet TA and outlet PCV, and a series of parallel capillaries. Six module geometries were designed with absent (0), moderate (4, 5), or high (8, 9, 10) degree of converging and diverging bifurcations; these internal bifurcations increase the number of capillary segments within a module while maintaining a similar number of parallel capillaries between all geometries. All capillary diameters were set to 5.5μm.

A steady-state dual-phase continuum computational blood flow model was then applied to the geometries, as developed by Goldman and Popel [24] using established rheological properties of the microcirculation [47, 48]. The boundary conditions were adjusted for (i) arteriole diameter (ii) inflow hematocrit (i.e. H_D), and (iii) driving pressure (ΔP) across the capillary module. Each boundary condition was adjusted over a physiological range, while keeping the other variables fixed: arteriole 10μm, venule 15μm, H_D 0.2, and ΔP 4mmHg.

Experiment	Module geometries	Range of boundary conditions	Analysis	Question
Arteriole diameter	10-8, 10-9, 10-10	6-14μm	RBC flow (mean, %CV) Plasma flow (mean, %CV) Hematocrit (mean, %CV)	Impact of arteriole diameter on blood flow and distribution in a module
Arteriole diameter	10-8, 10-9, 10-10	6-14μm	Capillary entrance pressure (mmHg)	Impact of arteriolar diameter and capillary position on capillary entrance pressure
Driving pressure (ΔP)	10-8, 10-9, 10-10	2-10 mmHg	RBC flow (mean, %CV) Plasma flow (mean, %CV) RBC velocity (mean, %CV) Capillary hematocrit (mean, %CV)	Impact of driving pressure on blood flow and distribution in a module
Hematocrit	10-0, 10-4, 10-5, 10-8, 10-9, 10-10	Inflow hematocrit	RBC flow (%CV)	Impact of hematocrit and module branching

		(H_d) 5%-35%	Plasma flow (%CV)	(low, moderate, high) on RBC and plasma distribution in a module
Hematocrit	10-4, 10-5, 10-8, 10-9, 10-10	Inflow hematocrit (H_d) 5%-35%	RBC flow (mean) RBC velocity (mean) Plasma flow (mean) Capillary hematocrit (mean) Relative viscosity (mean)	Impact of hematocrit on RBC and plasma flow in a module
Hematocrit	2-module, common arteriole: Even modules Length differential, even pressure Length differential, corrected pressure Capillary differential, even pressure Capillary differential, corrected pressure	Inflow hematocrit (H_d) 5%-35%	RBC flow per module (%CV) Plasma flow per module (%CV) RBC flow ratio between modules Plasma flow ratio between modules	Impact of hematocrit and asymmetric module resistance on RBC and plasma distribution

Table 3.1: Summary of experiments for computational modeling.
See figure 3.1 and 3.2 for details on capillary module geometry.
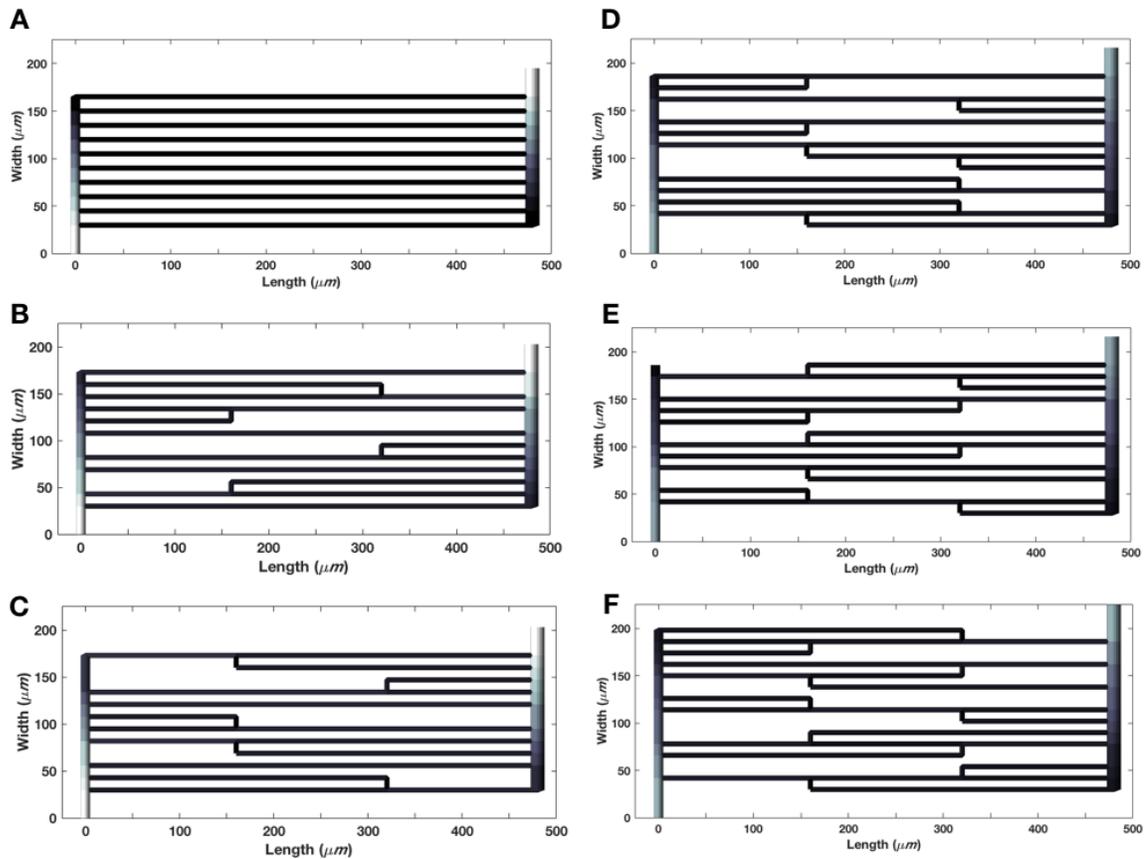
Figure 3.1: 1-module geometries used in computational modeling.
Each capillary module consists of a terminal arteriole (left) feeding a series of parallel capillaries and draining into a post-capillary venule (right); the arteriole and venule serve as manifolds for the parallel capillaries. The length of the modules is 480μm; diameters of the arteriole, capillaries, and venule are 10μm, 5.5μm, and 15μm respectively; all modules have approximately 10 parallel capillaries. Internal branching consists of converging and diverging bifurcations, with no branches (10-0, A), moderate degree of branches (10-4, B; 10-5, C), and high degree of branches (10-8, D; 10-9, E; 10-10,F).

Synthetic geometries were also designed for a single TA feeding a pair of modules (CM$_1$, CM$_2$), each draining to a different PCV (Figure 3.2); these modules had a moderate degree of internal bifurcations and a length of 480μm. Five experiments were simulated whereby the relative resistances and pressures were varied between modules. The cases were (i) balanced module resistances, (ii) CM$_1$ double the length of CM$_2$, (iii) CM$_1$ double the length of CM$_2$ with increased pressure gradient across CM$_1$, (iv) CM$_1$ with approximately half the parallel capillaries of CM$_2$, and (v) CM$_1$ with approximately half the parallel capillaries of CM$_2$, and with increased pressure gradient across CM$_1$. The cases with pressure differential between modules is intended to offset the differential resistance. For these experiments, inflow hematocrit was varied over a physiological range.
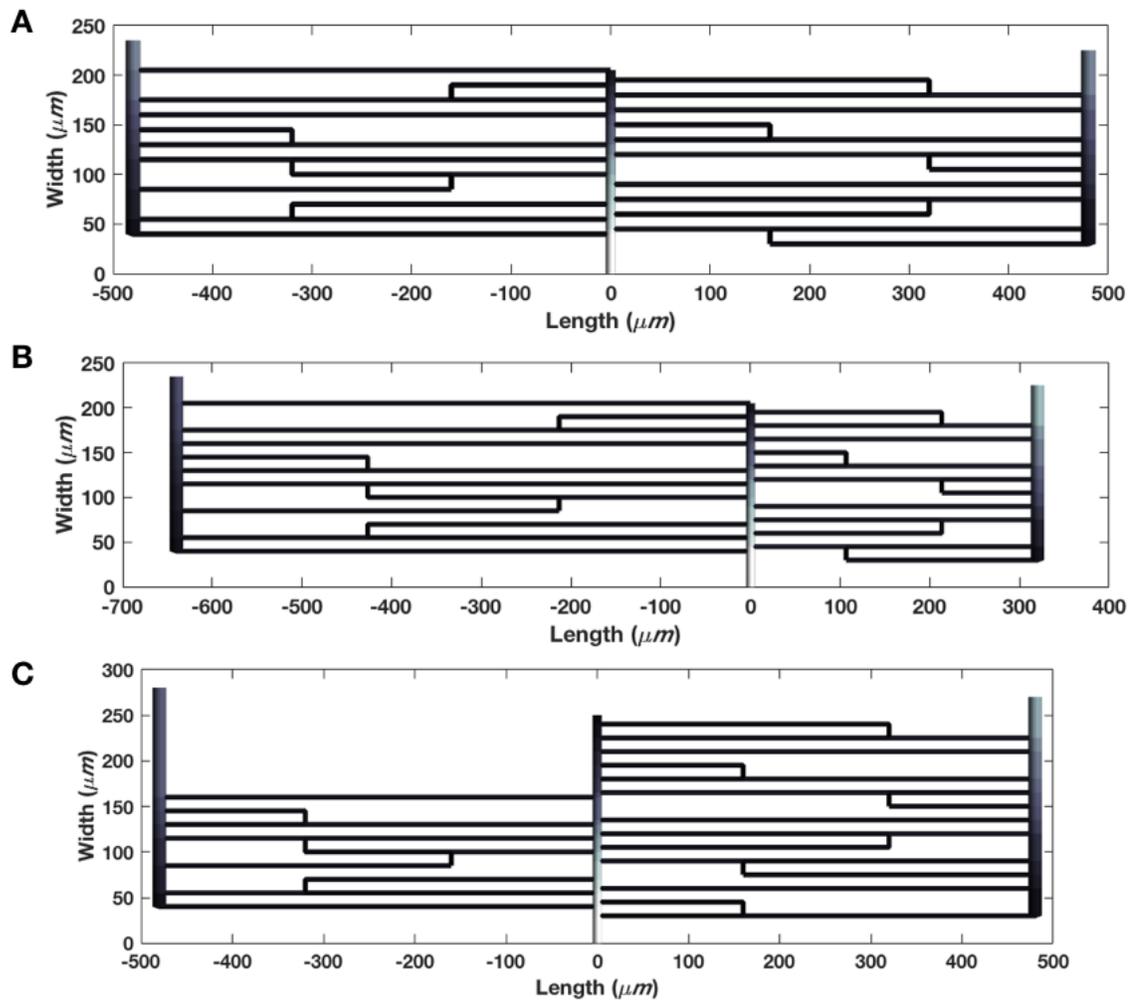
Figure 3.2: 2-module geometries used in the computational modeling.
A single common arteriole (center) supplies two capillary modules, each draining into a post-capillary venule (left, right). The number of internal branches is similar in all modules. Geometric resistances of the modules is varied, comparing (A) modules of equal length (480μm) and equal parallel capillaries (10), (B) modules of different lengths (640μm, 320μm) and equal parallel capillaries (10), and (C) modules of equal length (480μm) and different parallel capillaries (7, 12).

The model calculates RBC flow (Q_{rbc}, nL/s), plasma flow (Q_{plasma}, nL/s), tube hematocrit (H_T), discharge hematocrit (H_D), and pressure gradient (ΔP, mmHg) for all capillary segments within the module. Thus, these experiments describe the impact of each boundary condition on the mean and %CV values for capillary segments within a module. For the 2-module experiments, the proportional distribution of RBC, plasma, and blood flow were between modules was defined as the ratio of flow values, $\frac{Q_2}{Q_1}$.

3.2.5 Statistical Analysis

Correlations between experimentally-derived variables were undertaken using a linear mixed effects model (SPSS v26), as described in section 2.2.9 of this thesis. Briefly, this model is similar to simple linear regression, but accounts for random variations in slope and intercept that can occur between animals. The coefficient of determination (R^2) of the fixed effect defines the portion variance in the dependent variable that is determined by the independent variable over the entire dataset. Using PRISM v8 software package, the difference in heterogeneity (%CV) between RBC and plasma flow for capillary module were compared with a Student's paired t-test. 2-way ANOVA was used to determine the effect of variations to branching structure and hematocrit on RBC and plasma distribution (%CV) in synthetic modules. ANOVA analysis quantified whether each factor was a significant determinant of %CV and the amount of variance (R^2) attributed to each factor in the model (also called the standard omega squared). Statistical significance was considered for $p < 0.05$.

3.3 Results

3.3.1 Differential distribution of RBC and plasma flow in capillary modules derived from the experimental dataset

1491 capillary segments were analyzed, with a summary of capillary and module hemodynamics provided in Table 2.2 of this thesis. RBC supply rate was 13.96 (11.63) RBC/s which is equivalent to 9.073×10^{-4} (7.562×10^{-4}) nL/s of RBC flow; tube hematocrit was 13.19% (6.56) and discharge hematocrit was 19.12% (8.23); plasma flow was 3.722×10^{-3} (2.235×10^{-3}) nL/s and blood flow was 4.630×10^{-3} (2.820×10^{-3}) nL/s.

112 capillary modules had at least 67% experimental coverage and were included in the analysis, comprising 967 capillary segments. %CV for RBC and plasma flow represents the spatial distribution of hemodynamics for capillary segments in a module. As shown in Figure 3.3, mean %CV is 64.82% for RBC flow and 45.59% for plasma flow. Capillary modules had a mean difference of 19.23% (Student's paired t-test 15.70%, 22.76%; $p < 0.0001$) indicating that RBC flow is more spatially heterogeneous than plasma flow within capillary modules.
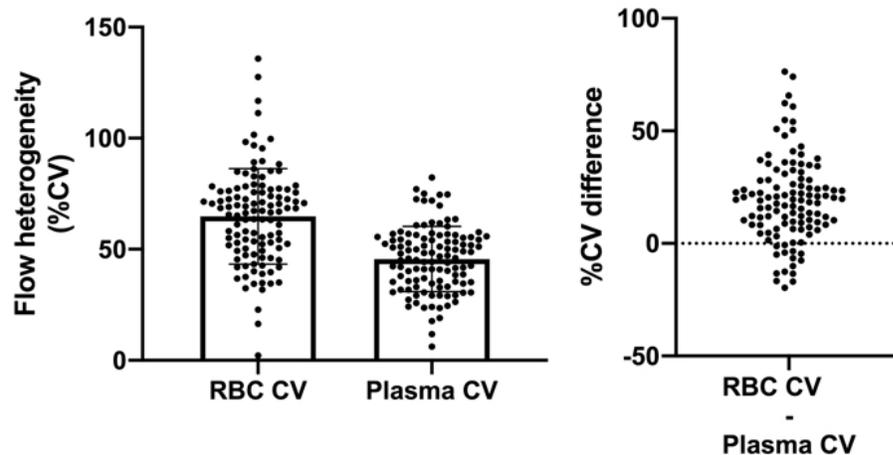
Figure 3.3: Comparison of RBC and plasma flow heterogeneity for capillary segments in a module.

Flow heterogeneity is defined as the coefficient of variation (%CV) for RBC and plasma flow between segments in a module, and is significantly higher for RBC flow versus plasma flow (mean difference of 19.23%; * p<0.0001 Student's paired t-test)

3.3.2 Hemodynamic relationships for capillary modules and module pairs derived from the experimental dataset

89 capillary modules with EDF protocol and at least 67% experimental coverage were analyzed. 8 modules did not contain length measurements which precluded resistance calculations, and 2 modules were rejected due to spurious topological data yielding significant resistance outliers. CM hemodynamics are listed in Table 3.2 for RBC flow, plasma flow, blood flow, viscosity, resistance, and driving pressure. Total blood flow in a capillary module is 4.316×10^{-2} ($2.262 \ 10^{-2}$) nL/s with a driving pressure of 3.236 (1.833) mmHg (range: 0.3498-8.159 mmHg).

	No. of measurements	Mean (SD)	%CV
RBC flow (nL/s)	89	8.547×10^{-3} (5.341×10^{-3})	62.50
Plasma flow (nL/s)	89	3.421×10^{-2} (1.797×10^{-2})	52.52
Blood flow (nL/s)	89	4.275×10^{-2} (2.257×10^{-2})	52.79
Viscosity (mmHg*s)	89	3.997×10^{-5} (6.688×10^{-5})	16.82
Resistance (mmHg*s/cm^3)	79	8.124×10^{7} (4.327×10^{7})	53.27
Driving Pressure (ΔP, mmHg)	79	3.236 (1.833)	56.54

Table 3.2: Hemodynamics for capillary modules in the experimental dataset.

The contribution of viscosity and geometric resistance to total module resistance was examined, as shown in Figure 3.4. Within the experimental dataset, module viscosity was only modestly correlated with module resistance (linear mixed effects: 2.0698×10^{12} [1.7278×10^{12}, 2.4116×10^{12}]; $R^2 = 0.10$, p<0.0001), while geometric resistance was strongly correlated with module resistance (linear mixed effects: 1.2723×10^{10} [1.1522×10^{10}, 1.3924×10^{10}]; $R^2 = 0.94$, p<0.0001). This data indicates that the overwhelming majority of module resistance in resting skeletal muscle is determined by geometry, with only a small portion determined by viscosity.
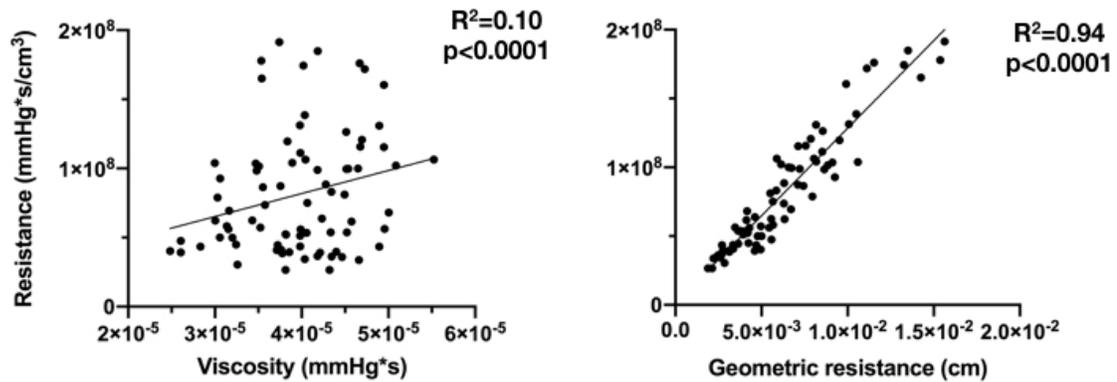
Figure 3.4: Contribution of viscosity and geometric resistance to overall module resistance in the experimental dataset.
Viscosity is derived from parametric equations described by Pries [48], and geometric resistance is derived from module length and the number of parallel capillaries $\left(\frac{l}{N_{par}}\right)$. In resting skeletal muscle, viscosity is weakly correlated with module resistance, whereas geometric resistance is a strong determinant of module resistance.

Hemodynamic relationships between CM resistance and flow are shown in Figure 3.5. CM resistance was not correlated with RBC flow (linear mixed effects: -2.8707 x 10^{-11}[-5.8673 x 10^{-11}, 1.2581 x 10^{-12}]; $R^2 = 0.05$, p=0.0602), but did trend towards being statistically significant despite the very weak R^2 value; CM resistance also has a weak negative correlation with plasma flow (linear mixed effects: -1.7396 x 10^{-10} [-2.6133 x 10^{-10}, -8.6581 x 10^{-11}]; $R^2 = 0.17$, p=0.0002) and blood flow (linear mixed effects: -1.9952 x 10^{-10} [-3.1151 x 10^{-10}, -8.7526 x 10^{-11}]; R^2=0.14, p=0.0007). Taken together, this data indicate that RBC flow and plasma flow are largely independent of CM resistance.
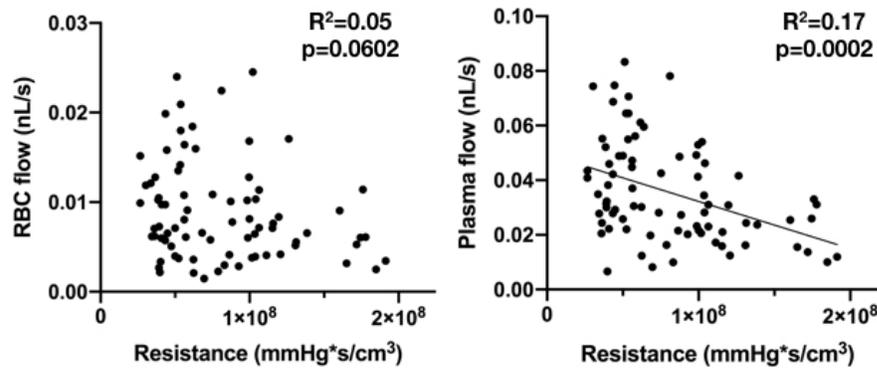
Figure 3.5: Correlation between module resistance and flow in the experimental dataset. RBC flow is not correlated with module resistance. Plasma flow has a weakly inverse correlation with module resistance.

As expected hemodynamically, driving pressure (ΔP) is strongly correlated with RBC flow (linear mixed effects: 1.764×10^{-3} [1.066×10^{-3}, 2.462×10^{-3}]; $R^2=0.40$, $p<0.0001$), plasma flow (linear mixed effects: 5.049×10^{-3} [3.094×10^{-3}, 7.005×10^{-3}]; $R^2=0.25$, $p<0.0001$), and blood flow (linear mixed effects: 6.950×10^{-3} [4.574×10^{-3}, 9.326×10^{-3}]; $R^2=0.30$, $p<0.0001$). This is because driving pressure was calculated directly from empirical measurements of flow, and flow had either no correlation (RBC) or a weak negative correlation (plasma, blood) with resistance.

In the experimental dataset, 22 module pairs were identified whereby each module had at least 67% experimental coverage. 13 module pairs shared a common arteriole, and 9 module pairs shared a common venule. Analysis was similar for module pairs with common arteriole and common venule, so results were pooled in a total dataset. As shown in Figure 3.6, the ratio of resistance (R1/R2) was not correlated with the inverse ratio of

blood flow (Q2/Q1) (linear mixed effects: 0.1972 [-0.40533, 0.7998]; $R^2 = 0.02$, p=0.5054); there was also no correlation with the ratio of rbc flow (linear mixed effects: 0.0902 [-0.7230, 0.9035]; $R^2 = 0.01$, p=0.8106) or plasma flow (linear mixed effects: 0.1674 [-0.4846, 0.8194]; $R^2 = 0.02$, p=0.5766). The ratio of resistance was not correlated with the ratio pressures (P1/P2) (linear mixed effects: 0.5106 [-0.0595, 1.0807]; $R^2 = 0.14$, p=0.0765), although there was a trend towards statistical significance.

As shown in Figure 3.7, the pressure differential between module pairs was low, with mean difference of 0.3293 (1.195) mmHg (range: -1.411 to 3.332 mmHg) indicating a balance of driving pressures between module pairs. 10/22 module pairs had a negative pressure differential, indicating that the module with lower resistance also received less driving pressure. There was no difference in pressure differential for module pairs that shared a common arteriole or a common venule (unpaired t-test: 0.4434 vs 0.1636, p=0.6013).
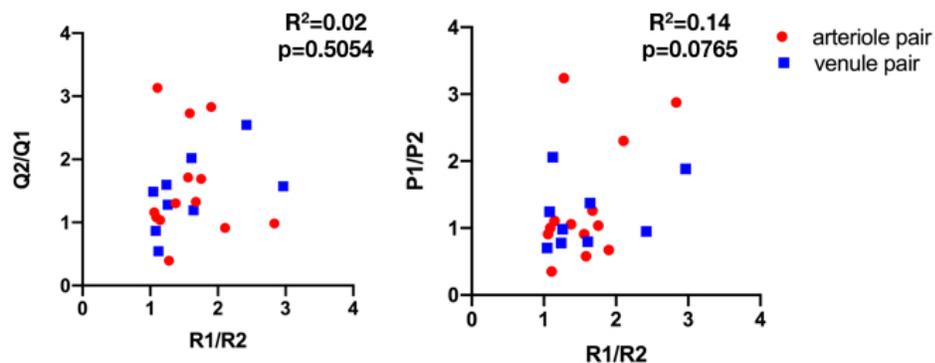
Figure 3.6: Hemodynamic relationships between module pairs.
Data is derived from 22 module pairs that share a common arteriole (n=13) or common venule (n=9). The ratio of resistances between modules is not correlated with the inverse ratio of blood flow. Similarly, the ratio of resistances between modules is not correlated with the ratio of driving pressures between modules.
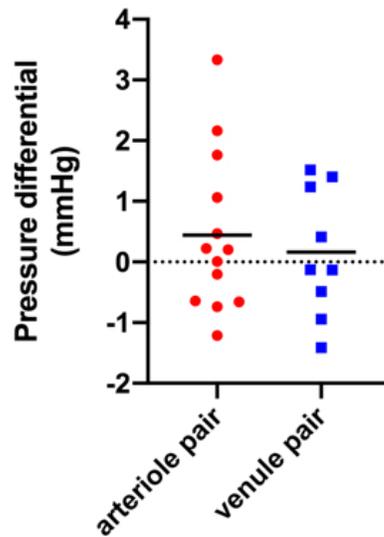
Figure 3.7: Pressure differential between module pairs.
Calculations were made for pairs sharing a common arteriole (n=13) or common venule (n=9), defined as the difference in driving pressures between modules ($\Delta P_1 - \Delta P_2$). Overall, mean pressure differential between pairs in each group was low (line), but exhibit a noticeable range. Mean values were not significantly different between arteriole or venule pairs.

3.3.3 Computational modelling of synthetic capillary modules

As expected hemodynamically, increasing CM driving pressure (ΔP) had a direct linear effect on RBC velocity and RBC supply rate for capillary segments in all CM geometries (Figure 3.8); linear increases were also observed for plasma flow and blood flow. RBC distribution (%CV) and capillary segment hematocrit (H_T and H_D) were not affected by changes to driving pressure. The hashed line in each graph indicates the average RBC velocity (245.40 μm/s) and RBC supply rate (13.96 RBC/s) for capillary segments the experimental dataset. Based on these values, the perfusion pressure for the average CM in

resting skeletal muscle is estimated between 4-6 mmHg, which is consistent with the physiological range of ΔP values listed in Table 3.2.
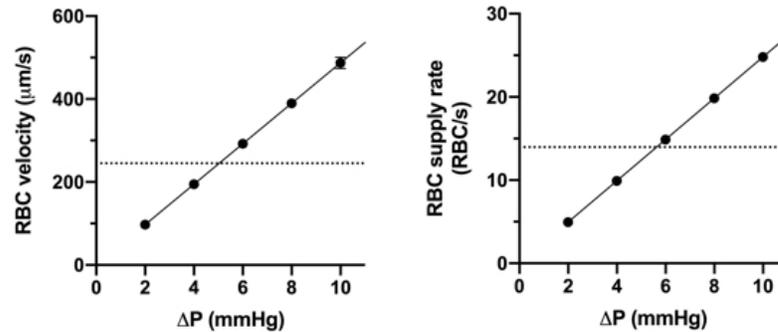
Figure 3.8: Influence of driving pressure (ΔP) on mean RBC velocity and RBC supply rate.
There is a linear relationship between driving pressure and RBC flow. Dashed lines indicate mean values for RBC velocity and RBC supply rate from the experimental dataset.

The diameter of the TA was varied from 6μm to 14μm. This adjusted the caliber of the inflow/outflow vessel and also the portion of the vessel within the CM. As shown in Figure 3.9, increasing TA diameter had a corollary effect on RBC and plasma flow within the 6-10μm range, but little effect on blood flow with further increases above 10μm. Variations in TA diameter significantly reduced plasma flow heterogeneity (i.e. %CV) for capillary segments within the module, but almost no effect on %CV for RBC flow. As shown in Figure 3.10, arteriolar dilation decreased mean capillary hematocrit, and also reduced hematocrit variability between capillary segments.
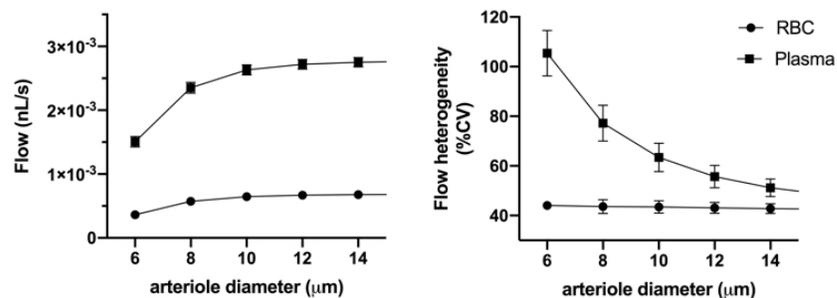
Figure 3.9: Influence of arteriole diameter of RBC and plasma flow.

RBC and plasma flow increase when the arteriole – immediately preceding the capillary module and within the module – is dilated from 6-10μm, but not significantly thereafter. Arteriole dilation significantly reduces plasma flow heterogeneity between capillary segments, but has little effect on RBC flow heterogeneity.
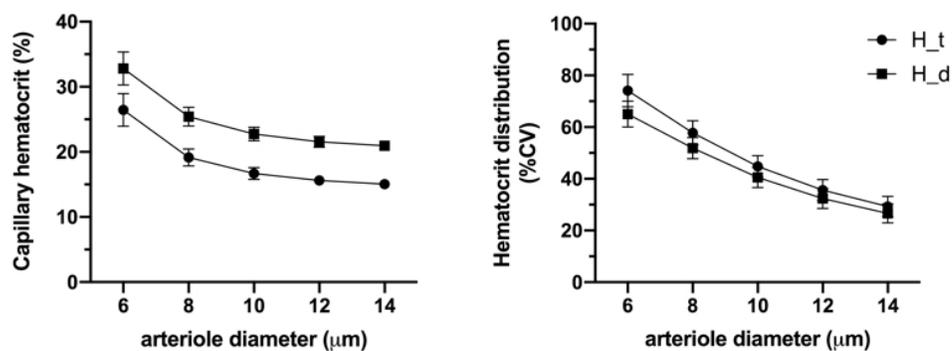
Figure 3.10: Influence of arteriole diameter on capillary hematocrit and hematocrit distribution.

Arteriole dilation reduces mean tube hematocrit (H_T) and discharge hematocrit (H_D) for capillary segments in a module. Similarly, arteriole dilation reduces hematocrit distribution, defined as the coefficient of variation of hematocrit between capillary segments.

As shown in Figure 3.11, for arteriole diameters above 6μm, the TA serves as a pressure manifold that maintains consistent pressure down its length despite feeding multiple capillaries within the module. For TA diameter 6μm, the pressure drop was approximately 1.5 mmHg between first and last capillary position (19.03-17.55 mmHg), whereas all other TA diameters had a pressure drop of less than 1mmHg.
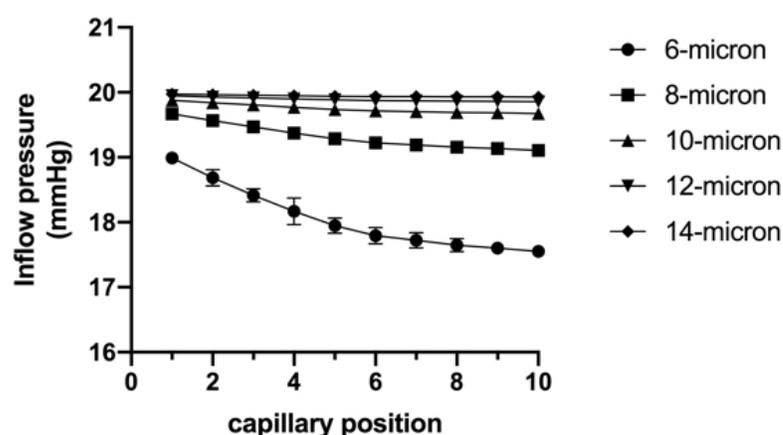
Figure 3.11: Hemodynamic interactions betwen the terminal arteriole in relation to capillary segments in a capillary module.
The terminal arteriole (TA) in the computational model comprises a short vessel segment preceding the module, and the portion of the arteriole within the module that feeds all the capillary segments (see Figure 3.1 for details). For TA diameter of 6μm, there is a moderate drop in pressure down the length of the TA. For all other TA diameters, the vessel serves as a manifold, with little pressure drop down its length. This ensures that all capillaries, regardless of position in the module, will be subjected to similar inflow pressures.

Variations to inflow hematocrit from 5%-35% were tested for 1-module geometries. As shown in Figure 3.12, increases to inflow hematocrit lead to a linear increase in mean discharge and tube hematocrit for capillary segments in the module; this increase in hematocrit is associated with an non-linear decrease in mean RBC velocity. Accordingly, the increase in RBC flow that is associated with increased hematocrit is non-linear, with the greatest increases to RBC flow occurring in the hematocrit range 5%-20%. Moreover, the reduction to plasma flow associated with increased inflow hematocrit is also exponential, following a similar profile to the reduction in velocity. This data demonstrates the interplay between module inflow hematocrit, capillary hematocrit, RBC velocity, and blood flow, and suggests an important contribution of inflow hematocrit to viscosity and module resistance – particularly when inflow hematocrit exceeds 20%. Given the dramatic hematocrit-dependent reduction to RBC velocity observed in the synthetic modules, the correlation between mean module lineal density (surrogate for hematocrit) and mean module RBC velocity was tested in the experimental dataset. A weak negative correlation was observed between module LD and RBC velocity (linear mixed effects: -1.2323 [-2.3741, -0.0895]; $R^2 = 0.04$, p=0.0348).
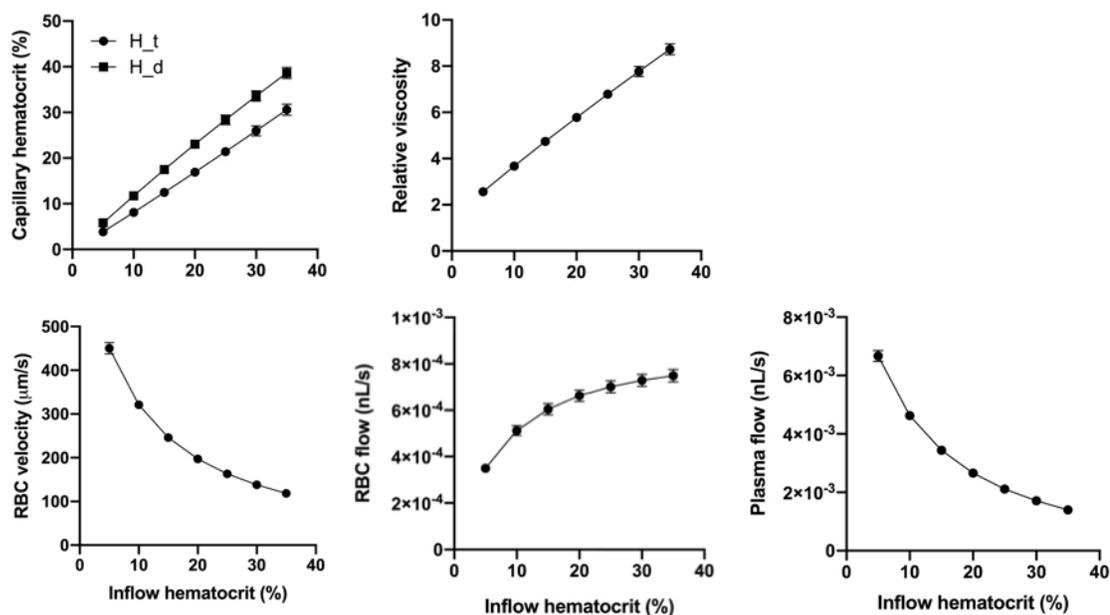
Figure 3.12: Effect of inflow hematocrit on mean capillary hemodynamics in a capillary module.

Increases to inflow hematocrit had a linear effect on mean capillary tube hematocrit (H_T), discharge hematocrit (H_D), and relative viscosity of capillary segments. Accordingly, mean capillary RBC velocity and plasma flow decreased in a non-linear fashion. Overall, these effects balanced, such that mean RBC flow in capillary segments increased in a non-linear fashion, with sharper increases in the inflow hematocrit range of 5%-20% compared to increases in inflow hematocrit above 20%.

As shown in Figure 3.13, increases to inflow hematocrit lead to reduction in RBC %CV (2-way ANOVA: R^2=0.26, p=0.0005). This effect was significantly affected by the number of internal branches (2-way ANOVA: R^2=0.71, p=0.0057), such that the module with no internal branches had a dramatic reduction in RBC %CV (39% to 3%), whereas this phenomenon was much more blunted for modules with moderate branching (51% to 34%) and high branching (56% to 42%). Notably, modules with any degree of branching demonstrated the greatest incremental reduction in RBC flow heterogeneity for the

hematocrit range 5%-20%, with little further reduction in RBC flow heterogeneity thereafter. By contrast, increases to inflow hematocrit lead to increase in plasma %CV (2-way ANOVA: R^2=0.37, p=0.0039), but this phenomenon is not affected by the number of internal branches in a module (2-way ANOVA: R^2=0.28, p=0.3684). Taken together, this data indicates that internal branching geometry has a substantial effect on RBC distribution within a module, but little effect on plasma distribution.
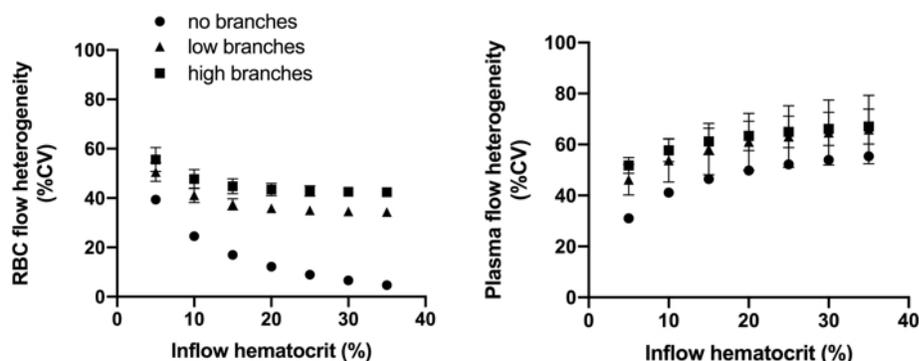
Figure 3.13: Effect of capillary module branching structure on RBC and plasma flow distribution.
Arteriole inflow hematocrit was varied for capillary modules with no branching, low degree, and high degree of internal branching (see Figure 3.1 for details). In all cases, increases to inflow hematocrit lead to a reduction in RBC flow heterogeneity, defined as the coefficient of variation in RBC flow between capillary segments; degree of internal branching significantly modulated this effect. Increases to inflow hematocrit increased plasma flow heterogeneity for all cases, which was not affected by the degree of internal branching structure.

Variations to inflow hematocrit from 5%-35% were also tested for 2-module geometries with a common arteriole. As shown in Figure 3.14, proportion of RBC flow between modules was approximately equal (i.e. Q2/Q1 ratio near 1) for the balanced module geometry. The proportion of RBC flow between modules was markedly

asymmetric (i.e. Q2/Q1 ratio above 2) for the uncompensated module geometries, such that the module with shorter length and more capillaries received more RBC flow; these differences in RBC flow between modules were easily compensated with corrections to driving pressure between modules. The proportion of plasma flow was also affected by asymmetric geometries, but to a lesser degree than RBC flow.
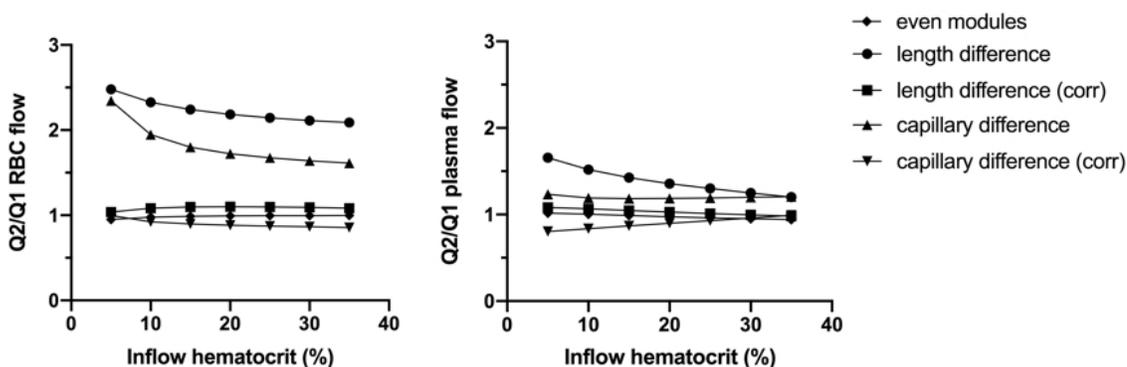
Figure 3.14: RBC and plasma flow ratios between modules sharing a common arteriole, as a function of inflow hematocrit.
Flow ratios are defined as the ratio of total RBC or plasma flow between each module. Balanced module resistances have balanced RBC flow (ratio ~1), whereas asymmetric resistances lead to asymmetries in RBC flow between modules with unequal lengths and number of parallel capillaries. These asymmetries are corrected with adjustments to post-capillary venule pressure that can titrate individual driving pressures between modules. Asymmetries in plasma flow are also noted for these geometries, but to a lesser degree than RBC flow.

As shown in Figure 3.15, RBC %CV values were impacted by variations to inflow hematocrit (2-way ANOVA: $R^2=0.90$, $p<0.0001$) and demonstrated similar curve profile to those for the 1-module geometries with moderate internal branching. However, RBC %CV within a module was similar for all of the 2-bundle geometries, either compensated or uncompensated by driving pressures (2-way ANOVA: $R^2=0.26$, $p=0.9924$). Plasma

%CV values were impacted by variations to inflow hematocrit (2-way ANOVA: $R^2=0.68$, p<0.0001), but were not affected by module geometries (2-way ANOVA: $R^2=0.14$, p>0.9999). The %CV values for plasma flow were substantially higher for 2-module geometries, likely on the basis of exaggerated plasma skimming. Taken together, this data indicates that for CMs that share a common TA, RBC and plasma distribution within each module is unaffected by variations to module resistance.
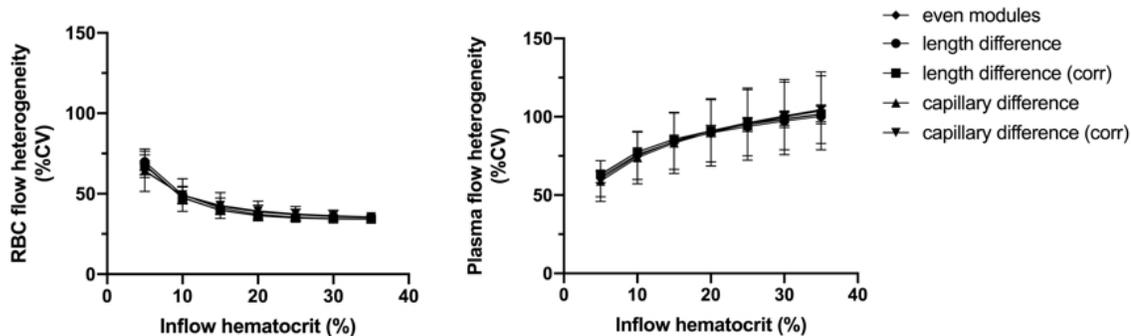
Figure 3.15: Effect of inflow hematocrit on RBC and plasma distribution for 2-module geometries.
Changes to inflow hematocrit lead to a reduction in RBC flow heterogeneity (%CV), and increase in plasma flow heterogeneity (%CV). This effect was not impacted by asymmetric resistances between modules (different length, number of capillaries), or by correction of this asymmetry with adjustments to module driving pressure.

3.4 Discussion

Using both experimental and computational methods, this study provides a detailed analysis of capillary module hemodynamics, and illustrates how RBC and plasma distribution are impacted by the structure of the capillary module and the biophysical properties of the microcirculation. By taking a systematic approach to the evaluation of single modules, followed by two connected modules sharing a common arteriole or venule, a realistic physiological framework is developed in a stepwise fashion that demonstrates the interaction of hemodynamic and rheological components to contribute to blood flow in capillary modules. Particularly, where experimental and computational results diverge, it becomes evident that multiple complex mechanisms of flow regulation must coordinate within a dynamic biological system to achieve the primary goal of adequate oxygen delivery within capillary networks.

Capillary RBC supply rate and capillary module topology were directly measured using intravital videomicroscopy, which provided a grounded truth from which to derive CM hemodynamics – flow, resistance and driving pressure (ΔP). To our knowledge, this study provides the first experimental measurements of these variables together at the level of the capillary module. Zweifach took the inverse approach, and measured pressure and flow through successive branch orders of the arteriolar and venous systems of the rat spinotrapezius muscle [63]. Using measurements from terminal arterioles (4A) and post-capillary venules (4V), he was able to infer the driving pressure and resistance across the capillary network, although capillary flow or the direct linkages between 4A and 4V vessels for individual capillary modules were not assessed. Nevertheless, estimates for

resistance across the capillary portion of the network were in agreement with the CM resistance values derived in this current study. Driving pressure across 4A-4V reported by Zweifach is higher than the mean ΔP in this study, but not outside the range of reported values, and discrepancies can easily be explained by the micro-pressure methods used by Zweifach that perturb the system while undertaking pressure measurements. Moreover, computational modeling in this study confirms that ΔP values derived from experimental data should align with mean experimental RBC flow values, within 1-2 mmHg difference between experimental and computational estimates (Figure 3.8). Taken together, these data suggest that CM driving pressure in resting skeletal muscle is modest – in the 3-6 mmHg range – which would imply that small changes to this value can have important consequences for the magnitude of blood flow in capillary networks.

Surprisingly, RBC flow and resistance for capillary modules are not correlated in this experimental dataset, and plasma flow demonstrates only a weak inverse correlation (Figure 3.5). Differences in correlation for RBC and plasma flow with CM resistance can partly be explained by the positive contribution of CM hematocrit to both RBC flow and resistance, with negligible or inverse effect of inflow hematocrit on CM plasma flow. Similar absence of correlation between RBC flow and resistance was noted by Klitzman and colleagues for individual capillaries and capillary networks [33], which they also remark as contrary to the a priori assumption that these variables should have an inverse relationship. Two-module experimental analysis in our study further supports these observations, when examining the correlation between resistance ratios and flow ratios for module pairs that share a common microvessel. While some pairs do show good agreement between these ratios (e.g. modules with 50% higher resistance have 50% less flow

compared to their pair), there are notable deviations that result in absence of correlation over the entire dataset (Figure 3.6). In these cases, the exceptions prove the rule: module pairs with similar resistance can have markedly different blood flow, and module pairs with markedly different resistance can have similar blood flow rates. These behaviors were not affected whether the modules shared a common arteriole or common venule. Taken together, this strongly suggests the presence of active flow regulation at the level of each capillary module.

If CM flow is largely independent from resistance, and distribution of flow between module pairs is not determined by their proportional resistance, attention then logically turns to the regulation of CM driving pressure as a method for flow regulation. For module pairs that share a common venule, it may seem obvious that arterioles would not necessarily have the same flow or pressure boundary conditions – nevertheless it is important to note that the above analysis confirms this hemodynamic condition. However, for module pairs that share a common arteriole, the question becomes more intriguing. Because these pairs are constrained by an arteriolar boundary condition, the lack of correlation between flow ratios and resistance ratios implies the need for post-capillary mechanisms of flow regulation to independently adjust venular pressure. Using a 2-module computational simulation, we show that even when module pairs have a two-fold difference in resistance (e.g. twice the length), balanced RBC flow can be achieved with only a 1 mmHg adjustment in venular pressure for both modules (Figure 3.14). Further, our experimental data show that the estimated differentials between driving pressures for module pairs is generally less than 2mmHg, and is not different whether the modules share a common arteriole or venule (Figure 3.7). Because these observations are made in resting skeletal muscle, it is unlikely

that the pressure regulation needs to be very tightly controlled, as blood flow and oxygen supply far exceeds the metabolic requirements of surrounding tissue [40]. This may also explain why pressure ratios were not correlated with resistance ratios in module pairs, as we hypothesized. During active hyperemia, however, these differences in resistance between module pairs may become more important, to ensure that the module with lower resistance does not divert blood away from its neighbor. Delashaw and Duling noted that module pairs sharing a common TA will behave synchronously when stimulated or inhibited with pharmacological or physiological interventions [11], however their study did not quantify the distribution of blood flow response between modules. Our current study adds to this line of inquiry, and suggests that consideration for flow regulation of module pairs requires two loci of flow control for each module, in order to compensate for any asymmetry in resistance.

These findings highlight the importance of understanding the properties of smaller functional units in the microcirculation before proceeding with larger network simulations. Recent studies in the field of neurovascular physiology have undertaken massive computational simulations of reconstructed complete cortical capillary networks [26, 28, 54]; these studies have proposed depth-dependent variations to capillary hematocrit within the rodent cortex and dominant contributions of capillary networks to overall network resistance. However, such models potentially fail to account for local mechanisms of flow regulation, such as the resistance-independent flow characteristics of CMs, which are non-evident and have significant implications for modeling design.

In order to further examine how flow might be regulated within these observed capillary modules, computational simulations of boundary conditions were undertaken for 1-module and 2-module geometries. We considered how isolated changes to driving pressure, arteriole diameter, and inflow hematocrit affect the magnitude and distribution of RBC and plasma flow within a module. This analysis has revealed that each of these boundary conditions has a particular impact on blood flow through a capillary module. As shown in Figure 3.8, variations to driving pressure are the most straightforward mechanism for achieving a direct change in blood flow, which is caused exclusively through modulation of RBC (and plasma) velocity, and with no effect on flow distribution or hematocrit within the module. By contrast, variations to the diameter of the arteriole – the portion of microvessel feeding the CM and within the CM itself - has non-intuitive hemodynamic characteristics. Specifically, this arteriole functions as a manifold (Figure 3.11), and maintains similar entrance pressures for all capillaries in the module, regardless of their position. While it is clear that variations to arteriolar diameters have important considerations for blood flow distribution within the larger resistance network [57], and that the position of terminal arterioles (4A) along the transverse arteriole (3A) can affect flow distribution between modules [18, 51], the biophysical interactions between 4A arterioles and their immediate daughter capillaries have not previously been considered. The likely explanation for this manifold effect is the short inter-capillary distance (~15μm) compared to the length of the capillaries (~480μm). Hemodynamically, this manifold will ensure that changes in 4A pressure have a similar effect on all capillaries within the module. Furthermore, arteriolar dilation does not significantly alter RBC flow distribution within the module, but does result in homogenization of capillary hematocrit between capillary

segments (Figure 3.10). This can partly be explained by the phase separation of blood flow at microvascular bifurcations, that will preferentially distribute RBCs towards the bifurcation with higher blood flow [45], causing plasma skimming in proximal capillaries. Fraser and colleagues showed that the bifurcation law is valid for bifurcations within a capillary module [19], but did not include inflow and outflow microvessels for these networks. Terminal arterioles will give rise to many capillaries in quick succession, and the proportion of blood flow into the proximal capillary is markedly skewed compared to the proportion of blood that continues in the arteriole for the remaining capillaries in the module; this phenomenon appears exaggerated when the diameter of the arteriole approaches the same as the capillaries. These computational findings suggest that the immediate point of interaction between the terminal arteriole and the capillary module is an important hemodynamic location for blood flow within microvascular networks, which merits further computational and experimental study.

To further examine these results, variations to inflow hematocrit were specifically tested. Using computational modeling, we showed that when all other parameters are equal, the relationship between inflow hematocrit and capillary hematocrit in a module was linear, whereas the relationship with RBC flow was non-linear, which resuleds in relatively minimal increases to overall RBC flow when hematocrit exceeds 20% (Figure 3.12). The main explanation for these findings is that increases to capillary hematocrit will cause a viscosity-dependent reduction in RBC velocity. Lower hematocrit vessels will have lower overall resistance and therefore higher RBC velocity and plasma flow, whereas capillaries with higher hematocrit will support higher RBC flow, but at the expense of increased resistance, lower RBC velocity, and reduced plasma flow. Moreover, 2-module simulations

with asymmetric geometries demonstrate substantial discrepancies in RBC flow between modules, whereas plasma flow was more balanced (Figure 3.14); this suggests that the preferential RBC flow to the module with lower geometric resistance (shorter length, more capillaries) will cause a viscosity-dependent increase in hemodynamic resistance that impairs plasma flow. Early work by Fung began to explore these concepts, by suggesting how local asymmetries to capillary hematocrit at bifurcations would eventually self-regulate through mechanisms of increased capillary resistance [22]. Recently, computational modelling has shown how RBC hemodynamics directly promote well-balanced velocities at bifurcations which are more conducive to efficient flow regulation [53]. Conversely, extreme variations to RBC velocity, and therefore RBC transit time, have been suggested to contribute to tissue dysoxia by affecting local oxygen availability [31]. Although it might be considered that RBC velocity and hematocrit distribution are of equal significance for oxygen exchange, theoretical analyses have shown that variations to hematocrit are a more efficient mechanism for increasing oxygen exchange with surrounding tissue [16, 36]. Overall, we conclude that spatial RBC distribution has an important effect on local RBC hemodynamics, particularly given the interactions between hematocrit and RBC flow.

Empirical analysis in the current study shows that viscosity contributes approximately 10% to overall module resistance at rest, compared to the dominant contribution of module geometry (length, parallel capillaries); similar to computational findings, this can be explained by the low hematocrit in resting capillary modules – rarely above 20%, often below 10% - which mitigate these effects. However, viscosity-dependent increases to capillary module resistance likely have important consequences for the

regulation of functional hyperemia, whereby capillary hematocrit increases towards systemic hematocrit, with simultaneous increase to RBC velocity as seen in skeletal muscle with contractions [7, 32], and cortical activation [34, 35]. In the skeletal muscle contraction small animal models, increases to mean capillary hematocrit are observed >20% but do reach the values of >40% encountered in the systemic circulation. As noted above, increases to RBC velocity can be achieved through increases to CM driving pressure, but will not increase capillary hematocrit or result in RBC flow homogenization. Conversely, isolated increases to inflow hematocrit will increase capillary hematocrit, but will have a detrimental effect to RBC velocity. Thus, we infer that functional hyperemia must occur through increases to inflow hematocrit and CM driving pressure together, which could be accomplished by dilation of the 4A arteriole, or through alterations to pressure and hematocrit in the 3A arterioles, as was proposed by Sweeney and Sarelius [61]. Taken together, these findings suggest that isolated adjustments to individual boundary conditions are unreasonable, and microvascular regulation of oxygen exchange requires mechanisms that account for the interactions between pressure, flow, and hematocrit.

The structure of the capillary module also appears to have important implications for RBC distribution. Similar to experimental findings of Ellis et al. [12], 1-module computational simulations show that increases to module supply rate (via increased hematocrit) cause a reduction in RBC flow heterogeneity between capillary segments in the module. The branching pattern of the module significantly alters this effect, whereby the simplified module with no branching achieves near complete homogenization of RBC flow, whereas moderate and high branching patterns will have an RBC heterogeneity of at least 35%-40%, regardless of increases to inflow hematocrit (3.13). This observation is

supported by Pries and colleagues, who demonstrated that network topology can significantly alter RBC distribution [43]. Furthermore, RBC flow heterogeneity is of a similar magnitude when modules are connected together and share a common arteriole, or if they are treated in isolation. Interestingly, we observe almost identical RBC flow heterogeneity for all 2-module geometries, regardless of asymmetry in lengths and capillary numbers between modules (3.15). From this, we can conclude that RBC heterogeneity is an intrinsic property of capillary networks, and arises from the interaction of network geometry and RBC rheology.

By applying the Fahraeus effect to capillary-RBC hemodynamics derived from intravital videomicroscopy, this study has demonstrated higher values for RBC %CV when compared with plasma %CV for capillary segments in a module (Figure 3.3). This is in accordance with a previous study by our group that demonstrated greater flow heterogeneity for RBC versus plasma in resting muscle before the onset of hyperinsulinemia [1]. In contrast, the computational simulations showed consistently higher %CV values for plasma compared with RBC distribution. There are a number of reasons why these discrepancies between experimental and computational results are to be expected. Firstly, the geometries for the synthetic networks are simplified reconstructions that do not perfectly reflect the internal branching structure of in vivo modules; moreover, only one geometric configuration of length (480μm) and parallel capillaries (~10) was used in computational modeling, in contrast to the many encountered in the experimental dataset. Secondly, the synthetic geometries do not account for variations in diameter between capillaries, or along the length of each capillary – both of which will affect their resistance, viscosity and flow distribution within a module [42, 55]. Thirdly, plasma is a

Newtonian fluid that can easily be divided at bifurcations, whereas RBCs are discrete cells that have non-linear behaviors are bifurcations. Lastly, and perhaps most importantly, the experimental data is derived from 2-minute video sequences, whereas the computational model is steady-state. Thus, time-dependent variations to RBC flow – via changes to arteriolar pressure and inflow hematocrit - are incorporated into the observed heterogeneity of experimental data, but are notably absent from computer simulations. For example, the proportional change from 5% to 15% inflow hematocrit results in a tripling of RBC flow, with only minor incremental reduction to plasma flow (95% vs 85%), amplifying the time-dependent alterations to RBC heterogeneity observed in vivo. Balogh and Bagchi identified temporal heterogeneity as more pronounced than spatial heterogeneity in artificial microvascular networks [3], and found significant discrepancies between time-averaged and time-dependent models of RBC flow [4]. Other time-dependent models have highlighted the emergence of non-linear behaviors including vasomotion [8, 17] and chaotic unsteady-state flow [23]. We can therefore conclude that temporal variations in microvascular flow have important contributions to RBC distribution and heterogeneity in capillary networks. The other missing elements from this current study are the discrete nature of RBCs which are absent in continuous fluid modeling. Cellular scale modeling of RBC flow in artificial microvascular networks has revealed biophysical properties, particularly the skewness of hematocrit profiles, that cause reverse partitioning in contrast to the classical bifurcation law [4, 37, 58]; these behaviors also result from cell-jamming at bifurcations that dramatically alters downstream pressure and hematocrit [3]. Other phenomena represented in discrete cell modeling are cell-cell interactions [5] and RBC

membrane deformability [29], each of which adds another layer of complexity when evaluating the distribution of RBCs in microvascular networks.

In conclusion, this study has demonstrated novel and non-intuitive relationships between flow and resistance at the level of the capillary module that suggest active flow regulation is occurring via control of module driving pressure; the interconnected structure of these CMs strongly supports the need for pre- and post-capillary loci of flow regulation. Computational simulations highlight the complex interactions between RBC flow, hematocrit, and resistance that are impacted by the unique structural properties of capillary modules; results suggest multiple mechanisms of flow regulation must act together to achieve the desired blood flow effects during functional hyperemia. Comparison between experimental and computational results suggests time-dependent mechanisms of flow regulation are an important factor that affects the regulation of RBC distribution and oxygen delivery in the microcirculation.

3.5 References

1.   **Akerstrom T, Goldman D, Nilsson F, et al** (2020) Hyperinsulinemia does not cause de novo capillary recruitment in rat skeletal muscle. *Microcirculation* 27:.

2.   **Bagher P, Segal SS** (2011) Regulation of blood flow in the microcirculation: role of conducted vasodilation. *Acta Physiol* 202:271–284.

3.   **Balogh P, Bagchi P** (2017) Direct Numerical Simulation of Cellular-Scale Blood Flow in 3D Microvascular Networks. *Biophys J* 113:2815–2826.

4.   **Balogh P, Bagchi P** (2018) Analysis of red blood cell partitioning at bifurcations in simulated microvascular networks. *Phys Fluids* 30:051902.

5.   **Barber JO, Restrepo JM, Secomb TW** (2011) Simulated Red Blood Cell Motion in Microvessel Bifurcations: Effects of Cell–Cell Interactions on Cell Partitioning. *Cardiovasc Eng Technol* 2:349–360.

6.   **Canham PB, Potter RF, Woo D** (1984) Geometric accommodation between the dimensions of erythrocytes and the calibre of heart and muscle capillaries in the rat. *J Physiol* 347:697–712.

7.   **Copp SW, Ferreira LF, Herspring KF, et al** (2009) The effects of aging on capillary hemodynamics in contracting rat spinotrapezius muscle. *Microvasc Res* 77:113–9.

8.   **Davis JM, Pozrikidis C** (2014) Self-sustained Oscillations in Blood Flow Through a Honeycomb Capillary Network. *Bull Math Biol* 76:2217–2237.

9.   **Davis MJ** (2012) Perspective: physiological role(s) of the vascular myogenic response. *Microcirculation* 19:99–114.

10.   **Davis MJ, Hill MA, Kuo L** (2011) Local Regulation of Microvascular Perfusion. In: Comprehensive Physiology. John Wiley & Sons, Inc., Hoboken, NJ, USA

11.   **Delashaw JB, Duling BR** (1988) A study of the functional elements regulating capillary perfusion in striated muscle. *Microvasc Res* 36:162–171.

12.   **Ellis CG, Wrigley SM, Groom AC** (1994) Heterogeneity of red blood cell perfusion in capillary networks supplied by a single arteriole in resting skeletal muscle. *Circ Res* 75:357–368.

13.   **Ellis CG, Ellsworth ML, Pittman RN, Burgess WL** (1992) Application of image analysis for evaluation of red blood cell dynamics in capillaries. *Microvasc Res* 44:214–25.

14.   **Ellis CG, Jagger J, Sharpe M** (2005) The microcirculation as a functional system. *Crit Care* 9 Suppl 4:S3-8.

15.   **Ellsworth ML, Popel AS, Pittman RN** (1988) Assessment and impact of heterogeneities of convective oxygen transport parameters in capillaries of striated muscle: Experimental and theoretical. *Microvasc Res* 35:341–362.

16. **Federspiel WJ, Popel AS** (1986) A theoretical analysis of the effect of the particulate nature of blood on oxygen release in capillaries. *Microvasc Res* 32:164–89.

17. **Forouzan O, Yang X, Sosa JM, et al** (2012) Spontaneous oscillations of capillary blood flow in artificial microvascular networks. *Microvasc Res* 84:123–132.

18. **Frame MD, Sarelius IH** (1993) Regulation of capillary perfusion by small arterioles is spatially organized. *Circ Res* 73:155–63.

19. **Fraser GM, Goldman D, Ellis CG** (2012) Microvascular Flow Modeling using In Vivo Hemodynamic Measurements in Reconstructed 3D Capillary Networks. *Microcirculation* 19:510–520.

20. **Fraser GM, Milkovich S, Goldman D, Ellis CG** (2012) Mapping 3-D functional capillary geometry in rat skeletal muscle in vivo. *Am J Physiol Circ Physiol* 302:H654–H664.

21. **Fraser GM, Sharpe MD, Goldman D, Ellis CG** (2015) Impact of Incremental Perfusion Loss on Oxygen Transport in a Capillary Network Mathematical Model. *Microcirculation* 22:348–359.

22. **Fung Y-C** (1973) Stochastic flow in capillary blood vessels. *Microvasc Res* 5:34–48.

23. **Geddes JB, Carr RT, Wu F, et al** (2010) Blood flow in microvascular networks: a study in nonlinear biology. *Chaos* 20:045123.

24. **Goldman D, Popel AS** (2000) A computational study of the effect of capillary network anastomoses and tortuosity on oxygen transport. *J Theor Biol* 206:181–94.

25. **Goldman D, Bateman RM, Ellis CG** (2006) Effect of decreased O2 supply on skeletal muscle oxygenation and O2 consumption during sepsis: role of heterogeneous capillary spacing and blood flow. *Am J Physiol Heart Circ Physiol* 290:H2277-85.

26. **Gould IG, Tsai P, Kleinfeld D, Linninger A** (2017) The capillary bed offers the largest hemodynamic resistance to the cortical blood supply. *J Cereb Blood Flow Metab* 37:52–68.

27. **Gutterman DD, Chabowski DS, Kadlec AO, et al** (2016) The Human Microcirculation: Regulation of Flow and beyond. *Circ Res* 118:157–172.

28. **Hartung G, Vesel C, Morley R, et al** (2018) Simulations of blood as a suspension predicts a depth dependent hematocrit in the circulation throughout the cerebral cortex. *PLOS Comput Biol* 14:e1006549.

29. **Hyakutake T, Nagai S** (2015) Numerical simulation of red blood cell distributions in three-dimensional microvascular bifurcations. *Microvasc Res* 97:115–123.

30. **Japee SA, Pittman RN, Ellis CG** (2005) A new video image analysis system to study red blood cell dynamics and oxygenation in capillary networks. *Microcirculation* 12:489–506.

31. **Jespersen SN, Østergaard L** (2012) The Roles of Cerebral Blood Flow, Capillary Transit Time Heterogeneity, and Oxygen Tension in Brain Oxygenation and Metabolism. *J Cereb Blood Flow Metab* 32:264–277.

32. **Kindig CA, Richardson TE, Poole DC** (2002) Skeletal muscle capillary hemodynamics from rest to contractions: implications for oxygen transfer. *J Appl Physiol* 92:2513–20.

33. **Klitzman B, Johnson PC** (1982) Capillary network geometry and red cell distribution in hamster cremaster muscle. *Am J Physiol* 242:H211-9.

34. **Lee J, Wu W, Boas DA** (2016) Early capillary flux homogenization in response to neural activation. *J Cereb Blood Flow Metab* 36:375–380.

35. **Li Y, Wei W, Wang RK** (2018) Capillary flow homogenization during functional activation revealed by optical coherence tomography angiography based capillary velocimetry. *Sci Rep* 8:4107.

36. **Lücker A, Secomb TW, Weber B, Jenny P** (2017) The relative influence of hematocrit and red blood cell velocity on oxygen transport from capillaries to tissue. *Microcirculation* 24:e12337.

37. **Mantegazza A, Clavica F, Obrist D** (2020) In vitro investigations of red blood cell phase separation in a complex microchannel network. *Biomicrofluidics* 14:014101.

38. **Murrant CL, Lamb IR, Novielli NM** (2017) Capillary endothelial cells as coordinators of skeletal muscle blood flow during active hyperemia. *Microcirculation* 24:1–10.

39. **Plyley MJ, Sutherland GJ, Groom AC** (1976) Geometry of the capillary network in skeletal muscle. *Microvasc Res* 11:161–173.

40. **Poole DC** (2019) Edward F. Adolph Distinguished Lecture. Contemporary model of muscle microcirculation: gateway to function and dysfunction. *J Appl Physiol* 127:1012–1033.

41. **Potter RF, Groom AC** (1983) Capillary diameter and geometry in cardiac and skeletal muscle studied by means of corrosion casts. *Microvasc Res* 25:68–84.

42. **Pries AR, Schonfeld D, Gaehtgens P, et al** (1997) Diameter variability and microvascular flow resistance. *Am J Physiol Circ Physiol* 272:H2716–H2725.

43. **Pries AR, Secomb TW, Gaehtgens P** (1996) Relationship between structural and hemodynamic heterogeneity in microvascular networks. *Am J Physiol - Hear Circ Physiol* 270:545–553.

44. **Pries AR, Secomb TW, Gaehtgens P** (1995) Structure and hemodynamics of microvascular networks: heterogeneity and correlations. *Am J Physiol Circ Physiol* 269:H1713–H1722.

45. **Pries AR, Ley K, Claassen M, Gaehtgens P** (1989) Red cell distribution at microvascular bifurcations. *Microvasc Res* 38:81–101.

46. **Pries AR, Ley K, Gaehtgens P** (1986) Generalization of the Fahraeus principle for microvessel networks. *Am J Physiol* 251:H1324-32.

47. **Pries AR, Secomb TW, Gaehtgens P, Gross JF** (1990) Blood flow in microvascular networks. Experiments and simulation. *Circ Res* 67:826–834.

48. **Pries AR, Secomb TW, Gessner T, et al** (1994) Resistance to blood flow in microvessels in vivo. *Circ Res* 75:904–15.

49. **Pries AR** (2019) Microvascular hemodynamics: System properties. *Biorheology* 56:1–13.

50. **Pries AR, Secomb TW** (2008) Blood Flow in Microvascular Networks. In: Microcirculation. Elsevier, pp 3–36

51. **Sarelius IH** (1993) Cell and oxygen flow in arterioles controlling capillary perfusion. *Am J Physiol* 265:H1682-7.

52. **Schmid-Schönbein GW, Skalak R, Usami S, Chien S** (1980) Cell distribution in capillary networks. *Microvasc Res* 19:18–44.

53. **Schmid F, Barrett MJP, Obrist D, et al** (2019) Red blood cells stabilize flow in brain microvascular networks. *PLOS Comput Biol* 15:e1007231.

54. **Schmid F, Tsai PS, Kleinfeld D, et al** (2017) Depth-dependent flow and pressure characteristics in cortical microvascular networks. *PLOS Comput Biol* 13:e1005392.

55. **Secomb TW, Hsu R** (1997) Resistance to Blood Flow in Nonuniform Capillaries. *Microcirculation* 4:421–427.

56. **Secomb TW** (2017) Blood Flow in the Microcirculation. *Annu Rev Fluid Mech* 49:443–461.

57. **Segal SS** (2005) Regulation of blood flow in the microcirculation. *Microcirculation* 12:33–45.

58. **Shen Z, Coupier G, Kaoui B, et al** (2016) Inversion of hematocrit partition at microfluidic bifurcations. *Microvasc Res* 105:40–46.

59. **Sherman TF** (1981) On connecting large vessels to small. The meaning of Murray's law. *J Gen Physiol* 78:431–453.

60. **Skalak TC, Schmid-Schönbein GW** (1986) The microvasculature in skeletal muscle. IV. A model of the capillary network. *Microvasc Res* 32:333–347.

61. **Sweeney TE, Sarelius IH** (1989) Arteriolar control of capillary cell flow in striated muscle. *Circ Res* 64:112–120.

62. **Tyml K, Ellis CG, Safranyos RG, et al** (1981) Temporal and spatial distributions of red cell velocity in capillaries of resting skeletal muscle, including estimates of red cell transit times. *Microvasc Res* 22:14–31.

63. **Zweifach BW, Kovalcheck S, De Lano F, Chen P** (1981) Micropressure-flow relationships in a skeletal muscle of spontaneously hypertensive rats. *Hypertension* 3:601–614.

CHAPTER 4: DYNAMIC TRACKING OF MICROVASCULAR HEMOGLOBIN CONTENT FOR CONTINUOUS PERFUSION MONITORING IN THE INTENSIVE CARE UNIT: PILOT FEASIBILITY STUDY

4.1 Introduction

The peripheral microcirculation is one of the physiological windows that can be assessed at the bedside for patients in the intensive care unit (ICU) with circulatory shock [61]. Perfusion status correlates better with ICU outcomes than macro-hemodynamics [1, 15], and there is emerging study of perfusion-guided resuscitation using clinical indicators such as capillary refill time, skin mottling, and body temperature gradients [23, 25]. Although these measurements can be standardized, they are often subject to inter-observer variability and lack refinement beyond rudimentary measures.

Microvascular monitoring has been proposed as an adjunct strategy for quantifying peripheral perfusion in the ICU [13, 37]. Near-infrared spectroscopy (NIRS) can be applied continuously and non-invasively to measure tissue oxygen saturation (StO2) of hemoglobin in skeletal muscle and overlying tissue [4]. Since venules contain the majority of blood in the microcirculation, StO2 can be viewed primarily as a measure of regional venous oxygen saturation [38]. However, a recent randomized controlled trial did not show

benefit for incorporating StO2 in a sepsis protocol [41], suggesting this may not be the correct target for microvascular resuscitation.

There is a need for physiologically-informed methods for evaluating the peripheral microcirculation that describe the dynamic process of oxygen delivery in microvascular networks. Traditionally, NIRS considers two distinct hemoglobin chromophores: oxy- (Hb-O2) and deoxy- (Hb) hemoglobin, with the sum of both chromophores denoted as total hemoglobin (HbT) [3]. Changes in HbT are proposed as a surrogate for changes in blood volume, assuming incorrectly that the microcirculation has a fixed hematocrit [34, 66]. In reality, red blood cells (RBCs) do not exist in exclusively oxy/deoxy states and contain millions of hemoglobin proteins with an aggregate RBC oxygen saturation. Furthermore, hematocrit and RBC flow in microvascular networks are highly heterogeneous [51], and temporal variations in HbT reflect changes in blood volume, hematocrit, and flow velocity within all three microvascular compartments (arterioles, capillaries, and venules) [4, 17].

We propose **microvascular hemoglobin content (MHC)** to denote the total hemoglobin contained in all the RBCs in the microcirculation. Although technically equivalent to HbT, the distinction arises from how this measurement is evaluated as a time-dependent physiological variable. MHC variability represents the continuous process of RBC distribution that is regulated within the underlying microcirculation, and we hypothesize that MHC may serve as a novel hemodynamic metric for monitoring microvascular function in the ICU. The goal of the current study is to (i) outline the theory and rationale for the technology, (ii) evaluate the feasibility of signal acquisition and signal

analysis in the intended clinical environment, and (iii) present the findings of this pilot cohort with an emphasis on signal characterization and descriptive statistics.

4.2 Methods

4.2.1 Study details

This is a prospective observational cohort study. Patients were recruited in a tertiary adult medical-surgical ICU (July 2017-April 2019) and all research practices were performed in accordance with institutional ethics protocol and approval (REB #108760). Participants were recruited within 48 hours of admission to the ICU, and consent was obtained from the patient or substitute decision maker prior to commencement of the study. The NIRS system was applied to the quadriceps, biceps, and/or deltoid.

Recordings were initiated immediately after recruitment, or as soon as possible permitting clinical workflow. The system was applied to the vastus medialis, vastus lateralis, biceps, and/or deltoid, with vastus medialis and biceps being the most frequent sites of application. The system was applied over the bulk of the muscle group to limit overlying subcutaneous tissue; location of the probe was also selected to minimize interference with patient positioning, lines, tubing, and medical care. Duration of recording was up to four hours at the bedside, or as long as permitted within clinical workflow.

Participants were excluded if they were outside the 48-hour window, or if consent was not possible to obtain; patients were also excluded with excessive subcutaneous tissue

(BMI > 35) or cutaneous pigmentation (e.g. jaundice, melanin) that might confound NIRS measurements.

This was a one-time study, with no additional follow-up, testing, or intervention other than the application of the NIRS system for MHC monitoring. Physiological variables (e.g. HR, MAP, SaO2%), doses of vasoactive medications, and ICU interventions (e.g. ventilation parameters) were recorded at the bedside; clinical history and laboratory values were obtained from medical records.

4.2.2 High-resolution NIRS for measuring microvascular hemoglobin content

Microvascular hemoglobin content (i.e. HbT concentration) is derived from NIRS signal sampled at high temporal resolution (10 Hz). For most NIRS wavelengths, variations in hemoglobin concentration (HbT) or saturation (StO2) can both affect tissue absorption. The isosbestic wavelength of hemoglobin defines the wavelength with identical extinction coefficients for Hb-O2 and Hb; in the near-infrared spectrum this occurs at approximately 798nm [32]. Therefore, changes in tissue absorbance at the isosbestic wavelength only detect variations in HbT concentration [3, 34]. In this study, MHC variability was measured using isosbestic NIRS, and can equally be calculated with two wavelengths to derive HbT as the sum of Hb-O2 and Hb hemoglobin chromophores [34].

This time-dependent HbT measurement also accounts for the contribution of melanin and myoglobin, that significantly affect NIRS absorption in peripheral tissue [9]. Because melanin and myoglobin have fixed tissue concentrations, they do not contribute

to the temporal variability in NIRS signal [4]; myoglobin saturation may vary within skeletal muscle, but the concentration is static. Thus, high-resolution NIRS specifically measures the temporal change in hemoglobin content, as a surrogate for RBC flow within the underlying microcirculation.

4.2.3 Engineering and system details

Measurements were acquired with a continuous-wave broadband NIRS system based on a modified off-the-shelf spectrometer (QE65000 Ocean Optics, Dunedin, FL) and a halogen lamp (Ocean Optics HL-2000-HP). Technical specifications and proof-of-concept of the NIRS system have been described previously [10].

Data capture was performed using SpectraSuite™ software (Ocean Optics, Inc.). Light intensities were recorded at the isosbestic wavelength 798nm with a sampling frequency of 10 Hz (100 ms integration time). Source detector distance (SDD) was 20mm (7 participants) and 15mm (29 participants). Shorter SDD interrogates a smaller volume of tissue and depth of penetration, but with higher light intensities recovered by the spectrometer; this modification was made when very low intensity signal was encountered for one patient early in the cohort.

Light intensity is converted to *change in optical density* (ΔOD) as follows: $\Delta OD(t) = log_{10} \frac{I(t_o)}{I(t)}$, where $I(t_o)$ is the initial intensity at time = 0, and $I(t)$ is the intensity at any subsequent time, t.

Assuming that tissue scattering does not change during the recording, ΔOD measures the change from baseline in HbT concentration in arbitrary units [55]. ΔOD time series (i.e. MHC tracings) were screened manually for artifacts (see section 4.2.5). Only continuous tracings of greater than 5 minutes with adequate signal quality were included in the analysis.

4.2.4 Continuous Wavelet Transform (CWT)

Application of continuous wavelet transform (CWT) for analysis of cardiovascular time series was first described by Stefanovska and colleagues [58], and has gained widespread use in the field of laser doppler flowmetry (LDF) of human skin [6, 33]. CWT is an attractive tool, as it provides good localization of signal in both time and frequency for non-stationary data. Using CWT, time series can be represented as power versus frequency versus time for physiological oscillations ascribed to components of the cardiovascular system [5]. Six "frequency bands" have been derived from pharmacological iontophoresis studies of human skin, and are proposed to represent mechanisms of peripheral and central blood flow control [5, 18, 21, 33] (Table 4.1): (1) B1 metabolic (2) B2 endothelial (3) B3 neurogenic (4) B4 myogenic (5) B5 respiratory (breath rate) and (6) B6 cardiac (heart rate).

Frequency Band	Frequency (Hz)	Period (seconds)	Cycles/minute
B0	0 – 0.005	> 200	< 0.3
B1 - Metabolic	0.005 – 0.0095	105.3 - 200	0.3 – 0.57
B2 – Endothelial	0.0095 - 0.02	50 – 105.3	0.57 – 1.2
B3 – Neurogenic	0.02 – 0.06	16.67 - 50	1.2 – 3.6
B4 – Myogenic	0.06 – 0.16	6.25 – 16.67	3.6 – 9.6
B5 – Respiratory	0.16 – 0.667	1.5 – 6.25	9.6 - 40
B6 – Cardiac	0.667 – 3.1	0.32 – 1.5	40 - 186

Table 4.1: Frequency bands used in the present study, that are attributable to physiological oscillations in the cardiovascular system.
Frequency ranges are adapted from previous studies [18, 33], with modification to the upper limit of respiratory band to include rapid breathing rates observed in the ICU. See references for details [5, 21, 57]

CWT analysis was applied in this study to ΔOD time series using the Morlet wavelet in Matlab v2016b (Figure 4.1). The total power for each frequency band was computed as the sum over the frequency range. B1 (ultra-low frequency) and B6 (high frequency) were removed from the analysis as they were most susceptible to artifacts, as described below. Thus, the final CWT signal is defined from B2-B5 and comprises three microvascular bands B2-B4 and the respiratory band B5. Using CWT, total signal power B2-B5 and for each frequency band is represented with mean, median, and coefficient of variation (%CV) over the duration of the recording; median power was the metric most often used for analysis in this study, being less impacted by extreme values than the mean. When applicable, CWT measurements were averaged for each muscle site, and muscle sites were averaged to calculate summary values for each patient.
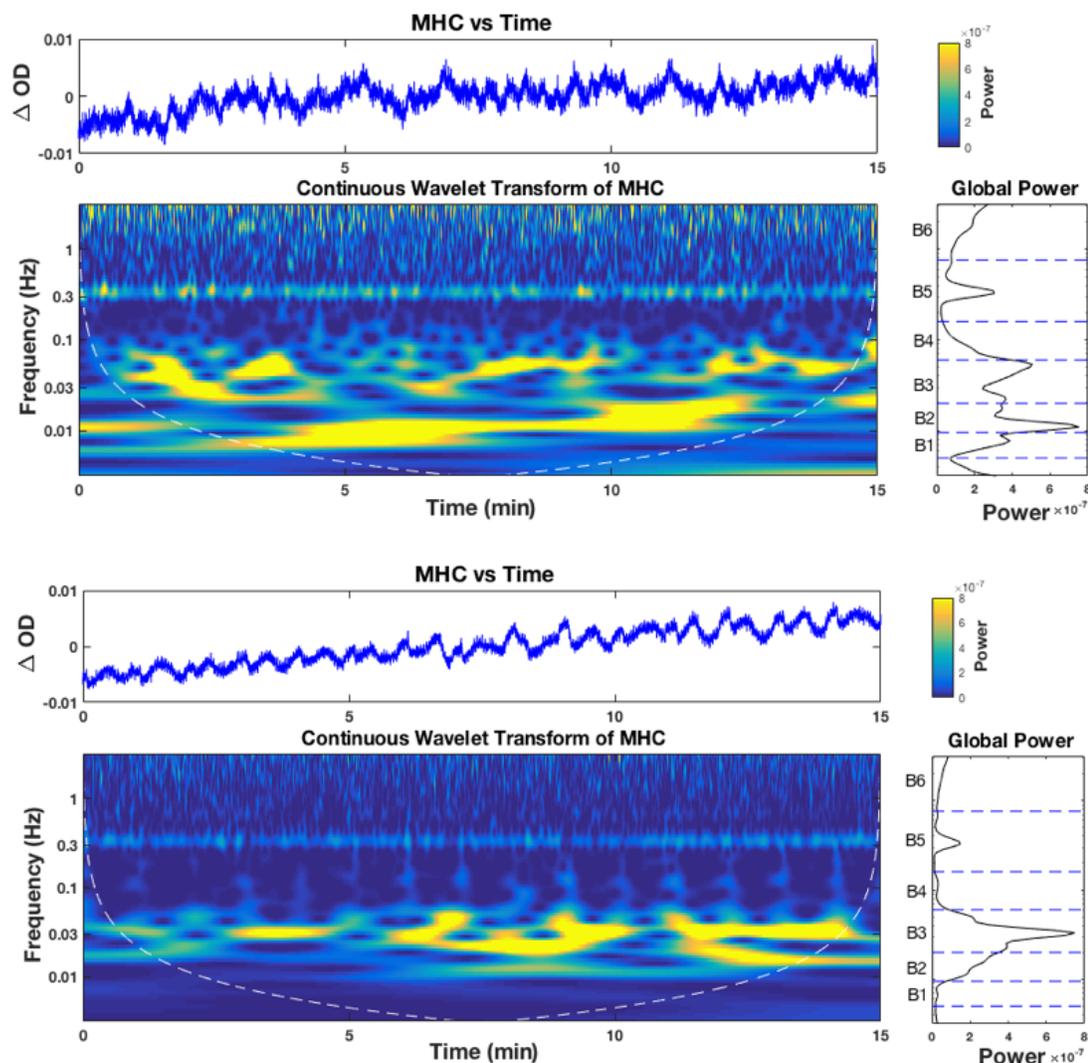
Figure 4.1: Application of continuous wavelet transform (CWT) to microvascular hemoglobin content (MHC) time series in peripheral tissue for continuous perfusion monitoring.

15 minutes of data is shown for two patients with cardiac arrest (upper) and sepsis (lower). MHC variability is defined as the change from baseline in total hemoglobin concentration, measured at high temporal resolution (10 Hz) with isosbestic near-infrared spectroscopy (ΔOD, arbitrary units). MHC time series demonstrates substantial temporal variability, as well as differences in variability patterns between patients.

Data is represented with standard time series (MHC vs time), CWT time-frequency projection (power vs frequency vs time), and the global wavelet power spectrum (GWPS) averaged over the recording (power vs frequency).

Dotted line in the CWT indicates data outside the cone of influence that is susceptible to edge effects. Dashed lines in the GWPS represent the boundaries of the frequency bands used for analysis in this study (B1=metabolic, B2=endothelial, B3=neurogenic, B4=myogenic, B5=respiratory, B6=cardiac).

The percentage contribution (%Power) of each frequency band relative to the total signal power was also quantified. For example, %Power of the respiratory band B5 is calculated as: $\%Power\ B5 = \frac{median\ Power\ B5}{median\ Power\ B2-B5} * 100$. This represents the contribution from the respiratory frequency range (0.16 – 0.667 Hz) to the total signal power. Similar calculations are used to quantify the contribution of frequency bands relative to the microvascular signal B2-B4.

4.2.5 MHC signal artifacts

Some patients underwent MHC monitoring with the NIRS system while also using intermittent pneumatic compression stockings. Representative MHC tracing from the vastus medialis of one patient is shown in Figure 4.2a and demonstrates a stereotyped waveform for venous occlusion. Although these MHC time series are not suitable for CWT analysis, this data supports the application of ΔOD as a straightforward measure of MHC variability in peripheral tissue.

Motion artifacts were easily identified as abrupt discontinuities in MHC signal (4.2b) and were more frequent for awake patients and during periods of stimulation. We observed an upsloping drift in MHC time series during initial application of the probe to the skin surface (4.2c); there is a subsequent stabilization in the signal over minutes to hours. Underlying physiologic variability is not affected by the artifact, except for B1 frequency band which is dominated by this slow drift. We interpret this to represent local heat-mediated vasodilation of cutaneous microvessels.

As shown with the CWT time-frequency projections in Figure 4.1, cardiac band B6 often comprises non-specific high-frequency noise, although in some cases the heart rate was detectable as a power stripe in the cardiac band (data not shown). Because this was an infrequent finding, B6 data was excluded from the analysis. The metabolic band B1 comprises the ultra-low frequencies and was most susceptible to the drift artifact described above; moreover, data from B1 often lies outside the cone of influence, where edge effects from the finite time data become important for making accurate determinations. Thus, B1 data was also excluded from our analysis.
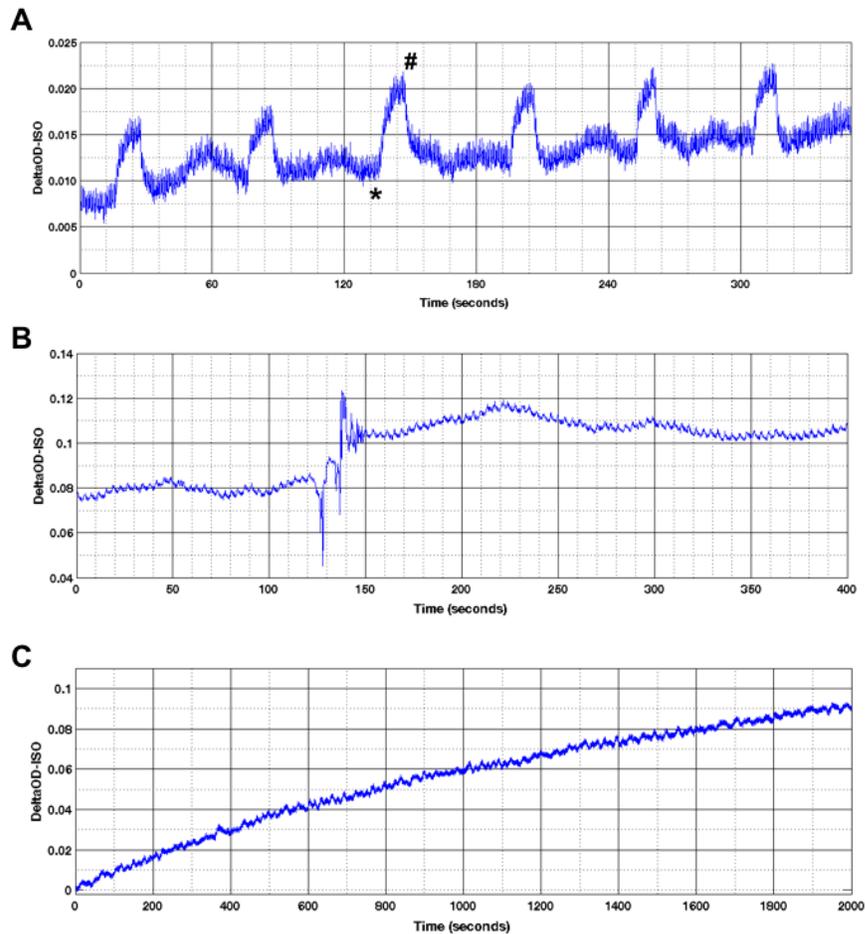
Figure 4.2: Common MHC artifacts encountered in the study.

MHC is derived from the change in optical density at the isosbestic wavelength 798 nm (ΔOD, arbitrary units).

a) MHC tracing is shown from the vastus medialis of a patient using sequential compression stockings cycled at a frequency of 60 seconds. MHC tracing demonstrates stereotypical waveform for venous occlusion, with accumulation of blood in the venous compartment during inflation (*) and rapid venous outflow at the time of deflation (#).

b) Motion artifact in MHC tracing noted as abrupt discontinuity in MHC signal.

c) Upsloping drift artifact in MHC tracing. This occurs over minutes to hours, and the underlying variability in MHC signal is not affected. We interpret this to be local heat-mediated vasodilation.

4.2.6 Statistical Analysis

Statistical analysis was performed using PRISM v8 software package. Lognormal distribution of median power values was assessed with D'Agostino Pearson test, with subsequent analysis performed using parametric tests on -logtransform of median power. Concordance between median power for frequency bands in the same patient was tested with a Pearson correlation matrix. Correlation between different muscle sites in the same patient was assessed with Pearson and Spearman correlation coefficient (r) for median power and %Power, respectively. MHC signal power was compared between patients requiring and not requiring vasoactive medication (vasopressors), patients with serum lactate greater or less than 2.0 mmol/L, and between SDD configurations using Student's unpaired t-test; %CV was compared between patients requiring and not requiring vasopressors using Mann-Whitney U test. Linear regression was used to calculate the coefficient of determination (R^2) between MHC signal power and systemic variables: mean arterial pressure (MAP), serum hemoglobin concentration ([Hb], g/L), arterial oxygen saturation (SpO2, %), and serum lactate (mmol/L).

Linear regression was used to assess correlation between MHC respiratory power B5 and %Power B5, and ventilator parameters - positive end-expiratory pressure (PEEP), driving pressure (ΔP), and tidal volume (Vt); tidal volume was measured as an index of body weight (cc/kg). These relationships were subsequently evaluated with multivariate regression to control for any interactions.

4.3 Results

4.3.1 Feasibility metrics from the pilot cohort

36 patients were recruited for the study with mean recording time 101.50 +/- 50.12 minutes (range: 0.00-221.10) per patient. After manually screening for signal quality and artifacts, the final data set comprised 31 patients with a mean recording time of 74.02 +/- 36.89 minutes (range: 5.83-148.70). Demographics for the final study cohort are provided in Table 3.2.

	N = 31 patients
Age (years)	62.10 +/- 16.55
Male (%)	61.3
Weight (kg)	82.12 +/- 17.67
MAP (mmHg)	75.30 +/- 12.73
HR (bpm)	83.32 +/- 15.68
Sepsis (%)	35.5
Cardiac arrest (%)	19.4
Vasopressors (%)	64.5
Mechanical ventilation (%)	90.3
FiO2	0.40 (0.2)
SpO2%	97 (3.5)
PEEP (cm H_2O)	10 (4)
Lactate (mmol/L)	1.4 (0.8)
[Hb] (g/L)	95 (34.5)

Table 4.2: Demographics for the patients in the final dataset included for analysis. Data are represented as mean +/- SD, median (IQR), or percentage of total cohort (n=31). MAP: mean arterial pressure; HR: heart rate; FiO2: fraction of inspired oxygen; SpO2: arterial oxygen saturation; PEEP: positive end-expiratory pressure; [Hb]: systemic hemoglobin concentration.

Signal quality for the final cohort was high, with median 74% (IQR 54-88) of recorded signal suitable for analysis; the most common reason for signal degradation was motion artifact. Of the five patients unsuitable for analysis, two were excluded due to measurements with compression stockings (this was a naïve error early in the study, but did demonstrate the venous occlusion waveform included in figure 4.2); one patient was excluded due to insufficient signal intensity (SDD of the NIRS system was subsequently modified, as described in methods); one patient was recruited but could not be measured due to clinical circumstances; and one patient was excluded due to excessive motion artifacts.

MHC tracings were recorded from 54 muscles with a mean duration of 42.49 +/- 22.34 minutes (range: 5.50-93.66) per muscle. 20/31 patients had recordings from multiple muscle sites, including three patient with recordings from 3 muscle sites. The main limitations for measuring multiple muscle sites was the presence of compression stockings on the lower extremities, patient positioning, lines and tubing, and change in clinical condition. Vastus medialis and biceps were the most common muscle sites for recording, and easiest to measure with patient positioning and clinical workflow; the deltoid muscle site was most vulnerable to motion artifacts and vastus lateralis was suboptimal due to patient positioning.

4.3.2 MHC signal demonstrates non-stationary temporal dynamics and inter-subject heterogeneity

Figure 4.1 (see above) illustrates 15 minutes of continuous MHC tracings, CWT projection, and global wavelet power spectrum (GWPS) for 2 patients in the cohort (cardiac arrest and sepsis). MHC signal demonstrates biological variability and complexity, and the pattern of MHC variability is not similar for these patients. Using CWT, the time-dependent changes in MHC power at various frequencies is illustrated, and the CWT projections are distinctive between subjects. The cardiac arrest MHC tracing demonstrates a combination of fast and slow frequency components with no discernable pattern throughout the recording; this is reflected in the GWPS with balanced distribution of power throughout the microvascular bands. By contrast, the sepsis MHC tracing is dominated by a slow, periodic and persistent oscillation with occasional episodes of correction – a phenomenon that has been described as vasomotion [47]. In the GWPS, this is represented by a singular broad peak in the neurogenic frequency band.

Median power, %Power, and %CV for MHC signal for the 31 patients in the final dataset is reported in Figure 4.3. Median power values in the cohort follow a lognormal distribution (p>0.05, D'Agostino Pearson test). MHC signal demonstrates substantial temporal variability, represented by the %CV of signal power versus time (Figure 4.3b).
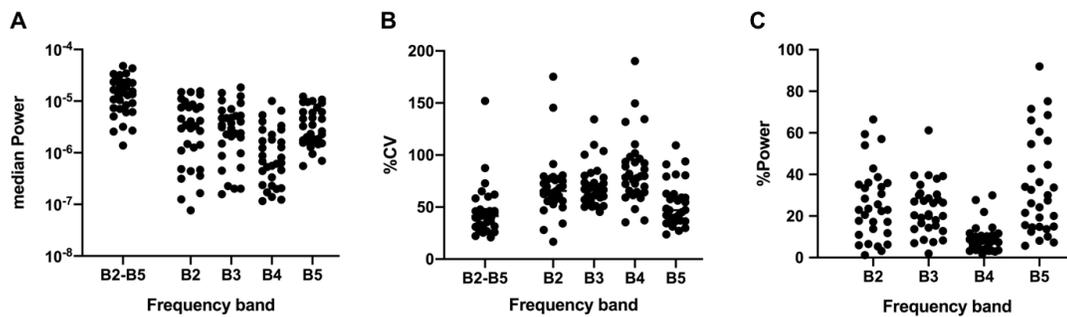
Figure 4.3: MHC signal characteristics for the patients included in the final cohort.

Data reported for total signal B2-B5 and for each frequency band (B2=endothelial, B3=neurogenic, B4=myogenic, B5=respiratory).

a) MHC median power values for patients in the cohort (n=31) follows lognormal distribution (p>0.05, D'Agostino Pearson test).

b) Temporal variation in each frequency band, expressed as coefficient of variation (%CV) of signal power vs time.

c) Percentage contribution (%Power) for each frequency band relative to total signal power B2-B5, calculated as (median Power band / median Power B2-B5).

Correlation matrix for the frequency bands is shown in Figure 4.4; microvascular frequency bands B2-B4 are more closely correlated with each other than the respiratory band B5. There was no significant difference in signal power between SDD 15mm and 20mm (4. 957 vs 4.733, p=0.2019).
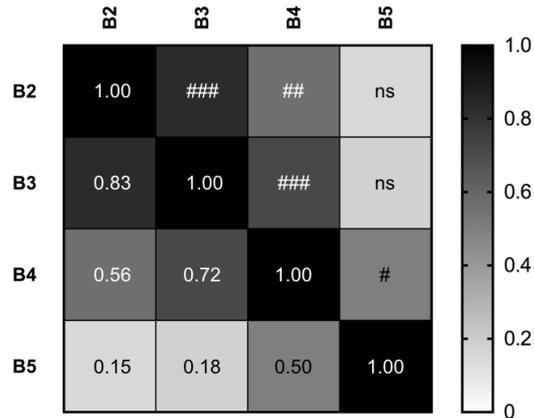
Figure 4.4: Correlation matrix between frequency bands for each patient.
Values represent Pearson correlation coefficient (r) is calculated on -logtransformed data for median Power. Microvascular bands B2-B4 are more strongly correlated with each other than the respiratory band B5.

p = 0.0035; ## p = 0.001; ### p ≤ 0.00001 ; ns p > 0.05

The %Power composition of MHC signal for each patient is shown in Figure 4.5 and is not consistent across the cohort. There is varying contribution to the overall MHC power from the microvascular bands B2-B4 versus respiratory band B5 (Fig. 4.5a). Furthermore, the proportions of each band within the microvascular signal B2-B4 is not consistent (Fig. 4.5b); some patients have balanced power between all three bands, while others have two or even one frequency component that dominates the signal composition.
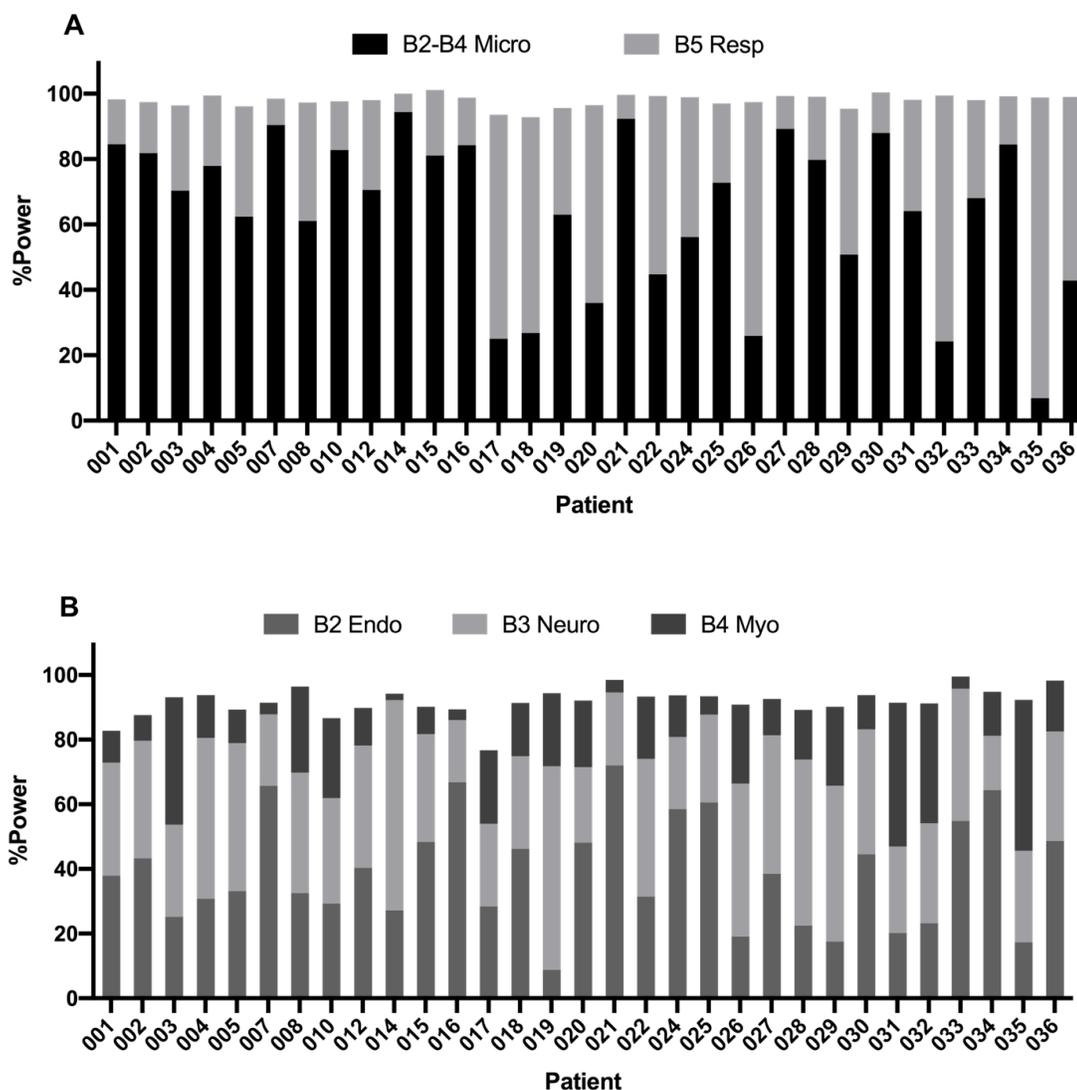
Figure 4.5: Signal power composition for each patient in the cohort.

Wavelet analysis demonstrates the percentage contribution (%Power) from each frequency band relative to overall signal power (B2=endothelial, B3=neurogenic, B4=myogenic, B5=respiratory). %Power composition is not consistent between patients in the cohort.

3a) %Power for microvascular bands B2-B4 and respiratory band B5 relative to overall signal B2-B5; %Power is calculated as (median Power / median Power B2-B5).

3b) %Power for each microvascular band relative to microvascular signal B2-B4; %Power is calculated as (median Power / median Power B2-B4).

4.3.3 MHC signal characteristics are concordant between muscle groups in the same patient and positively correlated with systemic hemoglobin and oxygenation levels

Pairwise comparison for signal power between muscle sites in the same patient demonstrates moderate correlation for microvascular bands B2-B4, but not for respiratory B5 (Figure 4.6). %Power was moderately correlated between muscle sites in all frequency bands (Figure 4.7). MHC microvascular power B2-B4 is positively correlated with systemic hemoglobin levels (Figure 4.8a; R^2=0.24, p=0.0055) and with SpO2 (Figure 4.8b; R^2=0.15, p=0.0410).
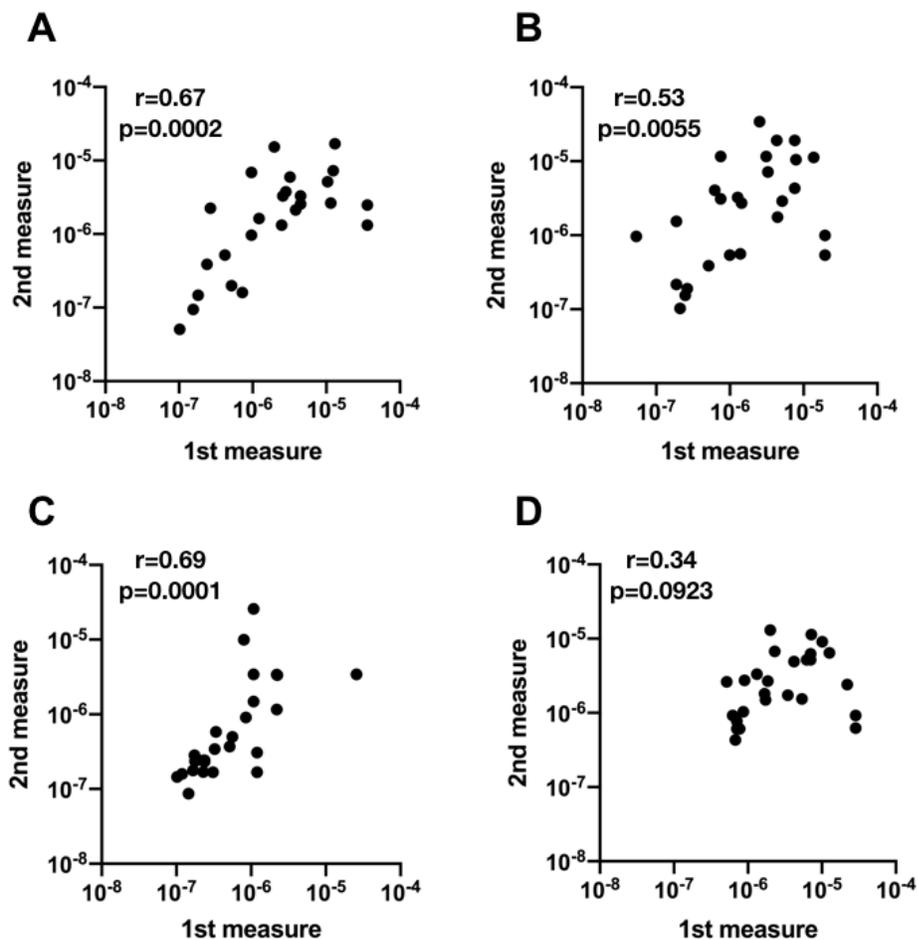
Figure 4.6: Correlation between MHC median Power in each frequency band for muscle sites in the same patient.

Pairwise comparisons (n=26) were made for patients with 2 (n=17) or 3 (n=3) muscle site measurements. Values represent Pearson correlation coefficient, r, derived from -logtransformed data for median Power for a) B2 endothelial band, b) B3 neurogenic band, c) B4 myogenic band, and d) B5 respiratory band. Median Power from microvascular bands B2-B4 are correlated between muscle sites. Median Power from respiratory band B5 is not correlated between muscle sites. ns: not significant p>0.05.
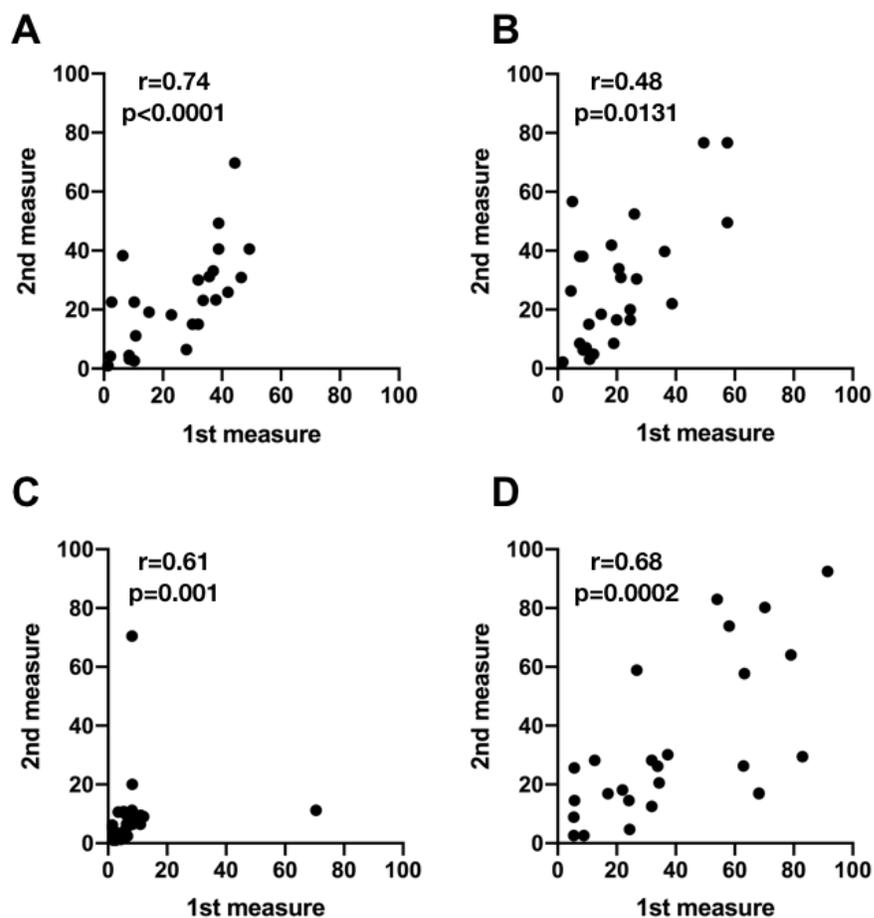
Figure 4.7: Correlation between MHC %Power in each frequency band for muscle sites in the same patient.

Pairwise comparisons (n = 26) were made for patients with 2 (17) or 3 (3) muscle site measurements. Values represent Spearman correlation coefficient, r derived from %Power for a) B2 endothelial band, b) B3 neurogenic band, c) B4 myogenic band, and d) B5 respiratory band. %Power is correlated between muscle sites for all frequency bands.
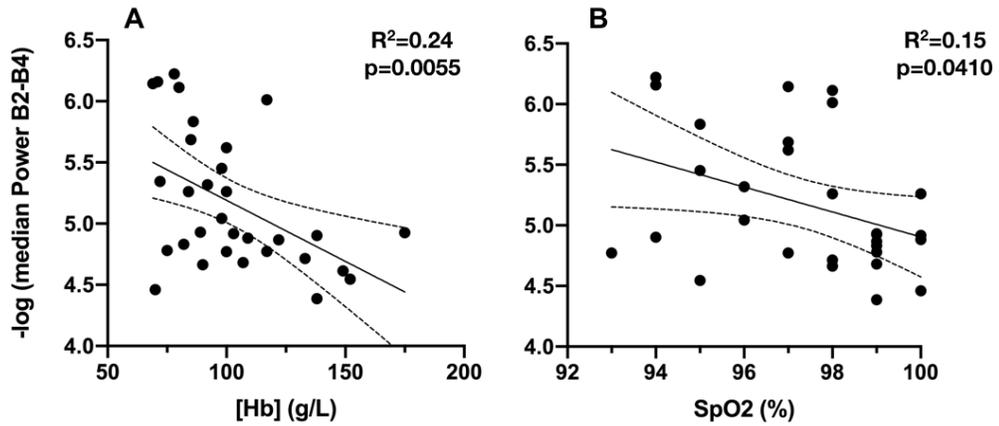
Figure 4.8: Correlation between MHC microvascular signal, systemic hemoglobin levels ([Hb], g/L), and arterial oxygen saturation (SpO2, %).

Note the -logtransform data where lower values indicate higher MHC signal power. Dotted lines represent 95% confidence intervals for line of regression.

a) MHC microvascular power B2-B4 is positively correlated with [Hb].

b) MHC microvascular power B2-B4 is positively correlated with SpO2

4.3.4 Mechanical ventilation directly impacts MHC in peripheral tissue

Respiratory frequency from the ventilator was readily detectable with MHC monitoring in this cohort. The effect of mechanical ventilation on MHC signal is demonstrated with ΔOD time series for three patients (Figure 4.9): the respiratory frequency is superimposed on the intrinsic variability of each MHC tracing. Similarly, CWT projection (Figure 4.1) identifies the ventilator effect as a distinct power stripe in the respiratory band B5.
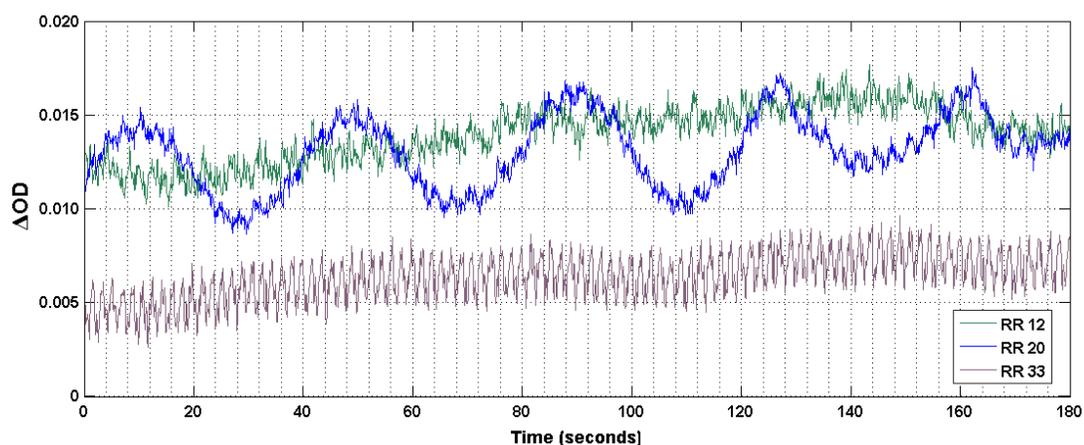
Figure 4.9: High-resolution NIRS demonstrates the interaction between mechanical ventilation and MHC signal in peripheral tissue.

MHC time series (ΔOD, arbitrary units) for three patients are shown. The mechanical ventilator is evident as a distinctive "saw-tooth" pattern superimposed on the intrinsic variability of the MHC signal. The frequency corresponds to the respiratory rate (RR, breaths per minute) delivered by the mechanical ventilator.

Linear regression shows a positive correlation between Power B5 and tidal volume (Figure 4.10a; R^2=0.22, p=0.0141), but no correlation with PEEP or driving pressure (p>0.05). %Power B5 is positively correlated with PEEP (Figure 4.10b; R^2=0.25, p=0.0065), but no correlation with tidal volume or driving pressure (p>0.05). These findings persisted with multivariate regression (Table 4.3).
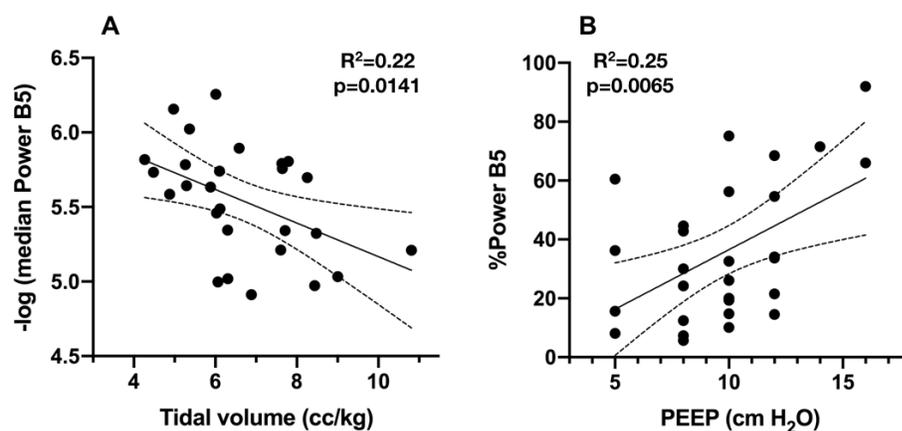
Figure 4.10: Correlation between MHC signal and mechanical ventilation parameters.

Note the -logtransform data where lower values indicate higher MHC signal power. Dotted lines represent 95% confidence intervals for line of regression. Multivariate models with all three ventilation parameters (PEEP, driving pressure, tidal volume) are shown in table 4.3.

a) MHC Power B5 is positively correlated with tidal volume.

b) MHC %Power B5 is positively correlated with PEEP.

	Beta	SE	| t |	p-value
Intercept	6.470	0.3847	16.82	< 0.0001
PEEP	-0.0243	0.0232	1.046	0.3064
ΔP	0.0062	0.0136	0.4581	0.6512
Vt	-0.1159	0.04461	2.598	0.0161

$R^2 = 0.25$ vs median Power B5; $F(3, 23) = 2.677$, p=0.0709

	Beta	SE	| t |	p-value
Intercept	-27.29	24.59	1.110	0.2784
PEEP	3.931	1.483	2.650	0.0143
ΔP	0.5308	0.8693	0.6106	0.5475
Vt	2.569	2.851	0.9010	0.3769

$R^2 = 0.28$ vs %Power B5; $F(3, 23) = 2.977$, p=0.0526

Table 4.3: Multivariate regression between MHC signal and mechanical ventilation parameters.
Median Power B5 and %Power B5 are set as dependent variables, with ventilator parameters positive-end expiratory pressure (PEEP, cm H_2O), driving pressure (ΔP, cm H_2O), and tidal volume (Vt, cc/kg) - as predictors. Tidal volume is positively correlated with median Power B5 (note the -logtransform data); PEEP is positively correlated with %Power B5.

4.3.5 MHC signal power is differentiated according to vasopressor status, but not mean arterial pressure or lactate

Vasopressor use was required in 20/31 patients (64.5%) in the cohort. Patients receiving vasopressors had significantly lower MHC signal power B2-B5 when compared to patients not receiving vasopressors (Figure 4.11a; 5.023 vs 4.715, p=0.0286), but there was no correlation between signal power and MAP (Figure 4.11b; R^2=0.02, p=0.4384). There was no difference in temporal variability (%CV) of MHC signal between vasopressor groups (46.1 vs 38.6, p=0.8870). Median serum lactate in the cohort was 1.4 (IQR 1.0-1.8) mmol/L, with 6/31 patients (19.4%) having lactate values greater than 2.0 mmol/L. Serum lactate was not correlated with MHC signal power (R^2=0.04, p=0.2600), and there was no difference in signal power between patients with lactate greater or less than 2.0 mmol/L (5.133 vs 4.991, p=0.5591).
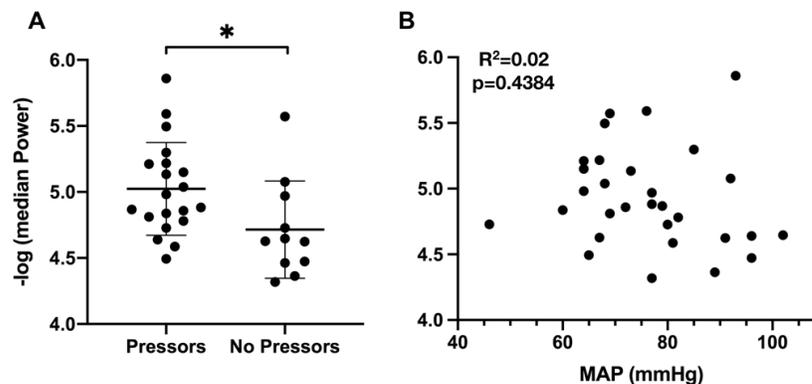
Figure 4.11: MHC signal power is differentiated according to vasopressor status, but is not correlated with mean arterial pressure.

Note the -logtransform data where lower values indicate higher MHC signal power. MAP: mean arterial pressure

a) MHC signal power B2-B5 is significantly reduced for patients receiving vasopressors (* p=0.0286, Student's unpaired t-test). Lines represent mean and standard deviation.

b) MHC signal power B2-B5 is not correlated with mean arterial pressure.

4.4 Discussion

4.4.1 General Discussion

This pilot study demonstrates that MHC monitoring in the ICU can provide continuous physiological data for assessing peripheral perfusion. Using high-resolution data sampling and a straightforward optical device, a signal with substantial biological variability was measured. Fundamentally, this variability underscores the physiology of RBC distribution, and should be viewed as the primary method by which oxygen delivery is regulated in the microcirculation [16]. Moreover, this is the first application of CWT to NIRS data from peripheral tissue in the ICU, representing a novel method for quantifying microvascular hemodynamics.

The main goal of this pilot study was to assess feasibility for MHC monitoring in the ICU, that was successfully demonstrated by signal acquisition from the large majority of patients in the cohort; the number of recruited patients that were invalidated was low, and for reasons that are easily corrected. Moreover, MHC signal quality was high, with a large majority of recorded data suitable for analysis. Motion artifacts were notable, but can been minimized in the future, as with other continuous physiological waveforms including pulse oximetry [46], cardiac telemetry [45], and arterial blood pressure [36]. Overall, this pilot study supports ongoing clinical investigation of MHC monitoring.

Tools for quantifying peripheral perfusion in the ICU have emerged in recent decades, as technology has made bedside evaluation of the microcirculation more accessible. Sublingual microcirculation has been evaluated extensively using handheld videomicroscopy [28], and alterations to the microvascular perfusion characteristics are seen following ICU interventions [14, 29, 44, 48], and correlated with adverse ICU outcomes [2, 24]. Dynamic assessments of peripheral perfusion using LDF [8, 39] or StO2-derived vascular occlusion tests [12, 42] also correlate with ICU outcomes, signifying the importance of the microcirculation in the pathophysiology of critical illness.

The strength of this current study is the simple application of this non-invasive optical technology, that may facilitate the adoption of MHC for monitoring deep tissue perfusion in many clinical settings. MHC is measured with NIRS using one or two wavelengths and well-accepted biomedical optics equations; the only requirement is high temporal resolution. MHC is recorded at the bedside in a similar fashion to cardiac telemetry and pulse oximetry, and is operator independent. In contrast, laser doppler and

sublingual systems monitor only superficial tissue beds, and require training for data collection and analysis; they are also not conducive to continuous real-time monitoring in a challenging ICU environment.

This pilot study introduces MHC as a novel continuous hemodynamic metric with substantial biological variability and signal complexity (Figure 4.1). These patterns of variability relate to the spatial and temporal complexity of the cardiovascular system that integrates signals from central, local, and neurogenic mechanisms. Time-frequency analysis using CWT highlights the presence of coupled oscillators that produce MHC time series with non-stationary and non-linear dynamics [22, 57]. These features are evident with high-resolution MHC data sampled at 10Hz, but are often overlooked when measuring StO2 with commercial NIRS systems that report values every 2-5 seconds. Furthermore, given the slower change of StO2 in skeletal muscle (i.e. regional venous oxygen saturation), StO2 functions mostly as a trend monitor over minutes to hours rather than second-to-second variability as observed with MHC.

MHC analysis in Figure 4.5 indicates that the signal composition (%Power from each frequency band) is not consistent between patients, and that physiological heterogeneity may exist regarding peripheral perfusion characteristics; this is not surprising in a cohort of patients with complex and diverse ICU diseases. Sub-classification according to physiological profile has been proposed for sepsis using organ failure models [20, 65], lactate kinetics [59], body temperature [7], and continuous vital signs [30, 63]. These subclasses (endotypes) have identified groups with differing mortality risks and treatment response profiles. By incorporating signal from the peripheral microcirculation, MHC may

eventually delineate physiological endotypes of perfusion that are not evident with macro-hemodynamic monitors.

This study suggests that MHC signal power may discriminate between patients according to vasopressor status but not according to MAP (Figure 4.10). This is consistent with prior studies that noted vasopressor use was a better surrogate for microvascular injury than MAP or cardiac index [24]. MHC power was lower for patients receiving vasopressors, and may reflect reduced oxygen delivery consistent with computational models [19]. The relationship between systemic hemodynamics and the microcirculation is disrupted in critical illness [27], and disparities often exist between macrohemodynamics and the degree of microvascular injury [2, 31]. The absence of correlation between MAP and MHC is consistent with the concept of the microcirculation as a distinct hemodynamic compartment, and the inability for systemic parameters to predict microvascular status. The lack of correlation between MHC and lactate may reflect the fact that most patients had normal lactate levels (< 2.0 mmol/L) at the time of monitoring, but also the differential kinetics between lactate clearance and microvascular perfusion [26]. These findings support the application of microvascular monitoring to enhance the hemodynamic management of patients with circulatory failure.

The interaction between mechanical ventilation and the circulatory system is well-described for the macrocirculation, but rarely has this impact been considered for the microcirculation. Using high-resolution NIRS, this study is the first to describe this phenomenon in skeletal muscle (Figure 4.9). Respiratory-induced intensity variation with mechanical ventilation has been demonstrated with cerebral NIRS to measure regional

venous saturation [62], and with pulse oximetry as a marker of volume responsiveness [43]. It is postulated that positive pressure decreases venous return and causes expansion of blood volume in the peripheral venous compartment [35, 62]. Measured here in another vascular bed, these findings support the hypothesis that mechanical ventilation is exerting a systemic impact on the microcirculation of many organs throughout the body. MHC monitoring directly quantifies the magnitude of hemoglobin content displaced by mechanical ventilation in peripheral microvascular networks, that will depend on the interaction between ventilator parameters, pulmonary mechanics, and venous hemodynamics (e.g. central venous pressure, blood volume, flow, capacitance). At this stage, it is unclear whether this phenomenon has any direct consequences on organ function, or the mechanisms through which these consequences could be mediated.

MHC signal is comparable in different muscle groups for the same patient (figures 4.6 and 4.7), suggesting a connection between central and peripheral blood flow control mechanisms throughout the body. Some of the concordance between muscle groups will arise from central signals that impact the entire system (e.g. heart rate, mean arterial pressure), but there are also semi-centralized mechanisms that operate throughout vascular networks (e.g. sympathetic tone). B2 endothelial and B3 myogenic bands are ascribed to local mechanisms of blood flow control, that may be similarly affected by systemic critical illness across the spatially distributed peripheral compartment.

Systemic hemoglobin and oxygenation levels are positively correlated with MHC microvascular signal power (figure 4.8), although these findings should not be overstated in a pilot cohort. It is well known from preclinical studies that the 'network Fahreaus effect'

explains the reduction in microvascular hematocrit compared with systemic hematocrit [50]; however, the relationship between systemic and microvascular hematocrit during interventions (e.g. experimental hemodilution) is not always straightforward [49]. In translational human studies, a NIRS-derived index of tissue hemoglobin was not correlated with systemic hemoglobin [11], and RBC transfusion has a variable impact on NIRS and sublingual microvascular perfusion [52, 54]. Because MHC measures the temporal change in hemoglobin content within the underlying tissue, it may track better with RBC flux and systemic hemoglobin levels. Reduction in signal power with decreasing arterial oxygen saturation may reflect a microvascular system with diminished physiological reserve [56]. These relationships and the possible impact of RBC transfusion on MHC signal require further exploration.

4.4.2 Study limitations and future considerations

The main technical limitation for the NIRS system used in the study is the contribution from superficial tissue to MHC signal with SDD 15mm and 20mm, and the variable depth of tissue penetration with these configurations; similarly adipose tissue thickness was not directly measured, but attempts were made to minimize this source of error with patient selection (BMI < 35) and probe positioning. Superficial contamination is a concern with NIRS, where discrepancies in oxygen metabolism and blood flow can exist between skin, adipose, and skeletal muscle [4]. Between these three tissues, skeletal muscle comprises the largest vascular bed with the greatest contribution to MHC variability. In this cohort, there was no difference for MHC signal power between the two SDD configurations, and CWT coherence is noted in prior studies for simultaneous

measurements from skin with laser doppler and skeletal muscle with NIRS [60, 64]. This suggests MHC variability may be a more uniform metric across tissue layers, and supports the application of CWT in the current study. The decision to shorten SDD in this study was driven by technical considerations relating to sensitivity of the spectrometer, rather than overall concerns with the application of the technology. The contribution and coherence of MHC signal from superficial and deep layers of peripheral tissue can be further characterized with spatially-resolved NIRS in future system iterations. Our broadband spectrometer recorded wavelengths from 650-900nm (data not shown), and this data can be used to compare signals derived from isosbestic versus other wavelengths, to inform design of other optical systems.

As illustrated with CWT projection in Figure 4.1, there is a clear demarcation of the respiratory band B5, yet the boundaries between microvascular frequency bands B2-B4 used from previous studies seem arbitrary; the GWPS also shows that the spectral peaks for these oscillators can fall outside of their intended band. Although these frequency components have been defined in previous studies and ascribed to regulatory systems [18, 33], their origins are proposed from indirect evidence and the underlying physiology of these oscillations is not well established [47]. Furthermore, some MHC tracings had a detectable heart rate, although this was not a consistent finding for most patients or recordings (data not shown). Overall, the results of this pilot study suggest that further work is needed to understand the true origins of these oscillations, how to measure them in the peripheral microcirculation, and how best to represent them using time-frequency projections.

Building on the findings of this pilot study, more work is needed to characterize the interactions between MHC and systemic hemodynamics. Using high-resolution NIRS, correlations between MHC and MAP can be investigated as continuous physiological waveforms, similar to the analysis developed for cerebral autoregulation [66]; systemic hemodynamic assessment can also include echocardiography or other non-invasive measures of cardiac output. Moreover, controlled studies can determine the effect of hemodynamic interventions (e.g. fluid bolus, MAP changes) on MHC signal. This current study demonstrates the impact of mechanical ventilation on peripheral tissue, and suggests that ventilator parameters may influence signal characteristics (figure 4.10). Future work should relate MHC signal to the hemodynamic effects of mechanical ventilation that have been used as a marker of fluid responsiveness (e.g. pulse pressure variation) [40].

Most importantly, while this pilot study demonstrates the feasibility of MHC monitoring in the ICU, it does not evaluate the efficacy of MHC as a diagnostic or prognostic tool. Given the substantial between-patient heterogeneity observed in this cohort, larger sample sizes will be required with the addition of healthy volunteers as a comparison group; MHC signal complexity also suggests that the best metrics for characterizing microvascular dysfunction are not yet established. Furthermore, studies have shown that microvascular monitoring may not discriminate between survivors and non-survivors during initial evaluation, and that metrics will only separate later in ICU stay [12, 53]. Thus, the prognostic ability of MHC monitoring is best evaluated with daily assessment to correlate MHC signal with ICU outcomes. This information is a pre-requisite before any consideration for incorporating MHC as a resuscitation target. Overall, the findings from this pilot study have provided vital information regarding the nature of this

novel hemodynamic signal, and will allow better refinement of system engineering, monitoring strategy, and the ability to successfully test numerous hypotheses in future studies.

In conclusion, microvascular hemoglobin content in peripheral tissue can be measured continuously in the intensive care unit with high-resolution NIRS and reflects the dynamic variability of hemoglobin distribution in the microcirculation. Mechanical ventilation directly impacts MHC in peripheral tissue. Results suggest that this novel hemodynamic metric should be further evaluated for diagnosing microvascular dysfunction and monitoring peripheral perfusion.

4.5 References

1. **Ait-Oufella H, Lemoinne S, Boelle PY, et al** (2011) Mottling score predicts survival in septic shock. *Intensive Care Med* 37:801–807.

2. **De Backer D, Donadello K, Sakr Y, et al** (2013) Microcirculatory alterations in patients with severe sepsis: Impact of time of assessment and relationship with outcome. *Crit Care Med* 41:791–799.

3. **Bakker A, Smith B, Ainslie P, Smith K** (2012) Near-Infrared Spectroscopy. In: Applied Aspects of Ultrasonography in Humans. InTech, pp 65–88

4. **Barstow TJ** (2019) Understanding near infrared spectroscopy and its application to skeletal muscle research. *J Appl Physiol* 126:1360–1376.

5. **Bernjak A, Clarkson PBM, McClintock PVE, Stefanovska A** (2008) Low-frequency blood flow oscillations in congestive heart failure and after beta1-blockade treatment. *Microvasc Res* 76:224–32.

6. **Bernjak A, Stefanovska A** (2007) Importance of wavelet analysis in laser Doppler flowmetry time series. *Annu Int Conf IEEE Eng Med Biol - Proc* 4064–4067.

7. **Bhavani S V, Carey KA, Gilbert ER, et al** (2019) Identifying Novel Sepsis Subphenotypes Using Temperature Trajectories. *Am J Respir Crit Care Med* 200:327–335.

8. **Bourcier S, Joffre J, Dubée V, et al** (2017) Marked regional endothelial dysfunction in mottled skin area in patients with severe infections. *Crit Care* 21:155.

9. **Davis ML, Barstow TJ** (2013) Estimated contribution of hemoglobin and myoglobin to near infrared spectroscopy. *Respir Physiol Neurobiol* 186:180–187.

10. **Diop M, Wright E, Toronov V, et al** (2014) Improved light collection and wavelet de-noising enable quantification of cerebral blood flow and oxygen metabolism by a low-cost, off-the-shelf spectrometer. *J Biomed Opt* 19:057007.

11. **Doerschug KC, Delsing AS, Schmidt GA, Haynes WG** (2007) Impairments in microvascular reactivity are related to organ failure in human sepsis. *Am J Physiol Circ Physiol* 293:H1065–H1071.

12. **Donati A, Damiani E, Domizi R, et al** (2016) Near-infrared spectroscopy for assessing tissue oxygenation and microvascular reactivity in critically ill patients: A prospective observational study. *Crit Care* 20:1–10.

13. **Dubin A, Henriquez E, Hernández G** (2018) Monitoring peripheral perfusion and microcirculation. *Curr Opin Crit Care* 24:173–180.

14. **Dubin A, Pozo MO, Casabella CA, et al** (2009) Increasing arterial blood pressure with norepinephrine does not improve microcirculatory blood flow: A prospective study. *Crit Care* 13:1–8.

15. **Dumas G, Lavillegrand JR, Joffre J, et al** (2019) Mottling score is a strong predictor of 14-day mortality in septic patients whatever vasopressor doses and other tissue perfusion parameters. *Crit Care* 23:1–9.

16. **Ellis CG, Jagger J, Sharpe M** (2005) The microcirculation as a functional system. *Crit Care* 9 Suppl 4:S3-8.

17. **Fantini S** (2014) Dynamic model for the tissue concentration and oxygen saturation of hemoglobin in relation to blood volume, flow velocity, and oxygen consumption: Implications for functional neuroimaging and coherent hemodynamics spectroscopy (CHS). *Neuroimage* 85:202–221.

18. **Folgosi-Correa MS, Nogueira GEC** (2011) Quantifying low-frequency fluctuations in the laser Doppler flow signal from human skin. In: Tuchin V V., Duncan DD, Larin K V., et al (eds) Proceedings of SPIE. p 789811

19. **Fraser GM, Sharpe MD, Goldman D, Ellis CG** (2015) Impact of Incremental Perfusion Loss on Oxygen Transport in a Capillary Network Mathematical Model. *Microcirculation* 22:348–359.

20. **Gårdlund B, Dmitrieva NO, Pieper CF, et al** (2018) Six subphenotypes in septic shock: Latent class analysis of the PROWESS Shock study. *J Crit Care* 47:70–79.

21. **Geyer MJ, Jan YK, Brienza DM, Boninger ML** (2004) Using wavelet analysis to characterize the thermoregulatory mechanisms of sacral skin blood flow. *J Rehabil Res Dev* 41:797–805.

22. **Glass L** (2001) Synchronization and rhythmic processes in physiology. *Nature* 410:277–84.

23. **Hariri G, Joffre J, Leblanc G, et al** (2019) Narrative review: clinical assessment of peripheral tissue perfusion in septic shock. *Ann Intensive Care* 9:1–9.

24. **Hernandez G, Boerma EC, Dubin A, et al** (2013) Severe abnormalities in microvascular perfused vessel density are associated to organ dysfunctions and mortality and can be predicted by hyperlactatemia and norepinephrine requirements in septic shock patients. *J Crit Care* 28:.

25. **Hernández G, Ospina-Tascón GA, Damiani LP, et al** (2019) Effect of a Resuscitation Strategy Targeting Peripheral Perfusion Status vs Serum Lactate Levels on 28-Day Mortality among Patients with Septic Shock: The ANDROMEDA-SHOCK Randomized Clinical Trial. *JAMA - J Am Med Assoc* 321:654–664.

26. **Hernandez G, Pedreros C, Veas E, et al** (2012) Evolution of peripheral vs metabolic perfusion parameters during septic shock resuscitation. A clinical-physiologic study. *J Crit Care* 27:283–8.

27. **Ince C** (2015) Hemodynamic coherence and the rationale for monitoring the microcirculation. *Crit Care* 19:S8.

28. **Ince C, Boerma EC, Cecconi M, et al** (2018) Second consensus on the assessment of sublingual microcirculation in critically ill patients: results from a task force of the European Society of Intensive Care Medicine. *Intensive Care Med* 44:281–299.

29. **Jhanji S, Stirling S, Patel N, et al** (2009) The effect of increasing doses of norepinephrine on tissue oxygenation and microvascular flow in patients with septic shock. *Crit Care Med* 37:1961–1966.

30. **Kamaleswaran R, Akbilgic O, Hallman MA, et al** (2018) Applying Artificial Intelligence to Identify Physiomarkers Predicting Severe Sepsis in the PICU. *Pediatr Crit Care Med* 19:e495–e503.

31. **Kanoore Edul VS, Ince C, Vazquez AR, et al** (2016) Similar microcirculatory alterations in patients with normodynamic and hyperdynamic septic shock. *Ann Am Thorac Soc* 13:240–247.

32. **Kim JG, Mengna Xia, Hanli Liu** (2005) Extinction coefficients of hemoglobin for near-infrared spectroscopy of tissue. *IEEE Eng Med Biol Mag* 24:118–121.

33. **Kvandal P, Landsverk SA, Bernjak A, et al** (2006) Low-frequency oscillations of the laser Doppler perfusion signal in human skin. *Microvasc Res* 72:120–127.

34. **Lee JK, Kibler KK, Benni PB, et al** (2009) Cerebrovascular reactivity measured by near-infrared spectroscopy. *Stroke* 40:1820–6.

35. **Leung TS, Tisdall MM, Tachtsidis I, et al** (2008) Cerebral tissue oxygen saturation calculated using low frequency haemoglobin oscillations measured by near infrared spectroscopy in adult ventilated patients. *Adv Exp Med Biol* 614:235–44.

36. **Li Q, Mark RG, Clifford GD** (2009) Artificial arterial blood pressure artifact models and an evaluation of a robust blood pressure and heart rate estimator. *Biomed Eng Online* 8:13.

37. **Lima A, Bakker J** (2012) Noninvasive monitoring of peripheral perfusion. *Appl Physiol Intensive Care Med 2 Physiol Rev Ed* 39–49.

38. **Mesquida J, Gruartmoner G, Espinal C, et al** (2013) Skeletal Muscle Oxygen Saturation (StO2) Measured by Near-Infrared Spectroscopy in the Critically Ill Patients. *Biomed Res Int* 2013:1–8.

39. **Mongkolpun W, Orbegozo D, Cordeiro CPR, et al** (2020) Alterations in Skin Blood Flow at the Fingertip Are Related to Mortality in Patients With Circulatory Shock. *Crit Care Med* 48:443–450.

40. **Monnet X, Marik PE, Teboul JL** (2016) Prediction of fluid responsiveness: an update. *Ann Intensive Care* 6:1–11.

41. **Nardi O, Zavala E, Martin C, et al** (2018) Targeting skeletal muscle tissue oxygenation (StO_2) in adults with severe sepsis and septic shock: a randomised controlled trial (OTO-StS Study). *BMJ Open* 8:e017581.

42. **Neto AS, Pereira VGM, Manetta JA, et al** (2014) Association between static and dynamic thenar near-infrared spectroscopy and mortality in patients with sepsis. *J Trauma Acute Care Surg* 76:226–233.

43. **Nilsson LM** (2013) Respiration signals from photoplethysmography. *Anesth Analg* 117:859–65.

44. **Ospina-Tascon G, Neves AP, Occhipinti G, et al** (2010) Effects of fluids on microvascular perfusion in patients with severe sepsis. *Intensive Care Med* 36:949–955.

45. **Patel SI, Souter MJ, Warner DS, Warner MA** (2008) Equipment-related Electrocardiographic Artifacts. *Anesthesiology* 108:138–148.

46. **Pollreisz D, TaheriNejad N** (2019) Detection and Removal of Motion Artifacts in PPG Signals. Mob Networks Appl. https://doi.org/10.1007/s11036-019-01323-6

47. **Pradhan RK, Chakravarthy VS** (2011) Informational dynamics of vasomotion in microvascular networks: A review. *Acta Physiol* 201:193–218.

48. **Pranskunas A, Koopmans M, Koetsier PM, et al** (2013) Microcirculatory blood flow as a tool to select ICU patients eligible for fluid therapy. *Intensive Care Med* 39:612–619.

49. **Pries AR, Fritzsche A, Ley K, Gaehtgens P** (1992) Redistribution of red blood cell flow in microcirculatory networks by hemodilution. *Circ Res* 70:1113–21.

50. **Pries AR, Ley K, Gaehtgens P** (1986) Generalization of the Fahraeus principle for microvessel networks. *Am J Physiol* 251:H1324-32.

51. **Pries AR, Secomb TW** (2008) Blood Flow in Microvascular Networks. In: Microcirculation. Elsevier, pp 3–36

52. **Sadaka F, Aggu-Sher R, Krause K, et al** (2011) The effect of red blood cell transfusion on tissue oxygenation and microcirculation in severe septic patients. *Ann Intensive Care* 1:46.

53. **Sakr Y, Dubois M-J, De Backer D, et al** (2004) Persistent microcirculatory alterations are associated with organ failure and death in patients with septic shock*. *Crit Care Med* 32:1825–1831.

54. **Scheuzger J, Zehnder A, Meier V, et al** (2020) Sublingual microcirculation does not reflect red blood cell transfusion thresholds in the intensive care unit-a prospective observational study in the intensive care unit. *Crit Care* 24:18.

55. **Scholkmann F, Kleiser S, Metz AJ, et al** (2014) A review on continuous wave functional near-infrared spectroscopy and imaging instrumentation and methodology. *Neuroimage* 85:6–27.

56. **Seely AJE, Macklem P** (2012) Fractal variability: an emergent property of complex dissipative systems. *Chaos* 22:013108.

57. **Stefanovska A** (2010) Coupled oscillators. Complex but not complicated cardiovascular and brain interactions. *IEEE Eng Med Biol Mag* 26:25–9.

58. **Stefanovska A, Bracic M, Kvernmo HD** (1999) Wavelet analysis of oscillations in the peripheral blood circulation measured by laser Doppler technique. *IEEE Trans Biomed Eng* 46:1230–1239.

59. **Thomas-Rueddel DO, Poidinger B, Weiss M, et al** (2015) Hyperlactatemia is an independent predictor of mortality and denotes distinct subtypes of severe sepsis and septic shock. *J Crit Care* 30:439.e1-439.e6.

60. **Thorn CE, Shore AC, Matcher SJ** (2007) Combined optical and near infrared reflectance measurements of vasomotion in both skin and underlying muscle. In: Chance B, Alfano RR, Tromberg BJ, et al (eds) Optical Tomography and Spectroscopy of Tissue VII. p 643421

61. **Vincent JL, Ince C, Bakker J** (2012) Clinical review: Circulatory shock - an update: a tribute to Professor Max Harry Weil. *Crit Care* 16:1–5.

62. **Wolf M, Duc G, Keel M, et al** (1997) Continuous noninvasive measurement of cerebral arterial and venous oxygen saturation at the bedside in mechanically ventilated neonates. *Crit Care Med* 25:1579–1582.

63. **van Wyk F, Khojandi A, Mohammed A, et al** (2019) A minimal set of physiomarkers in continuous high frequency data streams predict adult sepsis onset earlier. *Int J Med Inform* 122:55–62.

64. **Yano T, Lian CS, Afroundeh R, et al** (2014) Comparison of oscillations of skin blood flow and deoxygenation in vastus lateralis in light exercise. *Biol Sport* 31:15–20.

65. **Zhang Z, Zhang G, Goyal H, et al** (2018) Identification of subclasses of sepsis that showed different clinical outcomes and responses to amount of fluid resuscitation: a latent profile analysis. *Crit Care* 22:347.

66. **Zweifel C, Dias C, Smielewski P, Czosnyka M** (2014) Continuous time-domain monitoring of cerebral autoregulation in neurocritical care. *Med Eng Phys* 36:638–645.

CHAPTER 5: FINAL SUMMARY

The regulation of oxygen distribution within tissues is one of the primary functions of the microcirculation. This is achieved through numerous control and feedback mechanisms that carefully match supply with spatial and temporal accuracy to meet local tissue oxygen demands [13, 39]. Because oxygen is carried almost exclusively by red blood cells (RBCs), any study of microvascular oxygen exchange and its regulatory system must begin with these beautiful hemoglobin containers. Given the contribution of microvascular structure to the functional physiology of the microcirculation [36], the impact of capillary network structure (as the primary site of oxygen exchange) on RBC distribution is also particularly relevant. And while many overlapping principles in oxygen regulation exist across all organs, focus on skeletal muscle appears most appropriate due to the specialized role it serves in locomotion, and the dramatic ranges of oxygen consumption and blood flow that are required during the transition from rest to peak exercise.

The fundamental objective of this thesis was to characterize and quantify RBC distribution in skeletal muscle capillary networks. Philosophically, this was approached at different levels of scale ranging from individual capillaries to large capillary networks, employing numerous methodologies including preclinical animal experiments, in silico computational modeling, and translational investigation in humans with critical illness. With the information gained from this analysis, a physiologically-informed framework of microvascular control has emerged that is centered around the capillary module and capillary network, providing new insights into the potential mechanisms of flow regulation within the microcirculation. Lastly, we have developed new technology and applied these

physiological principles in the clinical setting, providing a successful linkage from bench to bedside.

Specifically, the following questions were addressed in the three research studies of this thesis: what is the structure of capillary networks in skeletal muscle, and the functional heterogeneity of RBC distribution therein ? (**Chapter 2**); can the hemodynamics of RBC flow and structural features of capillary modules illustrate mechanisms of flow regulation in capillary networks ? (**Chapter 3**); can variability of RBC distribution be measured in real-time in the ICU using non-invasive optical imaging? (**Chapter 4**).

5.1 Summary of results

In the first research study of the thesis (**Chapter 2**), we introduced a new paradigm of capillary network structure: the Capillary Fascicle. The Capillary Fascicle is a series of interconnected capillary modules spanning thousands of microns, organized into columns that align naturally with the dimensions of the muscle fascicle. Previous focus of capillary-myocyte oxygen exchange has mainly addressed small groups of capillaries and small volumes of muscle tissue [17]; alternatively, capillary-RBC hemodynamics have been recorded with no spatial localization [2]. In addition, the capillary module, as the basic functional unit of the microcirculation, has mostly been treated in isolation [34, 40] without consideration for how it might relate to broader capillary networks. These approaches have failed to address how blood flow might be coordinated over large distances for contracting skeletal muscle. Using intravital video-microscopy, this study provides the largest recorded dataset to date of capillary-RBC hemodynamics, and demonstrates the intrinsic

heterogeneity of capillary network topology (structure) and RBC hemodynamics (function) in resting skeletal muscle. Functional heterogeneity was spatially quantified between capillaries in a module and between modules in the total dataset, and also temporally quantified with repeated video recordings of the same capillary segments. Measurements of stopped-flow capillaries indicate that the overwhelming majority of skeletal muscle capillaries are perfused in resting skeletal muscle, conclusively undermining the theory of capillary recruitment that has persisted for decades despite a mountain of contradictory evidence [35]. Lastly, structure-function analysis indicates that capillary module hemodynamics are independent of module length or the number of parallel capillaries in a module, providing initial evidence that capillary modules are active participants in microvascular flow regulation. The main significance of this study is the large scale that characterizes the novel structure of the Capillary Fascicle, and its association with the muscle fascicle as the most likely target volume for oxygen delivery. Although capillary columns in skeletal muscle have been described to a certain degree in previous studies [40, 43], they have not been previously associated with specific structure in the muscle, nor evaluated over the expanse of many thousands of microns with such detailed hemodynamic analysis. In this regard, the Capillary Fascicle is a new paradigm for studying RBC distribution and oxygen delivery in skeletal muscle.

These observations regarding length-independence of RBC hemodynamics, and their implications for microvascular flow regulation have been expanded in the second study of this thesis (**Chapter 3**), using more detailed hemodynamic analysis complemented with computational modeling. We provide, for the first time, combined evaluation of capillary module flow, hemodynamic resistance, and driving pressure (ΔP) derived from

direct measurements of in vivo capillary perfusion. This analysis shows that the pressure drop across a capillary module is modest - in the single-digit mmHg range – establishing an important context and reference for further research into capillary hemodynamics. The most striking and significant finding from this study is the lack of correlation between capillary module resistance and RBC flow, and only weak correlation with plasma flow and blood flow. This is interpreted as supportive evidence that capillary perfusion is not passively determined by hemodynamic resistance; phrased another way, we observe the effects of active flow regulation at the level of the capillary module through adjustments to capillary module driving pressure. It should be noted that this evidence is circumstantial, and we are not observing these adjustments through test of dynamic interventions. Moreover, the interconnected structure of capillary modules allows further development of this theory by examining capillary modules that share a common microvessel. Passive microvascular flow would imply that blood flow distribution between these module pairs is determined by the ratio of their resistances. By demonstrating the absence of this relationship, with the requirement of a fixed boundary condition in module pairs, we can infer that pre- and post-capillary loci of flow regulation are necessary to independently adjust driving pressures for each module. Another functional consequence of the Capillary Fascicle structure is the need for precise regulation of capillary pressures over the entire length of the column to maintain proper flow direction within each module. This is truly remarkable given that the terminal arterioles supplying a fascicle may originate from vastly different sections of the arteriolar network [15].

This theory is a significant departure from current microvascular dogma which maintains that arterioles are the exclusive locus of flow regulation [1], and receive inputs

directly from surrounding tissue via diffusion of vasoactive metabolites. A consistent (albeit minority) theory has challenged this dogma, suggesting that capillaries are ideally situated to detect changes in tissue metabolism [31, 32], are indeed able to signal upstream along the arteriolar system to call for increased blood flow [9, 10, 41], and that oxygen-dependent ATP release from RBCs is an important initiator of this phenomenon occurring directly in capillary networks and propagated via conducted signaling [11, 14, 22]. Evidence from our current study aligns with this hypothesis by showing that RBC flow in capillary modules is independent of resistance, thereby requiring transmission of hemodynamic information from these modules and communication with the arteriolar system to regulate capillary perfusion.

The computational modeling in Chapter 3 is used to support the empirical observations and hemodynamic analysis from capillary modules. By systematically adjusting the boundary conditions within 1-module and 2-module geometries, we have gained insight into how these variables impact the magnitude and distribution of RBC and plasma flow in capillary modules. The main findings from these experiments were that: (i) changes to driving pressure have a direct linear effect on the magnitude of blood flow without any impact on flow distribution, (ii) changes to hematocrit, particularly above 20%, contribute to viscosity-dependent resistance in a capillary module, and (iii) heterogeneity of RBC distribution within a capillary module is primarily determined by the internal branching structure within a capillary module, and is unaffected by changes to geometric resistance (i.e. length or number of parallel capillaries). Furthermore, using the 2-module geometries, we showed how asymmetric module resistance can be compensated with relatively small adjustments to driving pressure between modules, providing further

support for the theory that post-capillary control of driving pressure is a feasible mechanism for regulating RBC perfusion in capillary modules. The last point of note from this study is the discrepancy in findings between computation and empirical analysis regarding RBC and plasma distribution within capillary modules. In computational studies, plasma flow was consistently more heterogeneous than RBC flow, whereas the opposite was observed in empirical analysis. We surmised that the biggest factors contributing to these differences were the absence of time-dependent variability for inflow hematocrit in the steady-state computational model, and the uniform diameter of capillaries within the synthetic modules. This was also supported by the evidence of temporal heterogeneity from primary capillary-RBC hemodynamics in Chapter 2.

The concept of time-dependent variability in RBC distribution was subsequently explored in a human study in the ICU (**Chapter 4**). Using high-resolution near-infrared spectroscopy (NIRS), we demonstrated the feasibility of monitoring microvascular hemoglobin content (i.e. total hemoglobin, HbT) and the detection of a biological signal with marked temporal heterogeneity and complexity over extended periods of monitoring at the bedside. While interrogating skeletal muscle tissue oxygen saturation (StO2) or individual hemoglobin chromophores (oxy/deoxy hemoglobin) with NIRS has been well-described in exercise science [23] and critical care [28], this study represents the first description of this new monitoring strategy for continuous assessment of RBC variability as a dynamic marker of microvascular function. This study was also the first to utilize wavelet analysis with skeletal muscle NIRS in the ICU, which demonstrated the wide range of perfusion phenotypes encountered in a heterogeneous cohort of ICU patients. The lack of correlation between systemic blood pressure and microvascular signal reinforces the

added value of microvascular monitoring in the management of patients with circulatory shock; the impact of common ICU interventions on the microcirculation - vasoactive medications and mechanical ventilation - was also documented with high-resolution near-infrared spectroscopy. Notably, the detection of mechanical ventilation is the first reported instance of this phenomenon in the peripheral circulation, further demonstrating the application of this new modality in the field of critical care.

Together, these three studies produce a cohesive and innovative paradigm for describing RBC distribution in skeletal muscle, and also point towards mechanisms of microvascular control and the role of capillary networks in regulating oxygen delivery. By moving from small groups of capillaries to the Capillary Fascicle – and therefore from a few myocytes to a muscle fascicle – we have matched the vascular supply of oxygen with the functional unit of muscle contraction. This larger scale also justifies the linkages between experimental observations in preclinical models and the interrogation of clinically-relevant volumes of tissue in human studies, with fascicular columns of capillaries evaluated in both circumstances. Yet, the interconnected structure of the Capillary Fascicle also explains how the basic unit of these capillary networks (capillary module) is still maintained. The advantage of these smaller units is to minimize the hemodynamic resistance for each module, and ensure that well-oxygenated RBCs are supplied within reasonable volumes of muscle tissue to maintain adequate oxygen delivery in resting and exercise conditions.

The updated paradigm in this thesis also establishes capillary networks as a central player and active participant in the process of microvascular flow regulation. The ability

of capillary networks to coordinate their own perfusion facilitates the accurate distribution of oxygen directly at the tissue level. Intuitively, this "capillary-centric" model aligns closely with philosophy of end-organ perfusion that is essential to the management of circulatory shock in critical care. Furthermore, because of the interconnected structure of capillary modules and capillary networks, changes to pressure, flow, and hematocrit cannot be treated in isolation. Rather, each of these variables has hemodynamic repercussions on the others, suggesting the need for multiple and overlapping effectors that act over wide ranges of hemodynamics and metabolic activity. Fundamentally, this system must exist far from equilibrium, and requires constant fine-tuning and feedback; intrinsic in this description is the fractal physiology that characterizes non-stationary and non-linear systems [20, 44]. In these circumstances, the health of the system in not determined by the maintenance of perfect homeostasis (i.e. constant and invariable physiological values), but rather the ability of the system to adapt and respond to stressors for efficient oxygen transfer [38], while operating "on the edge of instability" [30]. This paradigm explains how the structural complexity of capillary networks relates to temporal complexity of RBC perfusion, and how time series variability provides an evaluation of microvascular control and function. Moreover, when these regulatory systems fail, such as with sepsis and critical illness, this manifests through loss of temporal variability (and therefore loss in adaptability) , and also impaired spatial matching of oxygen supply and demand – leading to perfusion abnormalities, tissue hypoxia, and pathological supply dependency [21]. In the field of critical care, continuous bedside monitoring that incorporates these physiological principles may address the deficiencies that have limited the application of microvascular monitoring technologies in routine clinical practice.

5.2 Future considerations

Many avenues of inquiry have been opened by the results of this thesis that require further investigation. Experimental studies of capillary-RBC hemodynamics in the Capillary Fascicle, provided in Chapter 2 for resting skeletal muscle, should be expanded to included disease models such as sepsis [2, 12], heart failure [37], and diabetes [33]; in all of these diseases, RBC flow heterogeneity increases above baseline, with decreasing RBC supply rate and the proportion of perfused capillaries. Importantly, prior studies did not ascertain whether changes to capillary hemodynamics manifested equally across all capillary modules, or instead predominantly affected some modules while sparing others. The ability to spatially localize these functional changes may provide insight into how alterations to capillary hemodynamics contribute to pathological dysoxia. Similarly, the physiology of functional hyperemia should be investigated within the Capillary Fascicle paradigm. Using contracting skeletal muscle protocols [25, 37], we can expect to learn whether the structure-function relationships described in this thesis for resting skeletal muscle (e.g. lack of correlation between RBC velocity and lineal density for capillary segments; length-independence of capillary module hemodynamics) might present differently within this new condition of physiological stress.

Another knowledge gap that can be explored is the connection between the Capillary Fascicle and the rest of the microvascular network – arterioles and venules. Insights from cerebrovascular neuroscience have suggested that capillary networks and these resistance networks comprise two independent systems that fuse during vascular morphogenesis, the former being described as a mesh-like structure and the latter a quasi-

fractal branching tree [26]. This seems like an apt comparison for the organization of skeletal muscle, and the interactions between the Capillary Fascicle, arterioles, and venules. Computational modeling in this thesis identifies the point of interface between these two systems as an important hemodynamic location, but the exact anatomy requires further identification with advanced microcroscopy techniques (e.g. multiphoton, laser scanning confocal). Furthermore, studies of muscle contraction and pharmacological stimulation have demonstrated the ability of capillary networks to communicate with the arteriolar system [3, 7], but should be re-examined within the Capillary Fascicle with an eye towards the interconnected nature of capillary modules. This thesis discusses the particular hemodynamic consequences of module pairs sharing a common microvessel, the potential constraints this poses during functional hyperemia, and the need for post-capillary flow regulation to accommodate this physiology; all of these hypotheses require empirical validation. Notably, the ability of post-capillary venules to participate in microvascular control is very speculative, supported with old evidence for venular dilation during muscle contraction [27], and with description of venular ion channels, smooth muscle, and sympathetic innervation [29]. Moreover, computational modeling in this thesis suggests that functional hyperemia - causing increased capillary hematocrit and RBC velocity and decreased heterogeneity between capillary segments - would require simultaneous adjustments to multiple boundary conditions (e.g. pressure, diameter, hematocrit); evaluation of these assumptions with direct evidence for changes to upstream arterioles and downstream venules is therefore essential to characterize this fundamental process in skeletal muscle.

Missing from this thesis is any quantification of RBC oxygenation or computational modeling of oxygen transfer from the Capillary Fascicle into surrounding skeletal muscle. This is the natural step that follows from an understanding of RBC distribution, and is indeed the primary motivation for studying RBC distribution in the first place. As mentioned in Chapter 2, technical limitations precluded oxygen saturation measurements with the current intravital microscopy system; when these challenges are overcome, we can expect oxygen saturation measurements – at the inlet and outlet of capillary modules - to inform our understanding of oxygen transfer, and the heterogeneity of oxygen distribution in resting and active skeletal muscle in health and disease. Complementing this analysis, demarcation of fibre types, sizes and boundaries of the muscle fascicle will inform anatomical models over clinically-relevant scales and with clinically-relevant structures of locomotion. 3D rendering from anatomically faithful reconstruction has been shown to improve description of oxygen transport from small groups of capillaries [18], and from histological sections [6, 45]. The paradigm of the Capillary Fascicle therefore provides a new framework for modeling oxygen exchange in skeletal muscle, and enhances the ability to perform this modeling from large reconstructed capillary networks. One aspect to investigate using this information would be the role of diffusional oxygen exchange within capillary modules, and the potential for adjacent modules to coordinate oxygen exchange together; this analysis may further elucidate how oxygen delivery is accomplished within contracting muscle fascicles.

Building on the discoveries from the NIRS study in the ICU, further work is required to identify the appropriate applications of this technology in the clinical setting. Particularly, the connection between microvascular signal and ICU outcomes is not

established, nor is the relationship between the microvascular time series, systemic hemodynamics, and mechanical ventilation. Each of these knowledge gaps will entail dedicated experimental design, including both longitudinal and interventional studies in a large ICU cohort. Given the complexity of the NIRS time series, it is likely that machine learning [5, 42] or fractal variability analysis [4] will be needed, as will both time domain [46] and frequency domain [24] correlation techniques with systemic hemodynamics.

The time-dependent variability elucidated with human data can also be linked back with experimental and computational studies. For example, extended measurements of capillary-RBC hemodynamics may reveal oscillations similar to those identified using wavelet analysis, attributed to systems of microvascular control (e.g. neurogenic, myogenic, etc) that impact capillary perfusion. Time-dependent computational models with simulated and reconstructed vascular geometries will also highlight the interactions between Capillary Fascicle structure and temporal patterns of RBC flow, revealing emergent properties such as oscillations [8, 16] and non-linear behavior [19] observed with human data.

5.3 Final Summary

RBC distribution in capillary networks is the final product of microvascular oxygen delivery, and represents the interaction between network structure, biophysical properties of RBC rheology, and regulatory mechanisms of the microcirculation. Understanding this phenomenon necessitates an integrated approach that evaluates these components together, while also addressing the organ-specific requirements under which they are studied. In this

thesis, we introduced the Capillary Fascicle as a physiological framework that describes how RBC distribution is organized in skeletal muscle, and used hemodynamic analysis and computational models to understand how RBC distribution is regulated in capillary modules under normal resting conditions. We then applied these concepts to design and validate a NIRS system for monitoring RBC distribution in a clinical setting where impaired oxygen delivery produces life-threatening consequences. Taken together, the knowledge presented in this thesis expands the field of microvascular physiology and provides new opportunities to continue investigation in primary and translational domains of oxygen delivery and blood flow regulation.

5.4 References

1. **Bagher P, Segal SS** (2011) Regulation of blood flow in the microcirculation: role of conducted vasodilation. *Acta Physiol* 202:271–284.

2. **Bateman RM, Sharpe MD, Goldman D, et al** (2008) Inhibiting nitric oxide overproduction during hypotensive sepsis increases local oxygen consumption in rat skeletal muscle. *Crit Care Med* 36:225–231.

3. **Berg BR, Cohen KD, Sarelius IH** (1997) Direct coupling between blood flow and metabolism at the capillary level in striated muscle. *Am J Physiol Circ Physiol* 272:H2693–H2700.

4. **Bravi A, Longtin A, Seely AJ** (2011) Review and classification of variability analysis techniques with clinical applications. *Biomed Eng Online* 10:90.

5. **Cannesson M, Hofer I, Rinehart J, et al** (2019) Machine learning of physiological waveforms and electronic health record data to predict, diagnose and treat haemodynamic instability in surgical patients: protocol for a retrospective study. *BMJ Open* 9:e031988.

6. **Čebašek V, Eržen I, Vyhnal A, et al** (2010) The estimation error of skeletal muscle capillary supply is significantly reduced by 3D method. *Microvasc Res* 79:40–46.

7. **Cohen KD, Berg BR, Sarelius IH** (2000) Remote arteriolar dilations in response to muscle contraction under capillaries. *Am J Physiol Circ Physiol* 278:H1916–H1923.

8. **Davis JM, Pozrikidis C** (2014) Self-sustained Oscillations in Blood Flow Through a Honeycomb Capillary Network. *Bull Math Biol* 76:2217–2237.

9. **Dietrich HH** (1989) Effect of locally applied epinephrine and norepinephrine on blood flow and diameter in capillaries of rat mesentery. *Microvasc Res* 38:125–135.

10. **Dietrich HH, Tyml K** (1992) Capillary as a communicating medium in the microvasculature. *Microvasc Res* 43:87–99.

11. **Ellis CG, Milkovich S, Goldman D** (2012) What is the efficiency of ATP signaling from erythrocytes to regulate distribution of O(2) supply within the microvasculature? *Microcirculation* 19:440–50.

12. **Ellis CG, Bateman RM, Sharpe MD, et al** (2002) Effect of a maldistribution of microvascular blood flow on capillary O(2) extraction in sepsis. *Am J Physiol Heart Circ Physiol* 282:H156-64.

13. **Ellis CG, Jagger J, Sharpe M** (2005) The microcirculation as a functional system. *Crit Care* 9 Suppl 4:S3-8.

14. **Ellsworth ML, Ellis CG, Sprague RS** (2016) Role of erythrocyte-released ATP in the regulation of microvascular oxygen supply in skeletal muscle. *Acta Physiol (Oxf)* 216:265–76.

15. **Emerson GG, Segal SS** (1997) Alignment of microvascular units along skeletal muscle fibers of hamster retractor. *J Appl Physiol* 82:42–48.

16. **Forouzan O, Yang X, Sosa JM, et al** (2012) Spontaneous oscillations of capillary blood flow in artificial microvascular networks. *Microvasc Res* 84:123–132.

17. **Fraser GM, Goldman D, Ellis CG** (2012) Microvascular Flow Modeling using In Vivo Hemodynamic Measurements in Reconstructed 3D Capillary Networks. *Microcirculation* 19:510–520.

18. **Fraser GM, Goldman D, Ellis CG** (2013) Comparison of Generated Parallel Capillary Arrays to Three-Dimensional Reconstructed Capillary Networks in Modeling Oxygen Transport in Discrete Microvascular Volumes. *Microcirculation* n/a-n/a.

19. **Geddes JB, Carr RT, Wu F, et al** (2010) Blood flow in microvascular networks: a study in nonlinear biology. *Chaos* 20:045123.

20. **Goldberger AL, Amaral LAN, Hausdorff JM, et al** (2002) Fractal dynamics in physiology: Alterations with disease and aging. *Proc Natl Acad Sci* 99:2466–2472.

21. **Goldman D, Bateman RM, Ellis CG** (2006) Effect of decreased O2 supply on skeletal muscle oxygenation and O2 consumption during sepsis: role of heterogeneous capillary spacing and blood flow. *Am J Physiol Heart Circ Physiol* 290:H2277-85.

22. **Goldman D, Fraser GM, Ellis CG, et al** (2012) Toward a multiscale description of microvascular flow regulation: o(2)-dependent release of ATP from human erythrocytes and the distribution of ATP in capillary networks. *Front Physiol* 3:246.

23. **Grassi B, Quaresima V** (2016) Near-infrared spectroscopy and skeletal muscle oxidative function in vivo in health and disease: a review from an exercise physiology perspective. *J Biomed Opt* 21:091313.

24. **Highton D, Ghosh A, Tachtsidis I, et al** (2015) Monitoring cerebral autoregulation after brain injury: Multimodal assessment of cerebral slow-wave oscillations using near-infrared spectroscopy. *Anesth Analg* 121:198–205.

25. **Kindig CA, Richardson TE, Poole DC** (2002) Skeletal muscle capillary hemodynamics from rest to contractions: implications for oxygen transfer. *J Appl Physiol* 92:2513–20.

26. **Lorthois S, Cassot F** (2010) Fractal analysis of vascular networks: Insights from morphogenesis. *J Theor Biol* 262:614–633.

27. **Marshall JM, Tandon HC** (1984) Direct observations of muscle arterioles and venules following contraction of skeletal muscle fibres in the rat. *J Physiol* 350:447–459.

28. **Mesquida J, Gruartmoner G, Espinal C, et al** (2013) Skeletal Muscle Oxygen Saturation (StO2) Measured by Near-Infrared Spectroscopy in the Critically Ill Patients. *Biomed Res Int* 2013:1–8.

29. **Monos E, Bérczi V, Nádasy G, et al** (1995) Local control of veins: biomechanical, metabolic, and humoral aspects. *Physiol Rev* 75:611–666.

30. **Muñoz MA** (2018) Colloquium : Criticality and dynamical scaling in living systems. *Rev Mod Phys* 90:031001.

31. **Murrant CL, Lamb IR, Novielli NM** (2017) Capillary endothelial cells as coordinators of skeletal muscle blood flow during active hyperemia. *Microcirculation* 24:1–10.

32. **Murrant CL, Sarelius IH** (2015) Local control of blood flow during active hyperaemia: what kinds of integration are important? *J Physiol* 593:4699–4711.

33. **Padilla DJ, McDonough P, Behnke BJ, et al** (2006) Effects of Type II diabetes on capillary hemodynamics in skeletal muscle. *Am J Physiol Heart Circ Physiol* 291:H2439–H2444.

34. **Plyley MJ, Sutherland GJ, Groom AC** (1976) Geometry of the capillary network in skeletal muscle. *Microvasc Res* 11:161–173.

35. **Poole DC, Copp SW, Ferguson SK, Musch TI** (2013) Skeletal muscle capillary function: Contemporary observations and novel hypotheses. *Exp Physiol* 98:1645–1658.

36. **Pries AR, Secomb TW** (2008) Blood Flow in Microvascular Networks. In: Microcirculation. Elsevier, pp 3–36

37. **Richardson TE, Kindig CA, Musch TI, Poole DC** (2003) Effects of chronic heart failure on skeletal muscle capillary hemodynamics at rest and during contractions. *J Appl Physiol* 95:1055–1062.

38. **Seely AJE, Macklem P** (2012) Fractal variability: an emergent property of complex dissipative systems. *Chaos* 22:013108.

39. **Segal SS** (2005) Regulation of blood flow in the microcirculation. *Microcirculation* 12:33–45.

40. **Skalak TC, Schmid-Schönbein GW** (1986) The microvasculature in skeletal muscle. IV. A model of the capillary network. *Microvasc Res* 32:333–347.

41. **Song H, Tyml K** (1993) Evidence for sensing and integration of biological signals by the capillary network. *Am J Physiol Circ Physiol* 265:H1235–H1242.

42. **Sutton JR, Mahajan R, Akbilgic O, Kamaleswaran R** (2019) PhysOnline: An Open Source Machine Learning Pipeline for Real-Time Analysis of Streaming Physiological Waveform. *IEEE J Biomed Heal Informatics* 23:59–65.

43. **Tyml K, Ellis CG, Safranyos RG, et al** (1981) Temporal and spatial distributions of red cell velocity in capillaries of resting skeletal muscle, including estimates of red cell transit times. *Microvasc Res* 22:14–31.

44. **West BJ** (2010) Fractal physiology and the fractional calculus: A perspective. *Front Physiol* 1 OCT:1–17.

45. **Zeller-Plumhoff B, Daly KR, Clough GF, et al** (2017) Investigation of microvascular morphological measures for skeletal muscle tissue oxygenation by image-based modelling in three dimensions. *J R Soc Interface* 14:20170635.

46. **Zweifel C, Dias C, Smielewski P, Czosnyka M** (2014) Continuous time-domain monitoring of cerebral autoregulation in neurocritical care. *Med Eng Phys* 36:638–645.

Appendix A: Ethics Approval

Western

AUP Number: 2019-053
PI Name: Ellis, Christopher G
AUP Title: A Systems Approach to Sepsis: Pathological versus Adaptive Microvascular Response
Approval Date: 01/01/2020

 Official Notice of Animal Care Committee (ACC) Approval:
Your new Animal Use Protocol (AUP) 2019-053:1: entitled " A Systems Approach to Sepsis: Pathological versus Adaptive Microvascular Response"
has been APPROVED by the Animal Care Committee of the University Council on Animal Care. This approval, although valid for up to four years, is subject to annual Protocol Renewal.

Prior to commencing animal work, please review your AUP with your research team to ensure full understanding by everyone listed within this AUP.

As per your declaration within this approved AUP, you are obligated to ensure that:
   1) Animals used in this research project will be cared for in alignment with:
         a) Western's Senate MAPPs 7.12, 7.10, and 7.15

         b) University Council on Animal Care Policies and related Animal Care Committee procedures

   2) As per UCAC's Animal Use Protocols Policy,
         a) this AUP accurately represents intended animal use;
         b) external approvals associated with this AUP, including permits and scientific/departmental peer approvals, are complete and accurate;

c) any divergence from this AUP will not be undertaken until the related Protocol Modification is approved by the ACC; and

d) AUP form submissions - Annual Protocol Renewals and Full AUP Renewals - will be submitted and attended to within timeframes outlined by the ACC.

e) ██

3) As per MAPP 7.10 all individuals listed within this AUP as having any hands-on animal contact will

a) be made familiar with and have direct access to this AUP;

b) complete all required CCAC mandatory training ████████████ and

c) be overseen by me to ensure appropriate care and use of animals.

4) As per MAPP 7.15,

a) Practice will align with approved AUP elements;

b) Unrestricted access to all animal areas will be given to ACVS Veterinarians and ACC Leaders;

c) UCAC policies and related ACC procedures will be followed, including but not limited to:

i) Research Animal Procurement
ii) Animal Care and Use Records
iii) Sick Animal Response
iv) Continuing Care Visits

5) As per institutional OH&S policies, all individuals listed within this AUP who will be using or potentially exposed to

hazardous materials will have completed in advance the appropriate institutional OH&S training, facility-level training, and reviewed related (M)SDS Sheets.

████████████████████████████████

Submitted by: Copeman, Laura
on behalf of the Animal Care Committee
University Council on Animal Care

████████████████████
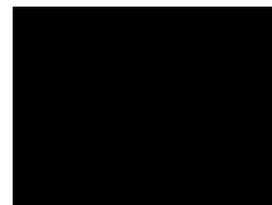
Animal Care Committee Chair

The University of Western Ontario
Animal Care Committee / University Council on Animal Care

████████████████████████

Western Research

Western University Health Science Research Ethics Board
HSREB Delegated Initial Approval Notice

Principal Investigator: Dr. Michael Sharpe
Department & Institution: Schulich School of Medicine and Dentistry\Anaesthesia, London Health Sciences Centre

Review Type: Delegated
HSREB File Number: 108760
Study Title: Optical Device for Monitoring Microvascular Function in Critically Ill ICU Patients
Sponsor: Canadian Institutes of Health Research

HSREB Initial Approval Date: March 20, 2017
HSREB Expiry Date: March 20, 2018

Documents Approved and/or Received for Information:

Document Name	Comments	Version Date
Data Collection Form/Case Report Form	MFM ICU Study Data Collection Form for Optical Device for Monitoring Microvascular Function in Critically Ill ICU Patients	2016/11/20
Western University Protocol	108760 Protocol - Clean	2017/03/14
Revised Letter of Information & Consent	MFM 108760 LOI - Clean	2017/03/14
Health Canada Correspondence	Correspondence between Keith St. Lawrence (Co-Investigator) and Health Canada regarding device.	2017/02/21
Revised Western University Protocol	References for Western Protocol	2017/02/21
Amendment	Change in PI	2017/02/21

The Western University Health Science Research Ethics Board (HSREB) has reviewed and approved the above named study, as of the HSREB Initial Approval Date noted above.

HSREB approval for this study remains valid until the HSREB Expiry Date noted above, conditional to timely submission and acceptance of HSREB Continuing Ethics Review.

The Western University HSREB operates in compliance with the Tri-Council Policy Statement Ethical Conduct for Research Involving Humans (TCPS2), the International Conference on Harmonization of Technical Requirements for Registration of Pharmaceuticals for Human Use Guideline for Good Clinical Practice Practices (ICH E6 R1), the Ontario Personal Health Information Protection Act (PHIPA, 2004), Part 4 of the Natural Health Product Regulations, Health Canada Medical Device Regulations and Part C, Division 5, of the Food and Drug Regulations of Health Canada.

Members of the HSREB who are named as Investigators in research studies do not participate in discussions related to, nor vote on such studies when they are presented to the REB.

The HSREB is registered with the U.S. Department of Health & Human Services under the IRB registration number IRB 00000940.
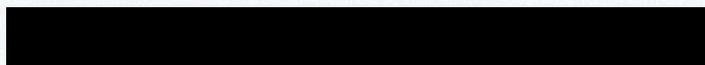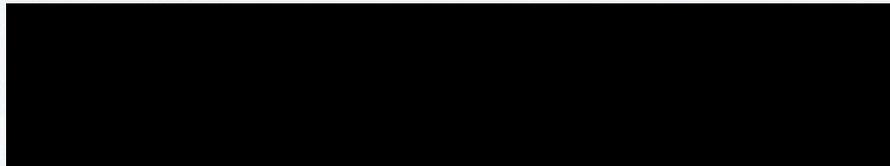
Appendix B: Copyright permissions

My Orders   My Library   My Profile

My Orders > Orders > All Orders

License Details

This Agreement between Dr. Asher Mendelson ("You") and Elsevier ("Elsevier") consists of your license details and the terms and conditions provided by Elsevier and Copyright Clearance Center.

Print   Copy

License Number	4966111279206
License date	Dec 11, 2020
Licensed Content Publisher	Elsevier
Licensed Content Publication	Microvascular Research
Licensed Content Title	Geometry of the capillary network in skeletal muscle
Licensed Content Author	M.J. Plyley,Gloria J. Sutherland,A.C. Groom
Licensed Content Date	Mar 1, 1976
Licensed Content Volume	11
Licensed Content Issue	2
Licensed Content Pages	13
Type of Use	reuse in a thesis/dissertation
Portion	figures/tables/illustrations
Number of figures/tables/illustrations	1
Format	both print and electronic
Are you the author of this Elsevier article?	No
Will you be translating?	No
Title	Experimental, theoretical, and translational studies of RBC distribution in capillary networks
Institution name	Western University
Expected presentation date	Mar 2021
Portions	Figure 3
Requestor Location	
Publisher Tax ID	
Total	0.00 USD
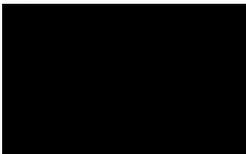
BACK

![Copyright Clearance Center RightsLink logo]

License Details

This Agreement between Dr. Asher Mendelson ("You") and Elsevier ("Elsevier") consists of your license details and the terms and conditions provided by Elsevier and Copyright Clearance Center.

[Print] [Copy]

License Number	4977131499676
License date	Dec 27, 2020
Licensed Content Publisher	Elsevier
Licensed Content Publication	Microvascular Research
Licensed Content Title	The microvasculature in skeletal muscle. IV. A model of the capillary network
Licensed Content Author	T.C. Skalak,G.W. Schmid-Schönbein
Licensed Content Date	Nov 1, 1986
Licensed Content Volume	32
Licensed Content Issue	3
Licensed Content Pages	15
Type of Use	reuse in a thesis/dissertation
Portion	figures/tables/illustrations
Number of figures/tables/illustrations	1
Format	both print and electronic
Are you the author of this Elsevier article?	No
Will you be translating?	No
Title	Experimental, theoretical, and translational studies of RBC distribution in capillary networks
Institution name	Western University
Expected presentation date	Mar 2021
Portions	Figure 2
Requestor Location	
Publisher Tax ID	
Total	0.00 CAD

[BACK]

Order Number: 1090266
Order Date: 13 Jan 2021

Payment Information

Asher Mendelson

████████████████████

Payment method: Invoice

Billing Address:

Customer Location:

██
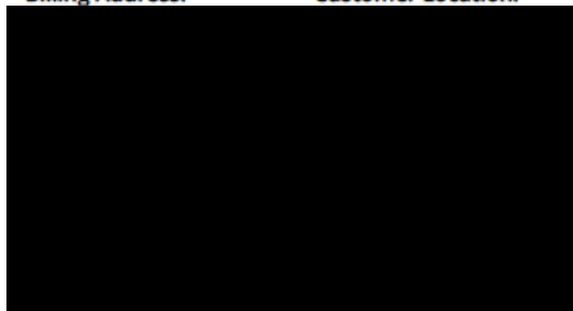
Order Details

1. Annual review of fluid mechanics

Billing Status:
Open

Order license ID	1090266-1
Order detail status	Completed
ISSN	1545-4479
Type of use	Republish in a thesis/dissertation
Publisher	ANNUAL REVIEWS
Portion	Image/photo/illustration

0.00 CAD
Republication Permission

LICENSED CONTENT

Publication Title	Annual review of fluid mechanics	**Rightsholder**	Annual Reviews, Inc.
		Publication Type	e-Journal
Date	12/31/1968	**URL**	http://arjournals.annu
Language	English		alreviews.org/loi/fluid
Country	United States of America		

REQUEST DETAILS

Portion Type	Image/photo /illustration	**Distribution**	Worldwide
		Translation	Original language of publication
Number of images / photos / illustrations	1		

Format (select all that apply)	Print,Electronic	**Copies for the disabled?**	No
Who will republish the content?	Academic institution	**Minor editing privileges?**	No
Duration of Use	Life of current edition	**Incidental promotional use?**	No
Lifetime Unit Quantity	Up to 4,999		
Rights Requested	Main product	**Currency**	CAD

NEW WORK DETAILS

Title	Experimental, theoretical, and translational studies of RBC distribution in capillary networks	**Institution name**	Western University
		Expected presentation date	2021-03-30
Instructor name	Asher Mendelson		

ADDITIONAL DETAILS

The requesting person / organization to appear on the license	Asher Mendelson

REUSE CONTENT DETAILS

Title, description or numeric reference of the portion(s)	Figure 5	**Title of the article/chapter the portion is from**	Blood Flow in the Microcirculation
Editor of portion(s)	N/A	**Author of portion(s)**	Timothy Secomb
Volume of serial or monograph	49	**Publication date of portion**	2017-01-01
Page or page range of portion	443-61		

My Orders   My Library   My Profile

License Details

This Agreement between Dr. Asher Mendelson ("You") and Springer Nature ("Springer Nature") consists of your license details and the terms and conditions provided by Springer Nature and Copyright Clearance Center.

Print   Copy

License Number	4991610492526
License date	Jan 17, 2021
Licensed Content Publisher	Springer Nature
Licensed Content Publication	Journal of Clinical Monitoring and Computing
Licensed Content Title	Dynamic tracking of microvascular hemoglobin content for continuous perfusion monitoring in the intensive care unit: pilot feasibility study
Licensed Content Author	Asher A. Mendelson et al
Licensed Content Date	Oct 26, 2020
Type of Use	Thesis/Dissertation
Requestor type	non-commercial (non-profit)
Format	print and electronic
Portion	full article/chapter
Will you be translating?	no
Circulation/distribution	5000 - 9999
Author of this Springer Nature content	yes
Title	Experimental, theoretical, and translational studies of RBC distribution in capillary networks
Institution name	Western University
Expected presentation date	Mar 2021
Requestor Location	
Total	0.00 CAD

BACK

My Orders   **My Library**   **My Profile**

My Orders > Orders > All Orders

License Details

This Agreement between Dr. Asher Mendelson ("You") and John Wiley and Sons ("John Wiley and Sons") consists of your license details and the terms and conditions provided by John Wiley and Sons and Copyright Clearance Center.

Print   Copy

License Number	5033110733969
License date	Mar 20, 2021
Licensed Content Publisher	John Wiley and Sons
Licensed Content Publication	Journal of Physiology
Licensed Content Title	The capillary fascicle in skeletal muscle: Structural and functional physiology of RBC distribution in capillary networks
Licensed Content Author	Asher A. Mendelson, Stephanie Milkovich, Timothy Hunter, et al
Licensed Content Date	Mar 18, 2021
Licensed Content Volume	0
Licensed Content Issue	0
Licensed Content Pages	20
Type of Use	Dissertation/Thesis
Requestor type	Author of this Wiley article
Format	Print and electronic
Portion	Full article
Will you be translating?	No
Title	Experimental, theoretical, and translational studies of RBC distribution in capillary networks
Institution name	Western University
Expected presentation date	Mar 2021
Requestor Location	
Publisher Tax ID	EU826007151
Total	**0.00 CAD**

BACK

Copyright Clearance Center Marketplace™

Order Number: 1112201
Order Date: 15 Apr 2021

Payment Information

Asher Mendelson

Payment method: Invoice

Billing Address:

Customer Location:

Order Details

1. Microcirculation

Billing Status:
Open

Article: Advances in Translational Imaging of the Microcirculation

Order license ID	1112201-1
Order detail status	Completed
ISSN	1549-8719
Type of use	Republish in a thesis/dissertation
Publisher	TAYLOR & FRANCIS
Portion	Chapter/article

0.00 CAD
Republication Permission

LICENSED CONTENT

Publication Title	Microcirculation	**Language**	English
Article Title	Advances in Translational Imaging of the Microcirculation	**Country**	United Kingdom of Great Britain and Northern Ireland
Author/Editor	Microcirculatory Society.	**Rightsholder**	John Wiley & Sons - Books
Date	12/31/1993	**Publication Type**	e-Journal

Appendix C: Curriculum Vitae

Asher Mendelson MDCM MSc FRCPC

EDUCATION & TRAINING

2015-2021	Western University PhD Candidate – Dr. Chris Ellis, Dr. Daniel Goldman Department of Medical Biophysics Schulich School of Medicine
2015-2017	Western University Research fellow, Critical Care Clinician Investigator Program Schulich School of Medicine
2013-2015	Western University Clinical fellow, Critical Care Schulich School of Medicine
2011-2013	University of British Columbia Master's of Science – Dr. Caigan Du Dept. of Experimental Medicine
2009-2013	University of British Columbia Resident, Internal medicine UBC Faculty of Medicine
2005-2009	McGill University MDCM, Faculty of Medicine
2004-2005	McGill University Pre-medical year *McGill Certificate of Merit*
2001-2004	Marianopolis College Combined DEC Music/Science *Marianopolis Scholar*

CERTIFICATION

2015	Fellow, Critical Care Medicine (Adult)
	Royal College of Physicians and Surgeons of Canada
2014	Fellow, Internal Medicine
	Royal College of Physicians and Surgeons of Canada
2013	USMLE Step 3
2011	USMLE Step 2 CS
2009	USMLE Step 2 CK
2007	USMLE Step 1
2010	LMCC 2
2009	LMCC 1

EMPLOYMENT & AFFILIATION

2020-present	Assistant Professor – Section of Critical Care
	Dept of Medicine, Rady Faculty of Health Sciences
	University of Manitoba, Winnipeg, MB
2019-present	Adjunct Scientist – Centre for Critical Illness Research
	Lawson Health Research Institute, Western University
	London, Ontario
2015-present	Clinical Associate – Department of Critical Care Medicine
	St. Mary's General Hospital and Grand River Hospital
	Kitchener, Ontario
2015-2017	Clinical Scholar and Adjunct Professor
	Division of Critical Care Medicine, Department of Medicine
	Schulich School of Medicine and Dentistry, Western University
2011-2013	Clinical Associate - Division of Critical Care Medicine
	Royal Columbian Hospital - Fraser Health Authority
	New Westminister, BC

ADMINISTRATION AND TEACHING

2020-2025	Canadian Sepsis Research Network
	Project co-lead, National Preclinical Sepsis Platform
2019-2020	*Shayla Scott*, undergraduate honors thesis
	Plasma flow distribution in the microvascular lattice

2019-2021	The Microcirculatory Society Co-chair, Clinician-Scientist Subcommittee
2019-2021	The Microcirculatory Society Trainee representative, Membership Committee
2019	*Timothy Hunter*, summer undergraduate project Geometric architecture of the microvascular lattice
2016-2018	ISPD 2018 World Congress – Vancouver, BC Member, Local Organizing Committee Member, Scientific Committee Co-Chair, Basic science pre-congress workshop
2018	*Shaun Milkovich*, summer undergraduate project In vivo hemodynamics of the microvascular lattice
2017-2018	*Edward Ho*, undergraduate honors thesis Hemodynamic implications of the lattice structure in skeletal muscle microvasculature
2016-2017	London Health Sciences Centre – London, ON Founder and Chair, Advanced Care Planning Committee
2015-2017	Schulich School of Medicine and Dentistry, Western University – London, ON Guest lecture: sepsis and inflammation Department of Physiology and Pharmacology MedSci 4200: Inflammation and Disease

RESEARCH FUNDING

CIHR Operating Grant
2020 – **Co-Investigator**
Sex differences in preclinical models of sepsis: systematic review
$112,500/1 yr

CIHR Operating Grant
2019 – **Co-Investigator**
Patient and Public Involvement in Preclinical Laboratory Research: A Scoping Review
$76,500/1 yr

CIHR Team Grant: Sepsis Research Network
2019 – **Co-Applicant**
Canadian Sepsis Research Network: Improving care Before, During, and After Sepsis
$5,700,000/5 yr

CIHR Planning and Dissemination Grant
2019 – **Principal Investigator**
National Preclinical Sepsis Platform: Developing a framework for accelerating innovation in Canadian sepsis research
$9,995/1 yr

CIHR Team Grant: Sepsis Research Network – Letter of Intent
2019 – **Collaborator**
Canadian Sepsis Research Network: Improving Care Before, During, and After Sepsis
$25,000/1 yr

CIHR Proof of Principle Program - Phase II
2014 – **Co-Investigator**
Preclinical Development of a Glucose-Free Peritoneal Dialysis Solution
$294,799/1 yr

CIHR Proof of Principle Program - Phase I
2012 – **Co-Investigator**
Novel Polymer Based Glucose-sparing Peritoneal Dialysis Solutions
for End-stage Renal Disease
$160,000/1 yr

Kidney Foundation of Canada – Biomedical Research Grant
2012 – **Co-Investigator**
Metabolic Benefits of Novel Glucose-Sparing Peritoneal Dialysis Solutions in Diabetics
$100,000/2 yr

PATENT & INDUSTRY

Patent US9919004B2: Polymer-based dialysate
Inventors: Jayachandran Kizhakkedathu, Caigan Du, **Asher Mendelson**, Gerald da Roza
Current Assignee: University of British Columbia
Date of Patent: March 20, 2018

PUBLICATIONS

1. **Mendelson AA**, Milkovich S, Hunter T, Vijay R, Choi YH, Milkovich S, Ho E, Goldman D, Ellis CG. The Capillary Fascicle in skeletal muscle: structural and functional physiology of RBC distribution in capillary networks. J Physiol; *accepted for publication*.
2. Guerraty M, Bargava A, Senarathna J, **Mendelson AA**, Pathak A. Advances in translational imaging of the microcirculation. Microcirculation; *accepted for publication*.

3. **Mendelson AA**, Lansdell C, Fox-Robichaud AE, Liaw P … Lalu MM. National Preclinical Sepsis Platform: Developing a framework for accelerating innovation in Canadian sepsis research. Intensive Care Med Exp; *accepted for publication*.

4. Zhang M, Macala KF, Fox-Robichaud A, **Mendelson AA**, Lalu MM. Sex- and gender-dependent differences in clinical and preclinical sepsis. Shock. 2021 Jan 4. doi: 10.1097/SHK.0000000000001717; *Epub ahead of print*.

5. **Mendelson AA**, Rajaram A, Bainbridge D, St Lawrence K, Bentall T, Sharpe M, Diop M, Ellis CG. Dynamic tracking of microvascular hemoglobin content for continuous perfusion monitoring in the intensive care unit: pilot feasibility study. J Clin Monit Comput. 2020 Oct 26; 1-13. doi: 10.1007/s10877-020-00611-x; *epub ahead of print*.

6. La Han B, Guan Q, Chafeeva I, **Mendelson AA**, da Roza G, Liggins R, Kizhakkedathu JN, Du C. Peritoneal and Systemic Responses of Obese Type II Diabetic Rats to Chronic Exposure to a Hyperbranched Polyglycerol-Based Dialysis Solution. Basic Clin Pharmacol Toxicol. 2018 Oct;123(4):494-503.

7. Du C, **Mendelson AA**, Guan Q, Dairi G, Chafeeva I, da Roza G; Kizhakkedathu J. Hyperbranched polyglycerol is superior to glucose for long-term preservation of peritoneal membrane in a rat model of chronic peritoneal dialysis. J Transl Med. 2016 Dec 13;14(1):338.

8. **AA Mendelson**. Book Review: Objective Structured Clinical Examination in Intensive Care Medicine. Can J Anesth. 2016. 63; 999-1000.

9. Du C, **Mendelson AA**, Guan Q, Chapanian R, Chafeeva I, da Roza G, Kizhakkedathu JN. The size-dependent efficacy and biocompatibility of hyperbranched polyglycerol in peritoneal dialysis. Biomaterials 2014 Feb;35(5):1378-89.

10. **Mendelson AA**, Guan Q, Chafeeva I, da Roza GA, Kizhakkedathu JN, Du C. Hyperbranched polyglycerol is an efficacious and biocompatible novel osmotic agent in a rodent model of peritoneal dialysis. Perit Dial Int. 2013 Jan;33(1):15-27.

11. **Mendelson AA**, Gillis C, Henderson WR, Ronco JJ, Dhingra V, Griesdale DEG. Intracranial pressure monitors in traumatic brain injury: a systematic review. Can J Neurol Sci. 2012;39(5):571-576

12. **Mendelson AA**, Al-Macki K, Chauvin P, Kost KM. Sclerosing Mucoepidermoid Carcinoma of the Salivary Gland: Case report and literature review. Ear Nose Throat J. 2010;89(12):600-3

13. *Mendelson AA*, Tamilia M, Rivera J, Hier MP, Sherman M, Garfield N, Black MJ, Rochon L, Gologan O, Payne RJ. Predictors of Malignancy in Preoperative Non-diagnostic Biopsies of the Thyroid. J Otolaryngol. 2009;38(3):395-400

14. **Mendelson AA**, Al-Khatib TA, Julien M, Payne RJ, Black MJ, Hier MP. Thyroid Gland Management in Total Laryngectomy: Meta-analysis and Surgical Recommendations. Otolaryngol Head Neck Surg. 2009;140(3):298-30

15. Al-Khatib TA, **Mendelson AA**, Kost KM, Zeitouni A, Black MJ, Payne MJ, Hier MP. Routine Thyroidectomy in Total Laryngectomy: Is it really indicated? J Otolaryngol. 2009;38(5):564-7

ACADEMIC PRESENTATIONS

Conference Proceedings:

1. National Preclinical Sepsis Platform: multicentre trials for basic science research in sepsis. Crit Care Med Jan 2021. 49 (1); 618. doi:10.1097/01.ccm.0000730804.60454.48

2. Insights on Microvascular Flow Regulation in Microvascular Units: A Computational Modeling Study. *Poster presentation (top 10 selection), Experimental Biology 2019 – Orlando, FL, April 2019*

3. Dynamic tracking of microvascular hemoglobin content in skeletal muscle of ICU patients with a custom near-infrared spectroscopy system. *Oral Presentation (top 10 selection), Canada Critical Care Forum – Toronto, ON, November 2018*

4. The microvascular lattice: and updated paradigm for flow distribution in capillary networks in skeletal muscle. *Poster Presentation, World Congress for Microcirculation - Vancouver, BC, September 2018*

5. The microvascular lattice: and updated paradigm for flow distribution in capillary networks. *Poster presentation, Experimental Biology 2018 - San Diego, CA, April 2018*

6. Vascular Stress Test: A macrovascular and microvascular method for assessing pressor responsiveness. *Oral presentation, Canadian Critical Care Translational Biology Group - Lake Louise, Alberta, January 2018*

7. Development of a near-infrared spectroscopy system to monitor microvascular function: pilot project in the ICU. *Oral Presentation, Canadian Critical Care Translational Biology Group - Lake Louise, Alberta, January 2018*

8. Design of an optical device for monitoring microvascular function. *Oral Presentation, Canadian Critical Care Translational Biology Group - Lake Louise, Alberta, January 2017*

9. Oxygen regulation, sepsis, and the microcirculation: potential role for the endothelial glycocalyx. *Oral presentation, Canadian Critical Care Translational Biology Group - Halifax, Nova Scotia, June 2016*

10. Hyperbranched polyglycerol is an emerging candidate for glucose-sparing PD therapy. *Oral presentation, International Society of Peritoneal Dialysis - Madrid, Spain, September 2014*

11. The efficacy and biocompatibility of a novel polymer-based solution in a rodent model of peritoneal dialysis. *Poster presentation, American College of Physicians - San Francisco, CA, April 2013*

12. Novel Polymer-based Biocompatible Peritoneal Dialysis Solution. *Oral presentation, ISPD 2014 World Congress - Kuala Lumpur, Malaysia, September 2012*

13. Novel Polymer-based Biocompatible Peritoneal Dialysis Solution. *Poster Presentation, Canadian Society of Nephrology - St John's, NFLD, April 2012*

14. Intracranial pressure monitors in traumatic brain injury: a systematic review. *Poster presentation, American Thoracic Society - Denver, CO, May 2011*

15. Thyroid Gland Management in Total Laryngectomy: Meta-analysis and Surgical Recommendations. *Oral Presentation, American Academy of Otolaryngology - Chicago, IL, September 2008*

16. Predictors of Malignancy in Preoperative Non-diagnostic Biopsies of the Thyroid. *Poster Presentation, Canadian Society of Otolaryngology - Jasper, AB, June 2008*

Invited Presentations:

1. Microvascular monitoring in the ICU: bench-to-bedside physiology and resuscitation science. *McGill ICU Grand Rounds – Montreal, QC, November 2019*

2. Microvascular monitoring for septic shock: can we quantify perfusion at the bedside? *Dalhousie ICU Grand Rounds – Halifax, NS, November 2019*

3. MCS President's Symposium: Clinical perspectives on the microcirculation (session chair). *Experimental Biology – Orlando, FL, April 2019*

4. Indigenous peoples' issues in training and research (session chair). *Critical Care Canada Forum – Toronto, ON, November 2018*

5. Microvascular monitoring in the ICU: physiology, knowledge gaps and translational medicine. *Ottawa Critical Care Research Rounds - Ottawa, ON, June 2018*

6. Strategic priorities in basic science and translational PD research (session chair). *ISPD 2018 World Congress - Vancouver, BC, May 2018*

7. Update on novel osmotic agents and glucose-sparing PD. *ISPD 2018 World Congress - Vancouver, BC, May 2018*

8. Resuscitation Science and how it influences clinical practice. *LHSC ICU Grand Rounds - London, ON, June 2016*

9. When oncology meets critical Illness: caring for cancer patients in the ICU. *Multidisciplinary Cancer Conference - Kitchener, ON, March 2016*

10. Novel Osmotic Agents in Peritoneal Dialysis: moving beyond glucose. *ISPD 2016 World Congress – Melbourne, Australia, February 2016*

11. When oncology meets critical Illness: caring for cancer patients in the ICU. *LHSC Oncology Grand Rounds - London, ON, September 2015*

12. Novel Osmotic Agents in Peritoneal Dialysis: Hyperbranched Polyglycerol. *ERA-EDTA Annual Congress – London, England, **May 2015***

13. Novel osmotic agents in PD: moving beyond glucose. *BC Renal Agency, Western Canada PD Days - Vancouver, BC April 2014*

14. Novel osmotic agents in PD: moving beyond glucose. *UWO Division of Nephrology Southwestern PD Symposium - London, ON, November 2013*

AWARDS

2019	Zweifach Student Travel Award – Microcirculatory Society
2018	CCCF Outstanding Trainee Abstract Award
2015	Western-McMaster ICU Resident Research Day – 2nd place
2013	ACP National Associates Abstract Competition Research Poster Winner – Basic Science
2013	UBC Internal Medicine Resident Research Day – Best podium presentation by a PGY- 4/5/6
2013	UBC Faculty of Medicine Graduate Award
2012	International Society for Peritoneal Dialysis – Young Investigator Award
2012	G.B. John Mancini Resident Research Achievement Award
2012	UBC Internal Medicine Resident Research Day – Best podium presentation by a PGY-3
2012	UBC Faculty of Medicine Graduate Award
2005	McGill Dean's Honor List
2005	McGill McConnell Award
2005	Hillel Montreal - Dr. Mark Cohen Scholarship
2004	Canada Millennium Scholarship Foundation - Local Excellence Award
2001	Secondary Diploma, Classical Piano - McGill Conservatory of Music
2000	Rensselaer Medal – Rensselaer Polytechnic Institute